

# HKJC 2015



## Proceedings of

**the HANU-Kosen Joint Conference  
on global network  
in a cross-cultural environment 2015**

Hanoi, December 2015



# **“HANU-KOSEN JOINT CONFERENCE ON GLOBAL NETWORK IN A CROSS-CULTURAL ENVIRONMENT 2015 (HKJC 2015)”**

## **CONFERENCE COMMITTEES**

### **I. STEERING COMMITTEE**

Prof. Dr. Nguyen Dinh Luan	President, Hanoi University, Vietnam, <i>Co-chair</i>
Prof. Dr. Tsutomu Hasegawa	President, Kumamoto College, Japan, <i>Co-chair</i>
Prof. Dr. Hiroshi Tsukamoto	President, Kitakyusyu College, Japan, <i>Co-chair</i>
Prof. Dr. Tran Quang Binh	Vice-President, Hanoi University, Vietnam, <i>Member</i>
Dr. Nguyen Thi Cuc Phuong	Vice-President, Hanoi University, Vietnam, <i>Member</i>
Prof. Dr. Nguyen Van Trao	Vice-President, Hanoi University, Vietnam, <i>Member</i>
Prof. Dr. Tran Quang Anh	Vice-Director, Post & Telecommunication Institute of Technology, Vietnam, <i>Member</i>

### **II. PROGRAM COMMITTEE**

Dr. Nguyen To Chung	Hanoi University, Vietnam, <i>Co-chair</i>
Prof. Dr. Yoshifumi Shimoshio	Kumamoto College, Japan, <i>Co-chair</i>
Dr. Nguyen Xuan Thang	Hanoi University, Vietnam <i>Co-chair</i>
Prof. Dr. Nguyen Xuan Hoai	Hanoi University, Vietnam, <i>Member</i>
Dr. Ta Quang Hung	Hanoi University, Vietnam, <i>Member</i>

Dr. Nguyen Viet Hung	Post & Telecommunication Institute of Technology, Vietnam, <i>Member</i>
Prof. Dr. Toyonori Matsuda	Kumamoto College, Japan, <i>Member</i>
Prof. Dr. Eiji Nishiyama	Kumamoto College, Japan, <i>Member</i>
Prof. Dr. Shinichiro Uemura	Kagoshima College, Japan, <i>Member</i>
Associate Prof. Dr. Akihiro Takahashi	Miyakonojo College, Japan, <i>Member</i>
Associate Prof. Dr. Tsutomu Iwashita	Ariake College, Japan, <i>Member</i>
Dr. Hiroshi Nishiguti	Sasebo College, Japan, <i>Member</i>
Prof. Dr. Hiroshi Tanaka	Okinawa College, Japan, <i>Member</i>
Associate Prof. Dr. Hiroyuki Kinjo	Kurume College, Japan, <i>Member</i>
Prof. Dr. Yasuo Matsuda	Kurume College, Japan, <i>Member</i>

### **III. ORGANIZING COMMITTEE**

Mr. Trinh Bao Ngoc	Hanoi University, Vietnam, <i>Co-Chair</i>
Mr. Nguyen Ngoc Tan	Hanoi University, Vietnam, <i>Co-Chair</i>
Ms. Pham Thi Thai	Hanoi University, Vietnam, <i>Co-Chair</i>
Mr. Nguyen Huy Quang	Hanoi University, Vietnam, <i>Co-Chair</i>
Mr. Luong Ngoc Minh	Hanoi University, Vietnam, <i>Co-Chair</i>
Mr. Hoang Anh Hung	Hanoi University, Vietnam, <i>Co-Chair</i>

Mr. Vu Minh Tuan	Hanoi University, Vietnam, <i>Member</i>
Ms. Vuong Thi Nhung	Hanoi University, Vietnam, <i>Member</i>
Ms. Hoang Thi Kieu Hoa	Hanoi University, Vietnam, <i>Member</i>
Ms. Trinh Thi Thu Huyen	Hanoi University, Vietnam, <i>Member</i>
Mr. Dang Hoang Giang	Hanoi University, Vietnam, <i>Member</i>
Mr. Pham Thi Hong Yen	Hanoi University, Vietnam, <i>Member</i>
Mr. Nguyen Trung Hieu	Post & Telecommunication Institute of Technology, Vietnam, <i>Member</i>



## CONTENT

<b>Conference session on Communication and Electronic Engineering .....</b>	<b>14</b>
Preparation of multilayer thin film for filtering specific light as magneto-optics devices <i>Sohsuke YAMADA, Tamiko OHSHIMA, Takeshi IHARA, Yoshihito YAGYU, Hiroharu KAWASAKI, and Yoshiaki SUDA .....</i>	15
Introduction of Arduino to signal light detection of a plasmons resonance absorption sensor I – Measurement of Stokes parameter <i>Yuki TANAKA, Kazuhito UMEKI and Toyonori MATSUDA .....</i>	18
Introduction of Arduino to signal light detection of a plasmons resonance absorption sensor II – Utilization to data transmission <i>Kazuhito UMEKI , Yuki TANAKA and Toyonori MATSUDA .....</i>	22
Diffractive Coupling of Localized Surface Plasmons in Quasi-Periodic Structures of Gold Nanospheres <i>Yasuhiro Kuranaga, Toyonori Matsuda and Mitsunori KAWANO .....</i>	26
Plasmon resonance absorption in a metal grating with a thin dielectric overcoating <i>Kengo KIYOTA and Toyonori MATSUDA .....</i>	30
Accuracy of TDR Measurement on Non-uniform Transmission Line <i>Naru HIRATA, Takuto OGATA and Yoshifumi SHIMOSHIO .....</i>	34
Detection of Partial Disconnection of Cable for Electrocardiography Monitor <i>Yuya YOSHIMURA and Yoshifumi SHIMOSHIO .....</i>	38
Equivalent Circuit Simulation of Variable Frequency Surface Acoustic Wave Resonator <i>Miyabi TANAKA and Hiroyuki ODAGAWA .....</i>	40
Research and design of short distance interactive RGB LED matrix blocks <i>LE Manh Hien, TRAN Duc Nam and NGUYEN Trung Hieu .....</i>	44
Led modules design using Binary Code Modulation (BCM) <i>NGUYEN Van Huy, NGUYEN Van Quan and VU Kha Khoi .....</i>	48
Measurement of Resistance and Internal Inductance of Wide Iron Plate <i>Takuto OGATA, Naru HIRATA and Yosifumi SHIMOSHIO .....</i>	52

Development of Simple and Low-cost Weeding Robot <i>Tsubasa MURAKAMI and Yoshifumi SHIMOSHIO</i> .....	56
Investigation of beta-gallium oxide phase transition temperature on sapphire substrates <i>Hiroshi OGATA, Hiroki ISHIMOTO, Shinichiro KOBA, Isao TSUNODA and Kenichiro TAKAKURA</i> .....	58
Development of evaluation method of the rubber vulcanization reaction by electrical current measurement <i>Jumpei YOSHIMATSU, Toyohiko GONDOH and Yasuyuki HIRAKAWA</i> .....	61
Properties of Sn-S thin films prepared by sulfurization <i>Kazuya IWASAKI, Shigeyuki NAKAMURA and Yoji AKAKI</i> .....	64
An Application of Embedded Programming and Electronics: A Field Research and Navigation Mobile Robot <i>TA Quyen, TA Vu, TRAN Nga, NGUYEN Mai, NGUYEN Chinh and NGUYEN Linh</i> .....	67
Miniaturized Notch antenna using capacitor <i>VU Viet Hoang, LE Cong Tuan and NGUYEN Viet Duc</i> .....	70
SmartFarm System - Environmental Monitoring and Device Management using Web browser <i>NGUYEN Tuan Anh</i> .....	73
Research and design of a short range wireless data transmitting device using sensor circuit <i>TRAN Duc Nam and NGUYEN Trung Hieu</i> .....	76
Research and manufacture health monitoring device using ZigBee wireless technology <i>HOANG The Viet and VU Kha Khoi</i> .....	80
Characteristics of UNCD/a-C:H Film Diodes for the Device Application <i>Kyosuke ONAGA and Chianami KANESHIRO</i> .....	84
Propagation Characteristics of SAW with Various Periodic Arrays <i>Taisei SAKAI and Chinami KANESHIRO</i> .....	88
Development of Sensor Network with Growth Rate Sensor for Agricultural Field <i>Sho YOSHIDA and Yoshihumi SHIMOSHIO</i> .....	92
Precise Positioning Measurement Using the Quasi-Zenith Satellite System (QZSS): an Influence of Positioning Environment Gives to Accuracy <i>Rei FUKUSHIMA and Shoichi TANIFUJI</i> .....	96

## **Conference session on Computer Science and Information Technology**

..... 100

Mobile Malware: Attacks and Defense <i>NGO Van Quyen and NGUYEN Xuan Thang</i> .....	101
A discussion of information systems analysis and design <i>LE Trong Tan and NGUYEN Xuan Thang</i> .....	105
The Golden Rules of User Interface Design <i>LE Duc Binh, NGUYEN Thi Mai and TRINH Bao Ngoc</i> .....	109
How Encapsulating Security Payload (ESP) protect your data <i>TRAN Quang Du and HOANG Thi Minh Ngoc</i> .....	115
A discussion of a Snake game implementation <i>NGUYEN Thi Thao and TRAN Nguyen Khanh</i> .....	120
Solving Notifying General News To Hanoi University Pupils – Hanu News Android Application <i>CHU Huu Thanh and NGUYEN Van Cong</i> .....	123
Social Network Analysis <i>NGUYEN Viet Anh, NGUYEN Phan Hung, DANG Thai Hoang and DO Thi Phuong Thao</i> .....	126
Tic-Tac-Toe Game and Artificial Intelligence <i>VU Anh Duc, PHAN San Thanh and TA Quang Hung</i> .....	129
Application of Game theory in Project Management <i>PHAM Thanh Trung, NGUYEN Minh Quan and VU Minh Tuan</i> .....	132
Multi-objective Optimization using Game Theory and Genetic Algorithm <i>DO Minh Thu, NGUYEN Minh Hoai and TRINH Bao Ngoc</i> .....	135
Multi-purpose artificial intelligent assistant humanoid graphical interface and AI approach to advanced human computer interaction <i>MAI Nguyen Binh Hung, LE Ngoc Hoa, BUI Trong Nam and BUI Minh Ngoc</i> .....	139
"Smart Monkey" Android Game <i>NGUYEN Van Manh, LUU Ngoc Diep, DO Tram Anh, TA Quang Tu, NGUYEN Viet Hung and NGUYEN Duc Minh</i> .....	144
Intelligent information system apply for healthcare system in Vietnam <i>HOANG Trung Hieu, TRAN Van Doanh and VU Minh Tuan</i> .....	147
Robotics for healthcare <i>TRAN Thi Giang, NGUYEN Thao Quyen and TRINH Bao Ngoc</i> .....	151

The Guidelines for Increasing Conversion Rates for Ecommerce Websites <i>BUI Thi Ngan, LE Thu Trang and NGUYEN Van Cong</i> .....	154
Lecture Archive System Using Web Camera <i>Yuki TSUTSUURA and Yoshifumi SHIMOSHIO</i> .....	158
Redundancy reduction using sparse representation for multi-view images of a light field camera <i>Taichi SUMI and Yoshimitsu KUROKI</i> .....	161
<b>Conference session on Architecture, Mechanical, Chemical, Biotechnology and Mathematic .....</b>	<b>164</b>
Experimental Study on Sliding Base-Isolator with Thermal Sprayed Molybdenum in Case of Change the Surface Roughness <i>Maiko BABA and Satoko ONO</i> .....	165
Effects of Cyclic Loading on Brittle Fracture in Notched Specimens <i>Tatsuya IKEDA and Tsutomu IWASHITA</i> .....	169
Study on “Skeletonics” in Cultural Festival <i>Kohei KAWAGOE, Hiroyuki SHIRAIWA, Natsuki TAKAGI and Akihiro TAKAHASHI</i> .....	173
Fatigue Property of Plasma Coating Film as Resistance to Hydrogen Entry and Hydrogen Embrittlement <i>Kazuki KOJIMA, Hiroshi NISHIGUCHI and Takayuki FUKUDA</i> .....	177
Study of the Adhesive Strength for Single Lap Joints in Consideration of Surface Properties <i>Keita OTA and Genji HOTTA</i> .....	179
Charpy Impact Property on Wrought Magnesium Alloy at Cryogenic Temperature <i>Kenta HATANAKA, Akihiro TAKAHASHI, Naoyuki YAMAMOTO, Hiromi MIURA, Masakazu KOBAYASHI and Yasuhiro NAKIYAMA</i> .....	182
Synthesis and Characterization of Novel Aromatic Polymer with Benzoxazine Functionality <i>Mizuki OTSUKA and Nobuyuki FURUKAWA</i> .....	186
Effect of Lactic acid bacteria on Awamori spirits quality <i>Shoya ARAKAWA, Masato MIYAHIRA, Shinya IKEMATSU, Makoto MIYAGI and Yasutomo TAMAKI</i> .....	188
On the study of the infinite decimal <i>Koki MURAOKA and Jo IDE</i> .....	192





**CONFERENCE SESSION ON**  
**COMMUNICATION AND ELECTRONIC**  
**ENGINEERING**



# Preparation of multilayer thin film for filtering specific light as magneto-optics devices

Sohsuke YAMADA<sup>1</sup>, Tamiko OHSHIMA<sup>2</sup>, Takeshi IHARA<sup>3</sup>, Yoshihito YAGYU<sup>4</sup>, Hiroharu KAWASAKI<sup>5</sup>, and Yoshiaki SUDA<sup>6</sup>

<sup>1</sup> Student, Advanced Course of Electrical Electronic Eng., National Institute of Technology, Sasebo College  
(1-1 Okishin, Sasebo, Nagasaki 857-1193, Japan)  
E-mail:ee1521@st.sasebo.ac.jp

<sup>2</sup> Associate Professor, Dept. of Electrical and Electronic Eng., National Institute of Technology, Sasebo College  
(1-1 Okishin, Sasebo, Nagasaki 857-1193, Japan)  
E-mail:ohshima@sasebo.ac.jp

<sup>3</sup> Assistant Professor, Dept. of Electrical and Electronic Eng., National Institute of Technology, Sasebo College  
(1-1 Okishin, Sasebo, Nagasaki 857-1193, Japan)  
E-mail:ihara@sasebo.ac.jp

<sup>4</sup> Associate Professor, Dept. of Electrical and Electronic Eng., National Institute of Technology, Sasebo College  
(1-1 Okishin, Sasebo, Nagasaki 857-1193, Japan)  
E-mail:yyagyu@sasebo.ac.jp

<sup>5</sup> Professor, Dept. of Electrical and Electronic Eng., National Institute of Technology, Sasebo College  
(1-1 Okishin, Sasebo, Nagasaki 857-1193, Japan)  
E-mail:h-kawasa@sasebo.ac.jp

<sup>6</sup> Professor, Dept. of Electrical and Electronic Eng., National Institute of Technology, Sasebo College  
(1-1 Okishin, Sasebo, Nagasaki 857-1193, Japan)  
E-mail:y-suda@sasebo.ac.jp

$[Er_2O_3/TiO_2]^6/[Er_2O_3]^2/[TiO_2/Er_2O_3]^6$  dielectric multilayer film was deposited on a glass substrate by a sputtering deposition method using  $Er_2O_3$  and  $TiO_2$  targets. We prepared the thin films at various conditions such as a radio frequency (RF) power,  $Ar/O_2$  gas flow rate, and a substrate temperature. Experimental results suggest that the crystallinity of these prepared films strongly depends on the substrate temperature, and the optical transmittance is shown 68% at the center wavelength of 490 nm.

## 1. Introduction

Unique optical properties of rare earth (RE) had been known since 1906 after the observation of sharp absorption lines in the spectrum of RE salts [1]. Nonetheless, they had been globally commoditized only in the late 1990s when the commercialization of Erbium(Er)-all-optical amplifiers boosted the telecommunication industry. Nowadays, Er doped fiber amplifiers (EDFAs) dominate in commercial systems providing efficient gain for wavelength division multiplexed (WDM) signal transmission in both C (1530–1565 nm) and L (1565–1625 nm) bands.

On the other hands,  $TiO_2$  is a unique material in view of its versatile properties which comprise high refractive index, wide band gap, and the resistance to chemical and physical impacts. This results in high applicability of  $TiO_2$  being an enabling material for manufacturing various stratified media, viz. antireflection coatings, optical waveguides, photonic crystals, and devices based on met-

al/ferroelectric/insulator/semiconductor structures, etc. The fertility of  $TiO_2$  thin films in the sphere of these applications is dictated by the demand for the highest refractive index  $n$ , lowest absorption coefficient  $\alpha$  and smoothest surface. This is feasible by employing several physical deposition techniques electron beam evaporation, pulsed bias arc ion plating, off-plane filtered cathodic vacuum arc, etc. In the case of multilayered structure preparation, the most adequate deposition techniques are magnetron sputtering and pulsed laser deposition (PLD) as they allow precise layer thickness control and preservation of stoichiometry during target-to-substrate material transfer. However, the former encounters problems at times, i.e. rather low deposition rates for some oxide materials (e.g.  $Er_2O_3$ ) and deficient stoichiometry (e.g. while depositing multicomponent films).

Sputtering deposition is a vapor deposition method for depositing thin films onto a substrate

using materials sputtered from a bulk target by means of the bombardment of energetic ions. The method suitable for preparation of large-area uniform amorphous and crystalline thin films for applications such as solar cells, liquid panel displays, and photocatalysts. The method's versatility has allowed the deposition of numerous types of functional thin films such as tungsten carbide, silicon carbide, chromium carbide, titanium carbide, cubic boron nitride, carbon nitride, and silicon nitride.

In this study, dielectric multilayer of  $\text{Er}_2\text{O}_3$  and  $\text{TiO}_2$  were prepared using sputtering deposition methods, and investigated the properties of the films. Especially, dielectric multilayer film, structured  $[\text{Er}_2\text{O}_3/\text{TiO}_2]^6/[\text{Er}_2\text{O}_3]^2/[\text{TiO}_2/\text{Er}_2\text{O}_3]^6$ , was prepared, and studied the property as optical magnetic films.

## 2. Experimental

Thin film fabrication was performed by conventional RF plasma deposition system, not shown here. In this experiment,  $\text{Er}_2\text{O}_3$  and  $\text{TiO}_2$  metal bulk targets were used. The purities of the powder targets were at least as high as 99.5%. The reaction chamber was evacuated to 1 Pa using a rotary pump and then to a base pressure of  $4 \times 10^{-4}$  Pa using a turbomolecular pump and rotary pump. The total deposition pressure ( $P$ ) was 0.5 Pa, and the input gas consisted of a mixture of oxygen (99.99%) and argon (99.99%) at a flow rate of 10 sccm. An RF magnetron plasma was generated at a frequency of 13.56 MHz and 30–100 W discharge RF power ( $P_{rf}$ ). Si(100) substrates were located 5.0 cm from the target. The substrates were cleaned by repeated bathing in an ultrasonic agitator and then rinsed in high-purity deionized water prior to loading into the deposition chamber. The deposition time was fixed at 120 min, the substrate temperature ( $T_s$ ) was increased from room temperature to 700 °C, and the gas mixture was varied from Ar: $\text{O}_2$  = 95:5. The deposition conditions are listed in Table 1.

The surface morphology of the films was observed using atomic force microscopy (AFM; JEOL JSPM4210). Film thickness was measured using an  $\alpha$ -step surface profiler (Kosaka Laboratory Surf-corder ET4000A). The thin film qualities were characterized by X-ray photoelectron spectroscopy (XRD; Rigaku RINT2100V) using  $\text{CuK}\alpha$  radiation

**Table 1** Deposition parameter and Deposition time per layer.

Material	$\text{Er}_2\text{O}_3$	$\text{TiO}_2$
Ar: $\text{O}_2$ ratio [sccm]	95:5	95:5
RF power [W]	200	200
Temperature [°C]	R.T.	R.T.
Pressure [Pa]	0.5	0.5
Time [s]	4816	6918

and X-ray photoelectron spectroscopy (XPS; JEOL JPS9010). Although it is not discussed in this report, all the observed thin film qualities were consistent independent of the target.

## 3. Results and discussion

We prepared the thin films at various conditions such as a radio frequency (RF) power, Ar: $\text{O}_2$  gas flow rate, and a substrate temperature. Fig.1 shows the crystallinity of the  $\text{Er}_2\text{O}_3$  film prepared by this method at room temperature measured by XRD. Fig. 2 also shows the crystallinity of the  $\text{Er}_2\text{O}_3$  film prepared by this method at substrate temperature 400°C. As the results, crystallinity of the film strongly depends on the substrate temperature.

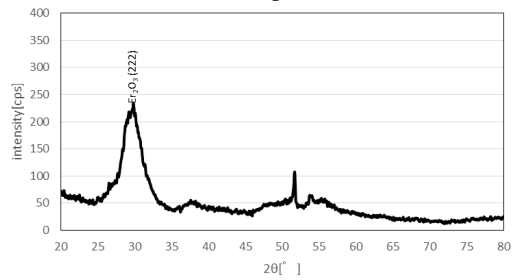


**Fig. 1** Crystallinity of the  $\text{Er}_2\text{O}_3$  film prepared by this method at room temperature.

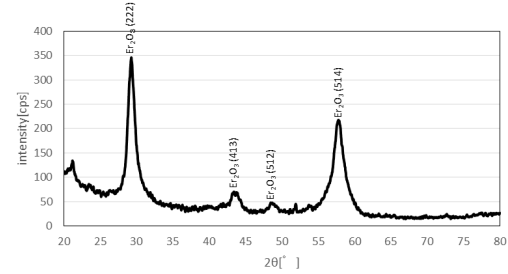


**Fig.2** Crystallinity of the  $\text{Er}_2\text{O}_3$  film prepared by this method at substrate temperature of 400°C.

Fig.3 shows the transmission spectra of the prepared multilayer film. In this research, wavelength of 200–1100 nm wavelength light was measured by UV-Vis-IR spectrometer. The highest transmittance is observed at 490 nm and 68%. And cut-off area's transmittance is about 10–20%. Ideal highest transmittance is more than 80% and cut-off area's transmittance is less than 10%.

Prepared multilayer film thickness was 1480 nm and 4.3%, and it is smaller than comparison ideal thickness 1529 nm.

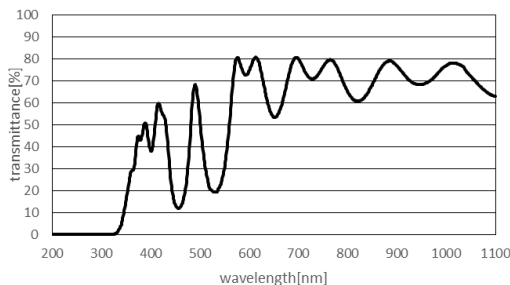


**Fig.3** The optical transmittance of prepared  $[Er_2O_3/TiO_2]^6/[Er_2O_3]^2/[TiO_2/Er_2O_3]^6$  dielectric multilayer.

#### 4. Conclusion

$[Er_2O_3/TiO_2]^6/[Er_2O_3]^2/[TiO_2/Er_2O_3]^6$  dielectric

multilayer film was deposited by prepared by a sputtering deposition method on a glass substrate using  $Er_2O_3$  and  $TiO_2$  targets. Experimental results suggest that the crystallinity of these prepared films strongly depends on the substrate temperature, and the optical transmittance of 68% at the center wavelength of 490 nm. As the results, it is necessary to change temperature and improvement multilayer's crystalline.

#### REFERENCES

- 1) A. M. Grishin, S. I. Khartsev, and D. O. Dzibrou, Enhanced photoluminescence in  $[Er_2O_3/TiO_2]^m$  photonic crystals, *J. Appl. Phys.*, **105**, 113122 (2009).

# Introduction of Arduino to signal light detection of a plasmons resonance absorption sensor I – Measurement of Stokes parameter –

Yuki TANAKA<sup>1</sup>, Kazuhito UMEKI<sup>1</sup>, Toyonori MATSUDA<sup>1</sup>

Advanced Course of Electronics and Information Systems Engineering.,

National Institute of Technology, Kumamoto Colegge

(2659-2,Suya, koshi-city, kumamoto 861-1102, Japan)

E-mail:ae15y-tanaka@g.kumamoto-nct.ac.jp<sup>1</sup>

E-mail:ae14umeiki@g.kumamoto-nct.ac.jp<sup>2</sup>

E-mail:tmatsu@kumamoto-nct.ac.jp

Surface plasmons resonance (SPR) sensors consisting of periodic structure are one of optical sensors for detecting a small change in a refractive index. We measure Stokes parameter  $S_3$  of the reflected light from the SPR sensor as output signals. We propose a compact photo detecting circuit for the measurement of  $S_3$  where a few of typical optical devices and simple electronic parts besides Arduino are composed. The experimental result obtained by the proposed signal light detection is good agreement with that by a commercially available polarization analyzer, Polarimeter. We can expect that the proposed light signal detection with Arduino enables us to downsize, lighten and cost-reduce the SPR sensor.

**Key Words :** polarization , surface plasmons, refractive index, Arduino, Stokes parameter.

## 1. INTRODUCTION

The authors have developed a surface plasmon resonance (SPR) sensor where periodic structures are used as a sensor head [1]. The SPR sensor can measure a change in a refractive index of a dielectric sample such as liquids or gases with high accuracy. The SPR sensor, however, becomes large in size and expensive in price since a commercially available polarization analyzer has been used as a signal detection component. In this presentation, we propose a light detecting device in the SPR sensor that can be largely reduced in size, weight and cost in comparison with a commercially available polarization analyzer.

## 2. PERIODIC-STRUTURES TYPE SPR SENSOR AND MEASURING PRINCIPLE

Figure 1 shows a schematic of an SPR sensor consisting of periodic structures made with noble metal such as aluminum or gold. A laser diode light is incident on the periodic structures through a sample with the angle of incidence  $\theta$ . At the specific angle of incidence  $\theta = \theta_{sp}$ , referred to as the resonance angle, surface plasmons are excited on the periodic structures. The occurrence of the surface plasmons is observed from the polarization state of the reflected light.

We next describe the measuring principle of a refrac-

tive index change of a sample in the SPR sensor. Figure 2 shows the stokes parameter  $S_3$  of the reflected light as functions of  $\theta$ , which is called the resonance curve. The resonance curve, e.g., black one where a refractive index of a sample  $n$ , is linearly changed to negative from positive before and after the resonance angle  $\theta = \theta_{sp}$  at which  $S_3$  becomes zero. When the refractive index of the sample is changed to  $n + \Delta n$  from  $n$ , the resultant resonance curve, expressed by green one, shifts to the right by  $\Delta n$ . Consequently if the angle of incidence is fixed to be  $\theta = \theta_{sp}$ ,  $S_3$  is changed from 0 to  $\Delta S_3$  when the refractive index is changed from  $n$  to  $n + \Delta n$ . We therefore measure the Stokes parameter  $S_3$  of the reflected light from periodic structures provided that the angle of incidence is fixed to be  $\theta = \theta_{sp}$ . The measured  $S_3$  varies linearly in response to a small change in a refractive index of a sample.

As shown in Fig. 3 we have assembled an SPR sensor consisting of periodic structures where a commercially available polarization analyzer, Polarimeter made in Thorlabs Inc., are employed for the measurement of the Stokes parameter  $S_3$ . Polarimeter, which is shown in Fig. 4, consists of an optical head and controller and is expensive in price. We therefore propose a photo detecting device for measuring  $S_3$  of the reflected light from the SPR sensor.

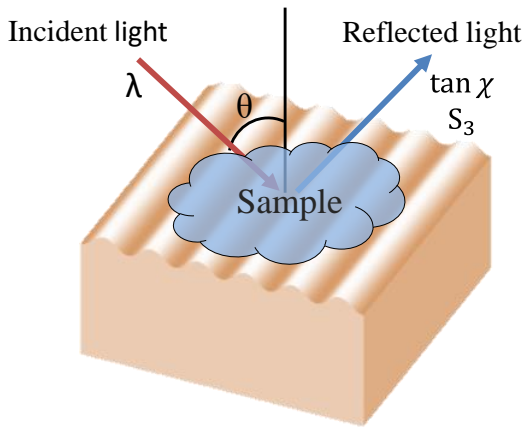


Fig.1 Principle of SPR-Sensor

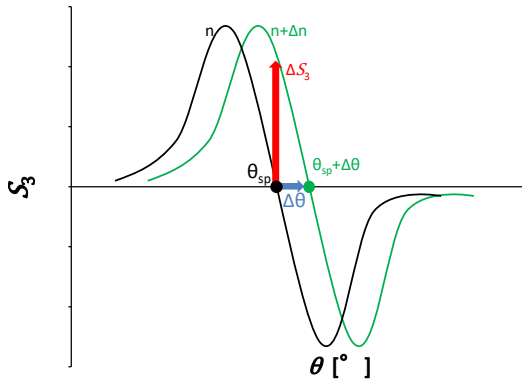


Fig.2 Resonance curve in the SPR sensor

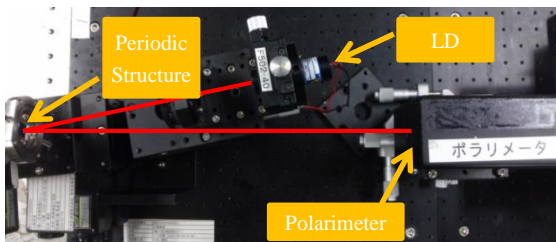


Fig.2 SPR sensor consisting of a Polarimeter



Fig.4 Polarimeter's head and control device

### 3. STOKES PARAMETOR $S_3$ AND ITS MEASUREMENT

We briefly describe Stokes parameters  $S_0, S_1, S_2$  and  $S_3$  that are used to express or measure the polarization state of light. In order to explain the parameters, let us consider light whose electric field is given as

$$\mathbf{E}^t = [E_x, E_y, E_z] = [A, B e^{j\delta}, 0] e^{j(\omega t - kz)}. \quad (1)$$

The light propagates along the z-direction and has an elliptical polarization based on the amplitude ratio  $\tan \alpha = B/A$  and the phase difference  $\delta$ . We focus on our attention to the parameter  $S_3$  because it is measured in the SPR sensor as stated above. The parameter  $S_3$  is defined as

$$S_3 = 2\sqrt{\langle A \rangle^2} \sqrt{\langle B \rangle^2} \sin \delta, \quad (2)$$

Where " $\langle \rangle$ " in formula represents the time average intensity of reflected light. Figure 5 shows the schematic diagram for measuring  $S_3$ . The incident light is transmitted through a quarter wavelength plate and a linear polarizer of the transmission angle  $\phi$ . The electric field of the transmitted light is given by

$$\mathbf{E}^o = \left( A \cos \phi + B e^{j(\delta + \frac{\pi}{2})} \sin \phi \right) \cdot [\cos \phi, \sin \phi, 0]$$

Thus, the intensity of the light is expressed by

$$I(\phi) = \langle A^2 \rangle (\cos \phi)^2 + \langle B^2 \rangle (\sin \phi)^2 - 2\sqrt{\langle A^2 \rangle} \sqrt{\langle B^2 \rangle} \sin 2\phi \sin(\delta) \quad (3)$$

The parameter  $S_3$  defined in Eq. (2) is obtained by the use of  $I(\phi)$  as follows:

$$S_3 = I(-\pi/4) - I(\pi/4) \quad (4)$$

In the actual measurement, we normalize the parameter by the intensity of the incident light. The normalized  $S_3$  is given by the equation

$$S_3 = \frac{I(-\pi/4) - I(\pi/4)}{I(-\pi/4) + I(\pi/4)} \quad (5)$$

Consequently we obtain the normalized  $S_3$  by measuring two quantities  $I(\pi/4)$  and  $I(-\pi/4)$  for the incident light and calculating Eq. (5).

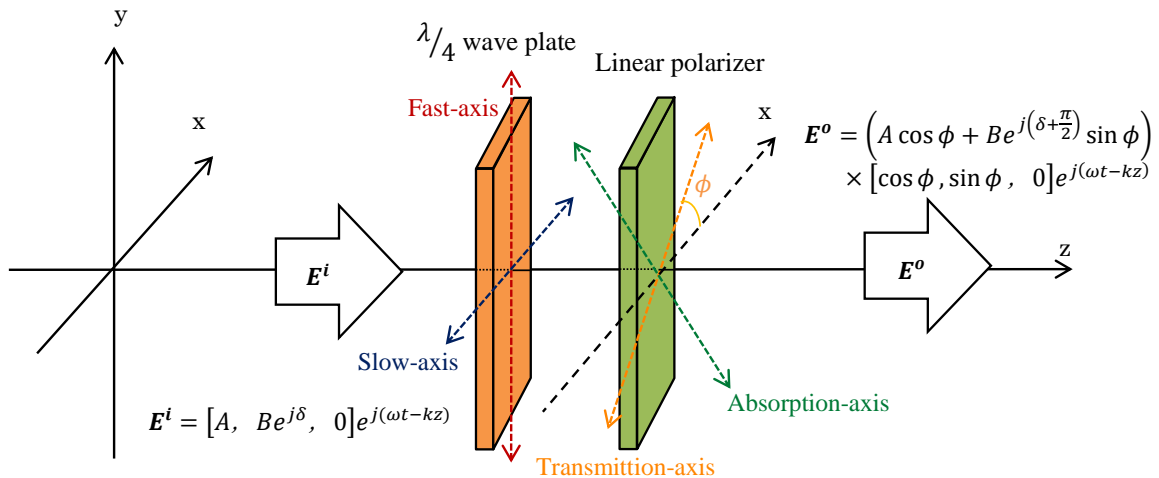


Fig.5 Construction of measurement

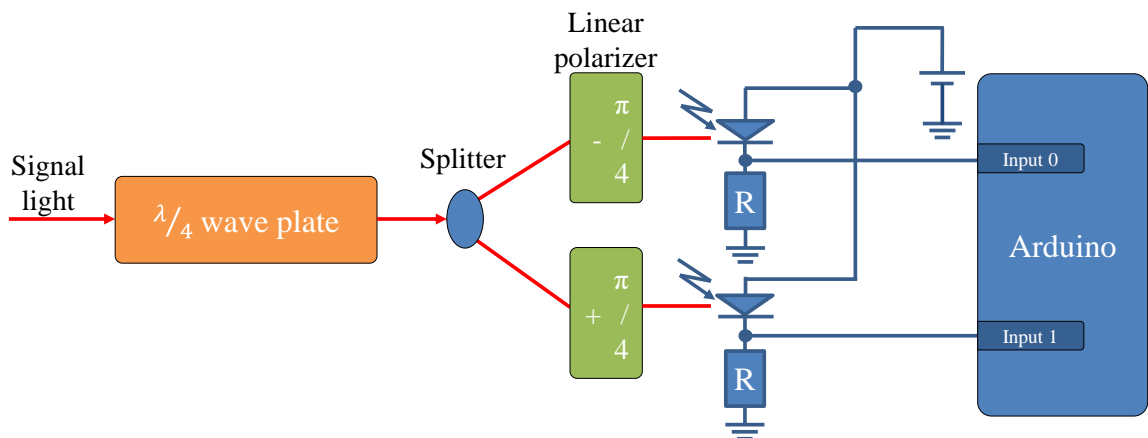


Fig.6 Block diagram of measurement device

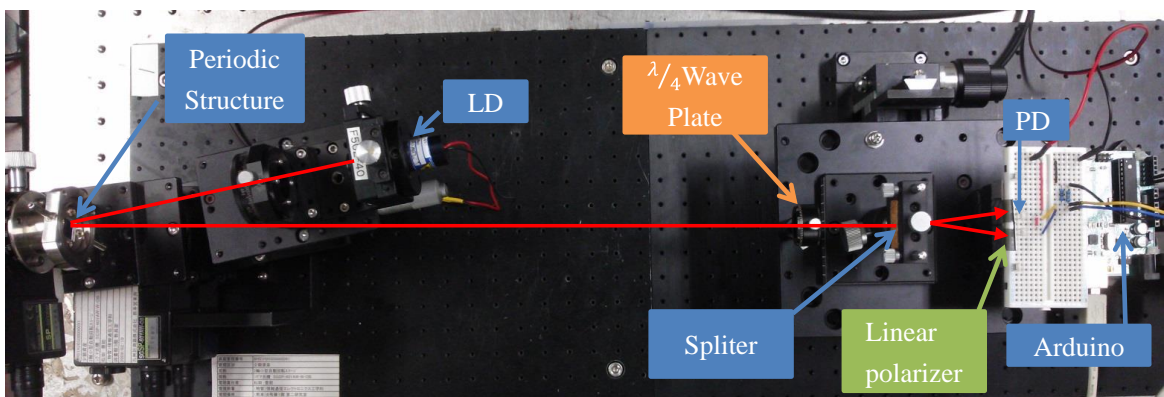


Fig.7 SPR sensor that uses proposed device

Figure 6 shows a schematic block diagram for measuring the normalized  $S_3$  of a reflected light from the SPR sensor. The reflected light is transmitted through quarter wavelength wave plate and then splits into two beams by a beam splitter. Each split beam light irradiates on a photo diode through linear polarizer of  $\phi = \pi/4$  or  $\phi = -\pi/4$ . The output of the photodiode, which corresponds to  $I(\pi/4)$  or  $I(-\pi/4)$ , is inputted into the analog terminal of Arduino which is connected to PC via a USB cable.

Figure 7 shows a light detecting device for measuring the normalized  $S_3$  of a reflected light from the SPR sensor that we assemble.

### 3. EXPERIMENTAL RESULTS AND DISCUSSIONS

Using the SPR sensor as shown in Fig. 7 we made an experiment on plasmon resonance absorption under the following conditions: periodic structures is a holographic aluminum grating, an incident light is an LD light of wavelength  $\lambda = 670\text{nm}$ , and a sample is air. In Fig. 8 we compare the resonance curve measured by Polarimeter with that obtained by the proposed device. From this figure we confirm the good agreement with both resonance curves. Table 1 illustrates the values of  $S_3$  by Polarimeter and that of the proposed device at several angle of incidence. The maximum error in  $S_3$  is within 4%. We thus confirm the validity of the proposed light detecting device from the experimental results.

### 5. CONCLUSION

We have proposed a detecting device for measuring the Stokes parameter  $S_3$  of the reflected light from the SPR sensor consisting of periodic structures. The detecting device can be largely reduced in size, weight and cost in comparison with a commercially available polarization analyzer. The validity of the proposed device experimentally demonstrates in comparison with Polarimeter. As the future work we are studying an application of the SPR sensor to a sensor network node through further simplifications.

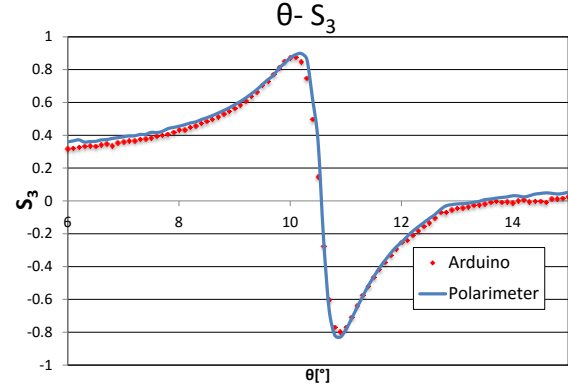


Fig.8 Comparison of the proposed method and Polarimeter

Table.1 The error in some point

$\theta [^\circ]$	S3		Error
	Polarimeter	Proposed	
6	0.360	0.320	-0.040
8	0.455	0.432	-0.023
10	0.871	0.874	0.003
12	-0.252	-0.243	0.009
14	0.031	0.004	-0.027

### Acknowledgments

This work was in part supported by JSPS KAKENHI Grant Number 15K00952.

### REFERENCES

- [1] T. Matsuda and H. Odagawa: US patent No. 8,976,360 SURFACE PLASMON SENSOR AND METHOD OF MEASURING REFRACTIVE INDEX .
- [2] C.F.Bohren and D.R.Huffman: Absorption and Scattering of Light by Small Particles, WILEY-VCH Verlag GmbH & Co.KgaA, Weinheim, 2004.
- [3] ThorLabs Inc. , Polarimeter System overview, [www.thorlabs.co.jp](http://www.thorlabs.co.jp), 2015.

# **Introduction of Arduino to signal light detection of a plasmons resonance absorption sensor II**

## **– Utilization to data transmission –**

Kazuhito UMEKI<sup>1</sup>, Yuuki TANAKA<sup>2</sup> and Toyonori MATSUDA<sup>3</sup>

<sup>1</sup> Student, Advanced Course of Civil Eng., National Institute of Technology,  
(Suya2659-2, Kohshi-shi, Kumamoto 861-1102, Japan)

E-mail:ae14umeki@g.kumamoto-nct.ac.jp

<sup>2</sup> Student, Advanced Course of Civil Eng., National Institute of Technology,  
(Suya2659-2, Kohshi-shi, Kumamoto 861-1102, Japan)

E-mail:ae15y-tanaka@g.kumamoto-nct.ac.jp

<sup>3</sup> Professor, Inst., Industrial Science, National Institute of Technology  
(Suya2659-2, Kohshi-shi, Kumamoto 861-1102, Japan)

E-mail:tmatsu@kumamoto-nct.ac.jp

We introduce a single-board microcontroller Arduino to the light signal detection component of the SPR sensor that we have developed. As a result, sensor outputs from the SPR sensor are measured by a simple photo detecting circuit and the light signal detection component is transmitted to PC with wired (USB) and wireless (Wi-Fi) communications. It is expected that the proposed light signal detecting with Arduino enables us to downsize, lighten and cost-reduce the SPR sensor.

**Key Words :** SPR sensor, sensor-network, Arduino, Wi-Fi communication

## **1. INTRODUCTION**

A wireless sensor network [1] has been actively studied in recent years due to the great potential to many industrial and consumer applications. A wireless sensor network consists of many nodes where each node is connected to one or a few sensors. The sensor network node is usually provided with the following components, a radio transceiver, a microcontroller, and a power source. It is therefore necessary to develop these functions included in the nodes in addition to sensing devices to construct a sensor network system

In this presentation we describe a basic study to apply a surface plasmon resonance (SPR) sensor [2] to a sensor network. An SPR sensor is one of optical sensors for detecting a small change in a refractive index of a dielectric sample such as liquids or gases. An SPR sensor has been put to practical use as a bio-sensor or a chemical sensor [2]. However, there are few applications of an SPR sensor to a sensor network. This is because most of commercially available SPR sensors are manufactured as precision equipment in a desktop type or a unit type. The usual SPR sensor, as it is, is not suitable for the application to a sensor network from viewpoints of both equipment component and cost.

The laboratory to which the author belongs has proposed an SPR sensor in which periodic structures instead of a prism are used as a sensor head [3]. The SPR sensor consisting of periodic structures can be assembled as a small-sized optical device. We introduce Arduino [4] to the light signal detection part of the SPR sensor so that it works as a sensor network node. The use of Arduino which is a single-board microcontroller realizes the functions included in a sensor network node, a radio transceiver, a microcontroller, and a power source. In the following sections, we first explain the SPR sensor consisting of periodic structures. We next introduce Arduino to a signal light detection part of the SPR sensor. We then connect Arduino to PC by wired (USB) and wireless (Wi-Fi) communications. We then make Graphical User Interface (GUI) on PC where measuring data are displayed and processed. We finally confirm data transmission of experimental results detected by the SPR sensor via USB and Wi-Fi communications.

## **2. SPR SENSOR CONSISTING OF PERIODIC STRUCTURES**

Figure 1 shows a schematic block diagram of an SPR sensor where periodic structures are over-coated on a glass substrate. The SPR sensor

detects a small change in a refractive index of a sample on periodic structures. A laser diode light is incident on the periodic structures through a sample. Surface plasmons are excited on the periodic structures at the specific angle of incidence  $\theta = \theta_{sp}$ , referred to as the resonance angle. The excitation of the surface plasmons in the SPR sensor consisting of periodic structures can be detected from the polarization state of the reflected light such as the ellipticity  $\tan \chi$  or Stokes parameter  $S_3$  that becomes to be zero at the resonance angle  $\theta_{sp}$ . In this presentation we adopt  $S_3$  as the parameter that detects the resonance angle. The excitation of surface plasmons depends strongly on the value of a refractive index of material on periodic structures. Stokes parameter  $S_3$  varies in response to the change in a refractive index of a sample when the angle of incidence is fixed at the resonance angle  $\theta = \theta_{sp}$ . Consequently, we can measure a refractive index change from the value of  $S_3$  of the reflected light in the SPR sensor.

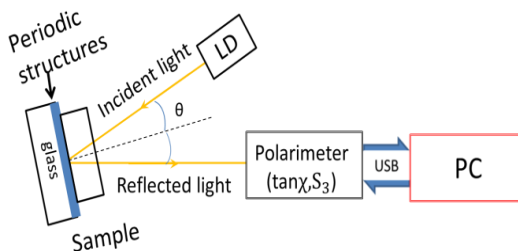


**Fig.1** SPR sensor consisting of periodic structures

We have employed a commercially available polarization analyzer, Polarimeter made in Thorlabs, Inc., for the measurement of Stokes parameter  $S_3$  in the SPR sensor. The polarization analyzer can measure all the parameters expressing polarization state of light with high accuracy. However, the use of the polarization analyzer is not suitable for the application of the SPR sensor to a sensor network because of its equipment component and cost.

To overcome such a problem, the authors proposed a signal light detecting device using Arduino in the SPR sensor consisting of periodic structures. The device is composed of two parts: One is a photo detecting circuit for detecting  $S_3$  of a reflected light from the SPR sensor; the other provides with the functions as a sensor network node, a radio transceiver, a microcontroller, and a

power source. As for the photo detecting circuit for the measurement of  $S_3$ , one of the authors presents in detail. In the following, data transmission using Arduino between a signal light detecting device and PC via wired and wireless connections is described.

### 3. DATA TRANSMISSION TO PC BY USB AND Wi-Fi CONNECTIONS

#### (a) Present apparatus

Figure 2 shows a schematic block diagram of the data transmission component that we propose in this presentation. Measuring data from a signal light detecting device are inputted into analog pins of Arduino. We transmit the measuring data inputted in Arduino to PC via wired USB and wireless Wi-Fi connections. We then make GUI with LABVIEW to display or process the measuring data  $S_3$  of the SPR sensor on PC.

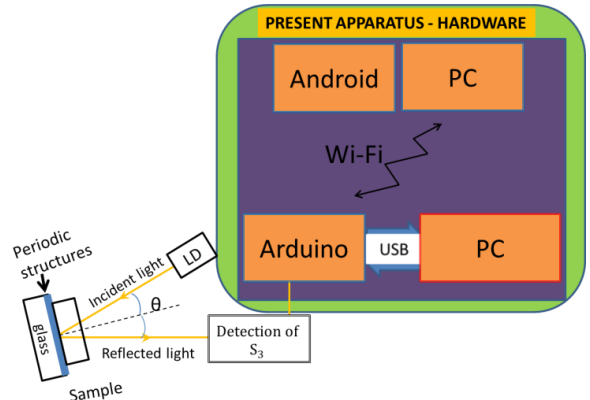


**Fig.2** Block diagram of present data transmission component in the SPR sensor

#### (b) USB connection

We connect Arduino to PC with a USB cable. Using the USB communication we perform the remote control of the angle of incidence  $\theta$  through the drive stage in a SPR sensor by means of LABVIEW on PC. The movement of the angle of incidence and the data acquisition of Stokes parameter  $S_3$  are synchronized on PC. Figure 3(a) shows the data transmission apparatus where a signal light detecting part of the SPR sensor is connected to a notebook PC with a USB cable. In the figure  $S_3$  is displayed on a display of the PC. In the figure a photograph of the data transmission apparatus with Wi-Fi communication is also included.

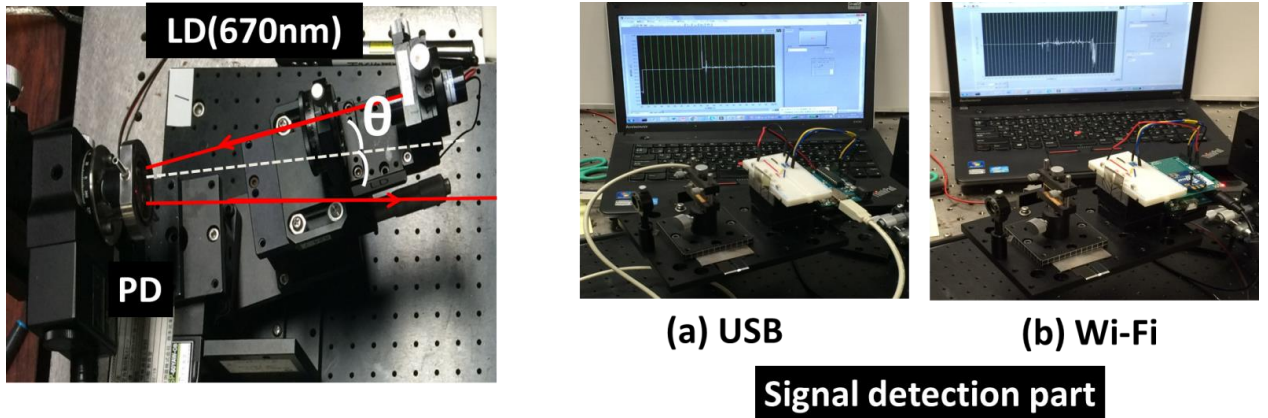


**Fig.3** Prototype circuit that a present SPR sensor of signal detection with Arduino using USB and Wi-Fi connection

#### (c) Wi-Fi connection

To expand the application of an SPR sensor, we need to provide data transmission by wireless communication with it. We adopt Wi-Fi (IEEE 802.11) that can connect to the Internet via a wireless LAN. Wi-Fi\_33 is available in many devices besides PC. In this study, we employ Arduino Wireless Proto Shield [5] and the XBee Wi-Fi(S6B) module [6]. Figure 4 shows a flowchart the implementation of data transmission between Arduino and PC with the Wi-Fi device.

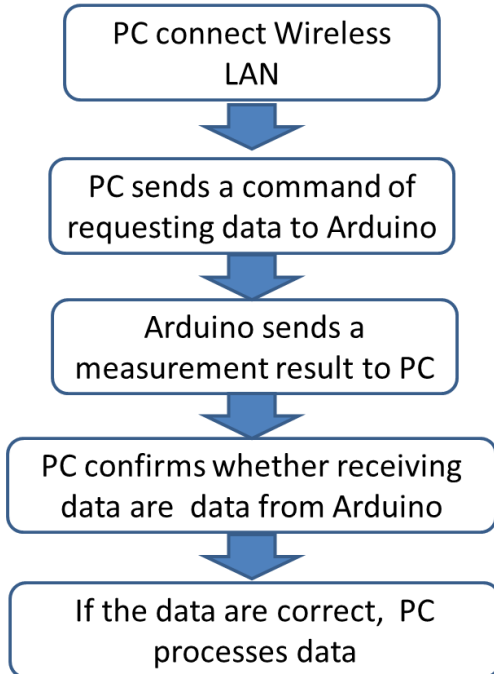


**Fig.4** Flowchart for data transmission between Arduino and PC with Wi-Fi communication.

## 4. EXPERIMENTAL RESULTS

#### (a) Confirmation of resonance curve

We made an experiment on the measurement of a refractive index change by three kinds of signal light detection in the SPR sensor, Polarimeter, Arduino with USB communication and one with WiFi. The experiments are made under the following condition: an incident light is a laser diode light beam of wavelength  $\lambda=670\text{nm}$  and intensity 1mW, and periodic structures are a holographic aluminum grating of period 556nm. We first fix the angle of incidence at the resonance angle,  $\theta = \theta_{sp}$ . The resonance angle is obtained as the zero cross of  $S_3$  in the resonance curve which is  $S_3$  as functions of  $\theta$ . Figure 5 shows the resonance curves obtained from three kinds of measurements stated above which are expressed as Polarimeter, USB and Wi-Fi on the figure. We confirm the good coincidence among them. From this figure we decide the resonance angle  $\theta_{sp}$ .

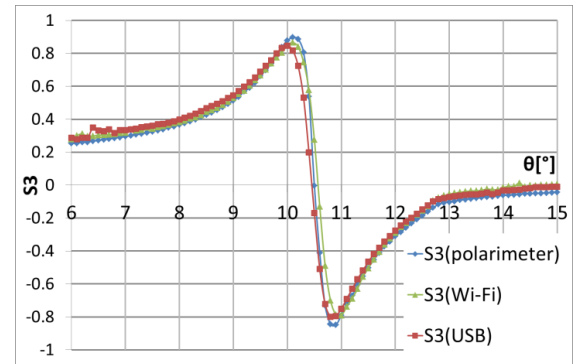


**Fig.5** Comparison of measurement result by USB with Wi-Fi and Polarimeter

#### (b) Time response of $S_3$

We next investigated the time response of  $S_3$  when the angle of incidence is fixed to be the resonance

angle  $\theta = \theta_{sp}$ . The time response, that is, the variation of  $S_3$  as function of time, represents the change in a refractive index of a sample. To make this experiment, we provide a chamber in which a holographic grating is placed. We inject three kinds of gases, air, hydrogen gas and carbon dioxide gas of 95 % concentration as the sample in the SPR sensor. Figure 6 shows the time response of  $S_3$  obtained by the three measurements (a) Polarimeter, (b) USB and (c) Wi-Fi. The experiments were made under the same condition: We filled air into the chamber for the first 30 seconds where  $S_3$  is nearly zero and then inject a hydrogen gas, air, and a carbon dioxide gas in sequence into the chamber. The measurement time is 60 seconds for each gas. We observe the detection of three kinds of  $H_2O$ , air, and  $CO_2$  for each measurement although the values of  $S_3$  for  $CO_2$  are different to each other.

## 5. CONCLUSION

We introduced Arduino to the light signal detection component of the SPR sensor that we have developed. We then connected Arduino to PC by USB and Wi-Fi communications. It is experimentally confirmed that the proposed signal light detection device with Arduino is available in the measurement of a refractive index change by the SPR sensor. It is expected that the proposed device enables us to downsize, lighten and cost-reduce the SPR sensor if we can improve the accuracy of data transmission in USB and Wi-Fi communications. The improvement of the data transmission is the research task from now on.

## REFERENCE

- [1] For examples,  
[https://en.wikipedia.org/wiki/Wireless\\_sensor\\_network](https://en.wikipedia.org/wiki/Wireless_sensor_network)
- [2] H.Raether : "Plasmons on surfaces of periodic profile", North-Holland Publishing Company, 1982, Surface Plasmons and Roughness, pp.384-393.
- [3] T. Matsuda and H. Odagawa: US patent No. 8,976,360 SURFACE PLASMON SENSOR AND METHOD OF MEASURING REFRACTIVE INDEX
- [4] Arduino – Home <http://www.arduino.cc/>
- [5] ARDUINO - Wireless Proto Shield  
<https://www.arduino.cc/en/Main/ArduinoWirelessProtoShield>
- [6] XBee Wi-Fi – DIGI  
<http://www.digi.com/products/xbee-rf-solutions/module/xbee-Wi-Fi?tab=productdocs&pid=5585>

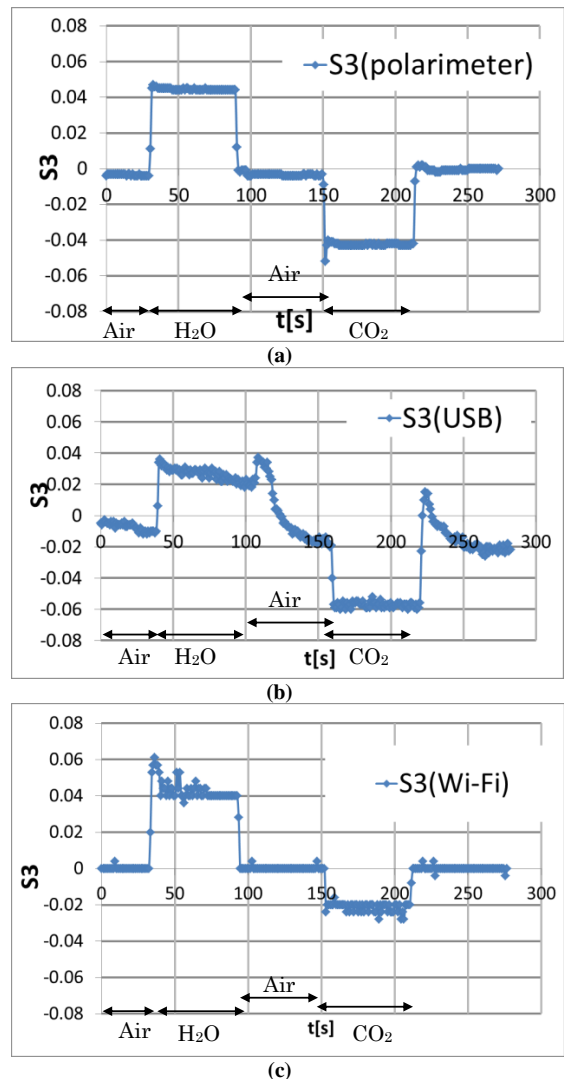


**Fig.6** Time response of  $S_3$

## Acknowledgments

This work was in part supported by JSPS KAKENHI Grant Number 15K00952.

# Diffractive Coupling of Localized Surface Plasmons in Quasi-Periodic Structures of Gold Nanospheres

Yasuhiro Kuranaga<sup>1</sup>, Toyonori Matsuda<sup>1</sup> and Mitsunori Kawano<sup>2</sup>

<sup>1</sup> Advanced Course of Electronics and Information Systems Eng.,

National Institute of Technology, Kumamoto College  
(Suya 2659-2, Koshi-shi, Kumamoto 861-1102, Japan)

E-mail:ae15kuranaga@g.kumamoto-nct.ac.jp

<sup>2</sup>Lumerical Solutions Inc. , Vancouver, British Columbia, Canada

The optical properties of periodic arrangement of finite gold nanospheres have been investigated in connection to localized surface plasmons (LSPs) by the computer simulation based on Generalized Multipole Technique. As a result, it is demonstrated that the LSPs excited on the nanospheres couple with each other and the resultant scattered field propagates along the row of nanospheres when the polarization of incident light is perpendicular to the nanosphere row. The coupling effect of LSPs results from the periodicity of the periodic arrangement of finite gold nanospheres.

**Key Words :** gold nanospheres, Localized Surface Plasmon, Generalized Multipole Technique

## 1. INTRODUCTION

Scattering and absorption of light from metal nanoparticles has been intensively studied due to the interesting property of localized surface plasmons (LSPs) [1,2] which are collective electron charge oscillations in a metallic nanoparticle. Many types of geometry including a single nanoparticle, clusters of nanoparticles, and 1D- or 2D-arrays of nanoparticles have been analyzed so far to study the interesting properties of LSPs.

One- or two-dimensional periodic structures of metal nanoparticles are attractive structures because they exhibit extremely narrow collective plasmon resonances (CPRs) [3] that are observed as remarkably sharp peaks in extinction spectra. The CPRs are associated with coherent coupling of LSPs through a diffracted mode generated by periodic structures consisting of nanoparticles. Most of theoretical studies on CPRs have dealt with 1D- or 2D- infinite periodic structures in which an infinite number of metal particles are placed at equally spaced positions along a line or on a plane.

On the other hand, quasi-periodic structures comprising finite number of nanoparticles are also of interest. In this paper we numerically investigate diffractive coupling of LSPs in 1D- or 2D-quasi-periodic structures of gold nanoparticles. We employ Generalized Multipole Technique (GMT) [4] for analyzing optical properties of quasi-periodic structures of gold nanoparticles. The results presented here facilitate our clear understanding of the mechanism of diffraction coupling of LSPs in nanoparticles.

## 2. NUMERICAL ALGORITHM OF GMT

In this section we simply explain the method for numerical analysis of optical properties of quasi-periodic structures comprising metal nanoparticles.

Figure 1 shows a coordinate system O-xyz and an aggregate of noble metal nanoparticles embedded in a homogeneous material V. The number of particles is  $L$  and each particle is numbered from  $\ell=1$  to  $L$ . A monochromatic plane wave with the wave vector  $\mathbf{k}^{\text{in}}$  is incident on an aggregate of metal nanoparticles. We denote by  $\mathbf{E}^{\text{sc}}$  the scattered electric field in V.

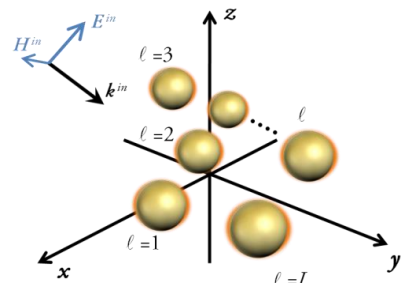


**Fig. 1** Coordinate system and an aggregate of metal nanoparticles.

In the numerical algorithm of the GMT, the approximate scattered electric field are expressed as

$$\mathbf{E}_N^{\text{sc}}(\mathbf{r}) = \sum_{\ell=1}^L \mathbf{E}_{\ell N}^{\text{sc}}(\mathbf{r}_\ell), \quad (1)$$

where  $\mathbf{E}_{\ell N}^{\text{sc}}(\mathbf{r}_\ell)$  is the scattered electric field from the  $\ell$ -th particle and is formed by

$$\mathbf{E}_{\ell N}^{\text{sc}}(\mathbf{r}_\ell) = \sum_{n=1}^N \sum_{m=-n}^n \left\{ a_{nm}^\ell(N) \mathbf{m}_{nm}^{(4)}(k\mathbf{r}_\ell) + b_{nm}^\ell(N) \mathbf{n}_{nm}^{(4)}(k\mathbf{r}_\ell) \right\} \quad (\ell = 1, 2, \dots, L) \quad (2)$$

Here,  $a_{nm}^0$  and  $b_{nm}^0$  are the expansion coefficients and  $\mathbf{m}_{nm}^{(4)}$  and  $\mathbf{n}_{nm}^{(4)}$  are the Hankel function-based spherical vector waves functions [2]. The unknown expansion coefficients are determined so that the scattered field satisfies the boundary condition.

To investigate the LSPs we evaluate the extinction efficiency  $Q_{\text{ext}}$  that is defined as the ratio of the sum of the extinction cross section and the geometrical cross section. We also show the electric field distributions when LSPs are excited in quasi-periodic structures of nanoparticles.

### 3. LSPs in QUASI-PERIODIC STRUCTURES

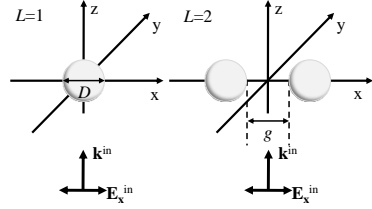
In the numerical examples presented here, all the nanoparticles are gold nanospheres with a diameter  $D=120\text{nm}$  and are assumed to be embedded in vacuum.

#### 3-1. LSPs excited on gold nanospheres

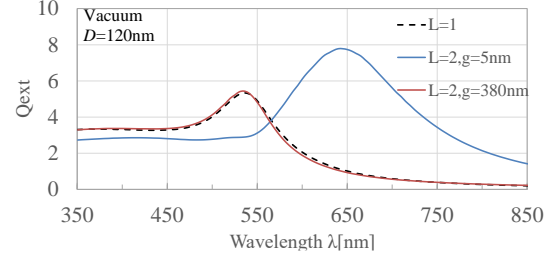
Before describing the LSPs in quasi-periodic structures we show the LSPs in a single gold nanosphere and two gold nanospheres with space  $g$  placed on the x-axis as shown in Fig. 2. The incident light of wavelength  $\lambda$  is illuminated from the negative direction of the z-axis. The incident light is polarized in the x-axis direction.

Figure 3 illustrates the extinction efficiency  $Q_{\text{ext}}$  for two gold nanospheres ( $L=2$ ) as functions of wavelength  $\lambda$  in the visible region. The extinction efficiency  $Q_{\text{ext}}$  of a gold nanosphere ( $L=1$ ) increases at the wavelength  $\lambda=535\text{nm}$  at which LSPs are excited. The extinction efficiency spectrum of two nanospheres with space  $g=380\text{nm}$  is almost agreement with that of a single nanosphere ( $L=1$ ). However, when the space is small  $g=5\text{nm}$ , the resonance wavelength exhibits redshift and the extinction efficiency increases compared with the case of a single nanosphere. This is because the LSPs of two nanoparticles interfere with each other.

Figure 4 shows the electric field distributions on the xy plane at the resonance wavelength: (a)  $\lambda=535\text{nm}$  for  $L=1$ , (b)  $\lambda=535\text{nm}$  for  $L=2$  of  $g=380\text{nm}$  and (c)  $\lambda=640\text{nm}$  for  $L=2$  of  $g=5\text{nm}$ . We observe the electric field distributions of LSPs excited on a single nanosphere from Fig. 3(a): Electric fields near the particle surface are enhanced and the enhancement quickly decays with distance from the surface. Figure 3(b) shows that there is no interaction between the LSPs of two nanospheres with the space  $g=380\text{nm}$ . Figure 3(c), however demonstrates the interference of the LSPs excited on each nanosphere when the two nanospheres are closely located and the resultant electric field is remarkably enhanced at the center of gap between particles.



**Fig. 2** A single gold nanoparticle and two gold nanoparticles.



**Fig. 3** Extinction efficiency spectra of a single gold nanoparticle and two gold nanoparticles.

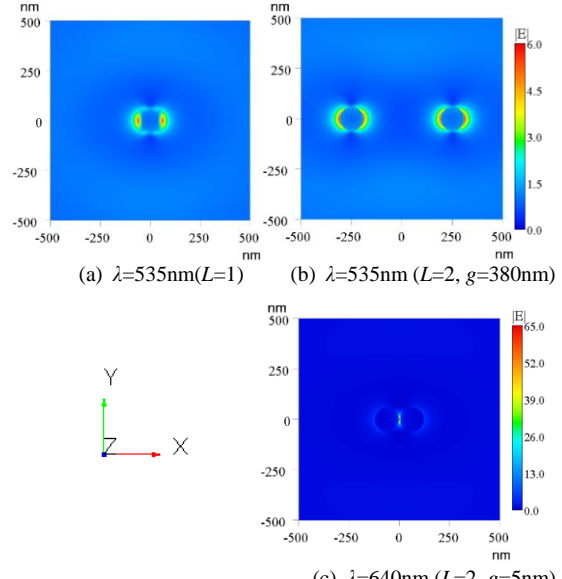


**Fig. 4** Electric field distributions of LSPs.

#### 3-2. LSPs of 1D-quasi-periodic structures

As shown in Fig. 5, we consider quasi-periodic structures where  $L$  nanospheres are placed at equally spaced positions along the x-axis. The incident light is irradiated from the negative direction of the z-axis.

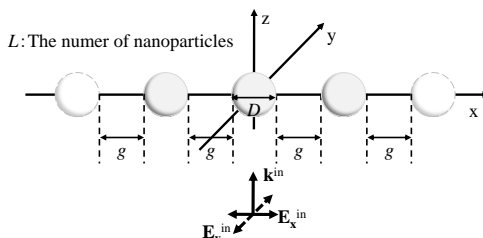


**Fig. 5** 1D- quasi-periodic structures

### (1) Influence of polarization of incident light

We first investigate the influence of the polarization of the incident light on the diffraction coupling of LSPs in the 1D quasi-periodic structures. Figure 6 shows the extinction efficiency spectra of the aggregate of  $L=3$  gold nanospheres when the polarization of the incident light is the x- or y-directions. The extinction efficiency spectrum for the x-polarized incident light is almost agreement with that of a single nanosphere. Redshift in the resonance wavelength and increment of  $Q_{\text{ext}}$  however occurs in the y-polarized incidence while the  $Q_{\text{ext}}$  for the x-polarized incidence is almost same as that of a single nanosphere. We therefore expect that the diffractive coupling of LSPs is remarkable when the polarization of the incident light is perpendicular to the row of nanospheres.

This is confirmed from the electric field distributions near the nanospheres when LSPs are excited. Figure 7 illustrates the electric field distributions of the  $L=3$  gold nanospheres aggregate at the resonance wavelength (a)  $\lambda=535\text{nm}$  and (b)  $\lambda=540\text{nm}$ , respectively, for the x- and y-polarization. From the electric field distributions we observe the scattered electric fields associated with the interference of the excited LSPs on each nanosphere: The scattered electric field based on LSPs propagates along the x direction and the strong interference occurs in the xz plane for the y-polarized incidence. We therefore focus our attention to the incident light polarized in the direction perpendicular to the row of nanospheres hereafter.

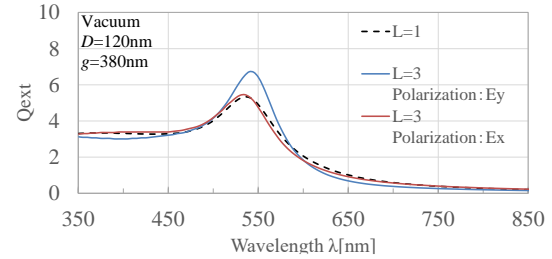


Fig. 6 Extinction efficiency spectra of  $L=3$  gold nanospheres.

### (2) Influence of the number of nanospheres

Next we investigate the influence of the number of nanospheres on the diffraction coupling of LSPs in the 1D quasi-periodic structures. Figure 9 shows the extinction efficiency spectra for the aggregates comprising various gold nanospheres  $L=1, 3, 5, 9, 25$ . The value of  $Q_{\text{ext}}$  increases and the width of the LSP resonance becomes narrower when the number of nanospheres increases. This demonstrates that the quality factor of the LSP resonance increases with the number of nanospheres. We further observe the change in the extinction efficiency spectrum for the  $L=25$  nanospheres near the wavelength  $\lambda=500\text{nm}$ . We therefore suppose that the effect by the nature of periodic structures appears at the wavelength 500nm that is equivalent to the interval of neighbouring nanospheres.

Figure 8 illustrates the electric field distributions of the  $L=9$  gold nanospheres aggregate at  $\lambda=540\text{nm}$  for the y-polarization incidence. We observe the enhancement of the electric field near the nanospheres aggregate in comparison with the  $L=3$  aggregate of Fig. 7(b).

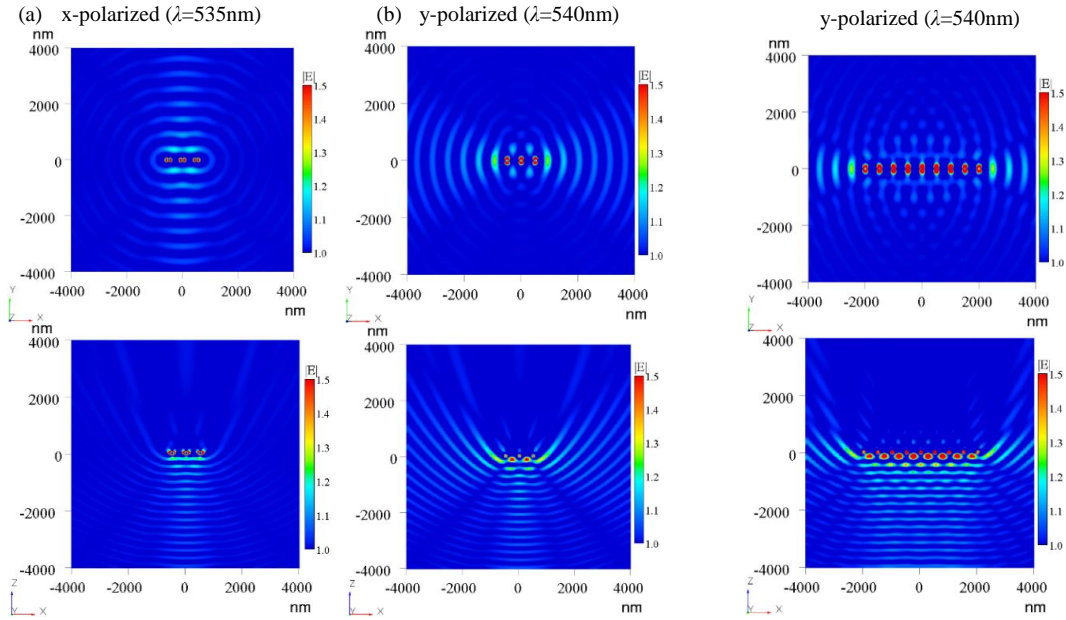
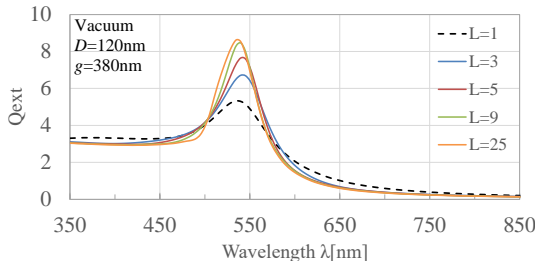


Fig. 7 Electric field distributions of the  $L=3$  gold nanospheres aggregate at the resonance wavelength.

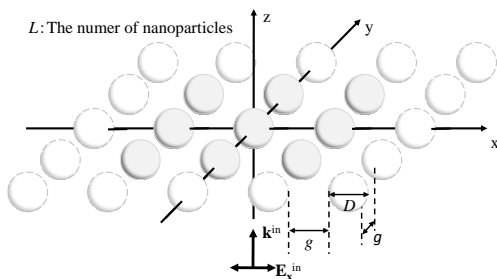
Fig. 8 Electric field distributions of the  $L=9$  gold nanospheres aggregate.



**Fig.9** Extinction efficiency spectra of gold nanoparticles arranged in a row.

### 3-3. LSPs of 2D-quasi-periodic structures

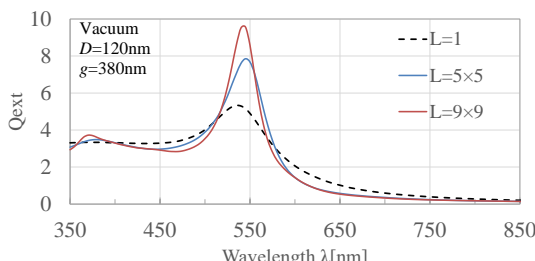
As an example of 2D-quasi-periodic structures, we consider an aggregate where gold nanospheres are placed on a square lattice with a common space  $g=380\text{nm}$  on the xy plane as shown in Fig.10. The incident light polarized in the x-direction is irradiated on the aggregate from the negative of the z-axis negative.



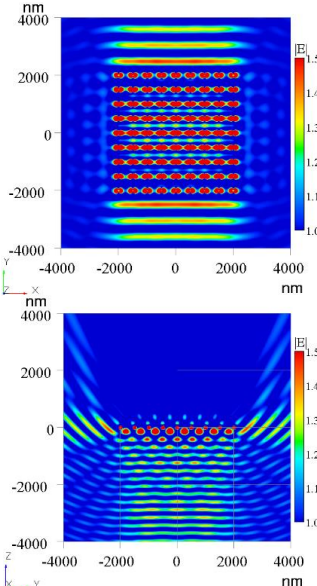
**Fig.10** Gold nanoparticles which are 2D quasi periodically arranged.

Figure 11 shows the extinction efficiency spectra  $Q_{\text{ext}}$  for the aggregates of  $L=5 \times 5$  and  $L=9 \times 9$ . As the similar to the case of 1D-quasi-periodic structures shown in Fig. 8, the quality factor of the LSP resonance increases with the number of nanospheres.

Figure 12 illustrates the electric field distributions for the 2D-quasi-periodic structures at the LSP resonance of  $\lambda=540\text{nm}$ . The scattered field based on LSPs propagates along the y direction which is perpendicular to the direction of polarization and the strong interference occurs in the yz plane.



**Fig.11** Extinction efficiency spectra of gold nanoparticles arranged on an x-y plane.



**Fig.12** Far field of  $L=9 \times 9$  gold nanoparticles arranged on a x-y plane(incident light polarized x-axis). At  $\lambda=545\text{nm}$

## 3. CONCLUSION

By employing the GMT, we have numerically examined scattering and absorption of light by 1D- or 2D-quasi-periodic structures comprising finite number of gold nanospheres. As a result, we observe the scattered field propagating along the row of nanospheres when the polarization of the incident light is perpendicular to the nanosphere row. The scattered field is associated with the coupling of LSPs excited on each nanosphere through the periodicity of the equally spaced arrangement of nanospheres. Especially the strong scattered field propagating along the direction perpendicular to the polarization direction occurs in 2D- quasi-periodic structures of  $L=9 \times 9$ .

## REFERENCES

- [1] B. Luk'yanchuk, N.I. Zheludev, S. A. Maier, ,N. J.Halas, P. Nordlander, H.Giessen and C. T. Chong: "The Fano resonance in plasmonic nanostructures and metamaterials", Nature Materials vol.9, pp.707-715(2010).
- [2] C.F.Bohren and D.R.Huffman: Absorption and Scattering of Light by Small Particles, WILEY-VCH Verlag GmbH & Co.KgaA, Weinheim, 2004.
- [3] S. Zou, N. Janel, and G. C. Schatz, "Silver nanoparticle array structure that produce remarkably narrow plasmon lineshapes," *J. Chem. Phys.* vol. 120, no. 23, pp. 10871-18075, June 2004.
- [4] M. Kawano, J. T. Blakely, R. Gordon, and D. Sinton, "Theory of dielectric micro-sphere dynamics in a dual beam optical trap", *Optics Express* vol. 16, pp. 9306-9317(2008).

# Plasmon resonance absorption in a metal grating with a thin dielectric overcoating

Kengo KIYOTA<sup>1</sup> and Toyonori MATSUDA<sup>2</sup>

<sup>1</sup> Advanced Course of Electronics and Information Systems Engineering,  
National Institute of Technology, Kumamoto Colegge  
(Suya 2659-2, Koshi city, Kumamoto 861-1102, Japan)

E-mail:ae15kiyota@g.kumamoto-nct.ac.jp

<sup>2</sup> Department of Information, Communication and Electronic Engineering,  
National Institute of Technology, Kumamoto Colegge  
(Suya 2659-2, Koshi city, Kumamoto 861-1102, Japan)

E-mail:tmatsu@kumamoto-nct.ac.jp

We examine surface plasmon resonance absorption of incident light energy by a metal grating with a dielectric overcoating thin film coating. Employing Yasuura's modal expansion method, we solve the diffraction problem by the grating and evaluate the diffraction efficiency and the ellipticity of the 0<sup>th</sup>-order diffracted wave. The plasmon resonance absorption is observed at the dip of a diffraction efficiency curve and at the zero-cross of an ellipticity curve. We examine the influence of the thickness of the dielectric overcoating on the angle of incidence, that is, the resonance angle at which plasmon resonance absorption occurs.

**Key Words :** surface plasmon, metal grating, dielectric overcoating, plasmon resonance absorption

## 1. INTRODUCTION

A metal grating has an interesting property called plasmon resonance absorption<sup>1)</sup>, which causes partial or total absorption of incident light energy in a visible region. The absorption has been the subject of many theoretical and experimental investigations due to the great potential to the application such as biosensors, surface enhance phenomena, and photonic bandgaps. The mechanism of plasmon resonance absorption has been made clear<sup>2)</sup>: The incident light couples with surface plasmons via an evanescent mode that is generated by periodic structures. The excitation of surface plasmons is affected by the surface state of metal gratings, material, groove profiles, dielectric overcoatings, etc.

In this paper, we investigate the dependence of plasmon resonance absorption on groove profiles and dielectric overcoatings which are the parameters of surface state in a metal grating. In the following section, we first formulate the diffraction problem by an aluminum grating with a thin dielectric overcoating. The groove profile of the grating is assumed to be arbitrary and is represented in finite Fourier series. We next briefly describe the numerical algorithm of Yasuura's method<sup>3)</sup> for solving the diffraction problem. Numerical results show the dependence of plasmon

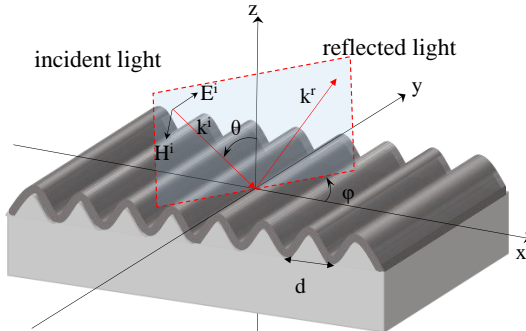


Fig.1 A metal grating with a dielectric overcoating

resonance absorption on a groove profile and the thickness of a dielectric overcoating. Experimental data on plasmon resonance absorption in a commercial aluminum grating are also included and compared with computation results.

## 2. FORMULATION OF THE PROBLEM

Figure 1 shows a metal grating with a dielectric overcoating and a coordinate system. The incident region over the grating is air ( $n_1 = 1$ ), a dielectric overcoating is  $\text{Al}_2\text{O}_3$  with a refractive index  $n_2$ , and the grating is made with aluminum metal with a complex

refractive index  $n_3$ . The grating surface is periodic in the x direction with a period  $d$ . The  $\text{Al}_2\text{O}_3$  overcoating film is periodically corrugated with a same period as grating surface  $d$ .

As incident light we consider a planewave with the wave vector

$$\begin{aligned} \mathbf{k}^i &= [\alpha \quad \beta \quad -\gamma] \\ \begin{cases} \alpha = k \sin \theta \cos \varphi \\ \beta = k \sin \theta \sin \varphi \\ \gamma = k \cos \theta \end{cases} \end{aligned} \quad (1)$$

Here,  $k$  is the wavenumber  $k = 2\pi/\lambda$ ,  $\theta$  is the angle of incidence and  $\varphi$  is the azimuthal angle between the x-axis and the plane of incidence. The electric field of the incident light is given by

$$\mathbf{E}^i(P) = \mathbf{E}_0 \exp(-jk^i \cdot P) \quad (2)$$

with  $\mathbf{E}_0$  being the amplitude vector of the incident electric field. The diffracted electric field in the upper region is denoted as  $\mathbf{E}^d(P)$  when the metal grating of Fig.1 is illuminated by the incident light.

We seek the diffracted electric field  $\mathbf{E}^d(P)$  by employing Yasuura's method. In that method, the diffracted electric field is expressed as a linear combination

$$\begin{aligned} \mathbf{E}_N^d(P) &= \sum_{m=-N}^N A_m^{\text{TE}}(N) \boldsymbol{\varphi}_m^{\text{TE}}(P) \\ &\quad + \sum_{m=-N}^N A_m^{\text{TM}}(N) \boldsymbol{\varphi}_m^{\text{TM}}(P) \end{aligned} \quad (3)$$

Here,  $\boldsymbol{\varphi}_m^{\text{TE}}(P)$  and  $\boldsymbol{\varphi}_m^{\text{TM}}(P)$  are vector modal functions of the  $m^{\text{th}}$ -order diffracted wave<sup>1)</sup>. The unknown expansion coefficients  $A_m^{\text{TE}}(N)$  and  $A_m^{\text{TM}}(N)$  are determined so that the approximate solutions satisfy the boundary condition in the sense of least squares. The superscript TE and TM mean that a relevant electric and magnetic field, respectively, are transverse to the z-axis.

To investigate the plasmon resonance absorption in the aluminum grating we evaluate the diffraction efficiency of the  $m^{\text{th}}$ -order diffracted wave by

$$\rho_m = \rho_m^{\text{TE}} + \rho_m^{\text{TM}} \quad (4)$$

where

$$\rho_m^{\text{TE}} = \frac{\gamma_m}{\gamma} |A_m^{\text{TE}}|^2 \text{ and } \rho_m^{\text{TM}} = \frac{\gamma_m}{\gamma} |A_m^{\text{TM}}|^2$$

with  $\gamma_m \geq 0$  being the propagation constant in the z-direction of the  $m^{\text{th}}$ -order diffracted wave.

In this presentation, we focus on our attention to the  $0^{\text{th}}$ -order diffracted wave ( $m = 0$ ), which is usually referred to as a reflection light. We consider the  $0^{\text{th}}$ -order diffraction coefficient  $\rho_0 = \rho_0^{\text{TE}} + \rho_0^{\text{TM}}$  and the ellipticity  $\tan \chi$  which is a parameter expressing a polarization state of the  $0^{\text{th}}$ -order diffracted wave. Plasmon resonance absorption is observed as the dip of the efficiency curve  $\rho_0$  and as the zero-cross of

the ellipticity curve  $\tan \chi$ . We therefore measure  $\rho_0$  and  $\tan \chi$  in experiment and evaluate them in computer simulation.

### 3. NUMERICAL ANALYSIS OF PLASMON RESONANCE ABSORPTION

#### 3.1 An aluminum grating and typical plasmon resonance absorption

Before describing numerical results obtained by the method stated above, we explain an aluminum grating that we made experiments on plasmon resonance absorption. It is a holographic grating of Edmund Optics Inc.<sup>4)</sup> as shown in Fig.2. Figure 3 illustrates an AFM image of the holographic grating. From the AFM observation we approximate the groove profile of the grating by a triangle with parameters  $H$ ,  $A$ , and  $D$ . The values of the parameters are read out from many AFM observations and the resultant average-values are as follows  $H = 72 \text{ nm}$ ,  $A = 377 \text{ nm}$ , and  $D = 553 \text{ nm}$ . We confirm that the base  $D$  agrees well with the period of the grating, 553 nm that is calculated from the groove density 1800 grooves/mm. In the computer simulation we use this triangle approximation as a groove profile of the holographic grating.

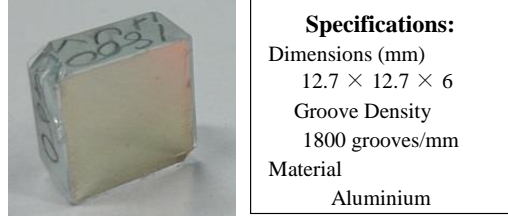


Fig.2 A holographic aluminum grating

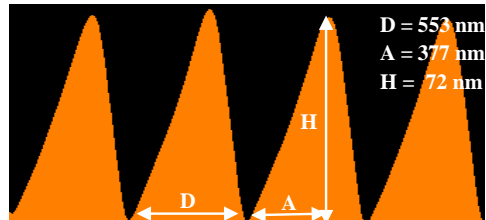
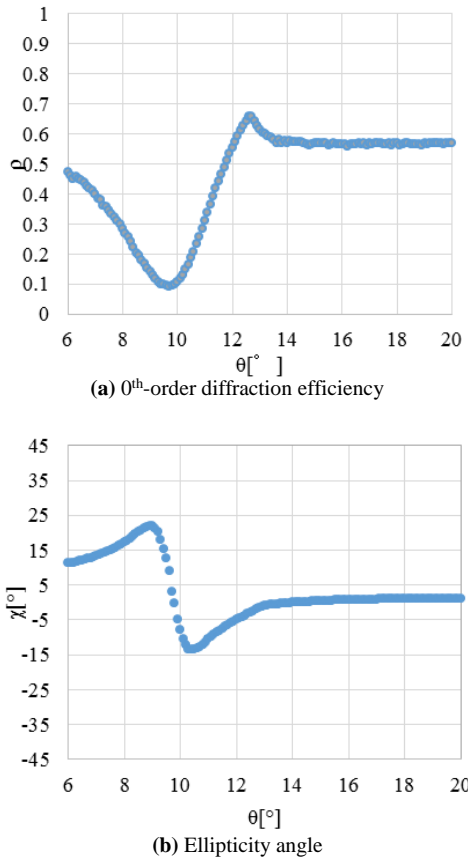


Fig.3 An AFM image of a holographic grating

We now show experimental data on plasmon resonance absorption in the holographic aluminum grating stated above. As an incident light we use the laser diode beam of  $\lambda = 670 \text{ nm}$ . The polarization of the incident light is p-polarized, that is, the electric field is parallel to the plane of incidence. Figure 4 shows the  $0^{\text{th}}$ -order diffraction efficiency  $\rho_0$  and the ellipticity angle  $\chi$  as functions of the angle of incidence  $\theta$

when the azimuthal angle  $\phi$  is fixed to be  $15^\circ$ . We observe the dip of the  $\rho_0$  curve and the zero-cross of the  $\chi$  curve at  $\theta = 9.7^\circ$  where plasmon resonance absorption occurs.



**Fig.4** Typical plasmon resonance absorption in an aluminum grating

### 3.2 Preparation for Computer simulation

We investigate optical properties of the plasmon resonance absorption in the holographic aluminum grating by the computer simulation stated in Section 2. To do so we consider an aluminum grating with an  $\text{Al}_2\text{O}_3$  film with thickness  $e$  whose cross section is illustrated by Fig.5, which is obtained from the approximation based on the AFM observation. We assume

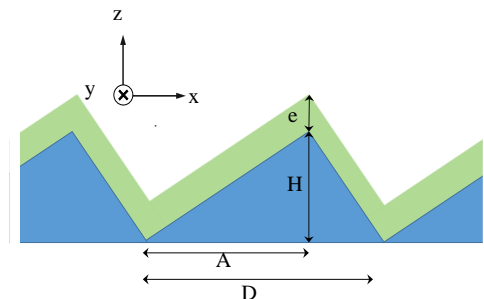


**Fig.5** Appriximate of diffraction grating by fourier series

that the corrugation profile of the  $\text{Al}_2\text{O}_3$  film is identical to that of the grating surface. We express the profile of the cross section by Fourier series expansion:

$$f(x) = \sum_{n=1}^M \left\{ a_n \cos\left(\frac{2n\pi x}{D}\right) + b_n \sin\left(\frac{2n\pi x}{D}\right) \right\}$$

$$a_n = \frac{D^2 H}{2n^2 \pi^2 (D - A)} \left\{ \cos\left(\frac{2n\pi}{D} A\right) - 1 \right\}$$

$$b_n = \frac{D^2 H}{2n^2 \pi^2 (D - A)} \sin\left(\frac{2n\pi}{D} A\right)$$
(5)

Figure 6 shows the groove profile measured by AFM (dots) and the 3<sup>rd</sup>-order approximation ( $M = 3$ ) of Fourier series expansion. We confirm the good agreement in nano size between the measured and approximated profiles of the grating surface for the parameters  $H = 72$  nm,  $A = 377$  nm, and  $D = 553$  nm.

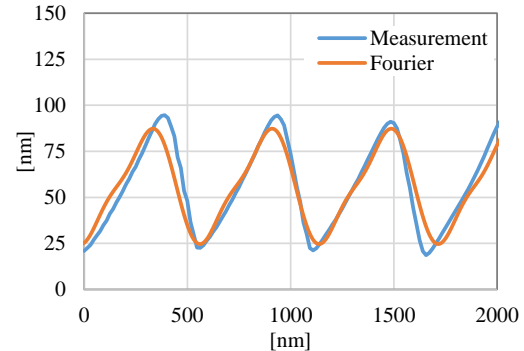


**Fig.6** Groove profiles

### 3.3 Simulation of plasmon resonance absorption

For the computer simulation of plasmon resonance absorption in the holographic grating of Fig.2 we use the 3<sup>rd</sup>-order approximation of Fourier series expansion as the groove profil of the grating and the corrugation profile of the  $\text{Al}_2\text{O}_3$  film. Parameters on incident light parameters are as follows: wavelength of incident light  $\lambda = 670$  nm, p-polarized incidence, and the azimuthal angle  $\phi = 15^\circ$ .

Figure 7 shows (a) the 0<sup>th</sup>-order diffraction efficiency  $\rho_0$  and (b) the ellipticity angle  $\chi$  as functions of  $\theta$  for some  $\text{Al}_2\text{O}_3$  film thickness  $e$ 's ( $e = 5, 10, 15, 20$  nm). In Fig.7 the parameter labeled "bare" means  $e = 0$  nm, that is, an aluminum grating without an  $\text{Al}_2\text{O}_3$  film. We estimate the influence of  $e$  on plasmon resonance absorption from this figure. The resonance angle  $\theta_{SP}$  shifts to lower value as the thickness  $e$  increases. This implies that the resonance angle can be controlled by the thickness of the dielectric over-coating on a metal grating.

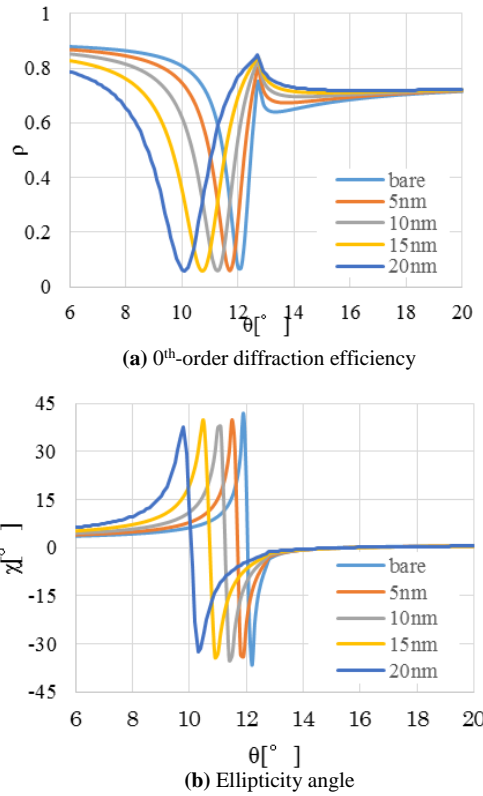


**Fig.7** Plasmon resonance absorption for some  $e$ 's

In Fig.8 we compare experimental data of plasmon resonance absorption with the simulation results where the 3<sup>rd</sup>-order approximation of Fourier series expansion and the sinusoid are considered as the groove profile of the grating with  $e = 20$  nm.

#### 4. CONCLUSION

We described the numerical algorithm based on Yasuura's method for analyzing plasmon resonance absorption of a metal grating with a dielectric overcoating. As numerical examples, we exhibited plasmon resonance absorption of an aluminum grating overcoated with an Al<sub>2</sub>O<sub>3</sub> film. As a result, the influence of the thickness of the overcoating on the resonance angle are made clear. The results are available in the investigation of optical properties of plasmon resonance absorption in a metal grating.

However, simulation results is not sufficiently coincident with experimental data in the resonance curves of  $\rho_0$  and  $\chi$ . As for comparison of simulation results and experimental data, therefore, there is necessity to continue to study from now on.

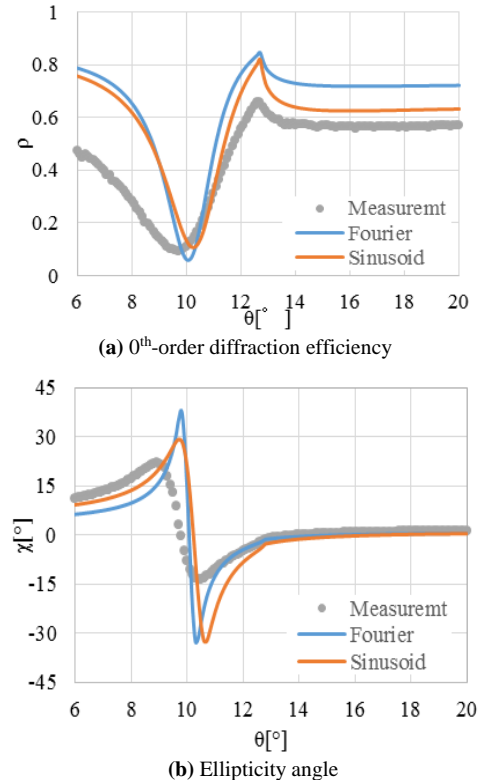


**Fig.8** Comparison of experimental data with simulation results in plasmon resonance absorption

#### REFERENCES

- 1) H. Raeter, "Surface plasmon and roughness," *Surface Polaritons*, V. M. Argranovich and D. L. Mills (eds.), pp. 331-403, North-Holland, New York, 1982.
- 2) M. Neviuer, "The homogenous problem," *Electromagnetic Theory of Gratings*, R. Petit (ed.), pp. 123-157, Springer-Verlag, Berlin, 1980.
- 3) H. Ikuno and K. Yasuura, "Improved point-matching method with application to scattering from a periodic surface", IEEE Trans. Antennas & Propag., vol. AP-21, no. 5, pp. 657-662, May 1973.
- 4) Edmund Optics Inc., <http://www.edmundoptics.com/>

# Accuracy of TDR Measurement on Non-uniform Transmission Line

Naru HIRATA<sup>1</sup>, Takuto OGATA<sup>2</sup> and Yoshifumi Shimoshio<sup>3</sup>

<sup>1</sup> Student, Advanced Course of Electronics and Information Systemos Engineering.

.Kumamoto National College of Technology,  
2659-2 Suya, Koshi, Kumamoto 861-1102 Japan  
ae14hirata@g.kumamoto-nct.ac.jp

This paper presents a research for a modeling of transmission line based on TDR measurement. TDR measurement can measure a characteristic impedance of a wire-harness that is installed in an automobile. The purpose of this study is to develop an equivalent circuit of a single-ended transmission line that is consisted of a wire-harness and the chassis of an automobile by TDR measurement. At first, we measured each trace, where the characteristic impedance is already known, on a PCB board. It has appeared some errors associated with multiple reflections and the rise time of an input pulse. A peeling program to remove the multiple reflections is developed. We measure a waveform varying the rise time. We make an experimental transmission line to extract an equivalent circuit from it. Then we calculate the values of L and C from the measured values by TDR measurement.

**Key Words :** *non-uniform transmission line, peeling, TDR measurement, multiple reflection, equivalent circuit*

## 1. INTRODUCTION

In general, an automobile which we always drive is equipped with many electronic devices. The electronic devices such as an engine control and a speed meter are systems for vital safety of humans and some devices such as a car navigation and an ETC are systems which provide a comfortable environment for us. All of these are realized by the operation of many electronic devices. A wire-harness which consists of many cables is used for these electronic devices to supply power for them and transmit various signals between them. The wire-harness consists of many single wires and many ground wires which are bundled. Many single wires of the wire-harness are connected to each electronic device. Many ground wires are connected to the chassis of an automobile. Therefore, the chassis of an automobile is used as a common ground of a signal transmission line. As many electronic devices are installed all over the automobile, the wire-harness is installed along the chassis in an automobile.

One single wire of the wire-harness and the common ground that is automobile chassis consist of a single-ended transmission line. As the wire-harness consists of many single wires, many single-ended transmission lines exist in the wire-harness. Generally, a single-ended transmission line generates noises easily and the noises effect to the signals

which are transmitted in other single-ended transmission line. The distance between single-ended transmission lines are near because many single wires and ground wires are bundled in a wire-harness. Therefore, there is a possibility that electromagnetic interferences occur between a single-ended transmission line and the other line. If the interferences occur, noises are generated on an electronic device that is connected to the single-ended transmission line where the noises are generated. The generated noises might cause troubles or undesired operation. Therefore, it is important to remove or reduce the interferences to keep safety and comfort of an automobile. If we can make the model of a wire-harness as a transmission line, we can investigate how to remove or reduce the interferences before the wire-harness is installed in an automobile. Therefore, we will make a transmission line model of a wire-harness.

There is an analyzing method such as FDTD (Finite Difference Time Domain) method for analyzing an electromagnetic interference and it is a full wave and spatial analyzing method of the electromagnetic interference. However, FDTD method needs much computational time and huge memory to build cells which represent the entire space of an automobile. On the other side, a method which treats the wire-harness as a transmission line has an advantage that it can analyze at a high speed and simulate electromagnetic

interferences under various conditions if we can make an appropriate equivalent circuit.

Single-ended transmission lines should be modeled as a distributed constant circuit. The distributed constant circuit consists of L and C and it is an equivalent circuit of a single-ended transmission line. The values of L and C in the equivalent circuit vary according to the distance between the single wire in a wire-harness and the chassis of an automobile. As a wire-harness is installed in an automobile along the chassis, the values of L and C vary when the distance between a single wire in a wire-harness and the chassis vary along the wire. Therefore, when we make an equivalent circuit, we have to consider the characteristic variations according to the distance of single wire and the chassis.

We use TDR (Time Domain Reflectometry) method to calculate the value of L and C of a single-ended transmission line. The TDR method is simple and easy to operate the equipment and easy to calculate the L and C. However, TDR measurement includes some measurement errors. Therefore we have to consider the accuracy of TDR measurement.

The purpose of this study is to develop an equivalent circuit of a single-ended transmission line that is consisted of a wire-harness and the chassis of an automobile. The longitudinal distance between a wire-harness and an automobile chassis varies at any positions in an automobile, thus the values of L and C in an equivalent circuit vary, too. In this study, we measure a voltage at input terminal of a transmission line and calculate the L and C values of the line. Then we can make an equivalent circuit of the line which consists of the cascaded many Ls and Cs.

## 2. THEORY AND METHOD

### (1) TDR theory

A TDR measurement is a method that a step pulse is applied to a transmission line and then a TDR equipment measures a voltage in time domain which is reflected in the line. As shown in Fig.1, TDR measurement instrument consists of a pulse circuit and a high-speed digital oscilloscope. At first, the pulse  $u(t)$  is applied to a transmission line that is connected to the TDR. If a reflection occurs in a transmission line, the reflected voltage,  $V_{ref}(t)$ , occurs and returns to TDR side. The measured voltage,  $V_{obs}(t)$ , is a sum of the applied pulse  $u(t)$  and voltage  $V_{ref}(t)$  that is generated by reflection and returned one. The measured voltage can be express as formula (1)

$$V_{obs}(t) = u(t) + V_{ref}(t) \quad (1)$$

If the reflection occurs, we can measure as shown

Fig.2As the internal resistance of TDR equipment and the rise time of the input pulse are already known, we can calculate the characteristic impedances by measuring the voltage,  $V_{obs}(t)$ . The measurement by TDR is carried in time domain. Thus the values of voltage and time are recorded at the same time. The propagation speed of a signal in a transmission line which has a permittivity of  $\epsilon_r$  is expressed as eq.(2).

$$v_p = \frac{3 \times 10^8}{\sqrt{\epsilon_r}} \quad (2)$$

If the permittivity is known, the propagation speed can be decided by eq.(2). Therefore, the position where the reflection occurred in the transmission line can be detected. Then, the characteristic impedance at the position can be obtained by calculation. And it is possible to make an equivalent circuit by the obtained characteristic impedance. The relation of the characteristic impedance between L and C of distributed constant circuit can be shown as eq. (3) and (4).

$$Z_0 = \sqrt{\frac{L}{C}} \quad (3)$$

$$LC = \sqrt{\mu\epsilon} \quad (4)$$

It is possible to make an equivalent circuit at any point by formula (3), (4).

### (2) TDR method

In a transmission line under testing, if there are sections where the characteristic impedance is not equal, multiple reflections occur at each section as shown in Fig.3. The measured voltage by TDR is a sum of reflected voltages from each section. The voltages by the multiple reflections cause an error in the measured voltage. Peeling program can remove the error according to the multiple reflections. In fig.3, the measured voltage by TDR is expressed as eq.(5).

$$V_{obs}(3) - u(3) = \Gamma_{01}u(2) + \Gamma_{12}T_{01}T_{10}u(1) + (\Gamma_{12})^2\Gamma_{10}T_{10}T_{01}u(0) + \Gamma_{23}T_{01}T_{12}T_{21}T_{10}u(0) \quad (5)$$

The formulas for removing the multiple reflections for one time and three times reflections are shown as eq.(4) and (5). However, an equation for removing the multiple reflections for more than five times is not derived here. When we calculate characteristic impedance, we have to calculate reflection coefficient. The procedure is as follows. Representing the measured voltage as  $V_{obs}(t)$ , and the summed up voltage included one time and three times reflections as  $V_{nwref}(k)$ , the reflection coefficient at each position

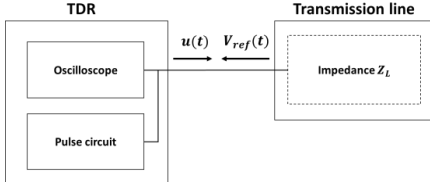


**Fig.1** Block diagram of TDR measurement.

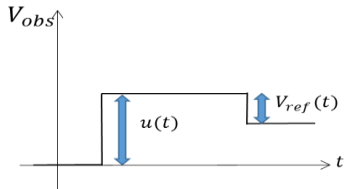


**Fig.2** The waveform measured by TDR

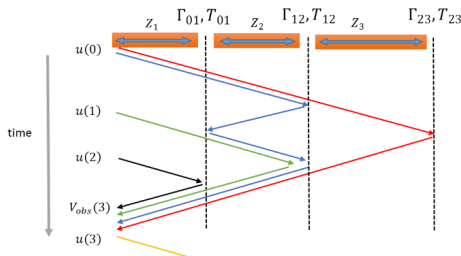


**Fig.3** Image of multiple reflection

can be represented as eq.(6). By repeating the procedure, the reflection coefficients at each sections can be obtained from eq.(6).

$$\Gamma_{k,k+1} = \frac{V_{obs}(k) - V_{nwref}(k)}{u(0)} \frac{1}{\prod_{j=1}^k T_{j-1,j} \prod_{j=1}^k T_{j,j-1}} \quad (6)$$

Characteristic impedance that we want to calculate is to be known a characteristic impedance of before step.

### 3. RESULT AND DISCUSSIONS

#### (1) Influence to a waveform by rise time

We used two transmission lines named as SMA1 and SMA3 with known characteristic impedance in order to confirm the effectiveness of TDR measurement to our purpose and investigate the accuracy of TDR measurement. The transmission line, SMA1, has uniform characteristic impedance which is  $50\Omega$  along the line. The transmission line, SMA3, has  $50\Omega$  and  $33.6\Omega$  characteristic impedance that changes alternately along the line. The dimension of the transmission line SMA3 is shown in Fig.4. The length of the  $33.6\Omega$  impedance section of SMA3 is designed that the section length changes gradually long. The length of a transmission line is associated with propagation time and the width is associated

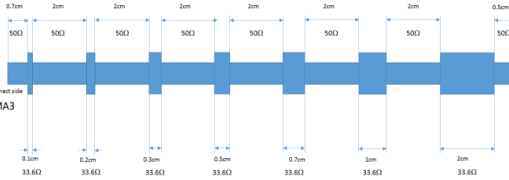


**Fig.4** Configuration of transmission line SMA3.

with characteristic impedance. Therefore, propagation time at each  $33.6\Omega$  section of SMA3 becomes gradually long. The internal resistance of TDR and the terminal end's resistance are  $50\Omega$ . We measured from the left side terminal of SMA3. The measurement results for SMA1 and SMA3 are shown in Fig.5 and Fig.6 as TDR. We used an input pulse with 35ps rise time in TDR measurement. The other curve in Fig.5 and Fig.6 named as SPICE is simulating result that is calculated for the equivalent circuit of SMA1 and SMA3 by SPICE program. In the simulation, the 0.01ps rise time for the input pulse was used. The 0.01ps is the shortest rise time which was used in a simulation by SPICE to know the influence of the rise time.

In the TDR measurement result for SMA1, the impedance of the transmission line, SMA1, is almost  $50\Omega$  and flat but not completely flat although it has uniform trace width. The reason is that the characteristic impedance of the measured transmission line is not perfectly  $50\Omega$  along the line although it is designed as  $50\Omega$ . As shown in Fig.5, the characteristic impedance vary abruptly at 0.2ns point. The variation comes from a connector connecting a TDR measurement cable to the transmission line of a PCB board. The reason why the simulated impedance is zero at the time before 0.2ns is that the simulation starts from 0.2ns although the measurement starts before it.

The measurement result for SMA3 is shown as “TDR” in Fig.6. The rise time and the voltage of input pulse is 35ps which is the same as the SMA1’s case. At each of  $33.6\Omega$  sections, the characteristic impedance must reach to  $33.6\Omega$ . However, they do not reach the value. The longer length of  $33.6\Omega$  section, the lower the characteristic impedance. If we compare the curve “SPICE:35ps” with the curve “SPICE: 0.01ps”, then we notice that the “SPICE:35ps” is similar with the curve of “TDR”. It means that the result by TDR measurement is influenced by rise time.

#### (2) Removing multiple reflections by peeling

As the curve “SPICE:0.01ps” shows a result which does not include much influence by the rise time because the rise time is very short. However, the curve does not show  $33.6\Omega$  at right side sections. As we assumed the reason is multiple reflections, a peeling program was executed to remove them on the waveform “TDR”. The curve “Peeling” shows the result.

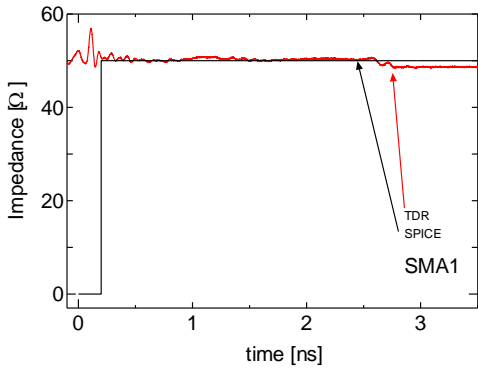


**Fig.5** Measured and calculated impedance for SMA1

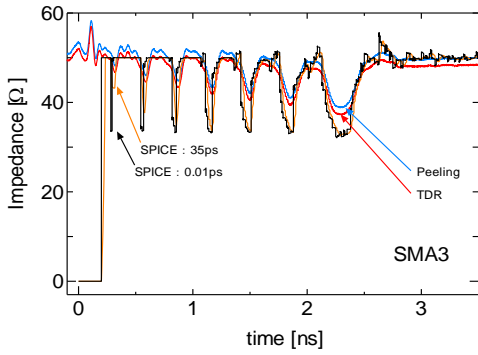


**Fig.6** SPICE waveform: 0.01ps and 35ps and peeling waveform: 35ps

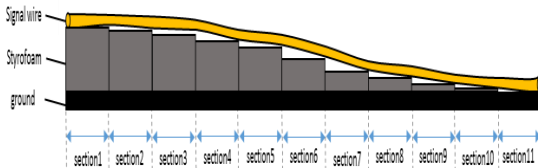


**Fig.7** Changing the height of conductor wire

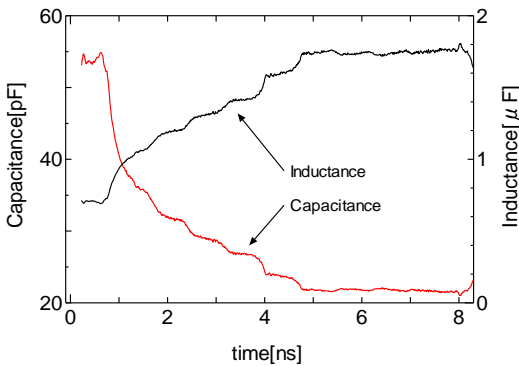


**Fig.8** Values of L and C.

As the curve shows, there is no apparent effect because the developed peeling program can remove only one-time reflection.

### (3) Changes of characteristic impedance by distance between signal wire and ground

Figure.7 shows a transmission line that the characteristic impedance varies along the line according to

the distance between a signal wire and a ground. As the line was made as it has different distance at each sections along the line, each section has different characteristic impedance. By measuring the characteristic impedance for each section, the values of L and C can be calculated. Figure.8 shows the changes of L and C. As shown as “inductance” in Fig.8, the value of L increases as the distance becomes longer. Similarly, the value of C decreases as the distance becomes longer. The measured two curves do not show complete step changes because the line itself were not mad as it has step change. It is difficult to make a transmission line which has step distance change because the signal wire has thickness. As the curves show, the values of C and L vary even in a section where the distance is same. It should be examined whether the obtained values are appropriate to represent an equivalent circuit of the transmission line.

## 4. SUMMARY

This paper described the accuracy of TDR measurement by investigating the effect of a rise time and multiple reflections. Then the impedance of a transmission line which consists of a signal wire and a ground has measured. The transmission line has many different impedances at each section along the line because the distance between a signal wire and a ground is different at each section.

As a result, it has just confirmed that the rise time influenced to the measured TDR waveforms but it could not be obtained how to extract the true waveforms. Although it has been executed to remove the influence of the multiple reflections by peeling, the one-time reflection removing did not much effect. Lastly the values of L and C of a transmission line have been calculated from the measured value. The transmission line has a characteristic impedance that changes along the line because of the distance difference between a signal wire and a ground. In the future, we will do follow things:

- 1) Program development to remove more than three-times reflections.
- 2) To check the validity of equivalent circuit for a transmission line which the distance between a signal wire and a ground varies and check.
- 3) To measure L and C of actual wire-harness and to make an equivalent circuit for it.

## REFERENCES

- 1) Ching-Wen Hsue and Te-Wen Pan: Reconstruction of Non-uniform Transmission Lines from Time-Domain Reflectometry, IEEE TRANSACTIONS ON MICROWAVE THEORY AND TECHNIQUES, VOL. 45, NO. 1, 1997.
- 2) Gresho, P. M., Chan, S. T., Lee, R. L. and Upson, C. D. : A modified finite element method for solving the time-dependent incompressible Navier-Stokes equations, part 1, *Int. J. Numer. Meth. Fluids*, Vol. 4, pp. 557-598, 1984.

# Detection of Partial Disconnection of Cable for Electrocardiography Monitor

Yuya YOSHIMURA<sup>1</sup>, Yoshifumi SHIMOSHIO<sup>2</sup>

<sup>1</sup> Student, Department of Information, Communication and Electronic Engineering,  
National Institute of Technology, Kumamoto College  
(2659-2 Suya, Koshi, Kumamoto, 861-1102 Japan)  
E-mail:hi11yoshimura@g.kumamoto-nct.ac.jp

<sup>2</sup> Professor, Advanced course, National Institute of Technology, Kumamoto College  
(2659-2 Suya, Koshi, Kumamoto, 861-1102 Japan)  
E-mail: shimoshi@kumamoto-nct.ac.jp

In this paper, a detection method to know the cable which is used for an electrocardiographic monitor is partially disconnected or not. When there is a partially disconnection in the cable, sometimes some noise appear in the signal from human to the monitor. Thus paramedical personals want to replace the cable prior to the disconnection occurs. Our study will be a helpful for them if the detection method can be realized.

**Key Words :** partial disconnection, electrocardiographic monitor, TDR, impedance measurement, noise

## 1. Introduction

Currently, a large number of researches on a detection of circulatory shunt or disconnection of wires have been conducted. However, studies on the detection of partial disconnection of wire have not been so popular yet. When a cable which is used for an electrocardiograph is partially disconnected, some noise may be appeared in the signal from human body to the electrocardiograph. Therefore paramedical personals who use an electrocardiograph want to change the cable before it is partially disconnected. The aim of this study is to be able to notify the paramedical personals to replace the cable prior to the disconnection occurs by detecting the position where the cable wire used for electrocardiograph is partially disconnected. In this paper, we investigate the change of impedance and reflection coefficients of the cable when it is partially disconnected and to find the method to notify that the cable has already partially disconnected.

## 2. Experiments

### 2.1 Measurement of reflection coefficient when a braided shield wire of coaxial cable is broken by piecemeal

As we had not enough information about the details of a cable that is used for an electrocardiograph at the beginning of this study, a coaxial cable was used for our first experiment. The coaxial cable which we used is a 1.5m long cable that consists of an inner wire of 0.5mm in diameter and a shield wire braided by 120 pieces of thin wires. We decided the cable length because the cable for an electrocardiograph is around 1.5m. The coaxial cable is connected to TDR (Time Domain Reflectometry) equipment. A reflected waveform is

measured every 5 pieces of thin wires are broken at the length of 25cm from cable end termination. The waveform which shows a reflected waveform is measured by TDR equipment. The measurement has repeated 24 times because the braided wire includes 120 pieces of thin wires. The changes in the reflected waveform every breaking the thin wires are observed by TDR equipment. The TDR equipment used here is Agilent 86100C. It can measure reflected waveform as voltage, reflection coefficient, and impedance. In this paper, the measurement is performed in voltage. Every breaking five thin wires of a braided shield, we observed the reflected waveform by using TDR equipment. The changes of the reflected waveforms according to the number of thin wires are shown in Fig.1.

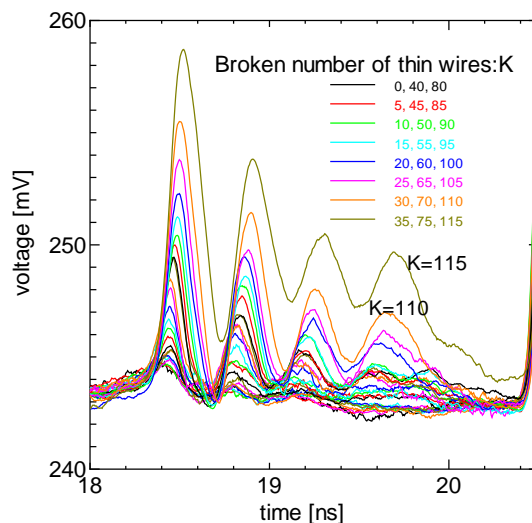


**Fig.1** Reflected waveform for the number of thin wires which are broken

As there are 120 thin wires in the braided shield, 24 lines appear in the figure. As shown in Fig.1, when the number of broke thin wires becomes large, it is obvious that the change in the reflected waveform also becomes large. The corrugations in the measured reflected waveforms seem to be caused by peeling off the cable jacket. The distance from a TDR input to the point where the reflected waveform voltage is biggest can be calculated from the graph. As the distance of the point shows the same value as the stranded wire which is connected to TDR equipment is broken, it can be said that the location where the shield wire is broken could be detected. The voltages of each curve at the point of 18.5ns where the change in Fig.1 is largest also be graphed. Then the voltage increases as it looks like a secondary function. If the reflected waveform can be measured within an accuracy of about 1mV, then the partially disconnected point of a shield wire of a coaxial cable seems to be possible to detect.

## 2.2 Impedance measurement when a stranded wire is broken by piecemeal

As we confirmed that the cable which is used for an electrocardiograph is a stranded wire, we did an experiment to know whether the impedance change can be detected or not when the wire is partially disconnected. The impedance change should be very small. A 30cm-long stranded wire is prepared and connected to an impedance analyzer. The impedance analyzer we used in this experiment is HP-4194A. It can measure the impedances from 100Hz to 40MHz.

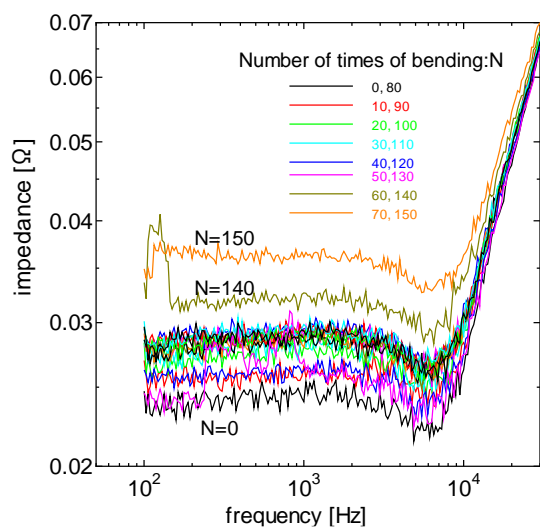


**Fig.2** Impedance characteristics for the number of bending.

To simulate the actual use condition of cable in a hospital, bend stress by hand is applied to the wire. The stress is applied by bending the center of the stranded wire 10 times for each measurement. Every applying the stress, the impedance of the wire is measured. The measurement is repeated and the change in the impedance is observed until the wire completely breaks. The electric signal applied the stranded wire to measure the impedance is an alternating current. The frequency of the applied signal varies from 100 Hz to 10MHz.

Figure.2 shows the frequency characteristics of measured impedances. Each curve shows the impedance values for the number of times where the stranded wire is bent. From Fig.2, there is a slight change in the impedance values at all frequency range because of noise. The drop of impedance at around 7 kHz may influenced by an internal inductance by a skin effect and also the increase at higher frequencies higher than around 10 kHz come from a high frequency effect by a skin effect too. The top line in Fig.2 shows a corrugation when the wire is perfectly broke. However, the impedance value does not reach infinity although the wire is already broke. The reason is that some of thin wires in the stranded wire still touch at some position. As a result, there is a possibility that we can know the partial disconnection of a cable for an electrocardiography monitor by detecting the impedance change at low frequency or DC. From Fig.2, it is shown that the impedance measurement needs the accuracy of about 1 mΩ to detect the partial disconnection of wire.

## 3. Conclusion and future works

In this paper, it was examined whether we can detect a partial disconnection of cable for electrocardiography monitor by measuring the impedance of cable. The impedance of cable changed according to the number of broke wires. Thus, it was shown that there is a possibility to detect the partial disconnection by measuring the cable impedance at low frequencies lower than 7 kHz or resistance at DC. In addition, as the TDR equipment can find the break point of the cable, it will be used if it is necessary to know the break position.

As the future works, the followings must be executed:

- to build a measuring circuit for measuring low-resistance with sufficient accuracy
- to decide the range of resistance value which shows the partially disconnected wire.
- to develop complete equipment to detect partial disconnection with sufficient accuracy.

# Equivalent Circuit Simulation of Variable Frequency Surface Acoustic Wave Resonator

Miyabi TANAKA<sup>1</sup>, Hiroyuki ODAGAWA<sup>2</sup>

<sup>1</sup> Student, National Institute of Technology, Kumamoto College  
(Koshi 861-1102, Japan)

E-mail:ae15m-tanaka@g.kumamoto-nct.ac.jp  
<sup>2</sup>Professor, National Institute of Technology, Kumamoto College

In information and communication systems, amount of communication data is increasing significantly, and higher speed and higher data density communication is required. Consequently, in mobile communication systems, developments of a high-frequency and broadband device with power saving and small size and weight become an important research subject. Surface Acoustic Wave (SAW) filters are currently used in mobile communication systems to meet the above characteristics. As increasing the data density, SAW filters having a low loss, flat pass band and enough out-of-band attenuation have been required for the future communication systems. Moreover, frequency tunable property is required to cover various frequency bands by one device. The purpose of this study is to examine a tunable SAW resonator obtained by applying a method to change SAW velocity and reflection coefficient by adding variable capacitance to a reflector part of the SAW resonator.

**Key Words:** Surface Acoustic Wave; Filter; Resonator

## 1. INTRODUCTION

Surface acoustic wave (SAW) filters have been applied to mobile communication systems taking advantage of the characteristics of small size and weight. Recently, frequency tunable filters and resonators which can support various kinds of communication methods are required<sup>1)</sup>.

The purpose of this study is to examine a tunable SAW resonator obtained by applying a method to change SAW velocity and reflection coefficient by adding variable capacitance to a reflector part of the SAW resonator

## 2. PRINCIPLES

### (1) Surface Acoustic Wave

SAW is the wave which energy is concentrated near the surface of the medium, and propagates in the surface. In the SAW devices, SAW is generated by interdigital transducer (IDT) on a piezoelectric substrate.

### (2) Piezoelectricity

Figure 1 shows schematic drawings of piezoelectric effect and inverse piezoelectric effect. When

pressure or stress is added to the piezoelectric material, dielectric polarization proportional to the stress and the electric charge of the plus and minus appears in both surfaces. This characteristic is called piezoelectric effect. Reversely, when electric field is added to the piezoelectric material, mechanical stress or displacement is occurred. It is called inverse piezoelectric effect.

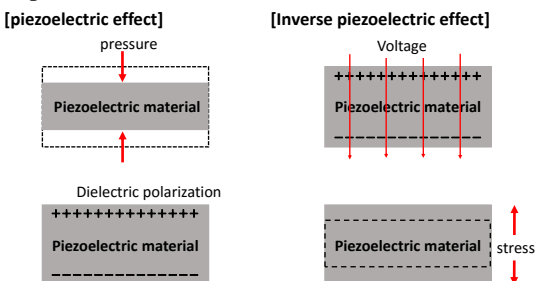


**Fig.1** Outline of piezoelectric effect and inverse piezoelectric effect.

### (3) SAW Filter

Figure 2 shows a structure of SAW filter. The SAW filter consists of a launching interdigital transducer (IDT) and receiving IDT which are fabricated on a piezoelectric substrate. The launching IDT converts input electrical signal to the SAW with inverse-piezoelectric effect and the receiving IDT

reconverts the SAW into an electrical signal with piezoelectric effect. It can take out only the signal having a same wavelength as the period of IDT, that is, it has the function of band pass filter.

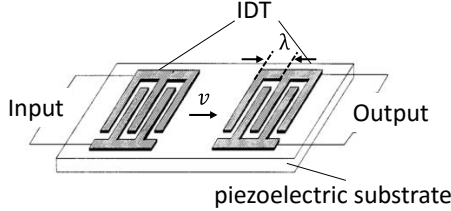


**Fig.2** Structure of the SAW filter.

The center frequency of SAW filter is given by following equation.

$$f = \frac{v}{\lambda}, \quad (1)$$

where  $v$  is velocity of SAW,  $\lambda$  is the period of the IDT. In conventional SAW filter, electrode period is fixed because IDT is fabricated by photolithography technique and the electrodes are deposited onto the piezoelectric substrate. In this structure, velocity of the SAW cannot be change. Therefore the frequency is unchangeable.

#### (4) Change of SAW velocity by electrical boundary condition

On the other hand, the propagation velocity of the SAW in the piezoelectric substrate is known to be change by electrical boundary condition of the surface. Figure 3 show open surface, short surface and intermediate surface.

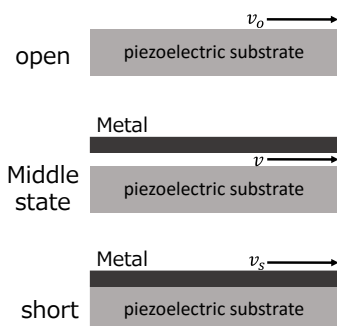


**Fig.3** State of the substrate surface.

As shown in Fig. 4, the velocity of SAW become lower when the surface of the piezoelectric substrate is shorted electrically. The relation between the velocity and electromechanical coupling coefficient of SAW  $k^2$  is given by equation (2).

$$k^2 = \frac{2(v_o - v_s)}{v_o}, \quad (2)$$

where  $v_o$  is the velocity in open surface, and  $v_s$  is the velocity in short surface.

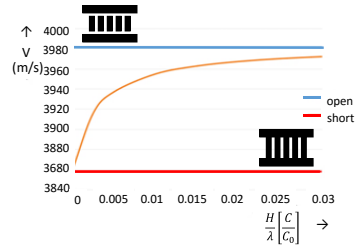


**Fig.4** SAW velocity as a function of distance between metal plane and surface of substrate.

In Fig.3 and Fig.4, electrical surface condition is changed by changing the distance between metal planed and surface of the substrate. Similar condition is obtained by using a variable capacitance which is connected to the IDT and the ground <sup>2)</sup>. In case the capacitance is small, surface condition is considered to be open. On the other hand, in case the capacitance is enough large, surface condition is considered to be short. Using this property, we can change SAW velocity continuously by changing the value of the variable capacitance. If we change the velocity using variable resistance instead of the variable capacitance, the energy loss occurs and the loss of the device will increase. Therefore we use variable capacitance.

#### (5) SAW Resonator

The velocity variable type IDT is applicable to not only the filter but also the resonator. The structure of a SAW resonator is shown in Fig. 5. In the resonator, drive IDT which has two pairs of electrodes is located at the center, and two reflectors which have 50 pairs of electrodes connected to the variable capacity are located at both side of the drive IDT. SAW made by drive IDT is propagate to both side and reflected back with the reflectors, and a standing wave of the SAW is generated.

In this variable resonator, following three effects are considered as a factor to change the resonant frequency.

1. Change of SAW velocity due to the electrical boundary condition.
2. Change of reflection coefficient of SAW at the reflector
3. Change of reflection in electric signal at the variable capacity

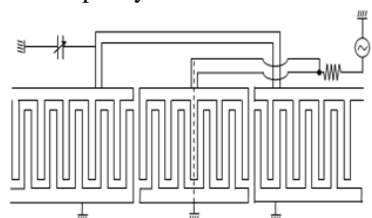


**Fig.5** Structure of tunable SAW resonator <sup>2)</sup>.

The purpose of this study is to clarify the contribution of the three effects using an equivalent circuit simulation. In this simulation, Al electrode and 128 ° Y-X LiNbO<sub>3</sub> substrate are used.

### 3. SIMULATION RESULTS

#### (1) Effect of SAW velocity change

As shown in Fig. 6, frequency responses are changed when the velocity of the reflector are changed. Approximately 2.6% of center frequency is changed when the boundary condition is changed from open to short.

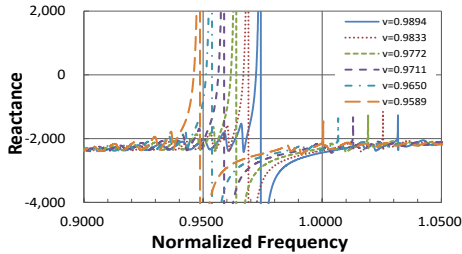


**Fig.6** Frequency response of SAW resonator when SAW velocity is changed.

#### (2) Effect of reflection coefficient change

As shown in Fig. 7, frequency response is changed as the reflection coefficient of the reflector is changed. When the reflection coefficient changed from open condition to short condition, approximately 1% change of the resonant frequency is provided.

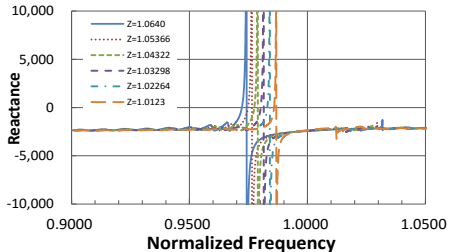


**Fig.7** Frequency response of SAW resonator as changing the reflection coefficient.

#### (3) Effect of variable capacitance

As shown in Fig. 8, frequency response is changed as the value of the capacitance is changed, because SAW is converted into electric signal at the reflectors, and the electric signal is reflected at capacitance and re-excited from the reflector. The frequency change of less than 1% is provided.

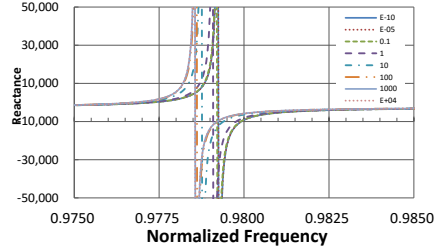


**Fig.8** Frequency response of SAW resonator when the variable capacitance is changed.

#### (4) Combination of SAW velocity, reflection coefficient and variable capacitance

Characteristic change by the SAW velocity, reflection coefficient and capacitance is shown in Fig. 9. Direction of the frequency shift caused by the effect of reflection coefficient is opposite to the other two effects. Therefore, only 1.8% of the frequency is changed.

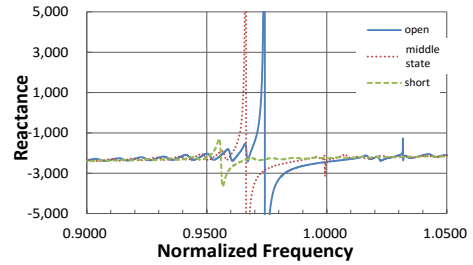


**Fig.9** Frequency response of SAW resonator as changing the SAW velocity, reflection coefficient and value of the capacitance.

### 4. FREQUENCY CHANGE BY THE REFLECTION COEFFICIENT

#### (1) Frequency shift by reflection coefficient

In a resonator, reflection of SAW is occurred over several electrodes because the each electrodes work as distributed reflector element as shown in Fig. 10. Equivalent reflection plane called penetration depth, which is obtained by adding the all reflections, can be defined in the SAW reflector. The penetration depth is inverse proportion to the reflection coefficient of one electrode. It means that when the reflection coefficient is large, penetration depth is small, and then the resonant frequency becomes high, because the wavelength of the standing wave in the resonator becomes short.

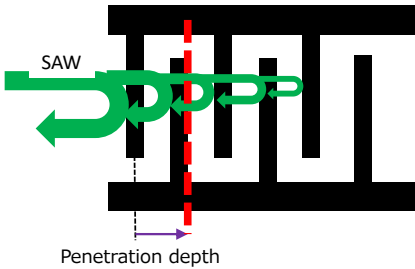


**Fig.10** Structure of reflector .

## (2) Method to reverse the frequency shift

As described in section 3 (4), frequency shift which is caused by the change of reflection coefficient is not the same direction to the other frequency shifts. Figure 11 shows the reflection coefficients in Al electrodes on  $128^\circ$  Y-X LiNbO<sub>3</sub> substrate as the function of electrode thickness. In this combination of the electrode and substrate, the reflection coefficient becomes small from open to short.

The reflection with film thickness of 0 is caused by only electrical reason. In this case, absolute value of the reflection coefficients in open and short condition are the same but the sign is opposite. However, when a film thickness becomes thick, a mechanical reflection is added to the electrical reflection, and then the value of the reflection coefficient changes. Therefore the absolute value of the reflection coefficients in short condition becomes smaller than that in open condition.

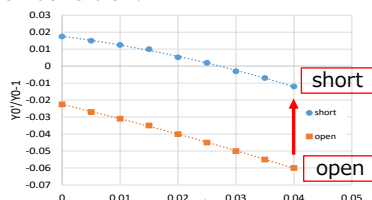


**Fig.11** Reflection properties of Al/128 ° Y-X LiNbO<sub>3</sub> as the function of electrode thickness.

If the reflection coefficient were to become large from open to short condition like Fig. 12, the frequency shift would be opposite to the case in Fig. 11. Figure 13 is a simulation results where we assume the relation of reflection coefficient in Fig.12.

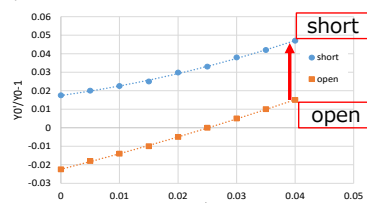


**Fig.12** Reflection properties of Al/128 ° Y-X LiNbO<sub>3</sub> as the function of electrode thickness.

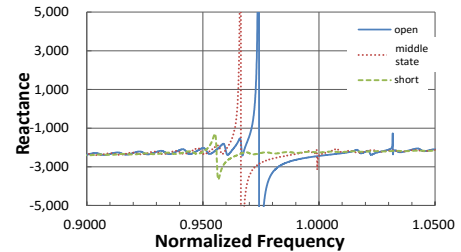


**Fig.13** Frequency response of SAW resonator assuming the relation of reflection coefficient is Fig.12.

About 3.5% of frequency change is provided. From this, it can be said that if we find the combination of the electrode material and substrate which shows the relation of the reflection coefficient in open and short condition like Fig. 12, the amount of the frequency shift becomes large.

## 5. CONCLUSION

In this study, we examine a tunable SAW resonator using SAW velocity change obtained by adding a variable capacitance to a reflector part of the SAW resonator.

In this variable resonator, three effects are considered as a factor to change the resonant frequency, and we clarified the relation of them by using equivalent circuit analysis. As the results, we make it clear that direction of the frequency shift by the effect of reflection coefficient is opposite to the other two effects in Al/128 ° Y-X LiNbO<sub>3</sub>, and we discussed the one of the possibility to change the direction of the frequency shift.

## ACKNOWLEDGEMNET

The authors wish to acknowledge Professor Kazuhiko Yamanouchi, emeritus professor of Tohoku University for the discussion about the tunable SAW resonator.

## REFERENCES

- 1) K.Yamanouchi, H.Odagawa and F.Iwai, "Tunable Transversal and Resonator Filters Using the Variable Velocity Inter-Digital Transducers with the Variable Capacitors and Gaps", IEEE Ultrason.symp. proc, 2014
- 2) Japan Society for the Promotion of surface acoustic wave device technologies 150 Committee, "Acoustic wave device technology" (in Japanese), SBN: 978-4274036309, pp217-227, 2004.

# Research and design of short distance interactive RGB LED matrix blocks

LE Manh Hien<sup>1</sup>, TRAN Duc Nam<sup>1</sup> and NGUYEN Trung Hieu<sup>2</sup>

<sup>1</sup> Student, Faculty of Electronics Eng., Posts and Telecommunications Institute of Technology  
(Km 10, Nguyen Trai Road, Hadong dist., Hanoi, Vietnam)  
E-mail: [nakihima@gmail.com](mailto:nakihima@gmail.com)

<sup>2</sup> Professor, Faculty of Electronics Eng., Posts and Telecommunications Institute of Technology  
(Km 10, Nguyen Trai Road, Ha dong dist., Hanoi, Vietnam)  
E-mail: [hieunt@ptit.edu.vn](mailto:hieunt@ptit.edu.vn)

**Abstract –** This article presents the research and design of RGB LED (Red-Green-Blue Light Emitting Diode) matrix blocks with ability of wireless interaction in short distance. Thanks to using LED Scanning method combines with 8-bit BCM (Binary Code Modulation), more than 16 million colors can be created in one pixel without depending on microcontroller's peripheral-control function. Besides, based on the result from the research of communication between 2 pieces of juxtaposed PCB (Printed circuit board), we also developed a method which allows communication through four edges among LED blocks.

**Keywords :** Interactive RGB LED matrix blocks , RGB LED matrix scanning using BCM.

## 1. INTRODUCTION

Nowadays, with the Internet of Things (IoT) trend, people want devices that can connect to each other. Adapt to this, we research and design wireless interactive LED RGB matrix blocks in short distance.

This paper will be presented as follow: Section 2 will describe the research of RGB LED scanning based on 8-bit BCM, we can create 16 million new colors from 3 basic colors on 1 pixel. Section 3 presents algorithm is used to control the interactive LED RGB matrix blocks. While, hardware and product design is describe in Section 4.

## 2. RGB LED SCANNING

We usually use PWM (Pulse Width Modulation) [1] method to control LED (Light Emitting Diode). It's simple but requires many peripheral from micro-controller, or IC (integrated circuit), this can enlarge the cost for fabrication. So we developed a LED matrix scanning technique using 8-bit BCM which can create 16 million colors without the need of complex peripherals for microcontroller, just use shift register ICs: 74HC595, MBI5024.

### (1) 8-bit BCM

With 8-bit BCM, we create 8 period of time, where each period is double the time of its precedent. It's similar to shift bit one time to left ( $<<1$ ), new value is double than the previous.

For example: 8-bit BCM and LED scanning, image dot 1x1, 40% bright

Solution: with 8-bit BCM  
 $DEC(40) = BIN(00101000)$

Each scanning one row, we have bright at bit 4,6 (as shown in figure 1)

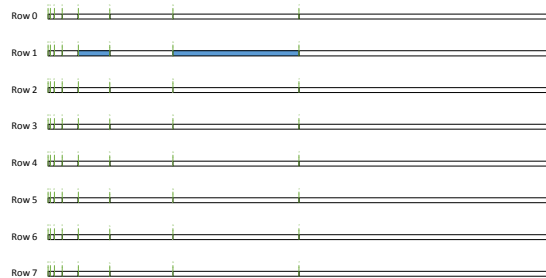


Figure 1 LED scan cycle using BCM

When start new period of time, some tasks are needed for the LED to work in right key point. As shown in the figure 2. The timeline from bit 4 to bit 7 in one cycle, called Tick\_bit which is described in figure 3.

We use timer to specify the time period of BCM bit . At the end of the bit period, Enable Pin of MBI5024 is pulled up and, then a pulse (short time high level pulse) is created on the latch pin (Latch) for updated data to display the next bit . The signals generated on Enable Pin and Latch Pin, you can easily create by using the Comparator of Timer. ShiftOut command is used to shift the display data (16 bits) to MBI5024 Pin. This instruction will be executed when received

rising edge of Enable pulse by sending requests to DMA (Direct Memory Access). Value transmitted in ShiftOut function will decide which bit is set, which bit is cleared.

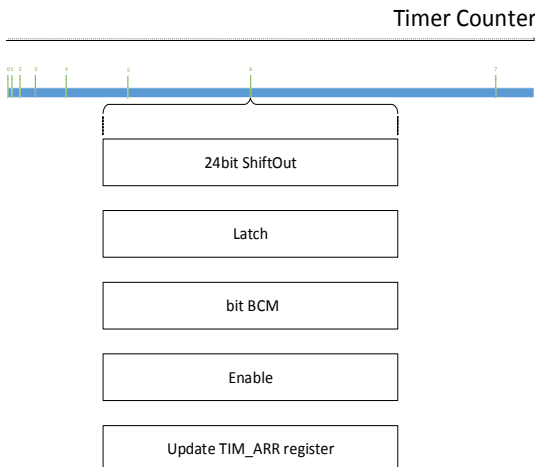


Fig. 2: Task in interrupt

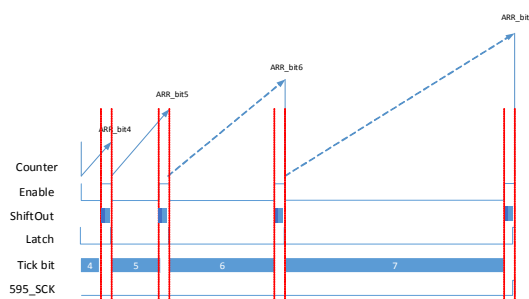


Fig. 3: Timeline

## (2) Compare between BCM and PWM

### - Hardware PWM

- Very well known method
- Easy to use
- Accurate output of a single frequency
- Suitable for all types of output: motors, LEDs, Servo motors.
- Can have a very high frequency

### - Software PWM

- Well known
- Multiple channels possible
- Suitable for all types of output: motors, LEDs, Servo motors.

### - 8-bit BCM

- Less well known
- Can run as many channels as you like
- Suitable for frequency insensitive outputs,

such as LEDs, bulbs and DC motors.

- Not suitable for servo motors.
- This is an excellent solution for LEDs.

## 3. TRANSMISSION BETWEEN LED BLOCKS

With new technology which enable data transmission between 2 pieces of PCB base on “capacitive technology” [2, 3, 4], we design 4 PCBs in 4 sides of each block. We have 4 LED blocks which can be arrange in 1X4 and 2x2 matrixes. We choose 1 LED block to be a leader, and the others are slave. Leader block will change the displayed data when we press the mode changing button. Others blocks will receive and analysis data on one side and transmit to other block through “connected” side.

### (1) Transmission algorithm

#### a) Transmitter algorithm

Figure 4 shows an algorithm for the transmitter.

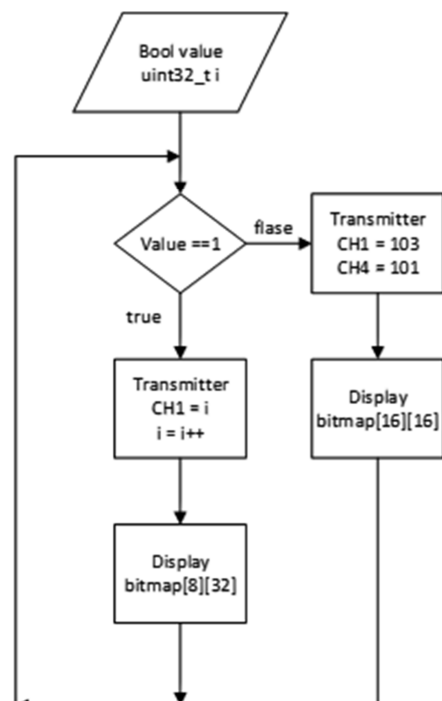


Fig. 4: Transmitter algorithmic diagram

#### b) Receiver algorithm

Receiver algorithm is presented in Figure 5.

### (2) Rotate bitmap algorithm

A rotate bitmap algorithm is used to solve the problem of how to rotate image bitmap in right way when moving the LED blocks.

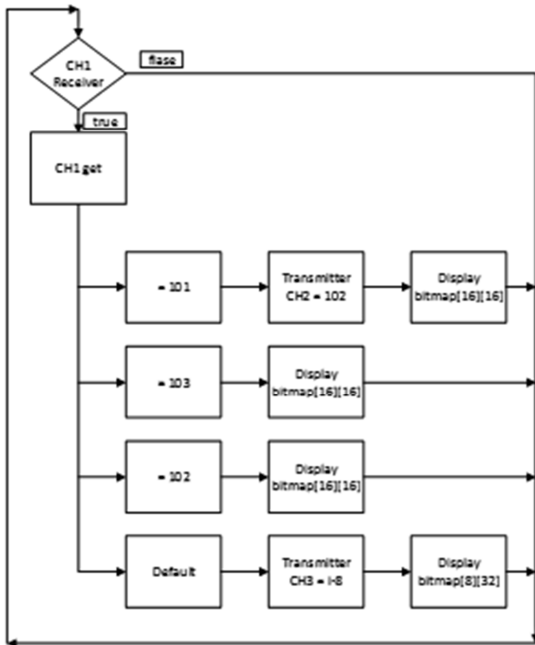


Fig. 5: Receiver algorithmic diagram

To do so, four matrixes bitmap are used in which the value zero stands for the boundary of the block. The proposed algorithm automatically figures out which way to change in the -Ox, -Oy, Ox, Oy axis.

Consider an example with a bitmap values:

`uint32_t bitmap[8][8] =`

```
{
{ 1, 2, 3, 4, 5, 6, 7, 8 },
{ 9, 10, 11, 12, 13, 14, 15, 16 },
{ 17, 17, 19, 29, 21, 22, 23, 24 },
{ 25, 26, 27, 28, 29, 30, 31, 32 },
{ 33, 34, 35, 36, 37, 38, 39, 40 },
{ 41, 42, 43, 44, 45, 46, 47, 48 },
{ 49, 50, 51, 52, 53, 54, 55, 56 },
{ 57, 58, 59, 60, 61, 62, 63, 64 };
};
```

After rotating bitmap 90 degree anti-clockwise, new bitmap values are:

`uint32_t bitmap_90[8][8] =`

```
{
{ 8, 15, 24, 32, 40, 48, 56, 64 },
{ 7, 15, 23, 31, 39, 47, 55, 63 },
{ 6, 14, 22, 30, 38, 46, 54, 62 },
{ 5, 13, 21, 29, 37, 45, 53, 61 },
{ 4, 12, 20, 28, 36, 44, 52, 60 },
```

```
{
{ 3, 11, 19, 27, 35, 43, 51, 59 },
{ 2, 10, 18, 26, 34, 42, 50, 58 },
{ 1, 9, 17, 25, 33, 41, 49, 57 }
};
```

The same process can be done with the rotating bitmap  $180^\circ$  or  $270^\circ$ .

## 4. HARDWARE DESIGN

### (1) Automatic power

We design auto power circuit to save energy; it can switch on/off flexibly. In ON mode, we can switch it on by a power button, or shaking the LED block. In one minute, without interact between LED block, it will automatically OFF. User can also switch off the system by shake the LED blocks 3 times or push the power button. Figure 6 shows the schematic of automatic power circuit:

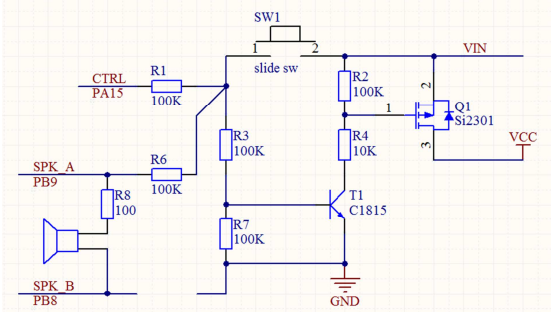


Fig. 6: Automatic power schematic

The operation of the schematic shown in figure 6 is explained as follow:

1. Using switch mode:
  - a. CTRL(PA15) pin is initiated at GPIO\_Output\_Pull\_Up by MCU. When SW1 is pressed, Q1 (Si2301) is On, then VCC will be activated by VIN
  - b. When OFF conditions is met. CTRL(PA15) is set to GPIO\_Output\_Pull Down.
2. Active by shaking mode:
  - a. A pulse is generated by buzz sensor, this make transistor T1 (C1815) to Enable state and then Q1 (Si2301) is ON
  - b. Q1 (Si2301) is OFF, when 3 pulses is detected.

### (2) Design a control circuit

We use ARM Cortex M3 – STM32F1. MBI5024 to control 24 row LED cathode, and 74HC595 to control 8 column LED anode.

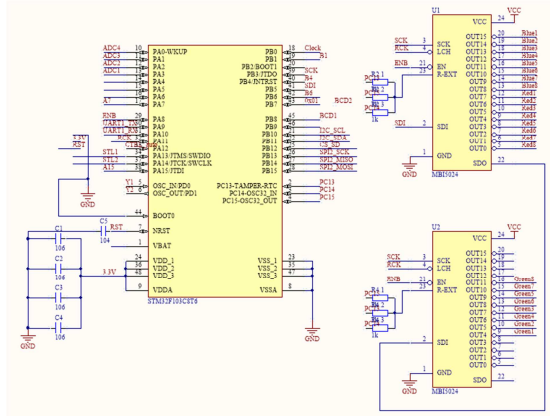


Fig. 7: Control schematic

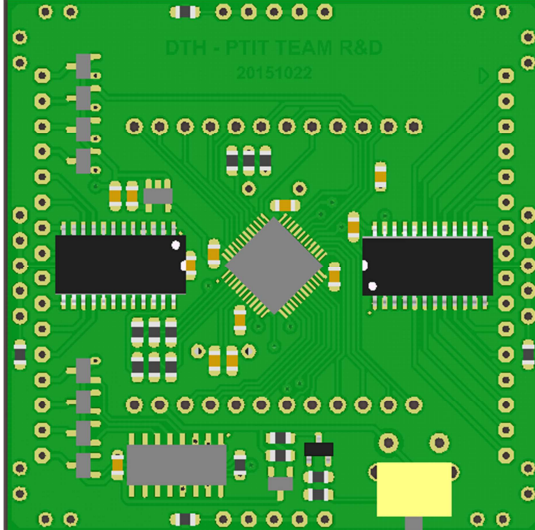


Fig. 8: PCB in 3D

## 5. CONCLUSION

After versions were tested and evaluated. The project was completed according to the target.

- Completely new RGB LED matrix scanning
- Flexible interact LED RGB matrix blocks
- Automatic power
- Easily create bitmap image

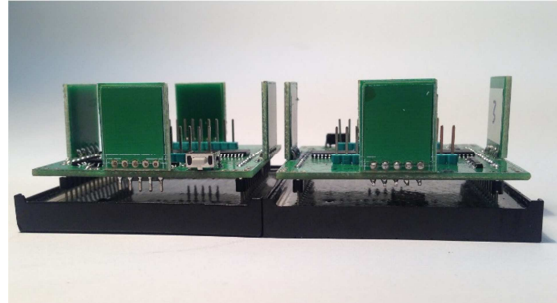


Fig. 9: Product photo



Fig. 10: Product photo

## REFERENCES

- 1) J. Huang, K. Padmanabhan, and O. M. Collins, "The sampling theorem with constant amplitude variable width pulses", IEEE transactions on Circuits and Systems, vol. 58, pp. 1178 - 1190, June 2011.
- 2) Narek Pezeshkian: Close-proximity communications system using capacitive coupled signal transfer, US8396136 B1.
- 3) George Kaplun, Alexander Rozin: Capacitive coupled bi-directional data and power transmission system, WO1998001905 A1.

(Received Nov 19, 2015)

# Led modules design using Binary Code Modulation (BCM)

NGUYEN Van Huy<sup>1</sup>, NGUYEN Van Quan<sup>1</sup>, VU Kha Khoi<sup>1</sup>

<sup>1</sup> Student, Faculty of Electronics Eng., Posts and Telecommunications Institute of Technology  
(Km 10, Nguyen Trai Road, Ha Dong Dist., Hanoi, Vietnam)  
E-mail: [huynguyend12dt1@gmail.com](mailto:huynguyend12dt1@gmail.com)

**Abstract--** This paper summarizes our research about LED brightness control methods using Binary Code Modulation (BCM). This is a new approach which uses the principle of turning LED On/Off in a very short interval so that human eyes can't distinguish and therefore, can control LED brightness. The applications of BCM in designing RGB LED Module and Ring LED using low-cost STM8 microcontroller which serve in the field of teaching and learning are also presented in this paper.

**Key Words :** binary code modulation, pulse width modulation, RGB LED, datasheet STM8.

## 1. INTRODUCTION

Nowadays, with the development of LEDs - we can see many of its applications in modern life: display unit, traffic lights, etc. LED has many advantages: Energy saving, a large variety of size, shape, color... It is very popular. A question raised: "Can we change its brightness? If yes then how?"

Push Width Modulation (PWM) is the most common method to do that. PWM adjusts output voltage, it's based on changing square pulse's width resulting in output voltage change. The parameters are: Time period (fixed) and Duty Cycle (variable)<sup>[1][2]</sup>. Figure 1 shows an example:

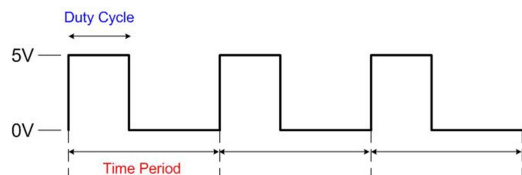


Fig. 1 Time period of each bit in BCM

PWM adjust duty cycles resulting in LEDs brightness changes. However, because PWM pins are usually limited on Microcontrollers, this method is more common in engine controlling than LEDs. There is another method called Binary Code Modulation (BCM). Similar to PWM, it turns LEDs on/off so fast human eyes can't see. The brightness level is a result of the average amount of time the LED is on versus when it is off. This is called duty cycle and although it can be the same percentage for both PWM and BCD, there is a fundamental difference.

While PWM usually uses a cyclical on/off cycle (30% on, 70% off, repeat) BCD uses a cumulative cycle. Each successive bit of binary code carries double significance compared to the previous bit. Now just assign a duty cycle based on your precision, and have an interrupt fire for each bit of the counter. With this method, we can use any I/O pins on Microcontrollers. In addition, it can be effectively combined with buffer IC like HC595, MBI5024<sup>[3]</sup>.

This method can be used for researches and LED modules designing using STM8 cheap Microcontrollers made by STMicroelectronics for studying, and teaching purpose.

## 2. BCM OPERATING PRINCIPLE

Binary Code Modulation (also known as Bit Angle Modulation) makes use of a key property of binary numbers<sup>[4][5]</sup> : As you work up through each digit (from the least-significant to the most-significant), the weight of each bit doubles in value.

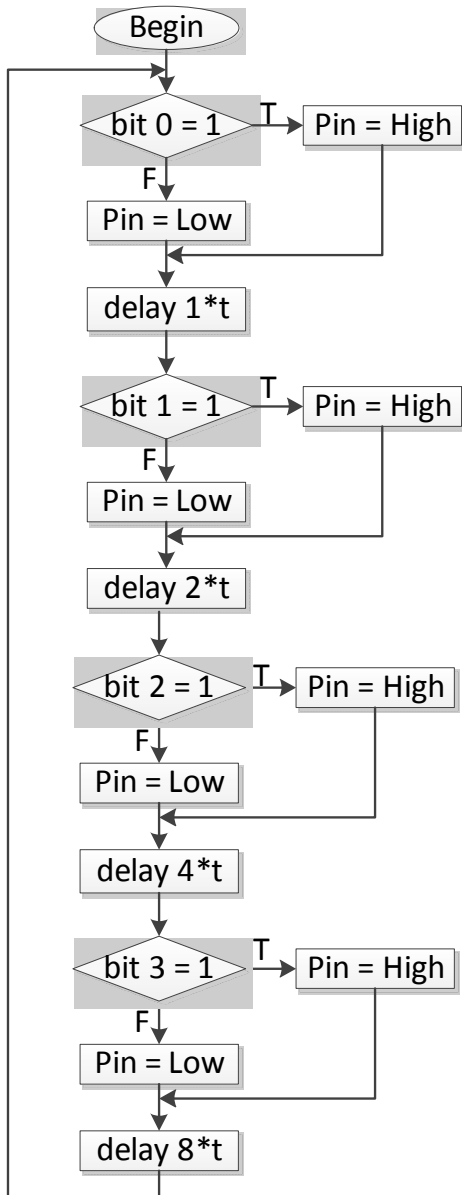


Fig. 2 Time period of each bit in BCM

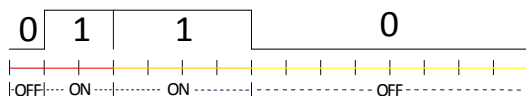
Considering a pulse diagram presented in Figure 2, If we have a 4-bit code e.g. 0110, it will represent a decimal value of 6 ( $0 + 2 + 4 + 0$ ). We'll turn the LEDs corresponded to the Binary bits. Then we can display an LED at a duty cycle of 6/15ths. We'll light the LED in the following manner:

- OFF for 1 tick (because the bottom bit is a 0)
- ON for 2 ticks (because the next bit is a 1)

- ON for 4 ticks (because the next bit is a 1)
  - OFF for 8 ticks (because the top bit is a 0)
- Figure 3 presents an algorithm diagram for this situation



**Fig. 3** The algorithm diagram



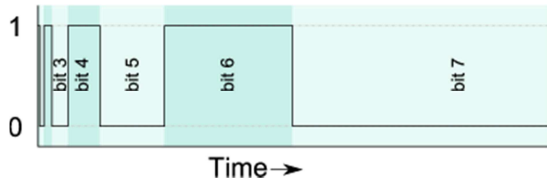
**Fig. 4** Time period of each bit in each cycle

Figure 4 shows the result if we repeat the cycle. This would mean that in each cycle of 15 ticks (1+2+4+8), the LED would be on for 6 ticks (0+2+4+6). This 4-bit process can be easily extended to 8-bits (or even

further). For example, to display an LED at 33% duty cycle with 8-bit precision, we simply take the 8-bit binary representation of 33%, which is 85/255ths or 01010101 in binary. Therefore, if we light the LED in the following manner:

- ON for 1 tick (because bit 0 is 1)
- OFF for 2 ticks (because bit 1 is 0)
- ON for 4 ticks (because bit 2 is 1)
- OFF for 8 ticks (because bit 3 is 0)
- ON for 16 ticks (because bit 4 is 1)
- OFF for 32 ticks (because bit 5 is 0)
- ON for 64 ticks (because bit 6 is 1)
- OFF for 128 ticks (because bit 7 is 0)

Then we will get the following output presented in Figure 5:



**Fig. 5** 85/255th duty cycle

It means that the LED will have been on for 85 of the total 255 ticks. That's 33% of the time, just as required. Now we can generalize what must be done in each time slice of the binary pattern:

- Set all LEDs according to bit n of their duty cycle value.
- delay for 2n ticks.

Note that the above process must be repeated for each of the bit positions in the duty cycle value.

An implementation of BCM would rely on interrupts to provide the delays between bit-changes. For n-bits of precision, n interrupts would fire per cycle, one interrupt for each bit-position. This overhead is fixed regardless of the number of channels. Therefore, if we use a 16 channels system instead of 8 channels, the overheads are the same.

This channel-independent overhead means that BCM is ideal for running large numbers of LEDs. It uses a predictable amount of processor power, regardless of the duty cycles chosen - There are no 'special cases' for 0% or 100% duty cycles.

The important thing is the length accurately doubles in each period of time. We will use the timer/counter on Microcontrollers to create it for each bit. Each time the timer ends we'll interrupt once for each bit. During interruption we only turn LEDs on/ off and reset the counter for the next interruption. Using BCM method to adjust LEDs brightness, we need to pay attention to 2 parameters: Cycle time needs to be less than 50ms and interruption time needs to be less

than bottom bit's

### 3. STM8 MICROCONTROLLER

The STM8 is a 8-bit microcontroller family made by STMicroelectronics. Similar to other microcontrollers, STM8s are equipped with basic peripheral devices like: GPIO, 10-bit ADC, 3 timer, UART interface, SPI, I2C, PWM, etc. 128 bytes EEPROM, 8k Flash. STM8s are able to operate at 2 power levels: 3.3V and 5V. This family also comes with a complete peripheral interface library, using C programming language and STVP translator. STM8 Microcontrollers load up programs using SWIM interface. Moreover, STM8s are much cheaper compare to other microcontrollers of the same speed like AVR, PIC. With the cost ranging from 6,000 to 20,000 VND/each, it is suitable for small applications<sup>[6][7]</sup>. Figure 6 shows a STM8S003F3 diagram.

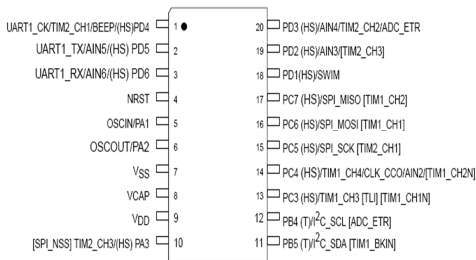


**Fig. 6** STM8S003F3 diagram

Instead of using DELAY we'll use a comparing interruption timer in Arduino. We must calculate HIGH and LOW value at each bit position and store them in an array called setLed. cTime stores compare value in counters. We only need to turn LEDs on/off and update OCR1A during interruption then increase the counter for the next bit.

### 4. COMPACT LED MODULE DESIGN

#### (1) Introduction

##### (a) RGB color model

RGB color space or RGB color system, constructs all the colors from the combination of the Red, Green and Blue colors<sup>[1]</sup>. The red, green and blue us 8 bits each, which have interger values from 0 to 255. This makes  $256 \times 256 \times 256 = 16777216$  possible colors<sup>[2]</sup>. When the red pixel is set to 0, the LED is turned off. When the red pixel is set to 255, the LED is turned fully on. Any value between them sets the LED to partial light emission<sup>[3]</sup>.

##### (b) System diagram

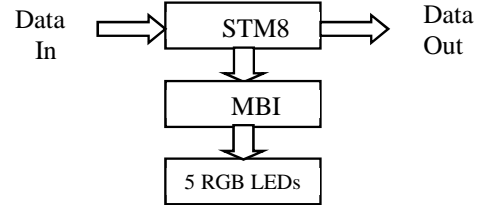


**Fig. 7** System diagram

The proposed system diagram is presented in Figure 7. The function of each block in the diagram is explained as the following:

- STM8 receives data and store the value to control 5 LED RGB. Each led consist of 3 bytes of data to control 3 colors Red, Green, Blue and have value from 0 to 255.
- After receiving enough data for 5 LEDs, it will transitory the data to the next module.
- STM8 uses BCM algorithm to control buffer currentent IC MBI 5024.
- LED is used to display.

#### (2) Frame data transmission and create interrupts BCM

##### (a) Frame data transmission

The module will receive data though the SPI interface. The transmission frame is described as follows:

- There are 32 zeros bits in the Start Frame that means the beginning of each transmission.
- LED Frame includes 32 bits 111 to detect the data frames, the next 5 bits are used to control the general brightness LED. The others 24 bits of data correspond with 3 colors R, G, B.
- End Frame includes 32 bits 1 to indicate the ending data transmission.

##### (b) BCM on STM8

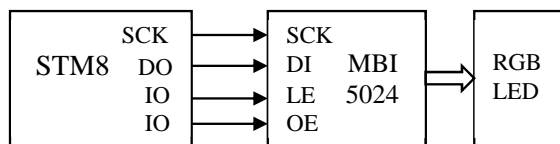


**Fig. 8** Connection diagram

The connection diagram is presented in Figure 8. The BCM is created by using the timer STM8 with 2 interrupts controller. Normally, a RGB Led needs 3 I/O pins to control it. In order to control 5 RGB Led, 15 I/O pins are needed. However, a STM8 has only two I/O pins so we will use the buffer IC (MBI 5024) to deal with the problem. MBI 5024 is an Integarted Circuit 16-bit shift registers serial input, parallel output, constant current is changed through an ex-

ternal resistor. MBI receives data from STM8 through SPI interface then sends the signal to the RGB LEDs.

### (3) PCB design

Figure 9 shows the PCB design of the system. LEDs are arranged on the top layer. Other chips such as STM8 or MBI 5024 are arranged on the bottom layer.

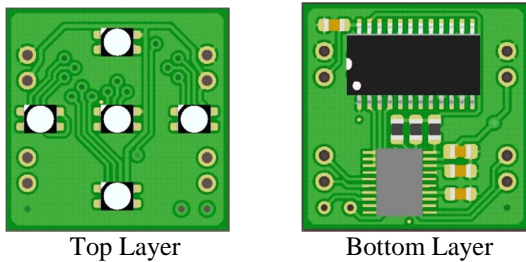


**Fig. 9** PCB design

## 6. CONCLUSION

The article introduced new methods to change the light intensity of RGB LED using Binary Code Modulation. The proposed method has some ad-

vantages over the normal methods such as PWM. In the experiment, the RGB LEDs module was designed. The module can receive data from other microcontrollers, then change the colors based on the received data.

## REFERENCES

- 1) F. Raab, B. Sigmon, R. Meyer and R. Jackson "L band transmitter using Kahn EER technique", *IEEE trans. On MTT*, pp.2200 -2224 1998
- 2) F. Raab "Intermodulation distortion in Khan-technique transmitter", *IEEE trans. on MTT*, 1996
- 3) M. Lentmaier, A. Sridharan, K. S. Zigangirov, and D. J. Costello, "Terminated LDPC convolutional codes with thresholds close to capacity," in Proc. IEEE Int. Symp. Information Theory (ISIT), Adelaide, Australia, Sep. 2005
- 4) Poynton, Charles A. (2003). *Digital Video and HDTV: Algorithms and Interfaces* Morgan Kaufmann.
- 5) Steve Wright (2006). *Digital Compositing for Film and Video*. Focal Press
- 6) Sun Lu, Jiang Jiu-chun, Yin Hang. Design of Procedure Downloads System Based on MC9S12 series MCU[J], Micro Computer and Information, 2010, 4-2: 64
- 7) STM8 SWIM communication protocol and debug module Technical Data[Z]. 2009

**(Received Nov 25, 2015)**

# Measurement of Resistance and Internal Inductance of Wide Iron Plate

Takuto OGATA<sup>1</sup>, Naru HIRATA<sup>1</sup> and Yosifumi SHIMOSHIO<sup>2</sup>

<sup>1</sup> Student, Electronics and Information Systems Engineering Course,  
National Institute of Technology, Kumamoto Colegge  
(2659-2, Suya, Koushi-shi, Kumamoto 861-1102, Japan)

E-mail:ae14ogata@g.kumamoto-nct.ac.jp, E-mail:ae14hirata@g.kumamoto-nct.ac.jp  
<sup>2</sup> Professor, Electronics and Information Systems Engineering Course,  
E-mail:shimoshio@kumamoto-nct.ac.jp

**Abstract** In this paper, we consider the measuremtn method of resistance and internal inductance of a wide iron plate. The wide iron plate is used instead of chassis of automobile to confirm the basic characteristics of it. First, we measured the resistance and inductance of a transmission line which consists of the plate and a conductor wire by Open-Short method. We obtained the resitance and internal inductance from the result by calculation. As the internal inductance relates with the permeability of the plate, it was measured and the relationship has been examined.

**Key Words :***Open-Short method, Mesh analysis, frequency characteristics*

## 1. INTRODUCTION

Many electric devices such as car navigation system and FM radio are equiped in an automobile to obtain more safety and more comfortable environment. For the automobile equiped many electric devices, it is important to know the electric characteristics of chassis. Because the electromagnetic interference generated by the electric devices may affect the performance or reliability of equiped electric devices because the impedance of the chassis.

An automobile chassis is used as a signal return line of electric devices or a reference potential. As the chassis has impedance characteristics, a potential difference arises at each point on the chassis when a current flows. The potential difference may cause a electromagnetic interference.

The chassis has complex mechanical structure because it is constructed by welding and screwing clamp. To investigate the basic characteristics of chassis, we assume the chassis which has complex mechanical structure as a wide conductor plate which has simplex structure. We measure the impedance characteristics of the conductor plate to confirm a frequency characteristics of resitance and inductance. When we measure the impedance such large plate, a long measurement cable is needed. Therefore, the the measured value includes the inductance by thelong measurement cable. To remove this undesired inductance, we proposed a new method using Open-Short method. It is a method for obtaining the primary constants ( $R$ ,  $L$ ,  $G$ ,  $C$ ) of a transmission line. In this paper, the resistance( $R$ ) and inductance( $L$ ) of a wide conductor plate are analyzed. Laying a thin copper wire on the conductor plate makes a single-ended trans-

mission line, and we measure the impedance characteristics of it by the Open-short method.

It is known that the the frequency characteristics of conductor wire and it includes high frequency effect by a skin effect [1]. At the low frequency area, there is no influence of high frequency resistance and the resistance is determined by the length, diameter, and resistivity of the conductor wire. Hence, measuring the resistance of the primary constants with good accuracy is difficult because the resistance is small at the low frequency area. About the inductance, as the conductor plate has permeability, it affects the measured inductance value. We examined the frequency characteristics of permeabilty at low frequency area by measuring the inductance of conductor plate.

## 2. OPEN-SHORT METHOD

A transmission line can be represented as an equivalent circuit by a distributed constant circuit which consists of primary constants:  $R$ ,  $L$ ,  $G$ , and  $C$  as shown in Fig. 1. The constants are measured by using an Open-Short method. By using the primary constants, the characteristic impedance of transmission line:  $Z_0$  and the propagation coefficient:  $\gamma$  are represented as Eq.(1) and (2).

$$Z_0 = \sqrt{\frac{R_0 + j\omega L_o}{G_0 + j\omega C_o}} \quad (1)$$

$$\gamma = \sqrt{(R_0 + j\omega L_o)(G_0 + j\omega C_o)} \quad (2)$$

where,  $R_0$ ,  $L_o$ ,  $G_0$ , and  $C_o$  show per unit length value. The propagation coefficient consists of attenuation constant::  $\alpha$  and phase constant:  $\beta$ .

$$\gamma = \alpha + j\beta \quad (3)$$

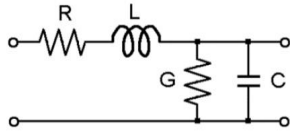


Fig. 1 Distributed constant circuit

The attenuation constant:  $\alpha$  and the phase constant:  $\beta$  for a transmission line with the line length:  $l$  are shown as follows.

$$\alpha l = \frac{1}{2} \tanh^{-1} \frac{2 \sqrt{\left| \frac{Z_s}{Z_f} \right|} \cos \frac{\theta_s - \theta_f}{2}}{1 + \sqrt{\left| \frac{Z_s}{Z_f} \right|}} \quad (4)$$

$$\beta l = \frac{1}{2} \tanh^{-1} \frac{2 \sqrt{\left| \frac{Z_s}{Z_f} \right|} \sin \frac{\theta_s - \theta_f}{2}}{1 - \sqrt{\left| \frac{Z_s}{Z_f} \right|}} \quad (5)$$

where,  $Z_f$  and  $Z_s$  are input impedance of the transmission line when the end terminal of the transmission line is open or short. Each value is represented as follows:

$$Z_f = |Z_f| e^{-i\theta_f} = \frac{Z_0}{\tanh \gamma l} \quad (6)$$

$$Z_s = |Z_s| e^{i\theta_s} = Z_0 \tanh \gamma l \quad (7)$$

where,  $\theta_f$  and  $\theta_s$  are phase angle of each input impedance. The primary constants are obtained from Eqs (1), (2), (6) and (7).

$$R_0 = \sqrt{\left| \dot{Z}_f \dot{Z}_s \right|} \frac{(\alpha l \cos \xi - \beta l \sin \xi)}{l} [\Omega] \quad (8)$$

$$L_0 = \sqrt{\left| \dot{Z}_f \dot{Z}_s \right|} \frac{(\alpha l \sin \xi + \beta l \cos \xi)}{\omega l} [H] \quad (9)$$

$$G_0 = \sqrt{\left| \dot{Z}_f \dot{Z}_s \right|} \frac{(\alpha l \cos \xi + \beta l \sin \xi)}{l} [S] \quad (10)$$

$$C_0 = \sqrt{\left| \dot{Z}_f \dot{Z}_s \right|} \frac{(-\alpha l \sin \xi + \beta l \cos \xi)}{\omega l} [F] \quad (11)$$

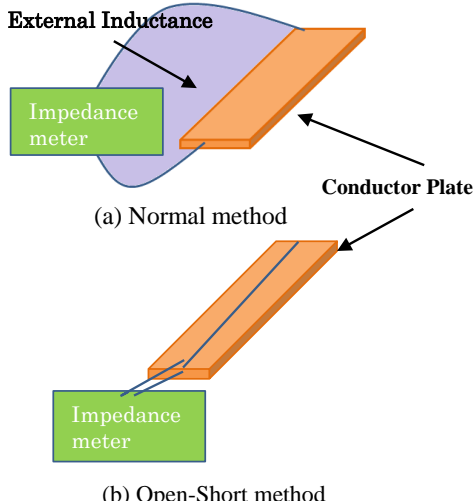


Fig. 2 Two kinds of impedance measurement.

where, phase angle of primary constant:  $\xi$  is

$$\xi = \frac{\theta_s - \theta_f}{2}. \quad (12)$$

As shown in Fig. 2(a), when the impedance of large plate is measured, a long probe is used to connect an impedance meter with the plate. Then the measured result includes the external inductance which is generated by the probe loop. Therefore it is difficult to obtain accurate measurement result because the external inductance affects measured value. Thus, we propose a new method that can extract a resistance and internal inductance of the conductor plate. The method is shown as Fig. 2(b). The resistance value which is obtained from Open-Short method includes the resistance of copper wire and conductor plate. The resistance of conductor plate is obtained by subtracting the resistance of copper wire from measured value.

### 3. Measurement of Impedance

As shown in Fig. 3, a conductor plate which size is 91cm in depth, 183cm in width, and 0.2cm in thickness was used and a copper wire is laid above the conductor plate. First we decided the plural measurement points on the conductor plate, and measure the impedance..

We measured the impedance by changing the height of copper wire above the conductor plate as shown in Fig. 4 to verify the influence of external inductance. The obtained inductance value which is obtained from the Open-short method should converge to the external inductance at high frequencies because an internal inductance becomes zero at high frequencies because of skin effect. The resistance of conductor plate changes depending on the measurement point in Fig. 4. Because the current distribution in the conductor plate which is affected by the electric field of copper wire. Figure. 5 shows the frequency characteristics of the internal inductance and the resistance which are calculated from measured impedance.

Figure. 5(a) shows that the resistance value is small when the wire is laid at middle of conductor plate because the current flows in the wide area of plate. However, the resistance converges almost same value at high frequencies because of skin effect. Figure. 5(b) shows the frequency characteristics of inductance. It can not be found any apparent characteristics from those results.

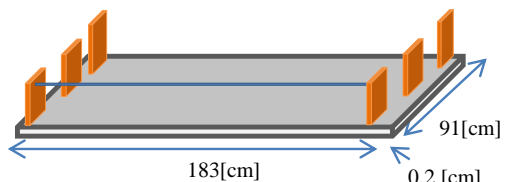


Fig. 3 Measurement of impedance on the conductor plate

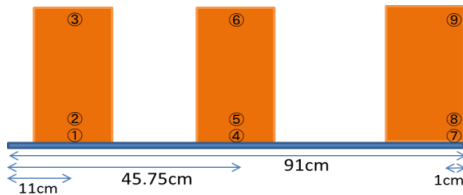
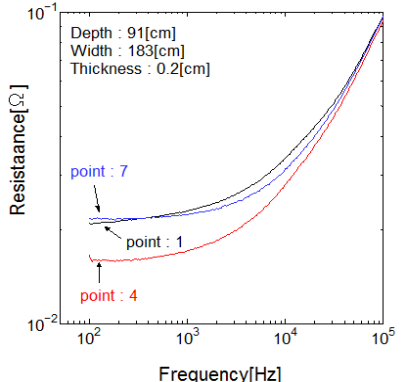
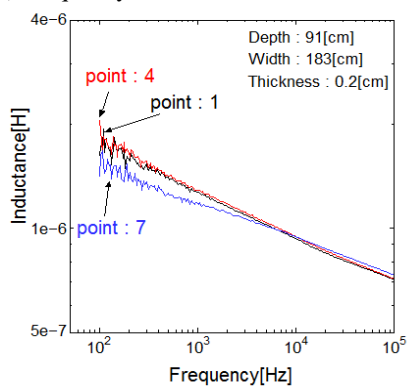


Fig.4 Measurement point of conductor plate



(a) Frequency characteristics of resistance



(b) Frequency characteristics of inductance

Fig. 5 Measured resistance and inductance.

### 3.1 Measurement of Inductance

The inductance of transmission line measured by the Open-short method includes three kinds of components as shown in Fig. 6. The measured inductance is  $L_m$ , the internal inductance of the copper wire which is laid above the conductor plate is  $L_{in,c}$ , the external inductance which is generated between the conductor plate and the copper wire is  $L_{ex}$ , and the internal inductance of conductor plate is  $L_{in,p}$ . As the internal inductance of copper wire is small to be neglected because the copper wire is very thin compared with the conductor plate. Thus the relationship becomes as follows:

$$\begin{aligned} L_m &= L_{in,c} + L_{in,p} + L_{ex} \\ &\approx L_{in,p} + L_{ex} \quad (\because L_{in,p} \gg L_{in,c}) \\ \therefore L_{in,p} &\approx L_m - L_{ex} \end{aligned} \quad (13)$$

We obtain the internal inductance of conductor plate by using Eq.(13).

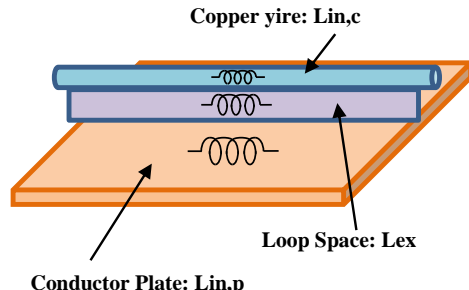


Fig. 6 Constitution of inductance of the conductor plate

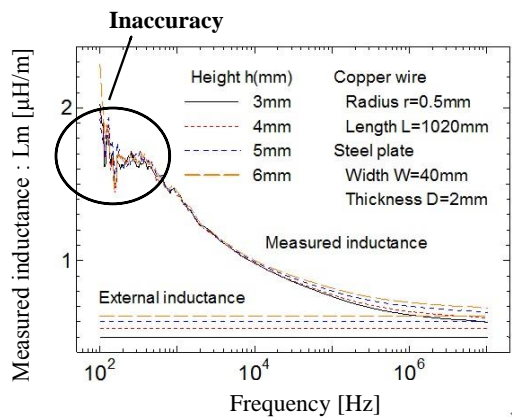


Fig. 7 Frequency characteristics of inductance

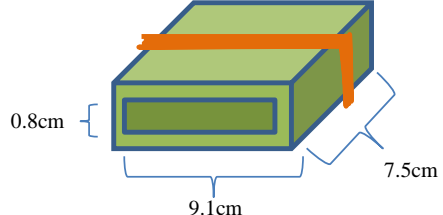


Fig. 8 Structure of air-core coil

Figure. 7 shows the frequency characteristics of measured inductance and calculated external inductance[1]. The measured inductance decreases at high frequency area and it converges to the external inductance value because the current is hard to flow in the conductor plate owing to skin effect. The calculated external inductance is flat because it is decided by the space between the wire and the plate and it has no frequency characteristic. It seems that the internal inductance of conductor plate at frequencies lower than 500Hz has flat frequency characteristics. It may relate to the permeability of the conductor plate. Therefore, we measure the frequency characteristics of inductance of iron plate and obtain permeability.

We make an air-core coil by winding coil around an insulator as shown in Fig. 8. The inductance when a conductor plate is inserted into the air-core coil is measured. The configuration of conductor plate is shown as follows:

Material : electro galvanized steel sheet  
Length : 1020[mm]  
Width : 20, 40, 80[mm]  
Thickness : 0.5, 1.0, 2.0[mm]

Figure 9 shows the frequency characteristics of a normalized inductance and relative permeability. The normalized inductance is obtained from dividing the measured inductance of the air-core coil inserted an conductor plate by the inductance of air-core coil itself. The relative permeability relates with internal inductance. Therefore, we define the relative permeability:  $\mu_s$  as below.

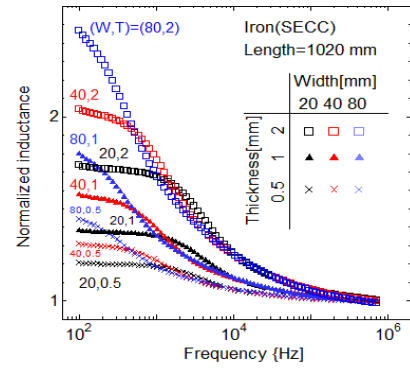
$$\mu_s = \frac{\mu}{\mu_0} = \frac{S}{S_p} \left( \frac{L_{measured}}{L_{aircore}} - 1 \right) \quad (14)$$

where,  $S$  is a cross section area of air-core coil and  $S_p$  is a cross section area of conductor plate. We confirmed that the change of inductance at low frequency area is flat and converges to the inductance of air-core coil itself at the high frequency area as shown in Fig. 9(a). The change at low frequency depends on permeability. Thus we are able to obtain the accurate characteristics of inductance against the previous result(Fig. 7). We obtained Fig.9(b) by calculating equation (14). It is evident from Fig. 9(b) that the permeability affects the internal inductance. Figure. 9(c) shows the details of the low frequency area in Fig. 9(b). The permeability becomes big value when both of width and thickness of conductor plate is narrow or thin. The thicknes of the plate may relates permeability. Thus, we have to examine the relationship.

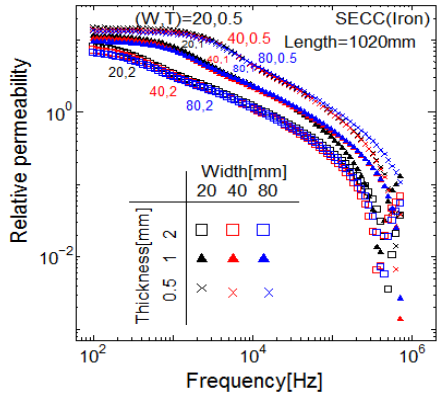
#### 4.Conclusion

We measured the impedance characteristics of a large conductor plate instead of automobile chassis to investigate the basic characteristics of the chassis. The basic characteristics are measured by Open-Short method to remove the influence of long measurement probe cable.

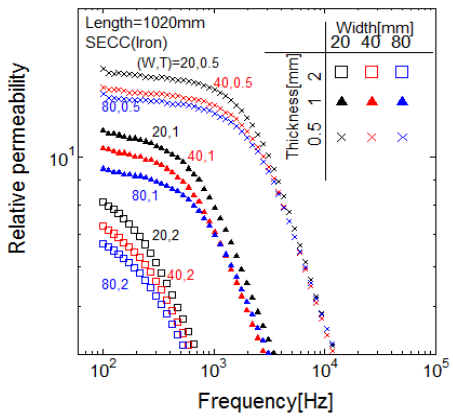
We confirmed that the resistance value and inductance value change depending on the place where the copper wire is laid above the conductor plate. As the measured resistance value is very small at low frequency area, it is difficult to obtain accurate value. Except this difficulty, the resistance value of the large conductor plate can be measured by Open-sort method. About the inductance, it also can be measured by using Open-hort method. If we subtract the external inductance, which is detrmined by the space between a copper wire and the conductor plate, from the measured inductance value, then the internal inductance of a conductor plate can be obtaianed. However, the permeability of conductor plate may infuence to the internal inductance. About the permeability, we need more investigation,



(a) Inductance value to air-core coil



(b) Relative permeability



(c) Details of relative permeability

Fig. 9 Frequency characteristics of normalized inductance and relative permeability

#### REFERENCES

- [1] T.Yokomitchi, Y.Shimoshio and Y.Miyazaki : Impedance Measurement Method for Wide and Flat Metal Plate by Using Open-Short Method, ISTS2013(2013).

# Development of Simple and Low-cost Weeding Robot

Tsubasa MURAKAMI<sup>1</sup>, Yoshifumi SHIMOSHIO<sup>2</sup>

<sup>1</sup> Student, Department of Information, Communication and Electronic Engineering,  
National Institute of Technology, Kumamoto College  
(2659-2 Suya, Koshi, Kumamoto, 861-1102 Japan)  
E-mail: te11t-murakami@g.kumamoto-nct.ac.jp

<sup>2</sup> Professor, Advanced course, National Institute of Technology, Kumamoto College  
E-mail:shimoshio@kumamoto-nct.ac.jp

In this paper, we describe the development of a simple and low-cost weeding robot. It is very hard for human to weed under hot or cold days. Actually the robot scratches and digs the ground surface a little. As it running for a long time and scratches many times, it can weed and any glass will not grow on there.

- *Key Words : weeding robot, crank, blade, geared motor, battery, Arduino*

## 1. Introduction

Recently various robots have been developed to assist human work. However, a weeding robot has not been developed yet because it is difficult to distinguish weeds from crops. In addition, there are several ways such as hand weeding or chemical weeding to remove weeds. But a hand weeding is time consuming and burden for farmers and the chemical weeding has a problem that the environment is contaminated. In this study, we are going to build a simple and low-cost robot that assists farmers' work. The robot under developing does not distinguish between weeds and crops to lower the cost and many difficulties in robot development. When the robot works in a field, the field where crop is grown will be enclosed by a wire or rope to prevent the robot entry to there. Thus a simple and low-cost robot can be realized.

## 2. Body structure and operation of Robot

### 2.1 Body structure

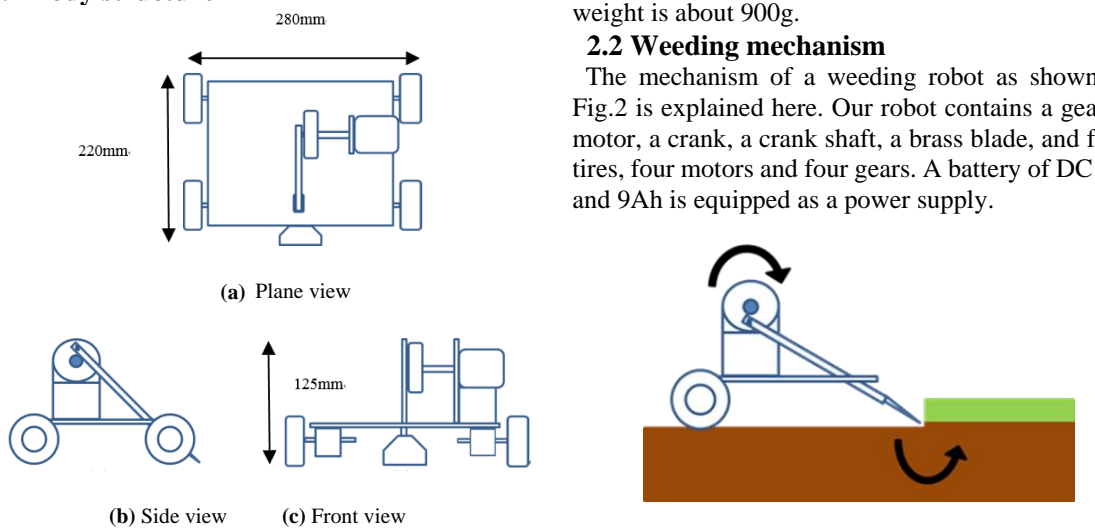


Fig.1 Body structure of robot under developing.

The robot under developing consists of two parts: weeding part and vehicle body part to run the robot. A crank mechanism is adopted for the weeding part. Comparing with other weeding mechanisms, it does not engulf weeds and it is safety. The vehicle body part uses tire to run the robot because it is easy to repair and good for stable running on the field. Figure 1(a) shows a plane view, Fig.1 (b) shows a side view, and Fig.1 (c) shows a front view of the robot respectively.

For the vehicle body part, a MDF (medium-density fiberboard) wooden board is used because it has stable strength and is suitable for machining. To scratch or cut weeds, a brass blade is used because it is suitable for machining although it has not enough strength for long-term use. As we are investigating whether the weeding mechanism or the shape of blade is suitable for our purpose, the wooden board and brass blade are used to develop several prototypes. The robot has the size that is 280mm in width, 220mm in depth, and 125mm in height. The total weight is about 900g.

### 2.2 Weeding mechanism

The mechanism of a weeding robot as shown in Fig.2 is explained here. Our robot contains a geared motor, a crank, a crank shaft, a brass blade, and four tires, four motors and four gears. A battery of DC 6V and 9Ah is equipped as a power supply.

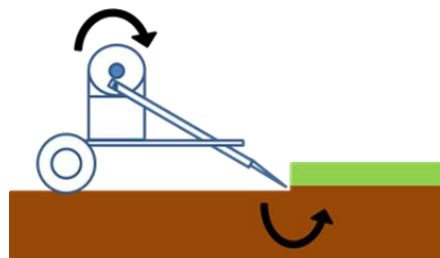


Fig.2 Weeding mechanism (Front tire is not drawn).

A crank is connected to the axis of a DC geared motor and a linked shaft to the crank moves back and forth according to the motor rotation. A brass blade is connected to the leading end of the crank shaft and it scratches ground surface so that the weeds on the ground surface are removed. Our robot cannot weed big weeds because the blade moves back and forth within only one or two centimeter and dig ground only one centimeter in depth. However the robot is always scratching ground surface so that any weeds do not grow.

The robot runs on a field and scratches the surface of the field. As our robot has no function to distinguish between weeds and crops, the robot weeds all of weeds and crops. To avoid weeding crops, a wire or a rope is used to keep the robot entering the crops filed. When the robot touches a rope or wire, then it turns to any direction which is decided randomly.

### 2.3 Running mechanism

Our robot is equipped with four tires, gears, and motors to run on a field. A small computer controller, Arduino UNO Rev.3, is used to control the running operation. To detect a wire or rope, several touch sensors are used. When the sensors detect a rope or wire, the robot turns automatically to random directions. Our robot which dissipates around 6W is able to run continuously for about 9 hours by using a 6V and 9Ah battery as power supply.

The width of the brass blade is 10cm. If the crank on the robot rotates at a speed of 5 turns/sec and the blade scratches 10cm<sup>2</sup>/turn, then the blade can weed 50cm<sup>2</sup>/sec. Thus the robot can weed 50x3600x9 = 162m<sup>2</sup> in nine hours.

## 3. Experimental result

### 3.1 Weeding movement

We have done to make the first prototype robot as shown in Fig.3 which has a function for weeding but it has no function to run although four tires are already equipped.

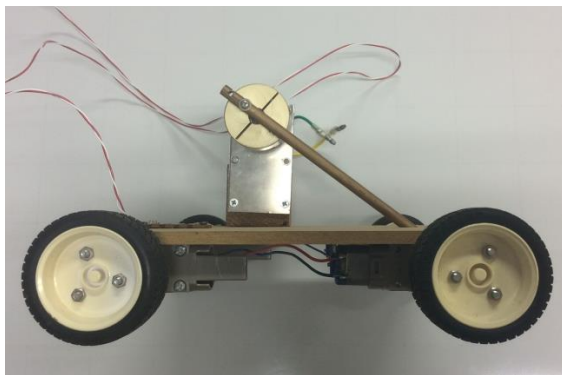


Figure.3 Developed prototype robot.

A test run by the developed prototype robot has performed on the blank space in our campus where weeds grow on it partially. As a result, it has confirmed that our robot can weed glasses by scratching and digging the ground surface. However, when the blade digs ground and the ground surface is hard, the front part of the robot rose up by the repelling force of the hard ground. To control this undesired force, it is essential to adjust the weight of robot keeping the blade from breaking.

### 3.2 Running movement

When the surface of the ground where a robot is running is irregular, it is impossible to keep stable run and weeding operation. Because the surface of ground where to be scratched by a blade is lower or higher than the bottom of the robot's tire at some places so that the blade cannot reach to the weed at there while the robot is running. To improve this unexpected movement of the robot, we will take one of the following countermeasures:

- (1) to use a large tire with suspension: if a large tire with suspension is used, then it can be reached to weeds even the ground surface is not flat.
- (2) to use a blade with suspension mechanism: if a blade with suspension is used, then the blade can reach to a ground surface.

## 4. Conclusion and future plan

We are developing a weeding robot for assisting humans who are working under heavy weather conditions and for preventing chemical prolusion by spraying herbicide onto the land. It will be very useful for humans if we could success to build it. Until now, we have made a very simple prototype robot using a blade, a crank and one geared motor for weeding and four tires, gears, and motors for running. Then we have examined whether it can actually weed or not.

As a result of test run, we have confirmed that the blade can remove weeds. However there are two problems and they need appropriate countermeasures. The first problem is rising up of the front part of the robot and it will be a good countermeasure to adjust the weight of the robot to control the rising up. The second one is moving away the blade from the surface of a ground by unflattens of the ground surface. We will examine three countermeasures that described in 3.2 to find which one is the best solution.

As the future tasks in addition to examine the above countermeasures, we have to make software to control the running function of the robot, especially to control turns when the robot touches a rope or wire which prevents entering the robot into crops field.

# Investigation of beta-gallium oxide phase transition temperature on sapphire substrates

Hiroshi OGATA<sup>1</sup>, Hiroki ISHIMOTO<sup>2</sup>, Shinichiro KOBA<sup>3</sup>, Isao TSUNODA<sup>4</sup>  
and Kenichiro TAKAKURA<sup>5</sup>

<sup>1</sup> Student, Department of Information, Communication and Electronic, Engineering,  
National Institute of Technology, Kumamoto College  
(2659-2, Suya, Koshi, Kumamoto 861-1102, Japan)  
E-mail:tel1ogata@g.kumamoto-nct.ac.jp

<sup>2</sup> Student, Advanced Course of Electronics and Information Systems Engineering,  
National Institute of Technology, Kumamoto College  
(2659-2, Suya, Koshi, Kumamoto 861-1102, Japan)  
E-mail:ae15ishimoto@g.kumamoto-nct.ac.jp

<sup>3</sup> Professor, National Institute of Technology, Kumamoto College  
(2627 Hirayamashin-Machi, Yatsushiro, Kumamoto 866-8501, Japan)  
E-mail:koba@kumamoto-nct.ac.jp

<sup>4</sup> Associate Professor, National Institute of Technology, Kumamoto College  
(2659-2, Suya, Koshi, Kumamoto 861-1102, Japan)  
E-mail:isao\_tsunoda@kumamoto-nct.ac.jp

<sup>5</sup> Associate Professor, National Institute of Technology, Kumamoto College  
(2659-2, Suya, Koshi, Kumamoto 861-1102, Japan)  
E-mail:takakura@kumamoto-nct.ac.jp

Gallium oxide ( $\text{Ga}_2\text{O}_3$ ) films are prepared by RF magnetron sputtering at room temperature. Phase transition of the films on sapphire substrates is studied by annealing with different temperature. As a result of the investigation, the films are changed into  $\beta$ - $\text{Ga}_2\text{O}_3$  from amorphous between 425°C and 450°C. Regarding optical transmittance, the former film kept high transparency of above 80%, and the latter film kept higher transparency of above 90% in the wavelength of over 350 nm.

**Key Words :** Gallium oxide, Phase transition, Transparent conducting oxide, Sapphire substrate, Sputtering

## 1. INTRODUCTION

Nowadays, the transparency conductive oxides (TCOs) are used for display, touch panel and solar battery. As the condition that the TCOs should meet, its conductivity is less than  $1 \times 10^{-3} \Omega\text{cm}$ , and the transmittance at the wavelength range between 380 nm and 780 nm is established more than 80%. The most of the TCOs are covered with Indium doped Tin Oxide (ITO) now. However, Indium is one of the rare metal, and it is expensive. The development of substitute materials reducing consumption of the Indium is demanded immediately,  $\beta$ - $\text{Ga}_2\text{O}_3$  attracts attention as the candidate material.

Previous studies show that  $\text{Ga}_2\text{O}_3$  films have five crystalline phases of  $\alpha$ ,  $\beta$ ,  $\gamma$ ,  $\delta$ , and  $\varepsilon$ <sup>1)</sup>. Of all phases,  $\beta$  phase is the most stable at high temperature<sup>2)</sup>. Various types of growth technique are available to obtain  $\beta$ - $\text{Ga}_2\text{O}_3$  films, such as molecular beam epitaxy

(MBE), pulsed laser deposition, sputtering and chemical vapor deposition (CVD)<sup>3-6)</sup>. Among these, we have fabricated  $\text{Ga}_2\text{O}_3$  films using RF magnetron sputtering at room temperature (RT). Because sputtering can deposit flat  $\text{Ga}_2\text{O}_3$  films to a large area in a shorter time<sup>7)</sup>. It is very effective method for the large area of the solar battery with  $\beta$ - $\text{Ga}_2\text{O}_3$ . After RT deposition, the films were annealed at high temperature to obtain  $\beta$  phase. From our previous study regarding  $\beta$ - $\text{Ga}_2\text{O}_3$  on silicon substrates, phase transition temperature from amorphous film to  $\gamma$  and  $\beta$  mixed phases is grown at over 600°C, and the  $\beta$  single phase is grown at 900°C<sup>8)</sup>. However, Oshima *et. al.* reported that  $\beta$ (-201) oriented film is epitaxially grown at 800°C as the most suitable growth temperature on sapphire ( $\alpha$ - $\text{Al}_2\text{O}_3(0001)$ ) substrate by MBE<sup>3)</sup>. It has been expected that  $\beta$ - $\text{Ga}_2\text{O}_3$  low temperature growth on sapphire substrates which enable epitaxial growth

by our method.

In this paper, we have clarified  $\beta$ -Ga<sub>2</sub>O<sub>3</sub> phase transition temperature on  $\alpha$ -Al<sub>2</sub>O<sub>3</sub>(0001). The Ga<sub>2</sub>O<sub>3</sub> films deposited at RT by RF magnetron sputtering, and annealed various temperature. After that, the crystalline structure and transmittance were evaluated.

## 2. EXPERIMENTAL

Preparation of the films were conducted using RF magnetron sputtering with 5N-sintered Ga<sub>2</sub>O<sub>3</sub> as a target. Films which thickness is 100 nm were deposited at RT on  $\alpha$ -Al<sub>2</sub>O<sub>3</sub>(0001) substrates. After deposition, annealing in nitrogen ambient up to 900°C for 10 min. Optical transmittance of the films evaluated using JASCO V-650. To investigate the crystalline structure of the grown films, X-ray diffraction (XRD, Pnalytical X'Pert PRO MRD) was used.

## 3. RESULT and DISCUSSION

Figure 1 shows the XRD  $\theta$ - $2\theta$  patterns of the as-deposited film and the films annealed up to 900°C for 10 min. There are no diffraction peaks observed for as-deposited and annealed films up to 425°C. In contrast, a diffraction peak corresponds to  $\beta$ (-402) is appeared at 450°C annealing. It could be say that  $\beta$ -Ga<sub>2</sub>O<sub>3</sub> phase transition temperature on  $\alpha$ -Al<sub>2</sub>O<sub>3</sub>(0001) is between 425°C and 450°C. Diffraction peaks correspond to  $\beta$ (-201) and  $\beta$ (-603) are observed at over 800°C as same as the former report<sup>9</sup>. Therefore, we could confirmed that  $\beta$ {-201} epitaxially grown on  $\alpha$ -Al<sub>2</sub>O<sub>3</sub>(0001) by RT deposition and post annealing. And here, these distinctive samples annealed at 425°C, 450°C and 800°C named as Sample1, Sample2 and Sample3, respectively. Sample1 and Sample2 correspond to the boundary of  $\beta$ {-201} oriented Ga<sub>2</sub>O<sub>3</sub> formation, and Sample3 corresponds to the high orientation film by high temperature annealing.

Figure 2 shows the optical transmittance of the Sample1, Sample2 and Sample3. All of samples kept high transparency of above 80% in the wavelength of over 350 nm. In addition, Sample2 and Sample3 spread a wavelength through 260nm. It could not confirm large difference of transmittance between Sample2 and Sample3. These results indicate that the annealing at 450°C is enough for high transmittance in visible light.

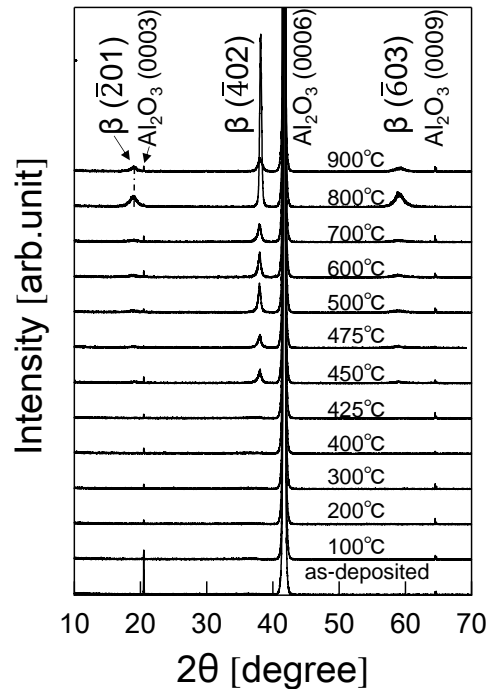


Fig.1 XRD  $\theta$ - $2\theta$  patterns of the as-deposited film and the films annealed up to 900°C for 10 min..

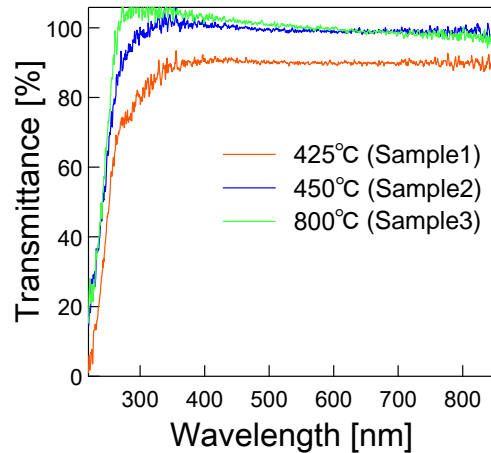


Fig.2 Transmittance of the films after the 425°C, 450°C and 800°C for 10 min annealing.

## 4. CONCLUSION

To investigate  $\beta$ -Ga<sub>2</sub>O<sub>3</sub> transition temperature on  $\alpha$ -Al<sub>2</sub>O<sub>3</sub>(0001) substrates by RF magnetron sputtering, the various temperature annealing is conducted to Ga<sub>2</sub>O<sub>3</sub> films. From XRD measurements, phase transition temperature is between 425°C and 450°C on  $\alpha$ -Al<sub>2</sub>O<sub>3</sub>(0001). The Ga<sub>2</sub>O<sub>3</sub> films annealed at 450°C has high transmittance as  $\beta$ -Ga<sub>2</sub>O<sub>3</sub>, and it could be said that the tempetarure enough to obtain  $\beta$ -Ga<sub>2</sub>O<sub>3</sub> film for TCOs.

## 5. ACKNOWLEDGMENTS

This work was supported in partly by Grant-in-Aid for Young Scientists (B) (No. 25820149).

## REFERENCES

- 1) R. Roy, V.G. Hill, E. F. Osborn : Polymorphism of  $\text{Ga}_2\text{O}_3$  and the System  $\text{Ga}_2\text{O}_3\text{-H}_2\text{O}$ , *Journal of the American Chemical Society*, No. 74, pp. 719-722, 1952.
- 2) Godhuli Sinha, Kalyan Adhikary, Subhadra Chaudhuri : Effect of annealing temperature an structural transformation of gallium based nanocrystalline oxide thin films and their optical properties, *Optical Materials*, No. 29, pp. 718-722, 2007.
- 3) Takayoshi Oshima, Takeya Okuno and Shizuo Fujita :  $\text{Ga}_2\text{O}_3$  Thin film Growth on c-Plane Sapphire Substrates by Molecular Beam Epitaxy for Deep-Ultraviolet Photodetectors, *Japanese Journal of Applied physics*, Vol. 46, pp.7217-7220, 2007.
- 4) Masahiro Orita, Hiromichi Ohta, Masahiro Hirano and Hideo Hosono : Deep-ultraviolet transparent conductive  $\beta\text{-}\text{Ga}_2\text{O}_3$  thin films, *Appl. Phys. Lett.* 77, pp. 4166-4168, 2000.
- 5) Katsuki Miyauchi, Tetsuichi Kudo and Tsuneo Saganuma : High ionic conductivity of Na- $\beta\text{-}\text{Ga}_2\text{O}_3$  thin film, *Appl. Phys. Lett.* 37, pp. 799-800, 1980.
- 6) Hyoun Woo Kim, Nam Ho Kim : Influence of postdeposition annealing on the properties of  $\text{Ga}_2\text{O}_3$  films on  $\text{SiO}_2$  substrates, *Journal of Alloys and Compounds*, No. 389, pp. 177-181, 2005.
- 7) M. Orita, H. Hiramatsu, H. Ohta, M. Hirano, and H. Hosono : Preparation of highly conductive, deep ultraviolet transparent  $\beta\text{-}\text{Ga}_2\text{O}_3$  thin film at low deposition temperatures, *Thin Solid Films*, Vol. 411, pp. 134-139, 2002.
- 8) Motoki Takahara, Suguru Funasaki, Jyun Kudou, Isao Tsunoda, Kenichiro Takakura, Hidenori Ohyama, Toshiyuki Nakashima, Mutsuo Shibuya, Katsuya Murakami, Eddy Simoen and Cor Cleays : Improvement of the Crystalline Quality of  $\beta\text{-}\text{Ga}_2\text{O}_3$  Films by High-Temperature Annealing, *Materials Science Forum* Vol. 725, pp. 273-276, 2012.
- 9) G. V. Chaplygin and S. A. Semiletov : Preparation, Structure and electrical properties of epitaxial films of  $\text{Ga}_2\text{O}_3$  on sapphire substrates, *Thin Solid Films* No.32, pp.321-324, 1976.

# Development of evaluation method of the rubber vulcanization reaction by electrical current measurement

Jumpei Yoshimatsu, Toyohiko Gondoh, Yasuyuki Hirakawa

National Institute of Technology, Kurume College  
1-1-1 Komorino, Kurume 830-8555, Japan  
E-mail: hirakawa@kurume-nct.ac.jp

**Abstract**— Variations of electric current with cure time during vulcanization process of rubbers were investigated and compared with the results by a conventional curemeter. As a result, the temporal variation of the current was in good agreement with the torque–cure time curves obtained by the curemeter. It was also found that this evaluation method is effective for the vulcanization process of the sample compound with carbon black.

**Primary categories**— Applied Physics/Basic Engineering

**Secondary categories**— General Applied Physics

**Keywords**— Rubber, Electrical Parameters, Vulcanization

## I. INTRODUCTION

The vulcanization is one of the most important processes of manufacturing rubber products. By the vulcanizing reaction, unique elastic properties are given to the products. Knowing an optimum vulcanization condition including cure temperature and cure time is essential in order to obtain rubber products with good properties. A traditional torque measurement by a curemeter is most commonly used for estimating the vulcanization condition, however; it is not possible to obtain real time information of the vulcanization reaction.

In-situ electrical current measurements method was

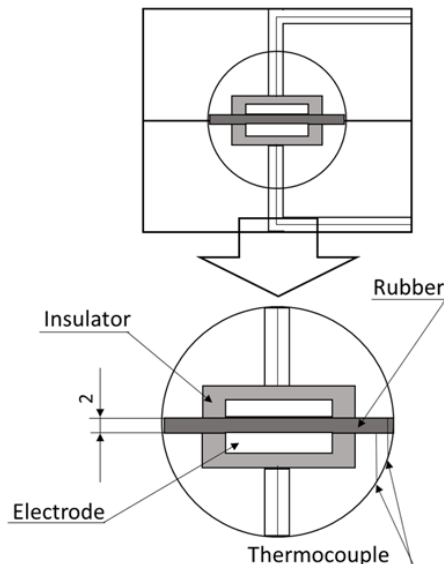


Fig. 1 Mold used in this study.

proposed by Gondoh et al<sup>1)</sup>. In this method, the electrical current with cure time under the constant electric voltage was measured, and it was suggested that the current-cure time curve had a good correlation with vulcanization reaction<sup>1,2)</sup>.

In this study, the fundamental electrical measurements of the rubber samples compounded with/without carbon black (CB) were performed during the vulcanization reactions, to experimentally confirm this technique as the estimation method for the rubber vulcanization.

## II. EXPERIMENTAL

Acrylonitrile-butadiene rubber (NBR) was used as a fundamental crude rubber material, because it allows larger electrical current. The NBR samples contained several additives including zinc oxide (5 phr), stearic acid (1 phr), sulfur (1 phr), N-cyclohexyl-2-benzothiazyl sulfenamide (1 phr), tetramethyl thiuram disulfide (1 phr), and dibenzothiazyl disulfide (1 phr) in addition to 100 phr crude NBR. The unit of “phr” or “per hundred rubber” means the relative weight when the crude rubber weight is 100 (in any units). The NBR compound was prepared using an internal mixer (rotational speed of 10 rpm). The sample compounded without CB was made as follows: after masticating the NBR crude rubber for 5 minutes, zinc oxide and stearic acid were added and mixed for 30 minutes. After that, sulfur and the other additives were added and mixed for 60 minutes. The sample contained CB was prepared as follows: after masticating the NBR crude rubber for 5 minutes, zinc oxide and stearic acid were added and mixed for 20 minutes. Then, sulfur and the other additives were added and mixed for 40 minutes. Finally, CB (20 phr) was added and mixed for 40 minutes. The reason why the procedures of making the samples were different between with or without CB is because the season of preparing the samples were different and the optimum procedure was selected for the season. The temperature of the rubber was controlled below 80 °C by a water-cooling system to suppress the unnecessary

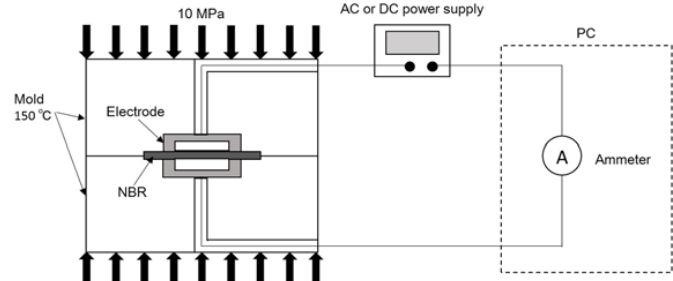


Fig. 2 Experimental setup.

vulcanization reaction. After mixing, the NBR compound was removed from the mixer and immediately put into a polyethylene bag to keep in a refrigerator.

A mold used for the vulcanization is shown in Fig. 1. This was also used for the electric measurement during vulcanization. The electrodes were made of stainless steel and were insulated from its surrounding mold by polytetrafluoroethylene seats. The upper and lower electrodes were separated by a distance of 2.0 mm. The total experimental setup was shown in Fig. 2.

The electric current was measured by a digital multimeter (DMM-522-PCI, CONTEC) equipped in PC. The AC power supply (CVFTI-250HA, TOKYOSEIDEN) and the DC power supply (Z100-2, TDK-Lambda) were used for the AC and DC measurements, respectively. The voltage was 100 V for both AC and DC and the frequency was 50 Hz for AC measurements.

The torque was measured by a curemeter (CURELASTOMETER W, A&D Company). The curemeter is a testing machine which measures torque applied to a rubber sample and obtains a torque-cure time curves. The torque measured by the curemeter is corresponded to the degree of the vulcanization in the sample. The optimum vulcanization time  $T_{90}$  is usually determined using the torque-cure time curve.

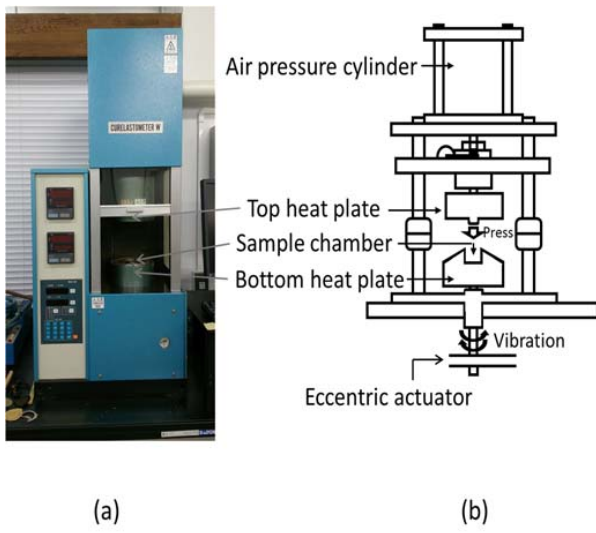


Fig. 3 Curemeter used in this study. (a) appearance and (b) structural drawing.

### III. RESULTS AND DISCUSSION

The results of the AC current and DC current measured are shown in Fig. 4. As shown in Fig. 4 (a), it was found that the remarkable inflection point of the AC curve was about 300 s. At this vulcanizing time of about 300 s, the DC curve also had an inflection point. It had been shown experimentally by previous measurements that the inflection point of the electrical current curve corresponds to the optimum vulcanization time ( $T_{90}$ ). By comparing these two-curves, it was found that the AC and the DC curves indicated similar tendency each other and also found that the AC curve approached a constant value and the DC curve gradually fell toward to zero.

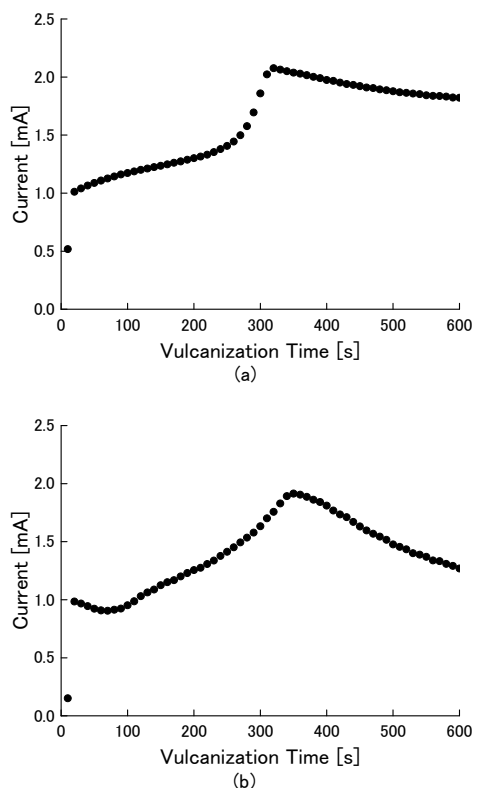


Fig. 4 Temporal variations of electrical current during vulcanization.  
(a) AC current and (b) DC current.

The comparison between the electrical current and the conventional parameters such as torques was attempted. Fig. 5 indicates the variation of torques with the cure time measured by the curemeter. From the results of Fig.4 and Fig.5, it was obvious that T90 in Fig.5 was coincident with the inflection points in Fig.4. This phenomenon was re-confirmed in this study as previous experiments. The AC current had almost constant current value after the inflection point (T90), while the DC current gradually decreased to zero current after T90 in Fig.4. It is reasonable to think that the AC current after T90 was generated by the capacitance component of the sample. To summarize the above, we concluded that the DC current only reflects the vulcanization reaction, and the inflection point is a real T90.

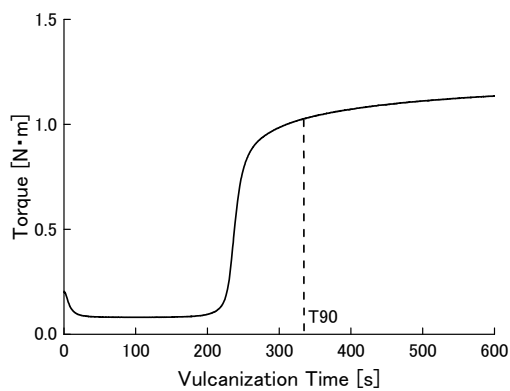


Fig. 5 Obtained torque vs cure time curve by the curemeter for no CB sample.

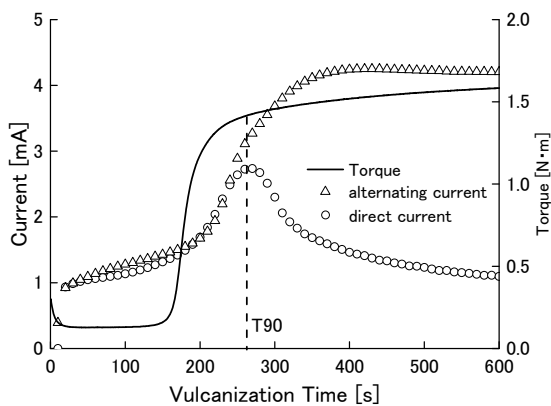


Fig. 6 Comparison between the electric current curves and the torque curve for the samples compounded with CB.

Carbon black (CB) is usually mixed in rubber products as a filler material to increase the product strength. To investigate whether electrical measurement is possible to apply samples contained CB, the sample which contained the same ingredient except for CB (SEAST 300, Tokai Carbon) and tested. The result was shown in Fig. 6. A correlation between the torque curve and the electrical current curve were clearly observed, even if CB was mixed with the sample. It was also found that the torque value at T90 was larger than that of Fig.5 whose sample did not contain CB and the T90 time became earlier than the T90 in Fig.4. These effects are reasonable and due to the CB addition. The electrical curves showed the same tendency. The inflection points of the current curves in Fig.6 appear at earlier time and the maximum values of the electrical curves in Fig.6 were higher than those in Fig.4. These facts were caused by CB which has high electrical conductivity and which has some effect for vulcanization. The result of Fig.6 indicates our in-situ electrical current method has a possibility that it can estimate vulcanization effect correctly.

#### IV. CONCLUSION

In conclusion, the possibility of estimation of the vulcanization reaction in two-kind rubber samples that had CB and no CB by electric measurements was shown experimentally. In the experiments, good correlation between electric current cure-time curves and conventional torque cure-time curves were confirmed for both samples. It is expected that by using this technique, the vulcanization process can be easily observed in real time.

#### REFERENCES

- [1] T. Mori, S. Etoh, Y. Matsuoka, T. Gondoh, M. Toh, and D. Okai, "Electric In-Situ Measurement of Vulcanization of Rubber", Proc. International Rubber Conference 1997, pp.1063-1068, Kuala Lumpur, 1997
- [2] R. Miratsu, Y. Hirakawa, T. Gondoh, K. Watanabe and T. Mori, "Changes of Electric Characteristics of Rubber during Vulcanization", 2012 national Symposium on Technology for Sustainability, Bangkok, 2012

# Properties of Sn-S thin films prepared by sulfurization

Kazuya IWASAKI<sup>1</sup>, Shigeyuki NAKAMURA<sup>2</sup> and Yoji AKAKI<sup>3</sup>

<sup>1</sup> Student, Advanced Course of Electrical and Computer Eng., National Institute of Technology, Miyakonojo Colegge  
(473-1 Yoshio Miyakonojo, Miyazaki 885-8567, Japan)  
E-mail:e14iwasaki@cc.miyakonojo-nct.ac.jp

<sup>2</sup>Professor, Dept. of Electrical and Electronic Eng., National Institute of Technology, Tsuyama Colegge  
(624-1 Numa Tsuyama, Okayama 708-8509, Japan)

<sup>3</sup> Assoicate Professor, Dept. of Electrical and Computer Eng., National Institute of Technology, Miyakonojo Colegge  
(473-1 Yoshio Miyakonojo, Miyazaki 885-8567, Japan)  
E-mail:akaki@cc.miyakonojo-nct.ac.jp

Sn thin films were deposited by thermal evaporation. After deposition of Sn, the thin films were annealed in a H<sub>2</sub>S atmosphere at temperature ranging from 100 to 500 °C for 1 hour. SnS thin films were obtained by annealing at 300 °C in H<sub>2</sub>S atmosphere. The absorption coefficient of thin films annealed from 250 to 450 °C was over 10<sup>4</sup> cm<sup>-1</sup> at photon energy above 1.3 eV. The thin films annealed at 300 °C had resistivity of 36.5 Ωcm and a direct band gap of 1.4 eV.

**Key Words :** tin sulfide, thin film, sulfurization

## 1. INTRODUCTION

At present, the materials mainly used for thin film solar cells are copper indium gallium selenide (Cu(In,Ga)Se<sub>2</sub>) or cadmium telluride (CdTe). Cu(In,Ga)Se<sub>2</sub> based solar cells have achieved the conversion efficiency more than 20%<sup>1)</sup>. However, their use has some problems, including the environmental impact of cadmium and the lack of abundance of indium, gallium, and tellurium. In contrast to these materials, tin sulfide (SnS) is non-toxic, abundant, and cheap. In addition, SnS has a direct energy band gap of 1.35 eV<sup>2)</sup>, which is closer to the optimum value of 1.4 eV, and has a high absorption coefficient (>10<sup>4</sup> cm<sup>-1</sup>). Therefore, SnS is a promising material for preparing the absorber layer of a thin film solar cell.

SnS thin films have been prepared using a variety of techniques such as sulfurization using sulfur powder<sup>2, 3)</sup>, vacuum evaporation<sup>4, 5)</sup>, chemical vapor deposition<sup>6</sup>, chemical bath deposition<sup>7</sup>, spray pyrolysis deposition<sup>8)</sup>, hot wall deposition<sup>9</sup>, sputtering<sup>10</sup>, and atomic layer deposition<sup>11</sup>. SnS thin film solar cell has been reported low efficiency below 5%<sup>11)</sup> compared with Cu(In,Ga)Se<sub>2</sub> and CdTe solar cells because SnS thin films using these method have low quality. In this paper, we report properties of SnS thin films prepared by sulfurization using H<sub>2</sub>S gas.

## 2. EXPERIMENTAL METHODS

Sn thin films were deposited onto glass substrates by thermal evaporation. The source material used was Sn powder with 99.99% purity. A pressure before the evaporation was below 2 × 10<sup>-3</sup> Pa and we do not control substrate temperature. After deposition of Sn, the thin films were annealed in a H<sub>2</sub>S atmosphere at temperature ranging from 100 to 500 °C for 1 hour.

The crystalline structure of the thin films was analyzed by X-ray diffraction (XRD, Rigaku SmartLab using Cu-Kα radiation), and the composition of the thin films was analyzed by energy dispersive X-ray spectroscopy (EDS, BRUKER QUANTAX FlatQUAD). The band gap of the thin films was determined from transmittance and reflectance measured by a UV-Visible-NIR Spectrophotometer (Hitachi U-4000). Resistivity of the thin films was measured by four-point prove method (Mitsubishi Chemical Loresta-EP MCP-T360). Morphological properties of the thin films were observed by a scanning electron microscope (SEM, Hitachi SU8020).

## 3. RESULTS AND DISCUSSION

Figure 1 shows XRD patterns of Sn-S thin films

annealed in H<sub>2</sub>S atmosphere and the JCPDS card of Sn (JCPDS card No. 00-004-0673), SnS (JCPDS card No. 00-014-0620), and SnS<sub>2</sub> (JCPDS card No. 01-083-1705). XRD patterns of the as-deposited film and films annealed from 100 to 200 °C corresponded to the Sn phase. Sulfurization did not occur because the melting point of Sn is 230 °C. Thin films annealed from 250 to 350 °C exhibited the orthorhombic phase of SnS. However, the films show diffraction peaks corresponding to not only the SnS but also the Sn phase. Further, thin films annealed from 400 to 500 °C showed mainly the SnS<sub>2</sub> phase.

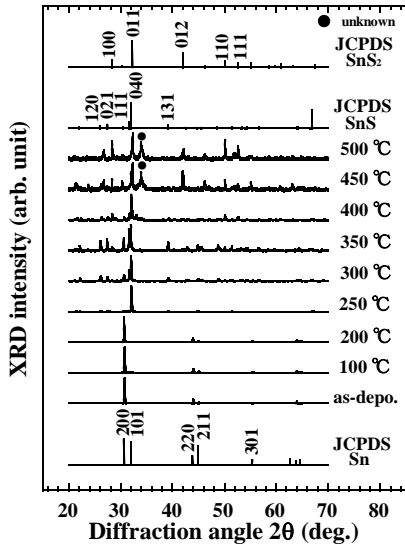


**Fig. 1** XRD patterns of Sn-S thin films annealed in H<sub>2</sub>S atmosphere.

Figure 2 shows the composition of Sn-S thin films annealed in H<sub>2</sub>S atmosphere. Sn/S ratio of thin films annealed at 300 °C was 0.97 which was a stoichiometry closest to SnS. However, the composition of the thin films annealed above 350 °C was considerably different from that of SnS. Sn/S

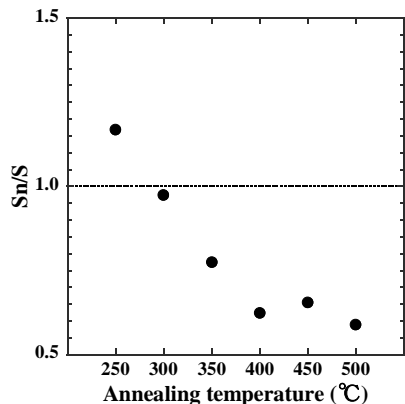


**Fig. 2** Sn/S ratio of Sn-S thin films annealed in H<sub>2</sub>S atmosphere.

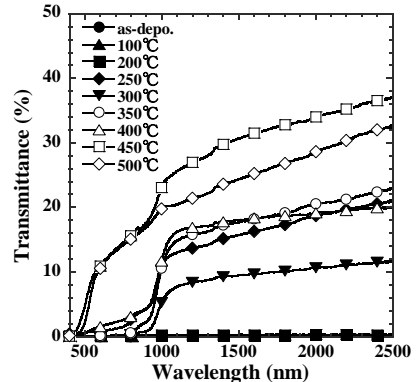
ratio of thin films annealed at 500 °C was 0.59 which was a stoichiometry closest to SnS<sub>2</sub>.

Figure 3 shows transmission spectra of Sn-S thin films. The transmittance of as-deposited film and films annealed 100 to 200 °C was almost 0% because of Sn metal. The transmittance of the thin films annealed from 250 to 400 °C was over 10% at above 900 nm and approximetary 0% at below 900 nm.

The absorption coefficient of the Sn-S thin films is calculated from the form using transmittance and reflectance,

$$\alpha = \frac{1}{d} \ln \left( \frac{(1-R)^2}{T} \right) \quad (1)$$

Where  $\alpha$  is absorption coefficient,  $d$  is film thickness determined from cross-sectional SEM images,  $R$  is reflectance of thin films,  $T$  is transmittance of thin films. Figure 4 shows absorption coefficient of the Sn-S thin films. The absorption coefficient of thin films annealed from 250 to 450 °C was over 10<sup>4</sup> cm<sup>-1</sup> at photon energy above 1.3 eV. This indicates that SnS crystals exists in the films. However, the absorption coefficient of thin films annealed at 500 °C was over 10<sup>4</sup> cm<sup>-1</sup> at photon energy above 2.4 eV.



**Fig. 3** Transmission spectra of Sn-S thin films annealed in H<sub>2</sub>S atmosphere.

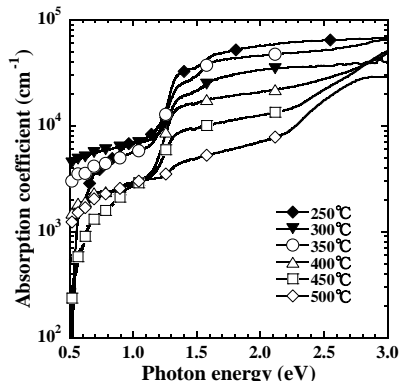


**Fig. 4** Absorption coefficient of Sn-S thin films annealed in H<sub>2</sub>S atmosphere.

The direct band gap of films annealed from 250 to 350 °C was 1.4-1.5 eV, which is similar to the direct band gap of SnS<sup>1)</sup>. However, the direct band gap changed with increasing annealing temperature and the band gap of the thin films annealed from 400 to 500 °C was 2.4-2.5 eV, which is similar to the direct band gap of SnS<sub>2</sub><sup>12)</sup>.

Figure 5 shows the resistivity of Sn-S thin films. The resistivity of thin films annealed under 200 °C was considerably low because of Sn metal. With increasing annealing temperature, the resistivity increased and the resistivity of the thin film annealed at 300 °C was 36.5 Ωcm. This value is close to reported value<sup>8)</sup>.

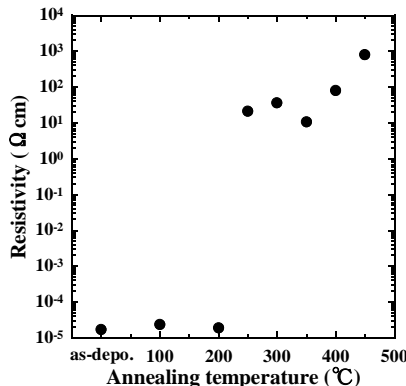


Fig.5 Resistivity of Sn-S thin films annealed in H<sub>2</sub>S atmosphere.

Figure 6 shows SEM images of as-deposited thin films and thin films annealed at 300 and 500 °C. The surface of thin films changed with increasing annealing temperature. The thickness of thin films annealed above 300 °C was higher than the as-deposited film thickness because of sulfurization. Composition distribution of the cross section of the thin film annealed at 300 °C showed insufficient diffusion of sulfur by EDS.

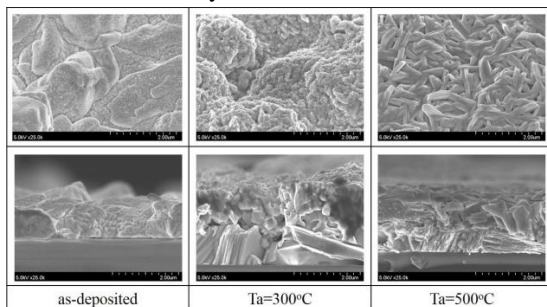


Fig. 6 SEM images of Sn-S thin films annealed in H<sub>2</sub>S atmosphere.

## 4.CONCLUSIONS

We prepared Sn-S thin films by sulfurization. Sn thin films were annealed in H<sub>2</sub>S atmosphere from 100 to 500 °C for 1 hour. XRD measurements and EDS measurements revealed that SnS thin films are obtained by annealing at 300 °C. Further, the direct band gap of thin films annealed at 300 °C was 1.4 eV, which is similar to the direct band gap of SnS. However, the Sn phase exists in the films because diffusion of sulfur is insufficient.

## REFERENCES

- P. Jackson, D. Hariskos, R. Wuerz, O. Kiowski, A. Bauer, T.M. Friedlmeier, M. Powalla: Properties of Cu(In,Ga)Se<sub>2</sub> solar cells with new record efficiencies up to 21.7%, *Phys. Status Solidi – Rapid Res. Lett.* Vol. 9, pp. 28-31, 2014.
- K. T. R. Reddy, P.P. Reddy, P. K. Datta, and R. W. Miles : Formation of polycrystalline SnS layers by a two-step process, *Thin Solid Films*, Vol. 403, pp. 116-119, 2002.
- M. Sugiyama, K. Miyauchi, T. Minemura, K. Ohtsuka, K.Noguchi, and H.Nakanishi : Preparation of SnS Films by Sulfurization of Sn Sheet, *Jpn. J. Appl. Phys.*, Vol. 47, pp. 4494-4495, 2008.
- A. Tanusevski, and D. Poelman : Optical and photoconductive properties of SnS thiin films prepared by electron beam evaporation, *Sol. Energy Mater. Sol. Cells*, Vol. 80, pp. 297-303, 2003.
- Y. Kawano, J. chantana, and T.Minemoto : Impact of growth temperature on the properties of SnS film prepared by thermal evaporation and its photovoltaic performance, *Curr. Appl. Phys.*, Vol. 15, pp. 897-901, 2015.
- L. S. Price, I. P. Parkin, A. M. E. Hardy, and R. J. H. Clark : Atmospheric Pressure Chemical Vapor Deposition of Tin Sulfides (SnS, Sn<sub>2</sub>S<sub>3</sub>, and SnS<sub>2</sub>) on Glass, *Chem. Mater.*, Vol. 11, pp. 1792-1799, 1999.
- D. Avellaneda, G. Delgado, M. T. S. Nair, and P. K. Nair : Structural and chemical transformations in SnS thin films used in chemically deposited photovoltaic cells, *Thin Solid Films*, Vol. 515, pp. 5771-5776, 2007.
- K. T. R. Reddy, N. K. Reddy, and R. W. Miles : Photovoltaic properties of SnS based solar cells, *Sol. Energy Mater. Sol. Cells*, Vol. 90, pp. 3041-3046, 2006.
- S. A. Bashkirov, v. F. Gremenok, V. A. Ivanov, V. V. lazenka, and K. Bente : Tin sulfide thin films and Mo/p-SnS/n-CdS/ZnO heterojunctions for photovoltaic applications, *Thin Solid films*, Vol. 520, pp. 5807-5810, 2012.
- K. Hartman, J. L. Johnson, M. I. Bertoni, D. Recht, M. J. Aziz, M. A. Scarpilla, T. Buonassisi : SnS thin-films by RF sputtering at room temperature, *Thin Solid Films*, Vol. 519, pp. 7421-7424, 2011.
- P. Sinsermsuksakul, L. Sun, S. W. Lee, H. H. Park, S. B. Kim, C. Yang, and R. G. Gordon : Overcoming Efficiency Limitations of SnS-Based Solar Cells, *Adv. Energy Mater.*, Vol.4, p. 1400496, 2014.
- B.Thangaraju, and P. Kaliannan : Spray pyrolytic deposition and characterization of SnS and SnS<sub>2</sub> thin films, *J. Phys. D: Appl. Phys.*, Vol. 33, p. 1054, 2000.

# An Application of Embedded Programming and Electronics: A Field Research and Navigation Mobile Robot

TA Quyen<sup>1</sup>, TA Vu<sup>1</sup>, TRAN Nga<sup>1</sup>, NGUYEN Mai<sup>1</sup>, NGUYEN Chinh<sup>1</sup>  
and NGUYEN Linh<sup>1</sup>

<sup>1</sup> Student, Faculty of Information Technology, Hanoi University  
(Km9 Nguyen Trai, Thanh Xuan, Ha Noi, Viet Nam)  
E-mail: tanvutdvp@gmail.com

This paper deals with a low cost solution to field research for a mobile robot using sensors. Firstly, this paper also presents a dynamic steering algorithm which ensures that the robot doesn't have to stop in front of an obstacle which allows robot to navigate smoothly in an unknown environment, avoiding collisions. The obstacle avoidance strategy has been described. Obstacle avoidance strategy and working of robot is greatly dependent on the detection of obstacles by sensors and corresponding response of robot. Secondly, gas detection, light detection, heat and moisture measuring methodologies using sensors are also presented. Working principle of sensors and limitation of their use has been discussed in details.

**Key Words :** Arduino, obstacle avoiding robot, light sensor, temperature-humidity sensor, motor shield

## 1. INTRODUCTION

Our world is now getting affected more and more heavily due to natural calamity. Disasters are exceptional and unstoppable events that are either man-made or natural, such as tsunamis, terrorist attacks, earthquakes, wildfires and floods etc. When stricken by a catastrophic natural disaster, such as Nepal Earthquake, Hurricane Katrina, or 2004 Indian Ocean earthquake and tsunami, emergency rescue operation is very critical to numerous lives. Many people trapped in the disastrous areas under collapsed buildings or landslides may have a large chance to survive if they are rescued in the first 72 hours. In order to make a plan and execute an effective rescue operation, rescue volunteers and experts have to carefully research the disaster region, detecting any hostile condition on the area.

As an effective back-up for the operation, this paper proposes a low-cost mobile robot base on a system of electronic sensors designed to detect light, gas, humidity and temperature in an unmanned area that can only be access by robots. These sensors collect data directly from the environment around them. After that, all information collected is sent to a programmed Arduino board, who will receive data and transmit it back to the rescue center using a radio transmitter module. At the head of the rescue campaign, another Arduino board with a radio receiver module is used to receive data and display to computer screens, giving volunteers an overview of the area.

The rest of this paper is structured as follow.

Section 2 will give reader a brief introduction into Arduino board, sensors, and Arduino programming language. Section 3 will mention some prior and related works, while section 4 discusses the algorithm and methodology in building the field researching robot. Section 5 raises a discussion on the advantages and disadvantages of our product and algorithm. Finally, section 6 provides some final conclusions and directions for future works.

## 2. BACKGROUND KNOWLEDGE

Arduino is an open-source platform used for building electronics projects. Arduino consists of both a physical programmable circuit board (often referred to as a microcontroller) and a piece of software, or IDE (Integrated Development Environment) that runs on your computer, used to write and upload computer code to the physical board.

The Arduino platform has become quite popular with people just starting out with electronics, and for good reason. Unlike most previous programmable circuit boards, the Arduino does not need a separate piece of hardware (called a programmer) in order to load new code onto the board – you can simply use a USB cable. Additionally, the Arduino IDE uses a simplified version of C++, making it easier to learn to program. Finally, Arduino provides a standard form factor that breaks out the functions of the micro-controller into a more accessible package.

Arduino IDE is the programming language is an implementation of Wiring, a similar physical computing platform, which is based on the Processing

multimedia programming environment.

**Sensor:** A sensor is a device that detects some type of input from the physical environment and converts it into a signal that can be read by an electronic device. The specific input could be light, heat, motion, moisture, pressure, or any one of a great number of other environmental phenomena. The output is generally a signal that is converted to human-readable display at the sensor location or transmitted electronically over a network for reading or further processing.

In this project we use lot types of sensor with the aim to answer the questions: what is the life condition we are discovering? Does it safe for human? Can human, animal or plan exist there? These sensors will collect the index about the temperature, humidity, amount of gas in the air and the topographic. Then the result will be sent to the computer and the computer will analyze and decide the life condition is suitable for the human or not.

### 3. OBSTACLE AVOIDING AND FIELD RESEARCHING ROBOT

#### (1) Proposed hardware

The project proposes mobile robot that can work in a destroyed- unknown area and helps executing rescue operation by collecting information about the environment around it and send all the data to operation center. This can help stretching an overview of the area, which is extremely useful in making rescue operating plans. The proposed system consists of a mobile robot and information displaying module.

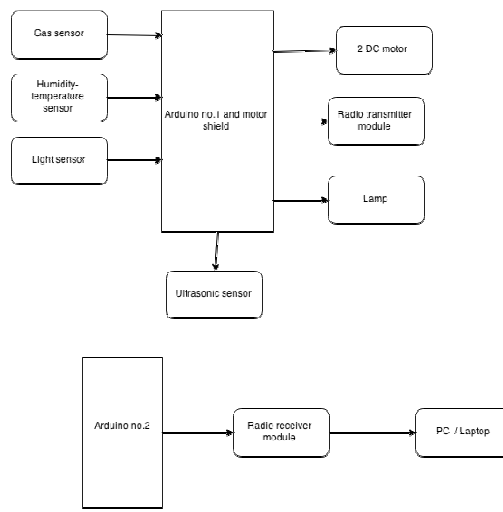


Fig.1 Overall system structure of the mobile robot

The mobile robot consists of six units namely sensor unit, picture collecting unit, Arduino micro-

controller unit, motor driver unit, light unit and transmission unit. The sensor unit is directly stick to the microcontroller through serial ports. These sensors detect current data about the surrounding environment and sends data to the microcontroller. The Arduino microcontroller is responsible for transmitting this information to rescuing center. An information display subsystem containing an Arduino microcontroller, a radio receiver module and a PC or laptop is used at the center to receive data and display it on computer screens, so that rescue team is given an overview of the area with multiple parameters.

#### (2) Obstacle avoiding and searching algorithm

In this project, a very simple obstacle avoiding algorithm is applied. A low cost ultrasonic sensor is deployed to calculate distance from the mobile robot to obstacle ahead. If the distance calculated is smaller than a certain number (eg. 20 cm in this case) the mobile robot automatically “knows” that there is an obstacle ahead. It will now turn left or right until there is no obstacle detected within given range.

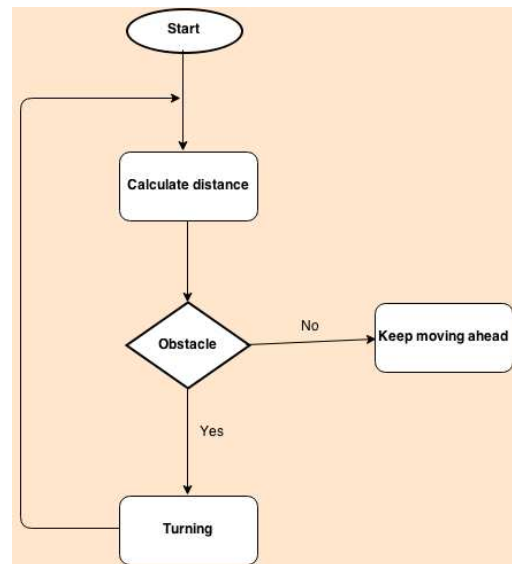


Fig.2 The block diagram of the obstacle-avoidance algorithm

#### (3) Principles of using sensors in environment researching

In order to collect environmental parameters, some sensors are deployed in this project. All of the sensors are of active type, which means when a current passed through a sensor, its current and/or voltage is changed. Naturally, this variation is directly proportional to the change in parameters. To make use of this characteristic, an Arduino-based embedded program is implemented to collect data

from the sensors, then calculate and show the parameters to users.

## 4. DISCUSSION

In an effort to apply programming in an embedded systems supporting rescue volunteer in executing operations, this paper raises a methodology to build a small mobile robot with simple, easy-to-find components. This is completely automatic system, by a pushing a button, the obstacle avoidance system controlled by the Arduino board and the ultrasonic sensor starts working and move the robot around the unnamed area; the other sensor also start collecting information automatically without people having to intercede anything. This is one of the most prominent features of our product, because automation is now becoming the popular trend that a lot of company is reaching to.

However, there exists some shortcoming remained in this project that should be solve in further development. First of all, using ultrasonic sensor as a solution to detect obstacles makes the robot become passive, it nearly moves randomly as it meets the obstacles, and it may ignore some important locations. In addition, the users cannot control the way it as the way they want, they also do not know where it goes and if it will return or not. Moreover, targets of low density, like foam and cloth, tend to absorb sound energy. This characteristic makes it extremely difficult to detect soft and low-density obstacles along the way. This could be one of the most serious shortcomings in this project.

## 5. CONCLUSION

With the aim use cheap electric materials to make a mobile robot for discovering the unnamed areas, saving human's life in the disasters. In this paper we create an effective and safe system to ensure that the life's condition of the whole unnamed area will be collected. By using different type of sensors, this system can detect the humidity, temperature, the amount of gas in the air record these index and send directory to a computer through a radio frequency module. These index will be analyzed and decided if it safe for human or not. It will improve the performance & efficiency of data transmission. It can be used popularly with the low cost components and basic principles about electricity.

For further development, it is suggested that more

modern and effective obstacle avoidance algorithm should be updated to help the robot to find better way in field researching. Some suggestions could be using InfraRed sensors and microcontrollers to draw a simple "map" of the nearby objects then decide which direction to go. Moreover, the whole system can be changed a little bit by replacing radio frequency module with a Bluetooth shield. With the later one, rescuers at the operation center can remotely control their robot via Bluetooth signal, deciding its direction base on the live video captured from attached phone. To perform this control, people have to prepare only a Bluetooth control application for mobile which can be found easily from Google's Playstore or Apple's Appstore. This will help reduce an enormous amount of resources needed to build robots. Besides, when provided with enough financial resources, developers can use an Arduino compatible camera module to help capturing live video while searching destroyed fields. Using this device, the robot can be considerably reduced in weight and size.

## REFERENCES

- 1) Michael Margolis, "Arduino Cookbook", 2nd Edition, O'Reilly Media, 2011.
- 2) Arduino (2015). "Arduino – Learn the basic." [Online] Available at: <http://www.Arduino.cc/en/Tutorial/HomePage> (Accessed: 14th April 2015)
- 3) Borenstein, J. and Koren, Y. (1988). "Obstacle Avoidance With Ultrasonic Sensors". IEEE Journal of Robotics and Automation, Vol. RA-4, No. 2, pp. 213-218.
- 4) Borenstein, J. and Koren, Y. (1989). "Real-time Obstacle Avoidance for Fast Mobile Robots". IEEE Transactions on Systems, Man, and Cybernetics, Vol.19, No.5, pp.1179-1187.
- 5) Hans-Petter Halvorsen, M.Sc. "Sensors and Actuators with Arduino", Telemark University College.
- 6) Lok Prasad Khanal. "OBSTACLE-AVOIDING ROBOT, a possible introduction project for engineering students", Bachelor thesis, Turku University of Applied Science, Finland. [Online] Available at: [https://www.thesus.fi/bitstream/handle/10024/71120/lok\\_final\\_thesis.pdf](https://www.thesus.fi/bitstream/handle/10024/71120/lok_final_thesis.pdf)
- 7) Johann B. & Yoram K., "Obstacle avoidance with ultrasonic sensors", IEEE journal of robotics and automation, vol. 4, no. 2, April 1998. [Online] Available at: [http://www-personal.umich.edu/~ykoren/uploads/Obstacle\\_avoidance\\_w\\_ultrasonic\\_sensors\\_IEEE.pdf](http://www-personal.umich.edu/~ykoren/uploads/Obstacle_avoidance_w_ultrasonic_sensors_IEEE.pdf)

(Received November 15, 2015)

# Miniaturized Notch antenna using capacitor

VU Viet Hoang<sup>1</sup>, LE Cong Tuan<sup>1</sup>, NGUYEN Viet Duc<sup>1</sup>

<sup>1</sup> Student, Post and Telecommunications Institute of Technology  
(Km 10, Nguyễn Trãi, Hà Đông, Hà Nội)  
E-mail: vuhoang5794@gmail.com

## Abstract

In this report, a Notch antenna originally designed to work at 900 MHz was added a capacitor at one end of its slot to change its operation frequency down to 700 MHz. This gives the antenna the ability to working in both GSM and future LTE network. Specifically, a 1pF capacitor was integrated in the antenna's design. Simulation results showed that its frequency changes from 900 MHz to 700 MHz with the tradeoff of its bandwidth, gain and efficiency. In detailed, its gain decreased from 2.42dBi to 1.8 dBi and its bandwidth down from 100 MHz to 20Mhz. However, its efficiency remains acceptable.

**Key Words:** Antenna, miniaturization, capacitor

## 1. INTRODUCTION

The proliferation of wireless communication applications lead to an increasing number of wireless services (Bluetooth, WIFI, GPS, GSM, ...) integrated in the limited small size of a mobile phone. Therefore, the miniaturization of antennas and especially its ability to operate simultaneously on multiple frequency bands are the research subject of many scientists around the world in general and Vietnam in particular. There are various ways to design self-configuring antenna, such as changing the properties of radiation, frequency characteristics, impedance bandwidth, or the polarization which has been researched and developed in recent years [1]. This research delves into operational structure and the parameters characteristic of a microstrip antenna. Then techniques of self-configuring miniature applied to microstrip antennas are researched. Specifically, we focus on the solution which use capacitor for the frequencies band of 700-900 MHz. This is the frequency range of mobile services, particularly 700 MHz frequency band is currently being studied for 4G generations after the liberation of analog TV frequency. Therefore, the miniaturization of antennas in this frequency range has potential in practice.

## 2. ANTENNA STRUCTURE

A notch antenna, consisting of a slot inside the metallic ground plane, is the complementary structure of the classical  $\lambda/4$  monopole, and has dual properties in terms of impedance and radiation behaviors. This kind of antenna presents the advantage of integration and miniaturization when loaded by a capacitor [2].

The notch antenna fed by a microstrip line is loaded with the varactor structure at the open-end of the slot as shown in Figure 1. The slot length is  $L = 46$  mm (or  $\lambda/0.7$ ) for the resonant frequency of 900 MHz without the varactor. The impedance matching is realized by varying the position of the feed line and the length of its extended part beyond the notch  $L_f$ . The used substrate is the commonly used FR4, with dielectric constant of 4.4 and 0.02 for loss tangent. Thickness of FR4 substrate is 0.8 mm. The microstrip line has width of 1.52 mm to make it a  $50 \Omega$  waveguide.

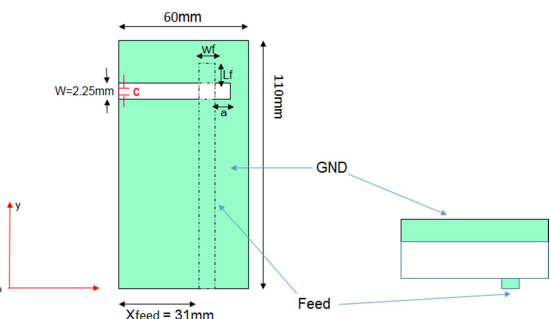


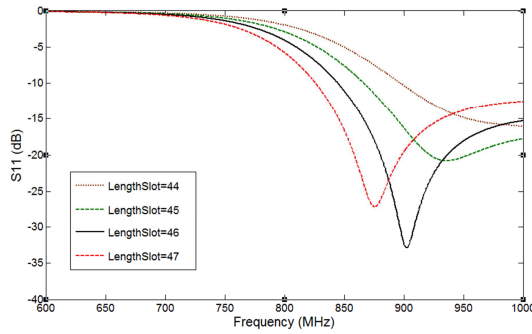
Fig.1 Antenna's structure

## 3. SIMULATIONS RESULTS

### (1) Role of Antenna's geometry

Antenna performance was simulated using Ansys HFSS[3] and CST Studio [4]. However, on the the results from HFSS is presented in this paper. CST results are very similar.

#### a) Slot's length



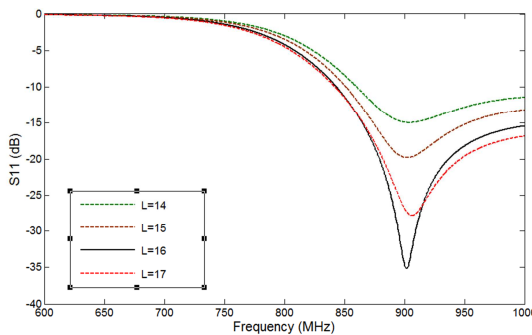
**Fig.2** Effect of slot's length on antenna's frequency

Figure 2 shows that when we change the length of the slot from 44 to 47(mm). As we know, in a Notch antenna, the length of slot has effect on its operating frequency. In our case, we need an antenna which operates at the frequency of 900 MHz. When the slot's length increase, the operating frequency decrease; in detailed when we change the length from 44 mm to 47mm the antenna frequency shift from 960 MHz to 860 MHz. Finally, we chose the slot's length of 46mm for the operation frequency of 900Mhz, the return loss(S11) is -35dB.

### b) Impedance Matching

Antenna's impedance matching can be obtained either by modifying the feed line position or the stub length above the slot or both.

Figure 3 shows us the antenna return loss when we change the length of the microstrip feed line. The parameter  $L_f$  is the length from the slot to the top of microstrip line feed. When we increase  $L_f$  from 14 to 16 mm, the return loss (S11) decrease from -15dB to -35dB and rise to -30 dB when  $L_f=17$ mm. So  $L_f=16$  is suitable for the impedance matching.



**Fig.3** Effect of microstrip stub's length to the impedance matching

In the other hand, Figure 4 shows us the return loss when we change the position of the microstrip feed line along the width of the antenna. Xfeed is the distance from the left edge of the antenna to the microstrip feed line. We examine this parameter in the range from 29mm to 32mm. And we can observe that

follow this figure with Xfeed=31mm, the antenna will work at the operation frequency 900Mhz and the return loss (S11) is -38dB. Here we fix  $L_f$  at 16 mm.

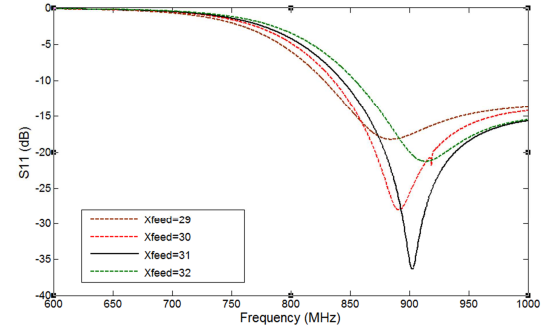


**Fig.4** Effect of feed line's position to the impedance matching

### (2) Notch loading effect

After adjust all the parameter, we choose the parameters set suitable with the antenna: slot's length is 46mm, feed line's position is 31mm, the length from the slot to the top of transmission feed line is 16mm. Figure 5 show the result of this parameters set, the return loss (S11) is around -35dB and the operation frequency is 900Mhz with bandwidth about 100Mhz

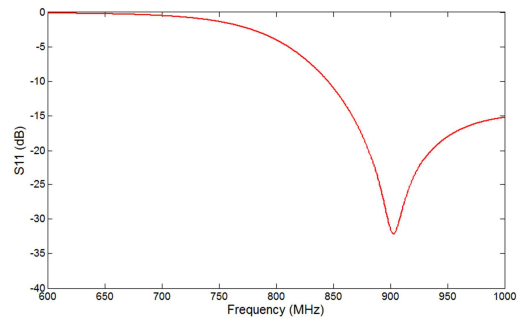


**Fig.5** Antenna return loss

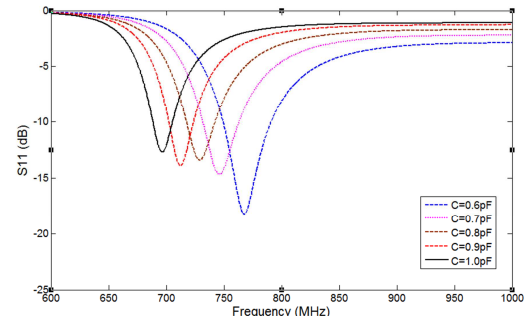


**Fig.6** Antenna return loss vs Capacitor value

Figure 6 shows the results of antenna's return loss when we integrate a capacitor on the open edge of the antenna. We can observe that when the value of capacitor change from 0.6pF to 1.0pF, the operation frequency decrease from 760Mhz to 700Mhz. Ac-

cording the figure, when the value of capacitor increase, the return loss ( $S_{11}$ ) increase from -19dB to -13.5dB and the bandwidth decrease from 50Mhz to 20Mhz.

### (3) Radiation pattern

Antenna's radiation pattern is presented in the Figure 7 and 8. Simulation results shows that with the integration of a capacitor in antenna structure, its gain from 2.42 dBi without the capacitor decrease to 1.8 dBi with  $C = 1\text{ pF}$ .

However, antenna efficiency still very good with the value of 92.3%

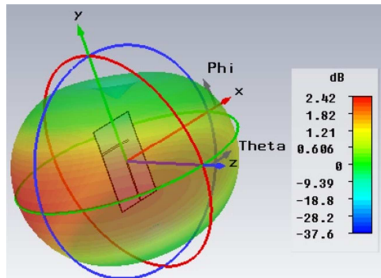


**Fig.7** Antenna's radiation pattern without Capacitor

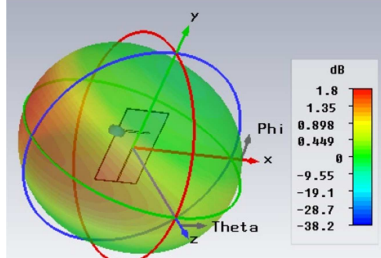


**Fig.8** Antenna's radiation pattern with  $C = 1\text{ pF}$

## 5. Conclusion

In this paper, the performance of a Notch antenna was examined. It showed that we can change the antenna's operation frequency from 900Mhz to 700Mhz by using a 1pF capacitor with the trait off of the bandwidth and gain. However, antenna efficiency is still acceptable when loaded with the capacitor. This shows us a potential way to design antenna which working in both GSM 900 MHz and 4G LTE 700 MHz. The frequency switching can be realize with the use of a varactor instead of the capacitor.

## REFERENCES

- [1] J. L. Volakis, C.-C. Chen, and K. Fujimoto, *Small antennas: miniaturization techniques & applications*. New York: McGraw-Hill, 2010.
- [2] C. Lach, L. Rudant, C. Delaveaud, and A. Azoulay, "A new miniaturized antenna for ISM 433 MHz frequency band," in *2010 Proceedings of the Fourth European Conference on Antennas and Propagation (EuCAP)*, 2010, pp. 1–5.
- [3] Ansys, *Ansys HFSS*. 2012.
- [4] CST, *CST Microwave studio* .

# SmartFarm System - Environmental Monitoring and Device Management using Web browser

NGUYEN Tuan Anh<sup>1</sup>

<sup>1</sup> Student, Faculty of Electronic Engineering, Posts and Telecommunications Institute of Technology  
(Km10, Nguyen Trai St, Ha Dong Dist, Ha Noi)  
E-mail: tuananh.d11dt1@gmail.com

Nowadays, technology is developing rapidly and strongly. Besides, the trend of developing IoT has been more popular in recent years. All industrial sectors and regions apply the scientific and technological achievements into production activities. Agriculture is not an exception. The demand for monitoring the environment and controlling devices remotely in agricultural production is also increasing.

Based on these reasons, the authors design a SmartFarm system for monitoring the environment condition and controlling devices using a web browser through Local Area Network (LAN) and Internet. The paper discusses various solutions for better management, and energy saving in a SmartFarm system.

**Key Words :** IoT, SmartFarm system, environmental monitoring, LAN and Internet, energy saving

## 1. INTRODUCTION

SmartFarm system is a system of devices controlled by a main controller. There are many wireless sensors nodes in the system. They create a wireless sensor system using WiFi to transmit data to the main controller. The main controller is able to schedule activities for devices in the system to work as a cycle. The main controller controls other devices based on the condition of the environment. The manager of the farm can observe the parameters about environment and the status of devices from a simple control panel, a web browser.

## 2. FEATURES

SmartFarm system is divided into 3 main modules as follows:

### Environmental monitoring:

- This module is a node in system.
- This module uses some sensors such as: moisture sensor, temperature sensor, humidity sensor, light sensor, and others sensor to detect the condition of environment. It sends data to the main controller by WiFi.
- This module use solar panel to get solar

energy, the purpose is self-supply for this module. By using solar energy, the system can protect the environment and save energy.

### Main controller:

- This module is the main part of system.
- This main module obtains data from “environmental monitoring” module. It analyzes and stores the data into common parameters. After that, it sends these parameters to the web browser. Besides, it controls status of relay to turn on/off devices in system such as: light bulb, water pumps, windows, and other devices.
- The above controlling is based on real time clock, and environment parameters for automatic purpose. User can also control it through web browser.

### Management:

- This module is web user interface.
- Web interface is used because it is the easiest way to manage the system through LAN and Internet. Users do not need to install any complex software. Instead, they only use a

web browser to access to the system.

- Thanks to the advances in web technology, web-based interface becomes more and more friendly and useful, presenting better ways to observe the status of environment and control the devices.

#### Benefits:

- With this self-supply environmental monitoring module, we can easily expand our multiple nodes. All we need is WiFi signal from LAN to sends data to main controller.
- We can surf our website from Internet without any money to keep it on Internet, we only need a Dynamic Domain Name System (DDNS) service which is provided by every Internet Service Provider.
- By using solar energy, we're also giving our hand to save earth.

## 3. PROBLEMS

SmartFarm system is divided into 3 main modules. Each module requires some different hardware and software solutions. Some requirements are listed below:

- **Environmental monitoring (1):** obtaining and calculating solar energy in an efficient way. Designing of environmental monitoring system and data transmission protocol.
- **Main controller (2):** real-time processing data from the environmental monitoring module. This module should be extendable to support more features in the future. The data processing approach should be automatic and intelligent.
- **Management (3):** web-based user interface should be friendly and fully functional. Users are able to access to the interface via LAN or via Internet.

## 4. DESIGN SOLUTIONS

### **(1) Environmental monitoring:**

- Obtaining and calculating solar energy in an efficient way:
  - Using ESP8266 WiFi module for transmission data to main controller purpose, it's also save energy.
  - Based on the level of energy consumption of the ESP-07, calculation show that 1-cell laptop battery 2200mAh is able to maintain operation of the ESP-07 within 20 hours since the end of the sun.
  - With the using of cell laptop battery 2200mAh, we only need to use a 5W solar panels that can ensure recharge batteries, and supply enough power for the ESP-07 also.
- Designing of environmental monitoring system and data transmission protocol:
  - There's only 1 ADC pin, and the voltage reference of the pin is 1V, it's restrictions of ESP-07. To solve this problem, we use HC595 for shift out purpose, we only turn on 1 sensor in one moment, other sensors are turned off in this moment.

ESP-07 has 3 WiFi mode: Access point mode, Station mode and Both. For the beginning of the project, we just need to use ESP-07 under Station mode. We use “*wifi.config*” command to set static IP for ESP-07, it will be easy for main controller to find ESP-07.

- ESP-07 and main controller will be communicate to each other as peer devices via LAN.

### **(2) Main controller:**

- Real-time processing data from the environmental monitoring module:
  - To obtain data from environmental monitoring, we use “*client.connect*” to access to ESP-07 static IP.
  - The data environmental monitoring sent to main controller is under “*char*” type, so if we want to compare to integer, we need to “*convert char to int*” before using it.
- Other requirements:

- In addition to relying on environmental parameters to decide to turn on/off the device in the system, and possibly extended scheduling for devices operating in real time, Intel Galileo board has the integrated real-time clock. Use the command:

```
system("date '+%H:%M:%S' > /tmp/time.txt");
```

to save time value to \*.txt file, then save it to a variable as “char” on Arduino IDE.

- Using Intel Galileo board, we can extend many others function, such as using webcams for monitoring security purpose, for OpenCV image processing, built-in microSD card slot web and image saving, use wifi card with PCI Express connection to increase the flexibility for the control board.

### (3) Management:

- Designing a web-based user interface:

- HTML and CSS is used to layout the website. Additionally, Java script is used create a dynamic website. We employed AJAX technique to update status of the devices and the parameters of the environment without reloading all parts of the website.

- To analyze the parameters, and to send them to the web server, we use the following XML snippet:

```
<?xml version = "1.0"?>
<inputs>
<tagnames>client.print(data)</tagnames>
</inputs>
```

- To allow users accessing the interface via LAN or Internet, the following solutions are considered:
  - 1) hiring a host and domain name and database
  - 2) using a DDNS service for the dynamic IP provided by Internet Service Provider.

We use the second method by configuring a “port

forwarding” rule for the static IP of the main controller. This technique can be easily done in the Intel Galileo board.

## 5. IMPLEMENTATION

Figure 1 below presents a SmartFarm system with three main modules.

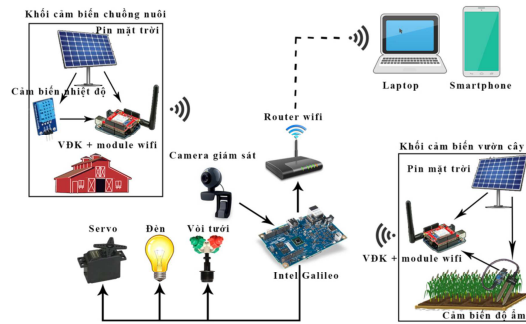


**Fig.1** SmartFarm System

## 6. CONCLUSION

The system works stably. The sensor nodes send data to the main controller regularly and accurately. In all experiment scenarios, the main controller is able to quickly respond to the command given by users. In most of case, users are satisfied with the web interface of the system.

## REFERENCES

- 1) <https://communities.intel.com/community/>
- 2) <https://www.arduino.cc/>
- 3) <http://www.instructables.com/id/intel/>
- 4) <http://www.w3schools.com/>
- 5) <http://startingelectronics.com/>

(November 20, 2015)

# Research and design of a short range wireless data transmitting device using sensor circuit

TRAN Duc Nam<sup>1</sup> and NGUYEN Trung Hieu<sup>2</sup>

<sup>1</sup> Student, Faculty of Electronics Eng., Posts and Telecommunications Institute of Technology  
(Km 10, Nguyen Trai Road, Hadong dist, Hanoi, Vietnam)  
E-mail: [tranducnam7@gmail.com](mailto:tranducnam7@gmail.com)

<sup>2</sup> Professor, Faculty of Electronics Eng., Posts and Telecommunications Institute of Technology  
(Km 10, Nguyen Trai Road, Hadong dist, Hanoi, Vietnam)  
E-mail: [hieunt@ptit.edu.vn](mailto:hieunt@ptit.edu.vn)

**Abstract--** This paper presents our research on the ability of interaction between two printed circuits board in short distance based on surveys, measurements and calculations of voltage value using ADC. As a result, an algorithms for data transmission was successfully build and two printed circuits board was designed and manufactured for demo.

**Key Words:** electric potential fields, capacitive coupling, data transmission circuit.

## 1. INTRODUCTION

Nowadays, Near Field Communication technology (NFC) has been researched and popularized widely around the world for short-range data transmitting combining with many software installed in our portable devices.. In recent studies, NFC technology is developed based on Radio Frequency Identification (RFID).

There are some researches on interactivity between circuits [1, 2] however their circuits design are bulky [3, 4]. Domestically, this research direction attracts scientist attention, but there are still no announced research results on scientific magazines, as well as application on electronic products yet.

This paper focus on studying a new interacting and transmitting method which is based on capacitive sensors between two circuits using ADC principles on Microcontrollers [3, 4, 7]. The goal is to design a prototype that can show off this ability and more over deepens our knowledge in this domain.

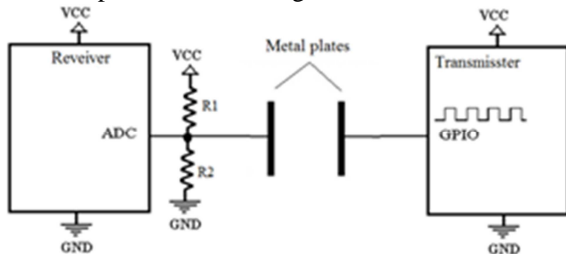


Fig. 1: Data transmission system.

Two circuits communicate with each other using 2 metal plates [1, 6, 7] (figure 1), which serve as two plates of a capacitor [10, 11] (the air layer in the middle serves as dielectric substance). Receiving base's voltage is divided to  $\frac{VCC}{2}$ . Transmitting base

detects square pulses, making the transmitting electric tension rapidly change between 0 & Vcc. When it is Vcc, an electric field appears from the transmitting base to the receiving base, making the receiving charge increases. ADC value measured on receiving base will be larger than  $\frac{VCC}{2}$ , otherwise when the value is 0 voltage value will be less than  $\frac{VCC}{2}$ .

Using capacitor's capacitance conversion, data can be transmitted from transmitting base to receiving base. Then the two devices will be able to communicate with each other [3, 4, 10, 11].

## 2. INTERACTIVITY BETWEEN TWO CIRCUITS IN A SHORT RANGE

When the transmitting base doesn't emit pulse, the receiving base's ADC voltage value is stabilized around  $\frac{VCC}{2}$ , with small fluctuation. When pulses are emitted, voltage's fluctuation will be larger. Recorded signal depends on transmitting base's square pulse frequency is presented in Figure 2: The capacitance is very small so resistor's value must be large enough to detect the transformation.

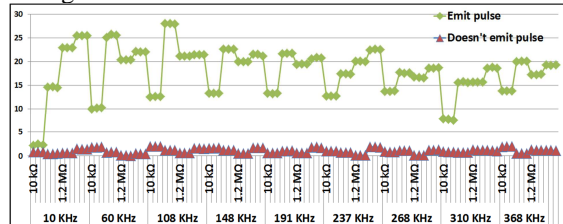


Fig. 2: Fluctuation according to R and F

In figure 3, with the same ADC sampling speed, with low frequency (19 & 38 KHz) we can only see a part of signal. When it is high enough (60 KHz), the

signal change continuously.

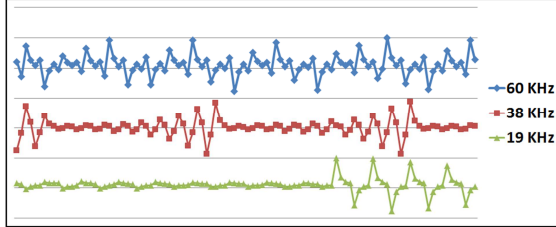


Fig. 3:  $R = 100k$

The more value of resistor, the longtime of charge/dis charge, we can easily see the voltage transformation (figure 4).

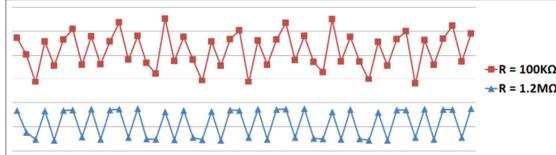


Fig. 4:  $F = 60KHz$

### 3. DATA TRANSMISSION METHOD SELECTION

#### (1) Data encoding

Using Pulse Length Coding, two binary bits 0 and 1 are encoded into two signals having the same cycle but different pulse widths (figure 5).

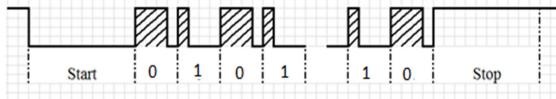


Fig.5: Data frame

#### (2) Data decoding

##### a) State decoding

By comparing a current sample value with the previous sample value, changes of the signal will be detected. Decode the current state of channels (figure 6):

- Rising edge: state = 1.
- Falling edge: state = 0.

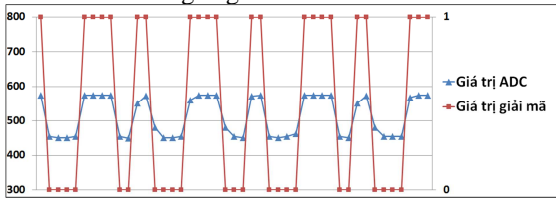


Fig. 6: State encoding

##### b) Measure Pulse Width

Measure the width (duration) of high and low levels of pulsed signals between each time signal's state is change

- Time high > time low: bit = 0.
- Time high < time low: bit = 1.

## 4. ALGORITHM

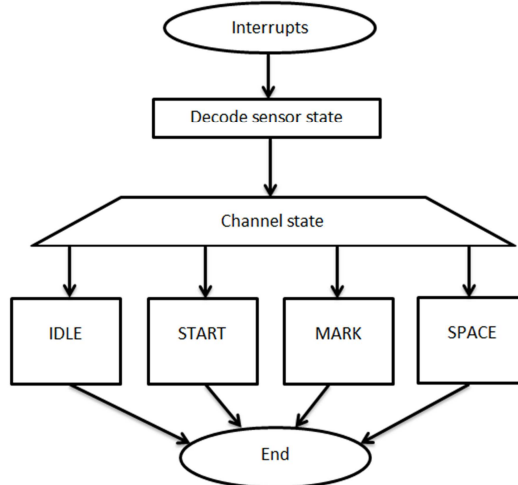


Fig. 7: Data decoding algorithm

In figure 7: The decoding process is divided into two stages:

- State decoding.
- Data decoding.

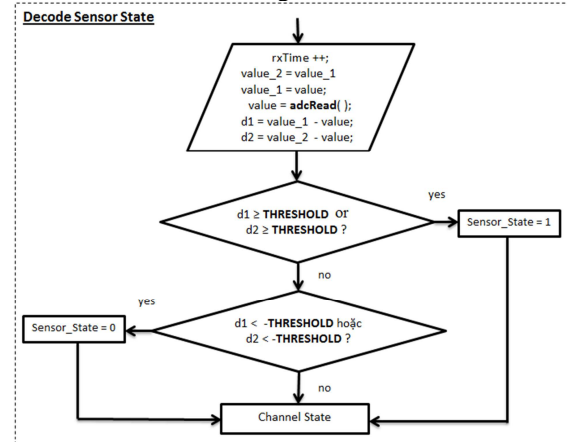


Fig. 8: Decode state algorithm

Compare new values with the old one to detect the signal state change (figure 8).

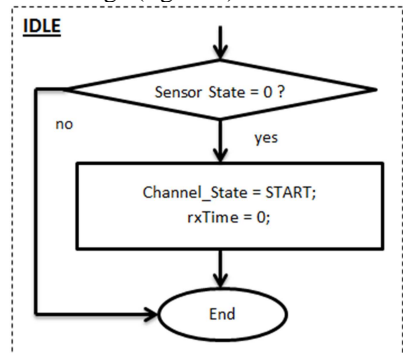
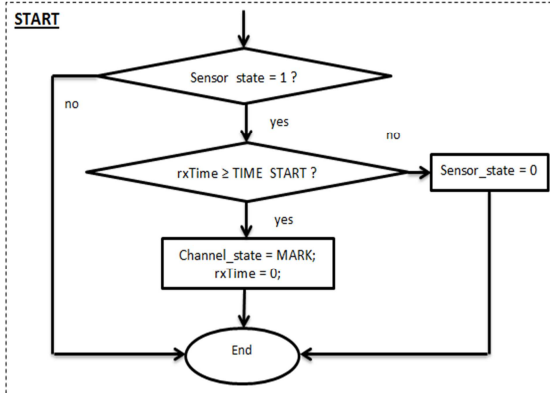


Fig. 9: IDLE

If the detected signal is pulled down to 0, then move

to START state (figure 9).



*Fig. 10: START*

If received START signal then system switches to receive data (figure 10).

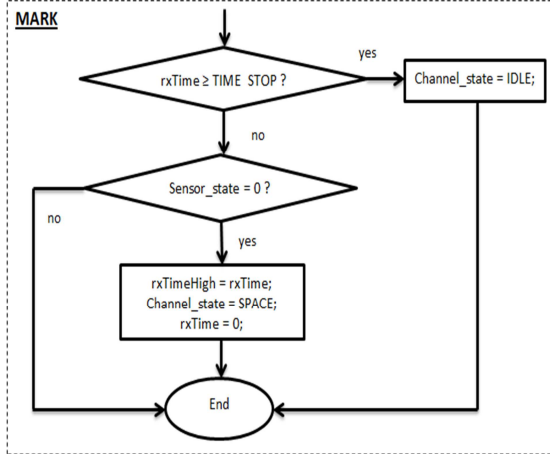


*Fig. 11: MARK*

If received STOP signal then system go back to IDLE state. If received falling edge then record high level pulse signal and move to SPACE state (figure 11).

If received rising edge then compare high level pulse with low level pulse to decode data. If we received not enough 8 bits then go back to MARK state to decode the next bit (figure 12).

## 5. DESIGNING WIRELESS DATA TRANSMITTING DEVICE

Applied research results on design, manufacture equipment for wireless data transmission in short range. Specifically, a peripheral module to communicate with the system through SPI is designed (figure 13).

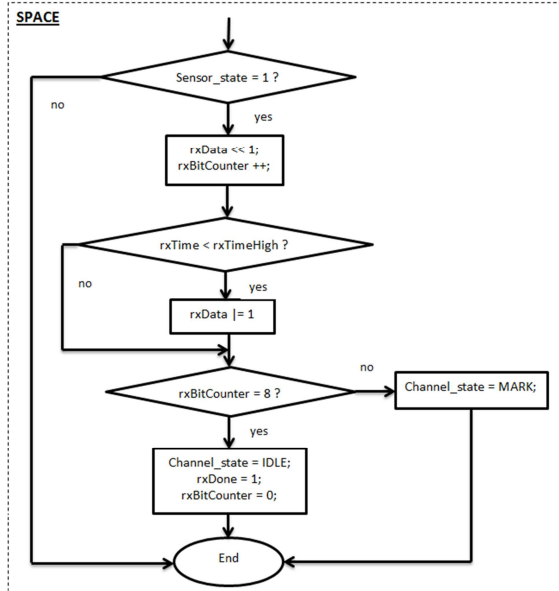


*Fig. 12: Space*

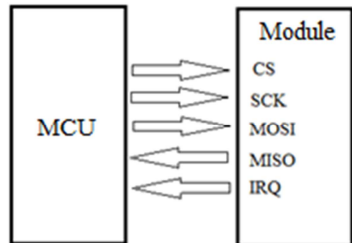


*Fig. 13: SPI Master-slave Interconnection*

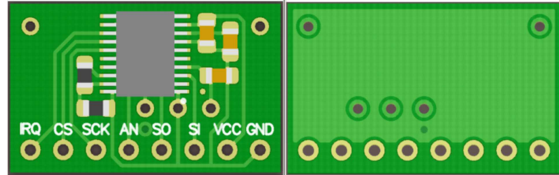


*Fig. 14: Top and bottom*

The bottom side is used as metal plate (figure 14). Features:

- Operating Voltage: 3.3 – 5 V.
- Small size: 2.1 x 1.3 centimeter.
- Max range: 2 cm.
- Max speed: 125 Kbps.
- Half duplex.
- Point-to-multipoint.

Using 1 byte SPI commands, you can active the Module data FIFOs or the register map during all modes of operation.

The STATUS register will indicate state of the data buffer. For reading, you send READ command then get data feedback from Module. For transmit-

ting, you send WRITE command then send data to it (figure 15).

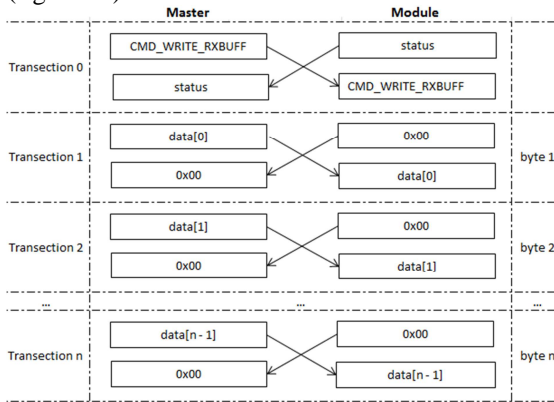


*Fig. 15: SPI write operation*

## 6. CONCLUSION

With the advantage is very low hardware requirements, this wireless data transmission method can be used and development on almost popular Microcontroller. This method can apply in security communications systems in short distance, electronics toys

## REFERENCES

- 1) Tadashi Minotani, Nobutarou Shibata, Mitsuru Shinagawa: Transmission device, electric field communication transceiver, and electric field communication system, US7583930 B2.
- 2) Tadashi Minotani, Mitsuru Shinagawa: Receiver, transceiver, and electric field communication system, US7801483 B2.
- 3) Shigeo Uoneda, Masato Hiramoto, Akira Kanayama: Capacitive coupling type data transmission circuit for portable electronic apparatus, US4763340 A.
- 4) Schyndel Andre Van: Wireless data transmission over quasi-static electric potential fields, US6336031 B1.
- 5) Narek Pezeshkian: Close-proximity communications system using capacitive coupled signal transfer, US8396136 B1.
- 6) George Kaplun, Alexander Rozin: Capacitive coupled bi-directional data and power transmission system, WO199801905 A1.
- 7) Yoshihiko Nekomoto, Yoshitaka Utsumi: Capacitive coupling, US5583525 A.
- 8) Kenji Doi, Masaru Hashimoto, Masaki Koyama, Yoshiko Suzuki, Tokuhisa Nishimura: Data transmission system using a human body as a signal transmission path, US6864780 B2.
- 9) Victor Allen Vega, John Howard Rolin: Wireless electrostatic charging and communicating system, US6879809 B1.
- 10) Reed Hoyt, John Lanza: Systems and methods for short range wireless communication, US 20060084380 A1.
- 11) Niels Kristian Kristiansen: A wireless communication device for inductive coupling to another device, US20100136905 A1.

# Research and manufacture health monitoring device using ZigBee wireless technology

HOANG The Viet<sup>1</sup>, VU Kha Khoi<sup>1</sup>

Student, Faculty of Electronics Eng., Posts and Telecommunications Institute of Technology  
(Km 10, Nguyen Trai Road, Hadong dist., Hanoi, Vietnam)  
E-mail: {[hoangtheviet93](mailto:hoangtheviet93), [khoivukha0509@gmail.com](mailto:khoivukha0509@gmail.com)}

In modern health care system, the demand for personal health tracing devices is increasing significantly. To solve this problem, we have developed a portable equipment which can monitor heart rate, blood pressure and health status. The measured data will be sent to the webserver to process and give out result in form of graphs so that users can monitor and judge their health status accurately. In some emergency situations, for example, someone may fall down or their heart rate goes down, a warning message will be sent to caregivers' phones immediately. This device is especially helpful for aged people.

**Keyword:** Zigbee, Health monitoring, heart rate, wearable sensor system.

## 1. INTRODUCTION

The elderly are more vulnerable to diseases and easily suffered from health problems than younger age groups. Health care needs of the elderly have increased fast. It is really necessary to have a remote health monitoring system based on wearable device. Health related information is gathered via body-worn wireless sensors and transmitted to the caregiver via an information gateway such as a mobile phone. Caregivers can use this information to implement interventions as needed.

This remote health monitoring device can monitor your heart rate, the operating status of the body like Activity, Sleep or free-fall, these parameters are extremely important. This information can be sent to the nurse or doctor, the information will be displayed as graphs so that they can be easily observed and monitored.

Beside that this device also sends reminders for tests and treatments, and alerts in case of potential hazardous conditions like free fall, heart rate go lower than threshold.

Despite the potential advantages of a remote monitoring system relying on wearable sensors like the one described above, there are significant challenges ahead before such a system can be utilized on a large scale. These challenges include technological barriers such as limitations of currently available battery technology as well cultural barriers such as the association of a stigma with the use of medical devices for home-based clinical monitoring. In the following section, we discuss key technologies enabling the development and deployment of wearable

technologies and remote monitoring systems.

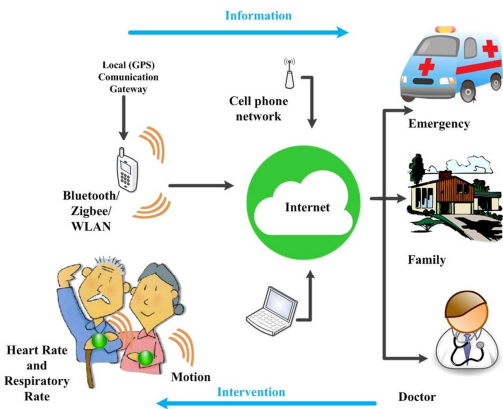


**Fig. 1** Illustration of health care system using wearable sensor

## 2. KEY TECHNOLOGIES

### (1) Medical Devices

#### a) Zigbee

Zigbee is a cheap wireless communications solution for embedded systems, the name of this protocol stems from the behavior of honeybees. Honeybee distributed on a large empty field, they perform a communication network to transmit information to the nest. They do this by forwarding the message follow zigzag shape until the nest received the mes-

sage.

A ZigBee network is a self-configuring, multi-hop network with battery-powered devices. This means that two devices that wish to exchange data in a ZigBee network may have to depend on other intermediate devices to be able to successfully do so. Because of this cooperative nature of the network, it is required that each device perform certain networking functions. These functions are determined by the logical *device type*.

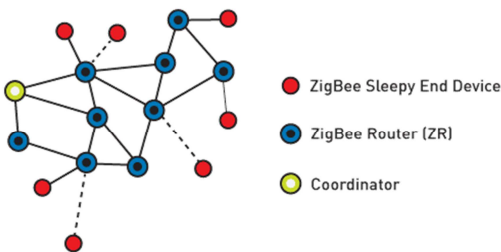


**Fig. 2** ZigBee networking protocol stack delivers robust and reliable mesh networking

**Coordinator:** This is the device that “starts” a ZigBee network. It is the first device on the network. The coordinator node chooses a channel and a network identifier (also called PAN ID) and then starts the network.

**Router:** As well as running an application function, a Router can act as an intermediate router, passing on data from other devices.

**EndDevice:** An end-device has no specific responsibility for maintaining the network infrastructure, so it can sleep and wake up as it chooses. End-devices only wake periodically to send and/or receive data to/from their parent. Therefore end devices can be powered by batteries for long periods of time.

### b) Heart Rate

This theory of heart rate measure is based on the principle of photoplethysmography (PPG) which is a non-invasive method of measuring the variation in blood volume in tissues using a light source and a detector.

Since the change in blood volume is synchronous to the heart beat, this technique can be used to calculate the heart rate. Transmittance and reflectance are two basic types of photoplethysmography. For the transmittance PPG, a light source is emitted in to the tissue and a light detector is placed in the opposite side of the tissue to measure the resultant light. Because of the limited penetration depth of the light through organ tissue, the transmittance PPG is applicable to a restricted body part, such as the finger or the ear lobe. However, in the reflectance PPG, the light source and the light detector are both placed on

the same side of a body part. The light is emitted into the tissue and the reflected light is measured by the detector. As the light doesn't have to penetrate the body, the reflectance PPG can be applied to any parts of human body.

In either case, the detected light reflected from or transmitted through the body part will fluctuate according to the pulsatile blood flow caused by the beating of the heart.

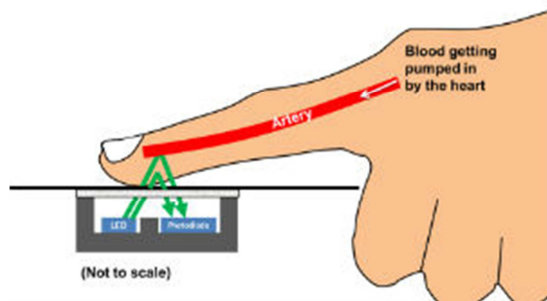


**Fig. 3** How a reflective optical heart rate monitoring solution works to measure the heart rate

### c) Activity status

For a human, experiencing a fall unobserved can be doubly dangerous. The obvious possibility of initial injury may be further aggravated by the possible consequences if treatment is not obtained within a short time. For example, many elderly individuals can suffer accidental falls due to weakness or dizziness—or, in general, their diminished self-care and self-protective ability. Since they tend to be fragile, these accidents may possibly have serious consequences if aid is not given in time. Statistics show that the majority of serious consequences are not the direct result of falling, but rather are due to a delay in assistance and treatment. Post-fall consequences can be greatly reduced if relief personnel can be alerted in time.

Activity status based on research into the principles of fall detection for an individual body, proposes a new solution for detection of fall situations, activity status utilizing the ADXL345,1 a 3-axis accelerometer from Analog Devices.

**ACTIVITY** is set when acceleration greater than the value stored in the THRESH\_ACT register is experienced.

**INACTIVITY** is set when acceleration of less than the value stored in the THRESH\_INACT register is experienced for longer than the time specified in the TIME\_INACT register. The maximum value for TIME\_INACT is 255 s.

**FREE\_FALL** is set when acceleration of less than the value stored in the THRESH\_FF register is experienced for longer than the time specified in the

TIME\_FF register. FREE\_FALL interrupt is mainly used in detection of free-falling motion. As a result, the FREE\_FALL interrupt differs from the INACTIVITY interrupt in that all axes always participate, the timer period is much shorter (1.28 s maximum), and it is always dc-coupled.

The fall-detection solution proposed here takes full advantage of these internal functions, minimizing the complexity of the algorithm—with little requirement to access the actual acceleration values or perform any other computations.

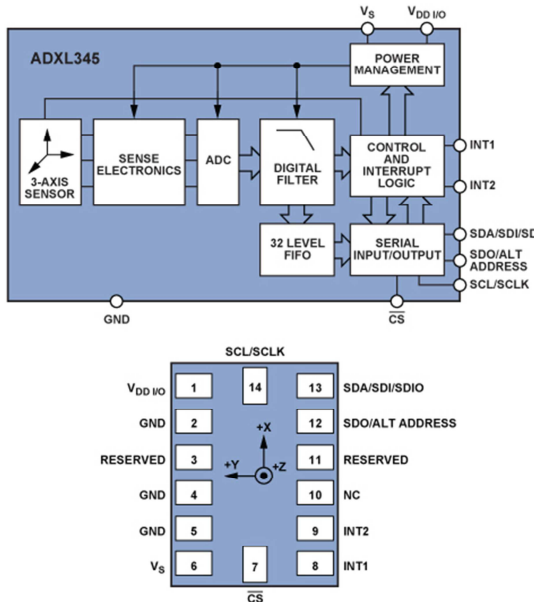


**Fig. 4** ADXL345 system block diagram and pin designations.

#### d) Medical Device Prototype

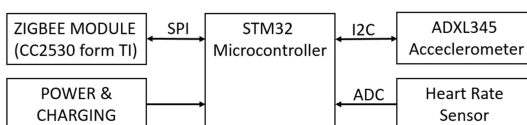


**Fig. 5** Medical Device Block

**STM32 Microcontroller:** is an 32-bit-ARM Cortex M core form ST Microelectronics. It read Heart Rate values from sensors, calculate them and Activity status form ADXL345, send the heart rate values and the activity status to the gateway via Zigbee module. It also displays information on the LCD for user.

**Zigbee Module:** is a Zigbee Network Processor (ZNP) based on CC2530 SoC contain 8051 microcontroller core form Texas Instrument. It run

Z-Stack(Zigbee protocols stack solution form TI) to handling data packet, communication to other Device (Gateway) in network and leave STM32 MCU free to handling other task.

**ADXL345 Accelerometer:** read 3 Axis Value, calculate them and export corresponding Interrupt(ACTIVITY, INACTIVITY, FREE\_FALL) with input Parameter form STM32 MCU like THRESH\_ACT, THRESH\_INACT.

**Heart Rate Sensor:** using SPRF359 IR sensor to mesuare Heart Rate follow the theory above, PPG Signal will pass 2 stage op-amps to filter unnecessary frequencies and increase the Amplitude of signal create conditions for ADC measurements correctly

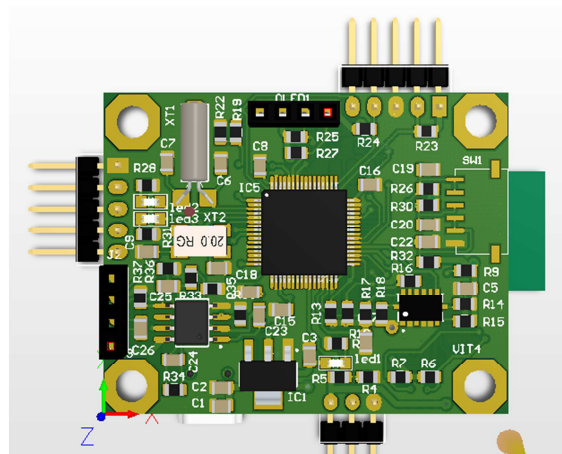


**Fig. 6** Medical Device in 3D

#### (2) Gateway device

Gateway is a device used to Health monitoring system to communicate with nurses through the internet and GSM, it is essential to keep track of information Activity status, the heartbeat of the elderly and immediately alert to a nurse if dangerous situations like fall.

Information from the medical device will be moved to the gateway via ZigBee, here gateways will be configured as coordinator, this information will be processed and posted to the database MySQL and webserver running on the gateway will obtain information from MySQL and displayed on graphs. Sim900A Module is used as a warning device, it uses the GSM network to communicate with the nurse's phone. If dangerous situation occurs a phone call or a sms message will be sent to the nurse's phone.

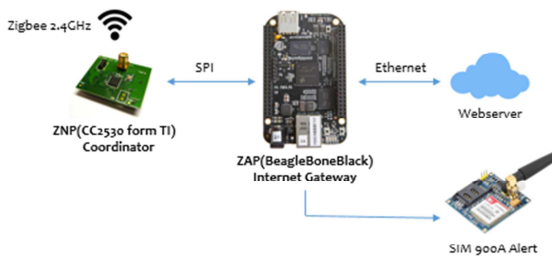


**Fig. 7** Gateway Device

## CONCLUSION

We have developed a portable and useful equipment to help the elderly with their health problems.

This device uses low power energy so user can bring it everywhere with you in daily life.

## REFERENCES

- 1) Ning Jia: Detecting Human fall with a 3-axis Digital Accelerometer, *Analog Device*, volume 43, July 2009
- 2) Zhilin Zhang, Zhouyue Pi, Benyuan Liu: "TROIKA: A General Framework for Heart Rate Monitoring Using Wrist-Type Photoplethysmographic Signals During Intensive Physical Exercise," IEEE Trans. on Biomedical Engineering, vol. 62, no. 2, pp. 522-531, February 2015
- 3) ADXL 345 datasheet, Analog Devices.
- 4) Ch Srikanth, D S Pradeep ,Sreeram Charan: Smart Embedded mediacial Diagnosis using BeagleBone Black and Arduino.

# **Characteristics of UNCD/a-C:H Film Diodes for the Device Application**

Kyosuke ONAGA<sup>1</sup>, Chianami KANESHIRO<sup>2</sup>

<sup>1</sup> Student, National Institute of Technology, Okinawa College  
Advanced course of Electronic Communication System Engineering  
(905 Henoko, Nago, Okinawa 905-2092 Japan)  
E-mail:ac144601@edu.okinawa-ct.ac.jp

<sup>2</sup> Professor, National Institute of Technology, Okinawa College  
Department of Information and Communication System Engineering

This paper presents the electrical properties of an ultrananocrystalline diamond/hydrogenated amorphous carbon composite (UNCD/a-C:H) films to clear and utilize device application. The UNCD/a-C:H films formed by the coaxial plasma gun technology were measured *I-V* characteristics to analyze electron-emission property as functions of space distance changes between film surface and collector electrode. The electron emission is related to electric field between collector electrode and UNCD/a-C:H surface. The experimental results indicate that UNCD/a-C:H films are realized the electron-emission property that will be attractive to apply functional devices.

**Key Words:** ultrananocrystalline diamond, UNCD/a-C:H, *I-V* characteristics, electron- emission

## **1. INTRODUCTION**

Recently, ultrananocrystalline diamond hydrogenated amorphous carbon composite (UNCD/a-C:H) films are studied on film formation technique which is comprising diamond crystallites with diameters of approximately 3–5 nm and an a-C:H matrix have been extensively investigated for their application <sup>1)</sup>. The UNCD/a-C:H film is attractive as a viewpoints of the following features: (a) It is easy to deposit different materials for realizing heterojunction, (b) surface morphology is extremely smooth, (c) Boron and Nitrogen doping are applied to realize *p*-type and *n*-type diamond film, respectively, and (d) physical properties are similar to diamond which are thermally stable up to at least 600 °C. Many researchers investigated the chemical properties of the UNCD/a-C:H films<sup>2-4)</sup>. Its unique optical and electrical properties that originate from the large number of grain boundaries (GBs) between the UNCDs and the amorphous carbon (a-C) are expected and tried to application of micro electro mechanical systems (MEMS) and semiconductor <sup>2,3)</sup>.

However, there is little literature about electric characteristics of UNCD/a-C:H film devices. To utilize device applications, it is important to

recognize the electric properties of UNCD/a-C:H film devices as well as the chemical properties of them.

The purpose of this paper is to examine a detail electric characteristics of UNCD/a-C:H film devices. In this paper, we investigate the electric properties of UNCD/a-C:H film device with simple diode structure. *I-V* and *C-V* measurements of test devices were carried out by using device measurement systems. Furthermore, the electron-emission characteristics of test device were analyzed by means of Fowler-Nordheim methods <sup>5)</sup>.

## **2. CHARACTERISTICS of ELECTRON EMISSION**

Fowler-Nordheim (FN) plots are used to analyze experimental data relating to cold field electron emission (CFE) <sup>5)</sup>. Many ways exist of presenting CFE data as FN plots, since any one of several "independent" variables (notably, voltage, barrier field, scaled barrier field, and macroscopic field), and any one of several "dependent" variables (notably, current, local current density, and macroscopic current density) can be used.

Based on  $I$ - $V$  measurement data, FN equation is shown as below<sup>5, 6)</sup>,

$$J = \frac{q^3 E^2}{8\pi h \phi t^2(y)} \exp\left(-\frac{8\pi\sqrt{2m}}{3hqE} \phi^{\frac{3}{2}} v(y)\right) \quad (1)$$

$$y = \sqrt{\frac{q^2}{4\pi\epsilon_0}} \frac{E^2}{\phi}$$

where  $J$  is current density,  $E$  is electric-field, and  $\phi$  is work-function of electron sources. And,  $t^2(y)$  and  $v(y)$  are correction terms due to the image-force effect as approximated  $t^2(y) \approx 1.1$  and  $v(y) = 0.95 - y^2$ .

Therefore, Eq. (1) is modified by logarithm as below,

$$\ln\left(\frac{I}{V^2}\right) = \ln(a) - \frac{b}{V} \quad (2)$$

where  $d$  is a distance between collector electrode and emission surface. The coefficients of  $a$  and  $b$  are determined

$$a = \frac{q^3 S \beta^2}{8\pi h \phi} \exp\left(9.8/\phi^{\frac{1}{2}}\right) \quad (3)$$

$$b = \frac{8\pi\sqrt{2m}}{3hq\beta} \phi^{\frac{3}{2}} \quad (4)$$

where  $S$  is the effective emission area and  $\beta$  means a coefficient due to electric-field and emitter characteristics. Therefore, the effective work function  $\phi$  is calculated from Eqs. (2)-(4). From Eqs. (1) and (2), when  $I/V^2$  changes exponentially as a function of  $I/V$ , it indicate that electron-emission occurs from the surface to collector electrode.

### 3. EXPERIMENTS

#### (1) Device structure

The UNCD/a-C:H films were formed by the coaxial arc plasma gun (CAPD) technology<sup>6)</sup>. One of the surface morphology by CAPD is that the film thickness distributed like a concentric circle. Therefore, the center of the film is thick rather than the edge of the substrate. The film thickness of center is about 340nm. Fig.1 shows device structure and UNCD/a-C:H film surface. The substrates were prepared  $n$ -type UNCD/a-C:H films with 8 at.% of Nitrogen concentration on silicon substrate.

#### (2) Measurement system and condition

Fig.2 shows experimental setup for measurement of electron-emission characteristics. The distance of collector electrode and substrate surface is varied the order from 7.5  $\mu\text{m}$  to 30  $\mu\text{m}$ . The emission area is

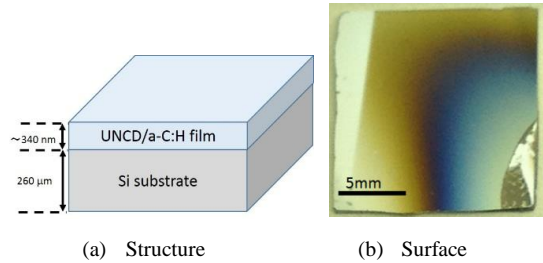


**Figure 1** Schematic illustration of (a) device structure and (b) photograph of surface morphology.

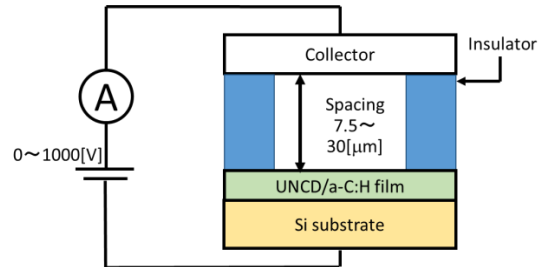


**Figure 2** Schematic illustration of experimental setup for measurement of electron emission. The space distance are varied.

about 1.0  $\text{mm}^2$ . The ranges of applied voltage are from changed 0 V to 1000 V, and the collector currents were measured by using electrometer. These  $I$ - $V$  characteristics were carried out under vacuum condition with  $10^{-6}$ - $10^{-5}$  Pa.

Furthermore, the static  $I$ - $V$  and  $C$ - $V$  characteristics of fabricated devices were measured by using semiconductor parameter analyzer.

### 4. EXPERIMENTAL RESULTS and DISCUSSION

#### Electron-Emission Characteristics

##### (1) Dependence on film thickness

Fowler-Nordheim (FN) plots are based on  $I$ - $V$  characteristics as function of the distance between collector electrode and UNCD/a-C:H film surface. Fig.3 (a) shows the possibility of electron-emission from UNCD/a-C:H films. The marks of the circles (O) and the cross (X) means the possibility of electron emission were observed or not, respectively. The detail  $I$ - $V$  data shows in Fig. 3 (b), which is Fowler-Nordheim plot based on  $I$ - $V$  characteristics. As shown in Fig.3 (b),  $\ln(I/V^2)$  vs.  $I/V$  shows that the slopes of the data is almost same. As shown in Eqs. (1)-(4), the slope value indicates the effective work function caused by electron-emission. Therefore, these characteristics imply that electron-emission is occurred from UNCD/a-C:H films to collector electrode.

The estimated values of the film thickness and the threshold voltage are summarized in Table I. The estimated values of the threshold voltage are 135 V, 333 V, and 208 V with 7.5  $\mu\text{m}$  of the space distance between collector and film surface. In addition, the slope values of FN plot are not dependent on the measurement point (film thickness). Therefore, it is expected that the chemical condition of UNCD/a-C:H film which formed by CAPD is almost same in surface.

Table II is summarized the threshold voltages to compare with the pulsed laser deposition (PLD) technology. The threshold voltages of CAPD are lower than that by PLD. This results means that the UNCD/a-C:H film formed by CAPD is attractive rather than that by PLD due to capability of low driving voltage.

## (2) Dependence on collector electrode distance

To investigate the dependence on the space distance between collector electrode and UNCD/a-C:H film. Fig.4 shows FN plots as a function of the space distance between collector electrode and substrate surface.

From these results, the estimated values of the threshold voltage are shown in Table III. The 250 V, 360 V, 526 V, and 667 V as a function of the distance, 7.5  $\mu\text{m}$ , 15  $\mu\text{m}$ , 22.5  $\mu\text{m}$ , and 30  $\mu\text{m}$ , respectively. The experimental results indicated the electric-field is affected the electron emission properties.

As shown in Fig.4,  $\ln(I/V^2)$  vs.  $I/V$  shows the slopes of the data is date of slope value is little difference. This result means that the electron emission is related to electric field between collector electrode and UNCD/a-C:H surface.

## 5. CONCLUSION

The electron-emission characteristics of UNCD/a-C:H film which formed by CAPD technology were investigated  $I$ - $V$  characteristics and analyzed by FN plot methods. The experimental results indicated as bellow;

- (1) The film chemical condition of UNCD/a-C:H film which formed by CAPD is almost same in surface area with  $\text{mm}^2$  because the slope values of FN plot are not dependent on the film thickness.
- (2) The electron emission is related to electric field between collector electrode and UNCD/a-C:H surface.

These results indicated that the coaxial arc plasma gun (CAPD) technology is applicable of formation of UNCD/a-C:H film rather than the pulsed laser deposition (PLD) technology.

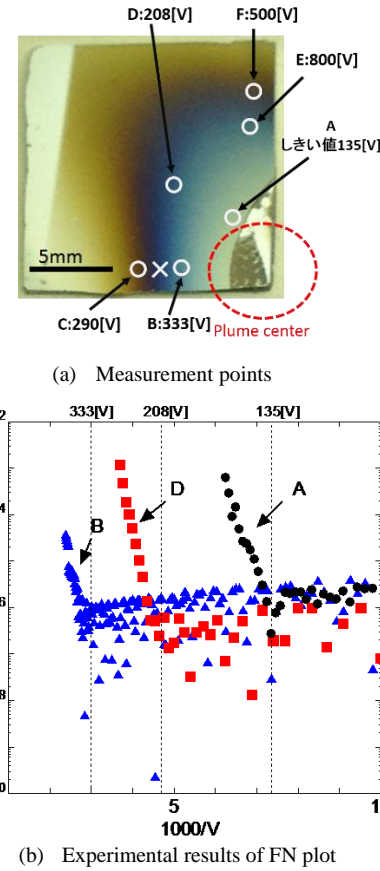


**Figure 3** Measurement points and  $I$ - $V$  characteristics based on FN plot.

**Table I** Summary of threshold voltage based on FN plot at measurement points.

Measurement Points	Approximately Film Thickness [nm]	Threshold Voltage [V]
A	340-280	135
B	280-220	333
C	160-100	290
D	280-220	208
E	280-220	800
F	220-160	500

**Table II** Comparison of the threshold voltages of UNCD/a-C:H films formed by PLD and CAPD.

Film Thickness[nm]	Approximate Threshold Voltage[V]	
	*PLD <sup>8)</sup>	CAPD
500	500	-
340-280	250	135
160-100	-	290

\*PLD Pulsed Laser Deposition

**ACKNOWLEDGMENT:** Authors thank Dr. Yoshitake who belong Kyushu University provided UNCD/a-C:H films. Authors also thank Dr. K. Higa who was a professor of NIT Okinawa gave fruitful advice.

## REFERENCES

- 1) O.A. Williams, M. Daenen, J. D'Haen, K. Haenen, J. Maes, V.V. Moshchalkov, M.Nesládek, D.M. Gruen, *Diamond Relat. Mater.* vol.15 (2006) p. 654.
- 2) T. Yoshitake, Y. Nakagawa, A. Nagano, R. Ohtani, H. Setoyama, E. Kobayashi, K. Sumitani, Y. Agawa, K. Nagayama, *Jpn. J. Appl. Phys.* vol.49 (2010) 015503.
- 3) S. Srinivasan, J. Hiller, B. Kabius, O. Auciello, *Appl. Phys. Lett.* vol.90 (2007) 134101.
- 4) A.R. Krauss, O. Auciello, D.M. Gruen, A. Jayatissa, A. Suman, J. Tucek, D.C. Mancini, N. Moldovan, A. Erdemir, D. Ersoy, M.N. Gardos, H.G. Busmann, E.M. Meyer, M.Q. Ding, *Diamond Relat. Mater.* vol.10 (2001) p.1952.
- 5) T. E. Stern, B. S. Gossling and R. H. Fowler, *Proc. R. Soc. Lond. A* 124, p.699 (1929).
- 6) E.L.Murphy, R.H. Good, *Phys. Rev.* vol.102, pp.1464-1473 (1956).
- 7) M. Egiza, H. Naragino, A. Tominaga, K. Murasawa, H. Gonda, M. Sakurai, and T. Yoshitake, Proceedings of Intellectual Exchange and Innovation Conference on Engineering & Sciences (IEICES), to be published.
- 8) T.Maebara, and K.Higa, The 60th JSAP Spring Meeting, 2013[Extended Abstracts], 28a-B1-7

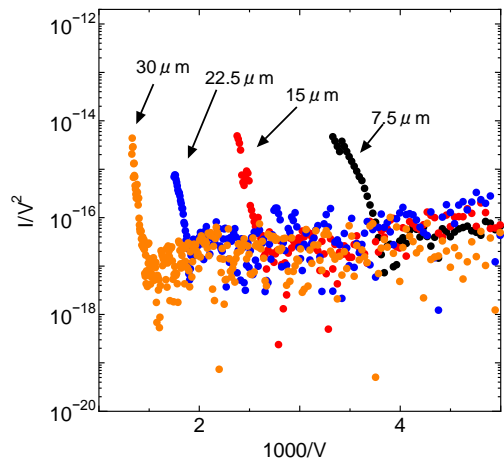


**Figure 4** FN plot based on *I-V* characteristics of UNCD/a-C:H film formed by CAPD.

**Table III** Summary of the threshold voltage and the slope of FN plots dependent on the space distance.

Distance between Collector and Surface [μm]	Threshold Voltage [V]	Slope Value of FN Plot
7.5	250	-8.68
15	360	-20.11
22.5	526	-24.9
30	667	-41.17

# Propagation Characteristics of SAW with Various Periodic Arrays

Taisei SAKAI<sup>1</sup>, Chinami KANESHIRO<sup>2</sup>

<sup>1</sup> Student, Advanced Course of Electronics and Communication System Eng., National Institute of Technology, Okinawa College  
(905 Henoko, Nago, Okinawa 905-2192, Japan)  
E-mail:ac154603@edu.okinawa-ct.ac.jp

<sup>2</sup> Professor, Dept of Information and Communication System Eng., National Institute of Technology, Okinawa College  
(905 Henoko, Nago, Okinawa 905-2192, Japan)  
E-mail:chinami@okinawa-ct.ac.jp

This paper presents that surface acoustic wave (SAW) devices with periodic arrays are attractive to control propagation frequencies. It is known that SAW with interdigital transducers has filtering characteristics itself. The controllable filters are realized by forming periodic arrays at SAW propagation path. To investigate the frequency control of SAW test devices with periodic arrays, the transmission characteristics were measured by the network analyzer. The various periodic patterns, such as line and space, dotted matrix array, and the other pattern, were examined. The experimental results indicated that the SAW device with periodic array could control the propagation frequency. The filtering characteristics are depend on periodic array pattern, such as line and space, dotted array.

**Key Words :** Surface Acoustic Wave (SAW), Frequency control, Filters, Periodic Arrays

## 1. INTRODUCTION

Surface acoustic wave (SAW) devices are attractive to apply many devices, such as RF filters, sensors and so on. Especially, SAW devices with interdigital transducers (IDTs) are used as SAW filters because of its property of controllable frequency. Surface acoustic wave (SAW) devices have been widely used in various applications and have several advantages: (a) extremely high sensitivity, (b) high SNR value, (c) small size, (d) wide operating frequency range (10 MHz to 1 GHz), and (e) ease of integration with planar processing technology. Because of these advantages, SAW technology is often applied in the fabrication of various electronic devices such as RF filters and sensors <sup>1-4)</sup>.

Many researchers tried to simulate and demonstrate filtering properties of ultrasonic propagation with periodic arrays <sup>6-8)</sup>. The non-linear effect is significantly important of ultrasonic propagation with periodic array. However, there is a little literature for SAW device with periodic array. To clarify SAW filter with periodic array, it is more attractive to realize combination device between SAW and optics, such as sonic crystal and photonic crystal.

The purpose of this paper is to examine fundamental propagation characteristics of SAW device with periodic array to utilize application devices of SAW filter. The propagation characteristics of test devices were demonstrated with periodic arrays, such as line and space, dotted array, and the other pattern.

## 2. SAW PROPERGATION METHODS

The generated SAW by electric field of IDTs are modeled by the rectangular model and/or the  $\delta$  function model <sup>9)</sup>. There are some models based on equivalent electric circuit used to model the behavior of piezoelectric ceramics plates. Mason's model is the most known <sup>10,11)</sup>. The fundamental component of SAW is shown by

$$A(\omega) \approx V_o \frac{\sin\left(\frac{2\pi f}{v_c} \cdot \frac{a}{2}\right)}{\left(\frac{2\pi f}{v_c} \cdot \frac{a}{2}\right)} \quad (1)$$

where  $v_c$  is the SAW velocity,  $V_o$  means electric field voltage determined by strip line,  $a$  is the space be-

tween electrodes as shown in Fig. 1.

The Bragg's law is applied to the reflected wave in case of the SAW propagation in periodic array as shown in Fig. 2 (a). The phase condition of the reflected wave is determined by

$$2d \sin \theta = m\lambda \quad (2)$$

Where  $d$  is the interval between the structure array,  $\lambda$  is wavelength of propagation wave, and  $\theta$  is the incident angle.

In SAW propagation, since the incident angle is  $90^\circ$  as shown in Fig. 2 (b), the relation between  $d$  and  $\lambda$  is

$$\lambda = \frac{m}{2d} \quad (3)$$

Furthermore, the center frequency of SAW is presented by

$$f_c = \frac{v_c}{2d} \quad (4)$$

Therefore, the propagation characteristics of SAW with periodic array are determined the phase difference between the original SAW and the reflected wave from the structural array.

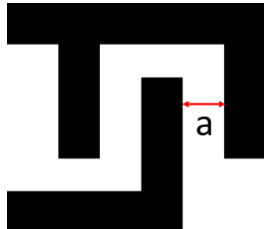


**Fig.1** Schematic illustration of IDT electrode.

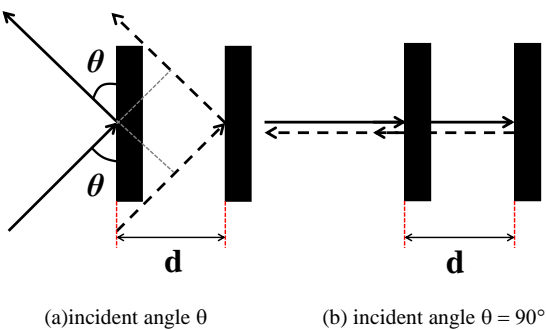


**Fig.2** Schematic illustrations based on Bragg's law  
(a) incident angle  $\theta$ , and (b) incident angle  $\theta = 90^\circ$ .

### 3. EXPERIMENTS

Ycut-Z LiNbO<sub>3</sub> substrates were used for base-substrate as piezoelectric material. The inter-digital transducers (IDTs) were formed on the LiNbO<sub>3</sub> surfaces by the radio frequency (RF) sputtering deposition. The specification of fabricated test devices are summarized in Table I. The IDTs consist of lines and spaces with 10  $\mu\text{m}$  and 25.5 pairs. The cross length of IDTs is 480  $\mu\text{m}$ . The length between input and output IDTs is 3.9 mm.

To examine propagation characteristics, the periodic array are formed at propagation path with various patterns, such as line and space, dotted matrix array, and wave guide, as shown in Table I. Such periodic patterns are formed metal deposition by RF sputtering technology.

The fabricated test devices were examined the transmission characteristics by using network analyzer. Figure 3 shows a schematic illustration of experimental setup. The frequency characteristics are survey in wide range from 300 kHz to 1.50 GHz at beginning. The detail examinations are carried out around the center frequency.

**Table I** Specifications of fabricated SAW devices.

Y-Z LiNbO <sub>3</sub> ( $v = 3470 \text{ m/sec}$ )	
IDT	25.5 pairs
Wave length	40 $\mu\text{m}$
IDT width	Single 10 $\mu\text{m}$
Cross length	480 $\mu\text{m}$
propagation path length	3.9 mm

#### Periodic Array Patterns

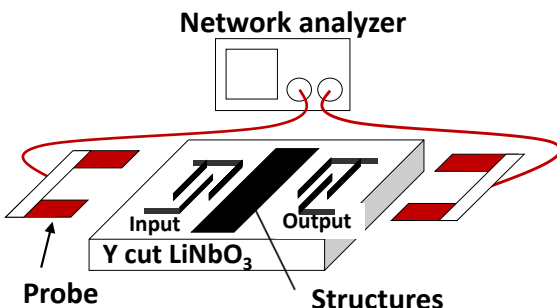
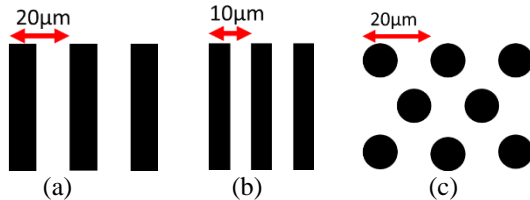


**Fig.3** Schematic illustration of experimental for frequency measurement.

## 4.EXPERIMENTAL RESULTS

Figure 4 shows experimental results of SAW transmission of fabricated devices. These horizontal axes are frequency, and these vertical axes are transmission. Fig. 4 (a) is the characteristics of SAW propagation with and without strip lines with 20  $\mu\text{m}$ . The original center frequency of dotted line as shown in Fig. 4 (a) is 85.9 MHz which is almost equal to theoretical value of 86.7 MHz calculated from  $f = v_c / \lambda$ . On the other hand, the stop-band characteristic is observed at the solid line which is the characteristics with strip lines in Fig. 4 (a). This result indicated that the phase of reflected wave from strip lines is reversed by the propagation wave.

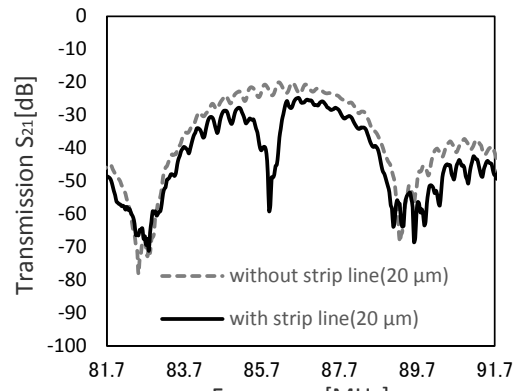
To compare the effect of phase difference from strip lines, figure 4 (b) shows the propagation characteristics of SAW with strip lines with 10  $\mu\text{m}$ . No stop-band was observed in case of the strip line with 10  $\mu\text{m}$ . This experimental result indicated that the phase of reflected wave from strip lines is in phase by the propagation wave.

To utilize wave-guide propagation characteristics, the transmission characteristics of SAW with dotted matrix array were investigated. Figure 4 (c) shows the propagation characteristics of SAW with the dotted matrix array.

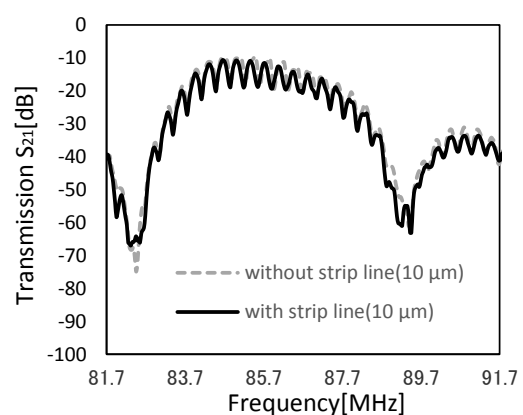
Figure 5 shows illustrations of expected interaction between propagation wave and reflected wave. In case of strip line as periodic structure as shown in Fig. 5 (a), the propagation wave faced the strip lines uniformly. As a result, the reflected wave goes to the opposite direction against the propagation direction. Based on the Bragg's law, when the phase difference between the propagation wave and the reflected wave is the same, the transmission characteristic of the SAW has the stop-band due to interaction of cancellation between the propagation wave and the reflected wave.

On the other hand, in case of dotted arrays as periodic structure as shown in Fig. 5 (b), the propagation wave faced the dots partly. The most of reflected waves are interacted with the propagation wave. Some waves propagate in free. Therefore, the ripples of main lobe are related to the period of the dotted matrix.

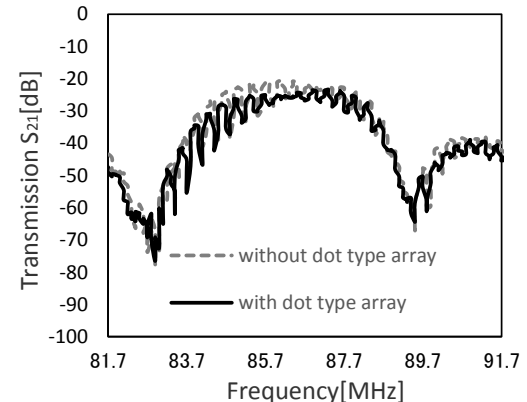
These experimental results indicate that the structural design is important to define the SAW propagation characteristics.



(a)Transmission S<sub>21</sub> without and with 20  $\mu\text{m}$  of strip lines



(b)Transmission S<sub>21</sub> without and with 10  $\mu\text{m}$  of strip lines



(c)Transmission S<sub>21</sub> without and with dotted matrix array

**Fig.4** Transmission characteristics of original SAWs and (a) with 20  $\mu\text{m}$  of strip lines, (b) with 10  $\mu\text{m}$  of strip lines, and (c) with dotted arrays.

## 5. CONCLUSIONS

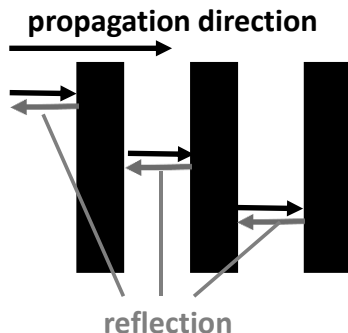
This paper presents the examination characteristics of SAW propagations with various periodic arrays. The summaries of the experimental results are below :

- (1) The stop-band is formed when the phase of SAW propagation is in phase with the reflected wave. This result indicated that the band-pass of SAW transmission can be controlled by the design of periodic array.
- (2) In case of SAW device with dotted array, no stop-band was observed on transmission characteristics. Change of transmission characteristics is shown the difference of periodic array patterns in the same period.

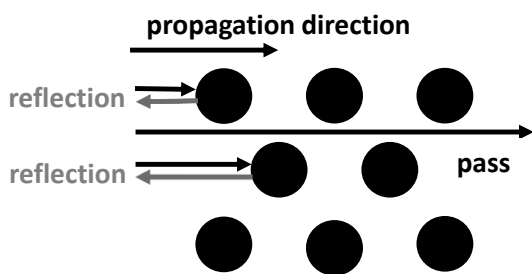
These results indicate that SAW device with periodic array could control the propagation frequency and filtering characteristics.

## REFERENCES

- 1) Hiroji Suzuki, Kenji Komine, Qixin Huang and Kohji Hohkawa, Jpn. J.Appl. Phys, Vol. 36, No. 5B, pp.3109-3114 (1997).
- 2) D.S.Ballatin, R.M. White, S. I. Martin, A. J. Rico, E.T.Zellers, G. C. Frye, and H. Wohltjen, "ACOUSTIC WAVE SENSORS" Chap. 5-6 pp.222-395 Academic Press.(1997) .
- 3) M. Feldmann and J. Henaff, Artech House Publishers (1989).
- 4) K. Hohkawa, T. Suda, Y. Aoki, C. Hong, C. Kaneshiro, and K. Koh, IEEE Transactions on Ultrasonics, Ferroelectrics and Frequency Control, pp. 466 – 474 (2003).
- 5) C.Kaneshiro and R. Gushiken, ECS Transactions,Vol.41 (20) pp.69-78 (2012)
- 6) R. Picó, I. Pérez-Arjona, V.J. Sánchez-Morcillo, K. Staliunas, Applied Acoustics. Vol. 74 pp. 945-948 (2013).
- 7) Serkan Alagoz, Applied Acoustics, Vol.76 pp. 402-406 (2014).
- 8) G. Gupta, K.-M. Lim, C.H. Chew, Wave Motion Vol.55 pp.1-9 (2015).
- 9) W. R. Smith, H. M. Gerard, and W. R. Jones, IEEE Trans. MTT-17, pp. 856-864 (1969).
- 10) W. P. Mason, "Electromechanical Transducers and Wave Filters, 2nd Ed. (D. Van Nostrand Company, Princeton, New Jersey, 1948).
- 11) A.Ballato, "Modeling Piezoelectric and Piezomagnetic Devices and Structures via Equivalent Networks", IEEE Trans. Ultrason., Ferroelect. and Freq. Contr. 48, pp.1189-1240 (2001).



(a) Schematic illustration of expected interaction between the propagation wave and the reflected wave in strip lines



(b) Schematic illustration of expected interaction between the propagation wave and the reflected wave in dotted matrix array

**Fig.5** Schematic illustrations of expected interaction between the propagation wave and the reflected wave in (a) strip lines and (b) dotted matrix array.

# Development of Sensor Network with Growth Rate Sensor for Agricultural Field

Sho YOSHIDA<sup>1</sup>, Yoshihumi SHIMOSHIO<sup>2</sup>

<sup>1</sup> Student, Advanced Course of Electronics-information Systems Engineering,  
National Institute of Technology, Kumamoto Colegge  
(Matsuo, Kumamoto-shi, Kumamoto 861-5280, Japan)  
E-mail:ae13yoshida@g.kumamoto-nct.ac.jp

<sup>2</sup> Professor, Inst., National Institute of Technology, Kumamoto Colegge  
National Institute of Technology, Kumamoto College  
(Suya, Koushi-shi, Kumamoto 861-1102, Japan)  
E-mail:shimoshio@kumamoto-nct.ac.jp

**Abstract** Recently, decreasing birthrate and aging population cause labor shortage in Japan. Therefore it is desired to promote efficiency of various things. Accordingly, as one of the ways to promote efficiency, a sensor network is used in various fields. A sensor network is also used in agriculture, and the research has been doing actively. A sensor network construction in agricultural field is described in this report. The purpose of this research is construction of the sensor network having new benefit. Conventional system does not have a function to measure growth rate of products yet. Therefore it will be a benefit to install growth rate measurement system. In addition, it is focused on easy introduction to a farmland. The growth rate system should be low cost and simple structure.

**Key Words :** sensor network, Arduino, XBee, greenhouse, growth rate

## 1. INTODUCTION

### (1)Background

In agriculture, there are many problems to be solved. Now the world population is increasing continuously. It causes lack of food sooner or later. Additionally decreasing birthrate and aging population cause labor shortage in Japan. Accordingly it is necessary for promoting efficiency of agriculture. As an environment of farmland depends on season and weather, farmers must work in hard condition. Additionally a farmland is very large. Therefore farmers have to walk long distance when they work. Farmers grow several kinds of product. Each product needs different conditions for each. Accordingly, it is necessary to provide suitable conditions for each

product to be grown up well. Farmers must observe farmland every day to manage it. As this is very tiring thing, farmland management using network technology is required. Recently a sensor network technology has been used to help farmland management. This background refers [1].

### (2)Purpose of research

Purpose of research is making sensor network system to help farmers' work. The aim of the system is shown in Fig.1. The system consists of sensor devices, wireless modules and server. The system consists of 3 steps: sensing, transmitting and data processing. By using the system, farmers can observe environment of farmland in their house.

The system in this research is assumed for using in a greenhouse and for managing plural products at the same time. If we introduce the system, it reduces work load, increases efficiency of farming and protects farmers from sunlight, rain etc. Now similar system exists already. Therefore, a growth rate sensor will be developed in this research for originality. Although a conventional system uses image data of products, it is not able to measure the growth rate quantitatively. In this research, it is investigated to obtain information about growth rate.

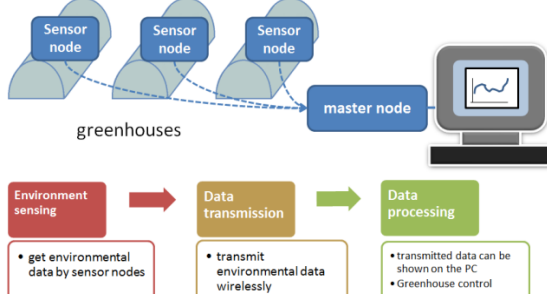


Fig.1 outline of system

## 2. ABOUT SENSOR NETWORK

A sensor network collects various data from many wireless sensor. Conceptual diagram of the sensor network is shown in Fig.2. The sensor network consists of one master node, plural sensor nodes and data server. Wireless sensor network can save cost because it does not need cables. Additionally, it does not have any limitations for installation place in a farmland. Sensor nodes collect various data around themselves. After collecting, sensor nodes transmit data to master node. Data which are received by master node are saved and retained in a data server. The retained data are provided for clients through browser. The processing flow described above is main function of sensor network. When we construct a sensor network, some conditions are required to wireless module. Conditions are shown below.

- A wireless module can work with battery. And it is required low power consumption.
- It is necessary that wireless module is small. A module can be installed at any place.
- Modules can construct a flexible network.
- A module is strong for a noise. A module can communicate anytime.
- A module is high security.

One of wireless standards, IEEE802.15.4, is regulated for these conditions. IEEE802.15.4 is a standard which is aim to construct a wireless sensor network system. Wireless modules having same ID become one group in this standard. This group is called Personal Area Network. The total number of module which can participate in Personal Area Network is numerous. Therefore it is possible to construct a large scale network. The connect time to a network is very short. Accordingly power consumption is low. A sensor network is used various field. For example agriculture, industry, building, house etc. A sensor network exists anywhere around us. When we construct sensor network, a main problem is cost because farmers cannot introduce system if system cost is high. A sensor network must be low cost.

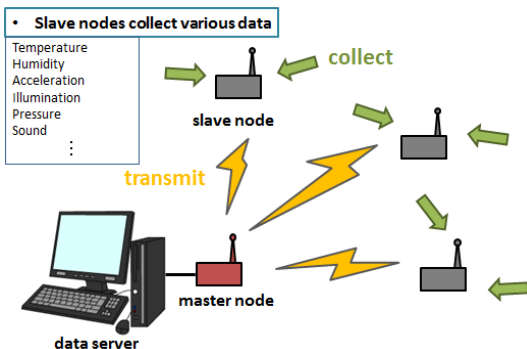


Fig.2 abstract of sensor network

Especially in agriculture, a system needs many sensor nodes to cover farmland. If each sensor node is expensive, total cost of system become very high. It is needed to achieve construction of sensor network with low cost.

## 3. SENSOR NETWORK CONSTRUCTION

### 3.1. PROCEDURE

The sensor network system is made by 4 steps. This

Research is preceded according to Fig.3. First, sensor node is made. An Arduino uno and some necessary sensors are used for sensor node. Second, wireless module is installed on the sensor node to transmit obtained data. A XBee is used. A XBee is one of the famous wireless module. Third, a data server constructed to retain environmental data of greenhouse. An apache and a MySQL are used for server construction. After making the base of sensor network, development of growth rate sensor system is proceeded to know growth rate of products. System construction refers [2].

### 3.2. DETAIL

#### (1)Sensor making

The sensor node is made by Arduino. At first, temperature and illuminance sensor are installed. After making base of sensor network system, more sensors will be installed such as humidity, soil etc. Each sensors change their output voltage or resistance when they receive environmental changes. Arduino get voltage value from sensor circuit. After that Arduino calculate environmental data from characteristic of sensors.

The sensor node is shown Fig.4 and circuit diagram is shown Fig.5. Environmental data is collected every one second. Serial data of environmental is shown Fig.6. The data in each line are divided with a comma. The data that are transmitted to master node is numerical value information only because sensor value are calculated and become the environmental

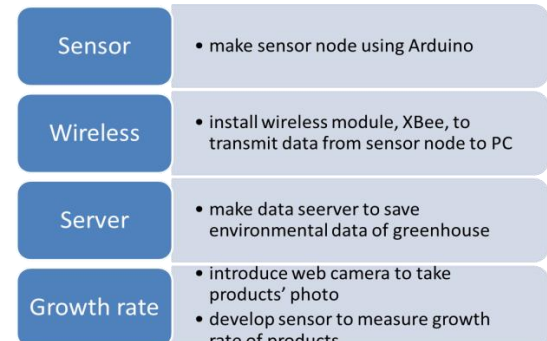


Fig.3 procedure of system construction

data by Arduino.

## (2)Introduction of wireless module

A XBee which is one of wireless module is used. A XBee change the serial data which are not wireless into the wireless one. A XBee is suitable for a sensor network. A feature of XBee compared with other wireless modules is shown below.

- XBee is inexpensive. It is about 4,000 yen for one.
- Transmission speed of XBee is relatively low. Therefore it is suitable for use with the sensor.
- communication distance is about 60m within doors and about 1500m in the open (XBee Pro).
- XBee moves only several millisecond and send only several byte data when transmit data. So battery life is very long.

XBee are installed to the sensor and PC. XBee installed on sensor is slave node. XBee installed to PC is master node. Slave nodes transmit sensing data to master node. Master node receives transmitted data and sends it to the server. When we set XBee, X-CTU is used. We can set Personal Area Network ID, destination ID, baud rate, sampling interval etc. And transmitted and received data on a X-CTU. Practically received data from sensor node are shown Fig.7.

## (3)Server making

A Xampp is used for server construction. A Xampp include an apache and a MySQL. An apache is used for server and a MySQL is used for database. A data server receives serial data which master node received from sensor node. And collected data are retained every uniformity time. Retained data are provided to clients. Data will be available on the PC or smartphone.

## (4)Measurement method of growth rate

Existing sensor network systems cannot measure growth rate of products. If the measurement system of growth rate were made, it helps to manage products. If collected data were referred with a growth rate, it would be a clue to know the suitable environment of each product. Therefore a sensor network system in agricultural field can be more useful one with a system knowing growth rate. In this research, the sensor which knows growth rate by thickness of stem of products is aimed. And this growth rate sensor should be installed on sensor network system.

In advanced research, measurement of growth rate is tried by image processing. Product photos are taken at some angles. Photos are processed by some methods. However, it is very complicated because it needs some cameras and restricts place for installa-

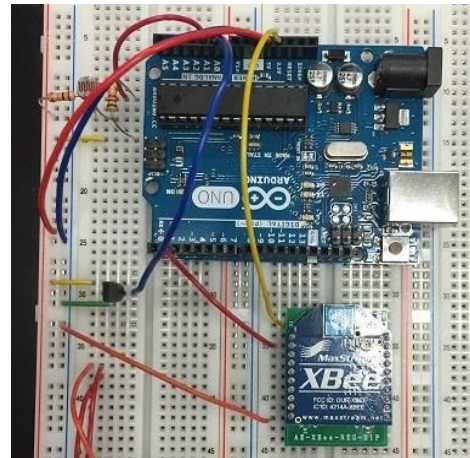


Fig.4 sensor node

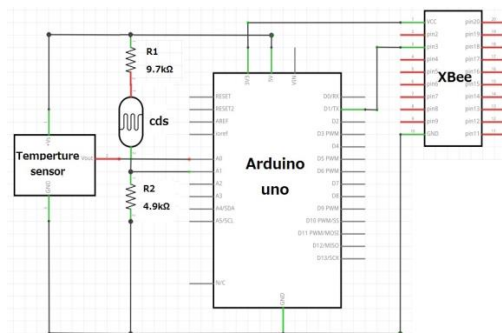


Fig.5 circuit diagram of sensor node

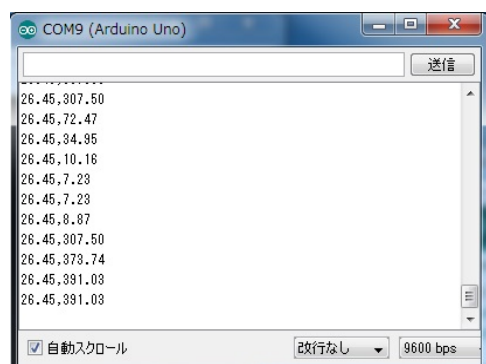


Fig.6 collected environmental data

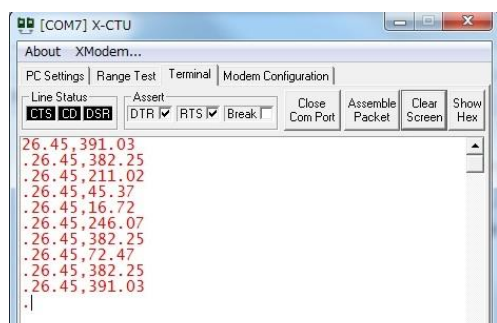


Fig.7 received data from sensor node

tion of web cameras. Additionally the method of image processing is very complicated. These problems are preventing development of system by image processing. In this research, thickness of stem of products is focused for low cost and simple measurement. The relationship between stems and growth of vegetables is shown in Table.1. Vegetables' stem gradually become thick along to the growth. This shows that it is possible to know the approximate growth rate of products. If the thickness of stem were measured by sensor, the growth rate could be shown to us.

A sensor mechanism which measures the thickness of stem is shown Fig.8. A sensor consists of a volume resistance and two insulation boards. Two insulation boards are attached to a volume resistance. To put the stem between two insulation boards, they are pushed by the stem and the knob of volume resistance is rotated. The thickness of stem is calculated by the value change of resistance. Using volume resistance has B curve. B curve has linear characteristic. The value of resistance is proportional to the rotation of the knob. A plastic board is used for insulation board. This sensor is low cost. There is no difficulty for installation to sensor network. There are two problems to be solved, method of fasten beside products and making strong structure. This sensor is cheaper than image processing system. There is no problem about place for installation. This sensor is easy to introduce into sensor network system. However, if the products did not have a stem, this sensor could not be used to measure a growth rate.

#### 4. CONCLUSION

In this research, easiness of introduction to farmland must be focused. The sensor network must be low cost. And it is desired that the system can be used simply. Important things for a sensor network construction are shown below.

- The system can be installed any place. Compact sensor node is need.
  - A battery life.is long.
  - The system can resist environmental change.
- Future works are shown below.
- The hardware of sensor node should be thought to be compact and durable.
  - Server system should be improved. It is needed to see and to search data easily.
  - The growth rate sensor should be completed and assessed.

Table.1 Thickness of the stem at the time of maturity of vegetables

example of vegetables having a stem	thickness of the stem after growth
tomato	1~2cm
broccoli	5cm
potato	1cm
eggplant	1cm
green pepper	2cm
cucumber	1~2cm
water melon	1cm
pumpkin	1~2cm
Japanese radish	3cm
parsley	5mm
garlic chive	5mm

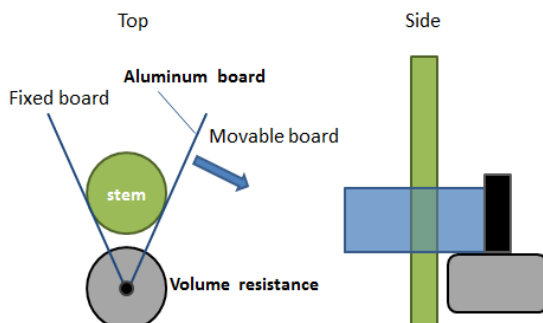


Fig.8 mechanism of growth rate sensor

#### REFERENCES

- [1]Tokihiro HUKATSU,"Sensor network system for agricultural applications",IEICE Electronics Express(ELEX)97(8),2014
- [2]Ryuji MICHINO,Syuhei KURODA,Koichi KIDO,"Design of an Environment Measuring System by Using Wireless Sensor Network", REPORTS OF KUMAMOTO INDUSTRIAL RESEARCH INSTITUTE No.51 2012.4-2013.3

# Precise Positioning Measurement Using the Quasi-Zenith Satellite System (QZSS): an Influence of Positioning Environment Gives to Accuracy

Rei FUKUSHIMA<sup>1</sup>, Shoichi TANIFUJI<sup>2</sup>

<sup>1</sup> Student, Advanced Course of Electric Communication System Engineering, National Institute of Technology, Okinawa College

(905 Henoko, Nago-shi, Okinawa 905-2192, Japan)

E-mail: ac154606@edu.okinawa-ct.ac.jp

<sup>2</sup> Professor, Information and Communication System Engineering, National Institute of Technology, Okinawa College

(905 Henoko, Nago-shi, Okinawa 905-2192, Japan)

E-mail: tanifiji@okinawa-ct.ac.jp

Positioning using Global Positioning System (GPS) is widely used. However, it can not be sufficient effect in buildings and mountain regions. So that Japan trying to complement the GPS positioning measurement using the Quasi-Zenith Satellite System (QZSS). It thought that can be positioning measurement in mm using the QZSS. However, it can not be obtained so much precise in the real. We want to know why that can not be positioning in mm. This paper shows the influence changes the positioning environment in single point positioning using GPS and QZSS. We researched the influence on the positioning accuracy. It changed temperature around receiver between 10 degree from 80 degree. Each of the positioning time was 1 hour. We thought that error of positioning accuracy is increase, because frequency of crystal oscillator is changed in changed temperature around receiver. However, we could not be confirmed the reason of error increasing. It is considered that frequency of crystal oscillator is corrected by the temperature compensation circuit inside the receiver. We confirmed that positioning error 2m-9m from the experimental results. This is caused by the difference in the number of visible satellites. The results confirm that positioning accuracy may have been guaranteed by temperature compensation circuit when rapid changed temperature around receiver. However, there are positioning errors so needed more accurate oscillator in the receiver.

**Key Words :** Global Position System(GPS), Quasi-Zenith Satellite System(QZSS), positioning accuracy, Crystal oscillator, temperature compensation circuit

## 1. INTRODUCTION

Global Positioning System (GPS) is one of the satellite positioning system and it is used for many field, car navigation system, ship and aviation, etc. It is operated by the United States Air Force 50<sup>th</sup> Space Wing of the USA. When the GPS receiver had the accurate clock same as GPS satellites. The multiplying the light velocity ( $c$ ) to the difference of the transmission time ( $T$ ) and reception time ( $t$ ). It can be known the distance between the satellite and the receiver. The position of the GPS satellite ( $(X_i, Y_i, Z_i)$ , the position of the receiver ( $x, y, z$ ). It holds the equation (1),

$$C(T - t)^2 = (X_i - x)^2 + (Y_i - y)^2 + (Z_i - z)^2 \quad (1).$$

Reception time ( $t$ ) is the value of the clock of the GPS receiver. If reception time is correct, there equations are requires at least to obtain the position of

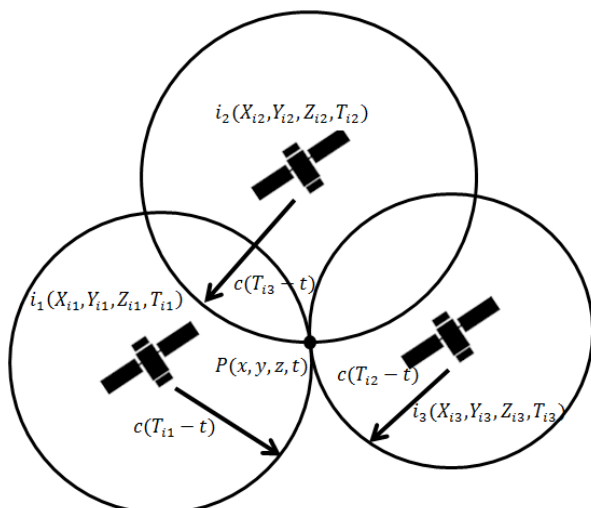


Fig.1 The principle of GPS

the receiver. However clock of the GPS receiver is less accurate.

Therefore, the reception time ( $t$ ) is unknown. By receiving signals from four satellites, it is obtain with for unknowns.

Quasi-Zenith Satellite System (QZSS) is a satellite system to complement and correct the GPS positioning. In future it will use multiple satellites that have the same orbital period as geostationary satellites with some orbital inclinations (their orbits are known as “Quasi-Zenith Orbits”). Quasi-Zenith orbits are the orbit tilted an angle the geostationary orbits and passing through the just above of Japan. we look at their orbits in the state that stopped the Earth, it looks like the satellite is moving so as to draw eight shaped. These satellites are placed in multiple orbital planes, so that one satellite always appears near the zenith above the region of Japan. The system makes it possible to provide high accuracy satellite positioning service widely covering the Asia and Oceania, including urban canyon and mountain terrain [2].

In this paper, we conducted a survey of the changes in the positioning accuracy due to a change in the positioning environment. Motivation of this attempt is that is not necessarily the environment where GPS and QZSS receiver is used in always stable. By changing the temperature around the receiver, the frequency of the receiver inside the crystal oscillator changes and clock of receiver will not be accurate. It can know the environment of surrounding receiver gives effect of positioning accuracy. We considered positioning error is increased. The purpose of this paper is the compare the pinpointing error with the normal temperature and change temperature.

## 2. EXPERIMENTAL PROCEDURE

Fig.2 shows schematic illustration of temperature change and process conditions.

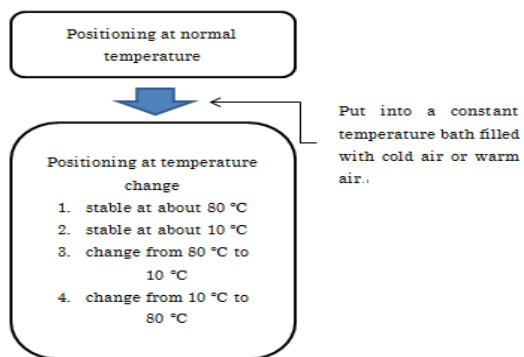


Fig. 2 temperature change and process conditions

We investigated positioning accuracy during the time of various changing the receiver temperature. Fig.3 shows temperature changes in experiments. Our experiments have four patterns. The horizontal axis is elapsed time from the start of measurement. The vertical axis is receiver temperature. Exp. No.1, the receiver temperature was stable at about 80 °C. Exp. No.2, the receiver temperature was stable at about 10 °C. Exp. No.3, the receiver temperature was changed from 80 °C to 10 °C. Exp. No.4, the receiver temperature was changed from 10 °C to 80 °C. Each of the measurement time was 1 hour. In the case of Exp. No.3 and No.4, the temperature was changed after 30 minutes from the start of measurement. Before the start of measurement, the receiver was observed four or more satellites, furthermore the positioning was stable.

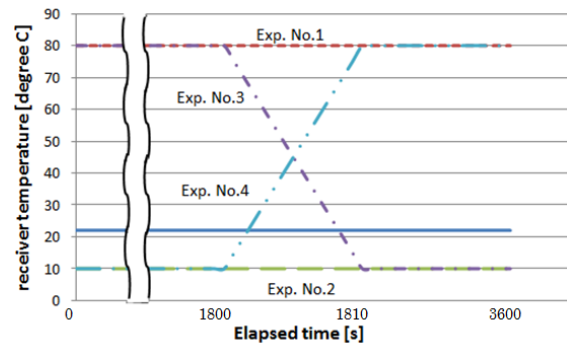


Fig.3 temperature changes in the experiments

We conjectured that there were no differences of positioning error between normal temperature and Exp. No.1 and No. 2. Because the receiver temperature was stable at high temperature or low temperature, it is possible to correct by the temperature compensated circuit. In addition, Exp. No.3 and No.4 compared with normal temperature, we conjectured large positioning errors were observed after 30 minutes. Because the receiver temperature was changed rapidly from high temperature to low temperature or low temperature to high temperature, it could not correct by temperature compensated circuit.

## 3. EXPERIMENTAL RESULTS

Fig. 3 to Fig. 6 show the experimental results of positioning error by the positioning environment. They compared with the results of same normal temperature. The horizontal axis is elapsed time from the start of measurement. The vertical axis is positioning error

between original position and measurement position.

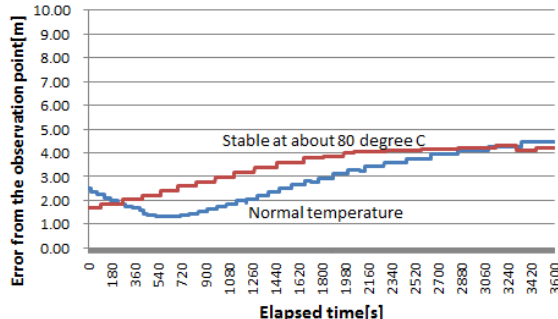


Fig. 4 Result of Exp. No.1

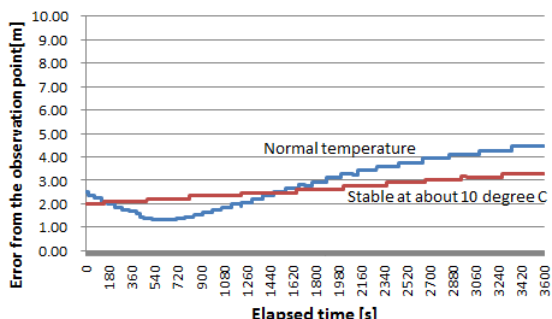


Fig. 5 Result of Exp. No.2

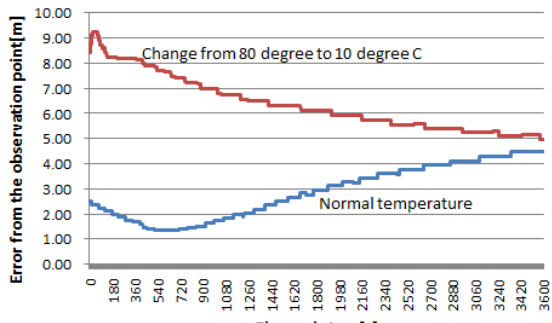


Fig. 6 Result of Exp. No.3

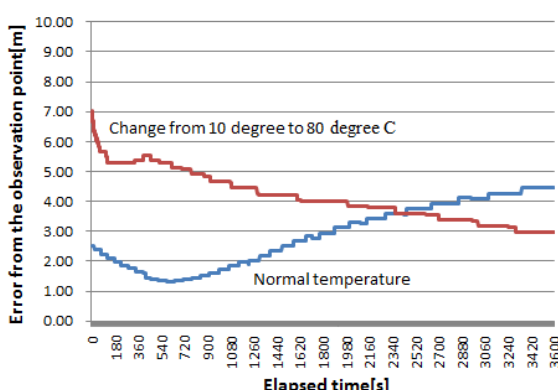


Fig. 7 Result of Exp. No.4

Fig.4 shows positioning errors of Exp. No.1 when the receiver temperature was stable at about 80 °C. The positioning error was 2m to 4m. The maximum error and minimum error are almost the same with normal temperature experiment because positioning errors were corrected by the temperature compensated circuit.

Fig.5 shows positioning errors when the receiver temperature was stable at about 10 °C. The positioning error was 2m to 3m. We obtained the result almost the same with normal temperature because positioning errors were corrected by the temperature compensated circuit.

Fig.6 shows positioning errors when the receiver temperature changed from 80 °C to 10 °C. The positioning error was 5m to 9m. Positioning errors were quietly large. However, the error was not increased after 30 minutes from the start of measurement. We speculated that the temperature compensated circuit could correct such the rapid temperature change.

Fig.7 shows positioning errors when the receiver temperature changed from 10 °C to 80 °C. The positioning errors were 3m to 7m. We speculated that the temperature compensated circuit could correct such the rapid temperature change.

From these results, we obtained same positioning accuracy of experiments normal temperature from Exp.No.1 and Exp.No.2. We speculated the positioning accuracy was decreased by rapid receiver temperature in Exp. No.3 and No.4. The positioning errors were corrected by the temperature compensated circuit. In addition, the temperature control was performed manually using hot water and cold materials in these measurements. Because of this, the experimental method was not precise. Furthermore, it is necessary constant temperature during the measurement.

Even so, the maximum error and minimum error was increased compare with normal temperature condition. Therefore, we considered more accurate oscillator in the receiver. Our receiver has Temperature Compensated Crystal Oscillator (TCXO). It was combined with crystal oscillator and temperature compensated circuit. It is used to correct the oscillation frequency due to temperature changing. TCXO has temperature compensation circuit to suppress output frequency deviation caused by surrounding temperature. The output signal from a temperature sensor is used to generate a correction voltage that is applied to a variable reactance in the crystal network. The reactance variations compensate for the crystal's frequency-temperature curve. The oscillation fre-

quency of TCXO of course affect to the positioning accuracy.

On the other hand, we were confirmed maximum error 9m in Exp. No.3 and minimum error 1m in normal temperature. The number of visible satellites affect to the positioning accuracy with GPS and QZSS [3]. There was difference of 7m to the maximum error and minimum error. Table 2 shows number of visible satellites for each experiment.

**Table 1** number of visible satellites for each experiment

Exp. No.	Number of visible satellites
Normal temperature	12
1	10
2	14
3	8
4	7

The number of visible satellites counted at the start of measurement within 10 seconds.

In normal temperature, positioning error was 1m to 4m, number of visible satellites was 12. In Exp. No.1, positioning error was 2m to 4m, number of visible satellites was 10. In Exp. No.2, positioning error was 2m to 3m, number of visible satellites was 14. In Exp. No.3, positioning error was 5m to 9 m, number of visible satellites was 8. In Exp. No.4, positioning error was 3m to 7m, number of visible satellites was 7. From these results, high positioning accuracy has many numbers of visible satellites.

#### 4. CONCLUSIONS

We measured effect of temperature changes for positioning accuracy using GPS and QZSS receiver. The main results were as follows.

- (1) We confirmed that no increased the positioning error when the receiver temperature was stable at high temperature or low temperature. The temperature compensated circuit could correct the oscillating frequency.

- (2) We confirmed that no increased the positioning error when the receiver temperature was rapid changed high temperature to low temperature or low temperature to high temperature. The temperature compensated circuit could correct the oscillating frequency.
- (3) Even so, the maximum error and minimum error was increased compare with normal temperature condition. Therefore, we considered more accurate oscillator in the receiver.
- (4) The number of visible satellites, more is better.

From these results, the effect of changes in the positioning environment gives to positioning accuracy. We confirmed that positioning accuracy may have been guaranteed by temperature compensation circuit when rapid changes temperature around receiver. However, there are still positioning errors, therefore the receiver need more accurate oscillator for precision positioning.

#### REFERENCES

- [1] Gerard Maral, Michel Bousquet and Zhili Sun, "Satellite Communicationn System, Fifth Edition," John Wiley & Sons, Ltd, pp.35-38, 2009.
- [2] QZSS Project Team Office of Space Applications JAXA, "Quasi-Zenith Satellite System," Japan Aerospace Exploration Agancy(JAXA), 2008.  
[http://qzss.jaxa.jp/01\\_e.html](http://qzss.jaxa.jp/01_e.html)
- [3] B.Hofmann-Wellenhof, H.Lichtenegger and J Collins, "Global positioning system: theory and practice," Springer-Verlag Wien, 2001.
- [4] Elliott D. Kaplan and Christpher J. Hegarty, "Understanding GPS: principles and applications second edition," Boston: Artech House, pp21-25, 2006.
- [5] Anil K. Maini and Varsha Agrawal, "Satellite Technology:Principles and Applications," Jhon Wiley & Sons, Ltd, pp63-67, 2011.
- [6] Nobunari Kubo, "A study on GPS Multipath Mitigation and its Practicability hor High Precise Positoning," Tokyo University of Marine Science and Technology, p33, 2005.



**CONFERENCE SESSION ON  
COMPUTER SCIENCE AND  
INFORMATION TECHNOLOGY**



# Mobile Malware: Attacks and Defense

NGO Van Quyen<sup>1</sup> and NGUYEN Xuan Thang<sup>2</sup>

<sup>1</sup> Student, Faculty of Information Technology, Hanoi University  
(Km9 Nguyen Trai, Thanh Xuan, Ha Noi, Viet Nam)

Email: nvquyen2404@gmail.com

<sup>2</sup> Professor, Faculty of Information Technology, Hanoi University  
(Km9 Nguyen Trai, Thanh Xuan, Ha Noi, Viet Nam)

Email: nxthang@hanu.edu.vn

In recent years, smartphones are used for several certain purposes like accessing online information or social network, making online payment, playing games and using other further applications that were once performed only by the computers. Additionally, plenty of sensitive data such as contact information, text messages, email or user's bank account is stored in mobile devices to make them a target for malicious activities. In this paper, we first discuss of mobile malware threats, highlights some emerging mobile malware and the ways they attack. Then we propose some security mechanisms that can be adopted in mobile devices to prevent the malicious attacks.

**Keywords:** Smartphones, Malware, Mobile devices, Security, Threat.

## 1. INTRODUCTION

The use of smartphones is rapidly increasing which directly leads to improved computational power and other utility functions. As a result of their popularity and functionality, smartphones are a burgeoning target for malicious attackers using mobile malware. Several years ago, mobile malware was just a proof-of-concept that was only mentioned in detective movies. Today, however, mobile malware has become a real threat. In<sup>1</sup>) the authors listed several certain malicious activities that can be performed by mobile malware such as stealing personal data and send it to attackers, paying online bills or transferring money.

The first virus for mobile phones was written by a member of a group known as 29A in June 2004. A reported made by Kaspersky Lab in 2014<sup>2)</sup> stated that there were a dramatic growth in the numbers of mobile malware in recent years. For example, the number of mobile malware samples analyzed in 2014 had exceeded the total samples discovered in the period from 2004-2013. In<sup>2)</sup>, according to the author, the number of mobile malware attacks per month increased tenfold – from 69,000 per month in August 2013 to 644,000 in March 2015. Specially, 53 percent of all mobile malware detections are now related to malware capable of stealing money. One of the more notable examples is *Svpeng*, designed to steal money from customers of three of Russia's biggest banks.

Mobile devices are now integrated into the fabric of our lives, so it's hardly surprising that the development of mobile malware is underpinned by a cybercrime business that includes malware writers, testers, mobile apps designers, web developers and botnet managers. In the next sections we continue discussing to mobile malware attacks and the defense strategy. We start with the definition of mobile malware in section 2.1. In section 2.2, some emerging mobile malware and the ways they attack are analyzed. Some effective defense strategies are proposed to mobile users in section 2.3. Finally, in section 3, we forecast the trend in mobile malware space by the conclusion.

## 2. MOBILE MALWARE

### 2.1 Definition

Today, smartphones permit users to install software applications from sources other than the mobile network operator which requires some controlling to mitigate attacks. Malware is a malicious code that can do anything in any other program can such as writing a message, stopping a running program, modifying a file etc. also, malware can be triggered periodically or lie dormant undetected until some event triggers the code to act. They are further classified into many types such as Trojans, bots, virus, backdoor, worms or rootkits. Figure 1 shows some basic types of malwares.

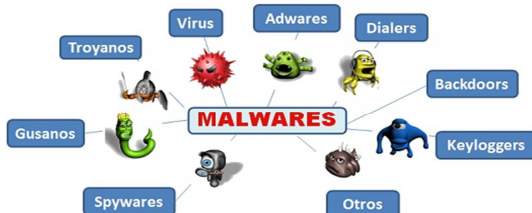


**Fig.1** Some basic types of malwares

## 2.2 Types of malware

According to <sup>3,4)</sup>, the types of malware currently popular are:

### Viruses

Malicious software self-replicating by inserting copies of itself into host programs or data files. The virus is usually triggered by the interaction of the user such as opening a file or run a program. Viruses are divided into two subcategories: viral translation and interpretation virus. Virus translation (Compiled viruses) is activated by an operating system, and Virus interpretation (interpreted virus) is triggered by an application.

### Worms

A program of "packaging", self-replicating, self activated without user intervention. Worms are divided into two types: Network services worms and "Post Parcels". The first one takes advantage of vulnerabilities in network services to propagate itself and infect other hosts. The second one is distributed by sending as attachments to emails or messages.

### Trojan Horses

A program that does not have the ability to copy, appear seemingly harmless but they are designed to perform some malicious actions on victims' computers such as stealing passwords and other sensitive personal information, tracking user activities or controlling the computer remotely.

### Spyware

A software installed on users' computer to collect their secure information without any permission from user.

### Adware

A software that automatically loads pop up, images and information ad to force users to read, view the advertising information. The software is not destructive but it would affect the performance of the devices and cause discomfort for users.

### Ransomware

A software infects a computer, it would control systems or computers then requires victims to pay for restoring the systems.

### Rootkit

A technique that allows the software to conceal its identity in the system, the antivirus software then it can support for other modules to destroy and take advantage of the system.

According to the Android Mobile malware report by Liviu Arsene in July 2012 <sup>5)</sup> Trojans, exploits and adware have become the most popular and strictly mobile threats throughout the world. The report revealed that India is the country most affected by malware and adware. The second and third places are occupied by the United States and Romania. The United Kingdom and France have close percentages as well, placing them in the top five countries affected by Android malware. This report also revealed that malware coders are mostly using Trojans or aggressive adware bundled with a wide range of applications.

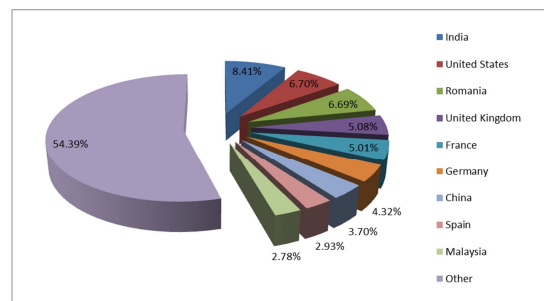


**Fig.2.** Android mobile malware rate in July 2012

Another example of mobile malware is a research <sup>6)</sup> carried out by Lookout – a security firm works for Android Authority. They have discovered a new type of adware on Android devices. It is able to infect the Android device and impossibly removed if the device is infected because the adware will automatically turn itself into a system application and can not be removed even though users use restore factory settings. Also, it would have rights to access the databases on the devices and easily steal all secure data stored on the machine. This kind of malicious code was found out on over 20,000 Android applications, familiar ones like Facebook, NYTimes, Okta, Twitter, Candy Crush,... However, the important point is that the software is not installed from Google Play app store, but from untrustable websites.

### **3. DEFENSE STRATEGY**

#### **3.1 Detection**

Various mobile malware detection techniques have been outlined in <sup>7,8)</sup>. Some common techniques are Static analysis, Dynamic analysis, Application permission analysis, Cloud-based detection, Battery life monitoring.

##### **Static analysis**

A quick, inexpensive approach to find malicious characteristics or bad code segments in an application without executing them. The techniques are widely used in a preliminary analysis, when suspicious applications are first evaluated to detect any obvious security threats.

##### **Dynamic analysis**

Unlike static analysis, dynamic analysis involves executing the mobile application in an isolated environment, such as a virtual machine or emulator, so that researchers can monitor the application's dynamic behavior. Dynamic analysis is primarily used in taint tracking or system call tracing.

##### **Application permission analysis**

Permissions play a key role in mobile applications: they convey the application's intentions and back-end activities to the user. In smartphones, permissions are clearly defined, so application authors must acquire appropriate permissions.

##### **Cloud-based detection**

Because of limited computational power and energy sources, smartphones don't carry fully featured security mechanisms. In that case, a cloud service which provides malware detection can come in handy.

##### **Battery life monitoring**

Because smartphones have limited battery capacity, observing energy consumption sometimes identifies malicious applications, which consume more energy than benign ones. If normal user behavior, current battery state, and other domain-specific details such as signal strength and network traffic are known, it's possible to detect hidden malicious activities more precisely.

#### **3.2 Defense**

To safeguard users, it is essential to have a defense strategy. In general, a prevention-based system should complement the detection-based system. The following prevention techniques are proposed in this paper to help users against malicious activities.

#### **Avoid risky application stores**

User should only permit the installation of apps from trusted sources, such as Google Play and Apple App Store. However, companies should also consider building enterprise application stores to distribute corporate custom apps and sanctioned consumer apps. In that case a chosen security vendor can help user set up an app store and advise which applications are safe.

#### **Consider the security of over-the-air networks**

Generally speaking, over-the-air (i.e., Wi-Fi) networks are insecure. For example, if a user is accessing corporate data using a free Wi-Fi connection at an airport, the data may be exposed to malicious users sniffing the wireless traffic on the same access point. Companies must develop acceptable use policies, provide VPN technology, and require that users connect through these secure tunnels.

#### **Use up-to-date Anti-virus software**

Although malware exists for iOS and BlackBerry, those operating system interfaces don't support anti-malware. However, the risk of infection is highest for Android, where security software is already available. User should make sure all their Android devices are protected by anti-malware software.

#### **Avoid jailbreak or root devices**

Jailbreaking/root is the process of removing the security limitations imposed by the operating system vendor. This activity also means breaking the security model and allowing all apps, including malicious ones, to access the data owned by other applications.

#### **Be careful with permissions**

User should read the permissions that will be granted to an app before installing it. If a simple application is asking for permission to send and receive SMS or MMS messages, consider that a red flag. Be sure that the requested permissions are commensurate with the expected function of the application.

### **4. CONCLUSION**

Smartphone usage has been rapidly increasing and is increasingly becoming more sophisticated device. The increasing popularity makes them a perfect target for attackers. Smartphones are increasingly being equipped with sophisticated software and software system which open up avenues for sophisticated malware attacks. Based on the study on various research papers and online sources, we propose that all the stake holders

have to realize the importance of securing mobile phones from mobile malware. Complementing the detection systems, there should effort to improve prevention mechanisms like cloud-sharing alternatives, trustable application stores, etc. Finally, we recommend that all users should make themselves educated with the threats and methods to remain safe. It is a reality that moile malware is widespread and would continue to surge.

## REFERENCES

- 1) Felt, Adrienne Porter, et al: A survey of mobile malware in the wild. *Proceedings of the 1st ACM workshop on Security and privacy in smartphones and mobile devices*. ACM, 2011.
- 2) Emm, D. : *Kaspersky Security Bulletin*. 2014.  
Retrieved from: <https://securelist.com/analysis/kaspersky-security-bulletin/68052/kaspersky-security-bulletin-2014-malware-evolution/>
- 3) You, I., & Yim, K.: Malware obfuscation techniques: A brief survey. In *2010 International conference on broadband, wireless computing, communication and applications* (pp. 297-300). IEEE, 2010.
- 4) La Polla, M., Martinelli, F., & Sgandurra, D. : A survey on security for mobile devices. *Communications Surveys & Tutorials, IEEE*, 15(1), 446-471. 2013
- 5) Arsene, L: *Android Mobile Malware Report – July 2012*.  
Retrieved from: <http://www.hotforsecurity.com/blog/android-mobile-malware-report-july-2012-3066.html>
- 6) Lookout: *Mobile Threat report*, 2014.  
Retrieved from:  
<https://www.lookout.com/resources/reports/mobile-threat-report>
- 7) Chandramohan, M., & Tan, H. B. K. : Detection of mobile malware in the wild. *Computer*, 9(45), 65-71. 2012.
- 8) Peng, S., Yu, S., & Yang, A. .. Smartphone malware and its propagation modeling: A survey. *Communications Surveys & Tutorials, IEEE*, 16(2), 925-941. 2014

**(Received November 15, 2015)**

# A discussion of information systems analysis and design

LE Trong Tan<sup>1</sup> and NGUYEN Xuan Thang<sup>2</sup>

<sup>1</sup> Student, Faculty of Information Technology, Hanoi University  
(Km9 Nguyen Trai, Thanh Xuan, Ha Noi, Viet Nam)  
E-mail: tanlt5c12@s.hanu.edu.vn

<sup>2</sup> Professor, Faculty of Information Technology, Hanoi University  
(Km9 Nguyen Trai, Thanh Xuan, Ha Noi, Viet Nam)  
Email: nxthang@hanu.edu.vn

Today the application of information technology has become an indispensable companion for every person in contact, communication and daily work. Therefore, the analysis and design of information systems is extremely important and plays a key role to help people in the areas of management and automation to increase productivity. This paper will discuss of the Information Systems and the Systems Development Life Cycle. Based on this, we highlight and compare the effectiveness between two different methods for Information System analysis and design.

**Key Words:** information system, analysis, design, object-oriented

## 1. INTRODUCTION

The word “system” covers a very broad spectrum of concepts in our daily life for example: the water system in the city, the transportation system, the social system, the natural system, etc. Generalization to a simple concise way, the “system” is a collection of many elements, have the relationship of mutual interaction and work together towards common goals.<sup>1)</sup>

The elements of the system (or the system components) can be very diverse<sup>2)</sup>. For instance, in the solar system, the elements are the Sun, Earth, Mars, etc. The element is not necessarily rudimentary. It is simple but can be a complex entity (and to an extent can be considered a subsystem).

Many people think of data as synonymous with information; however, information actually consists of data that has been organized to help answer questions and to solve problems. An information system is any organized system for the collection, organization, storage and communication of information. So, the purpose of an information system is to turn raw data into useful information that can be used for decision making in an organization.

### (1) Classification of Information System

#### (a) Transaction processing systems (TPS)

A transaction processing system<sup>3)</sup> provides a way to collect, process, store, display modify or cancel transactions. Most of these systems allow multiple transactions to take place simultaneously. The data that this system collects is usually stored in databases which can be used to produce reports

such as billing, wages, inventory summaries, manufacturing schedules, or check registers.

#### (b) Management information systems (MIS)

A management information system is an information system that uses the data collected by the transaction processing system and uses this data to create reports in a way that managers can use to make routine business decisions in response to problems. Some of the reports that this information system creates are summaries, exceptions and Ad Hoc reports. All this is done to increase the efficiency of managerial activity.

#### (c) Executive information systems (EIS)

Monitor competitive environment and strategic Planning<sup>5)</sup>.

#### (e) Decision support systems (DSS)

Explore impact of available options or decisions (What-if scenarios)<sup>6)</sup>.

#### (f) Communication support systems

Facilitate communication internally and with customers and suppliers.

#### (g) Office support systems

Help employees create and share documents.

## 2. SYSTEM LIFE CYCLE<sup>7)</sup>

#### (1) Definition

System life cycle (**Fig. 1**) is an organizational process of developing and maintaining systems. It helps

in establishing a system project plan, because it gives overall list of processes and sub-processes required for developing a system<sup>4</sup>.

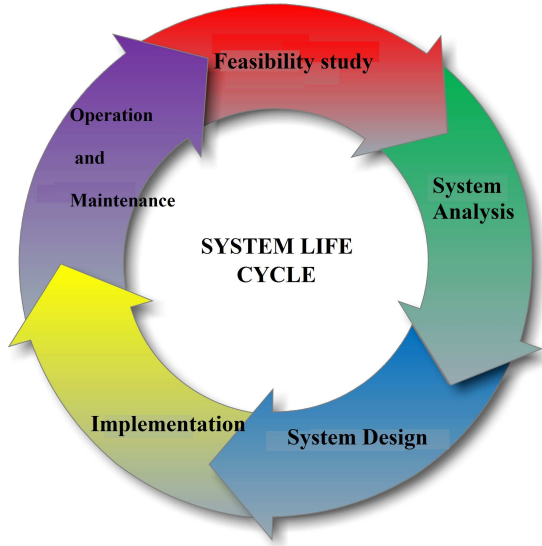


**Fig.1:** System life cycle

## (2) The steps

### a) Feasibility Study

At this step, the team analyzes if a software can be made to fulfill all requirements of the user and if there is any possibility of the software not being useful any more. Using this information, they find out if the project is financially, practically and technologically feasible for the organization to take up. There are many algorithms available, which help the developers to conclude the feasibility of a software project.

### b) Systems Analysis

During this step, the developers decide a roadmap of their plan and try to bring up the best software model suitable for the project. System analysis includes, Understanding of software product limitations, learning system related problems or changes to be done in existing systems beforehand, identifying and addressing the impact of project on organization and personnel, etc. The project team analyzes the scope of the project and plans the schedule and resources accordingly.

### c) System design

During the design, the developers bring down knowledge of requirements and analysis on the desk and design the software product. The inputs from users and information gathered in requirement gathering phase are the inputs of this step. The output

of this step comes in the form of two designs: logical design and physical design. Engineers produce meta-data and data dictionaries, logical diagrams, data-flow diagrams and, in some cases, pseudo codes.

### d) Implementation

This means installing the software on user machines. At times, software needs post-installation configurations at user end. Software is tested for portability and adaptability. Integration related issues are solved during implementation.

### e) Operation and Maintenance

This phase confirms the software operation in terms of more efficiency and less errors. If required, the users are trained on, or aided with the documentation on how to operate the software and how to keep the software operational. The software is maintained timely by updating the code according to the changes taking place in the environment during the user's end or technology. This phase may face challenges from hidden bugs and real-world unidentified problems.

## (3) Software Development Paradigm

### a) Waterfall Model

The Waterfall Model (**Fig. 2**) is the simplest model of software development paradigm. It says the all the phases of SDLC will function one after another in linear manner. That is, when the first phase is finished, then only the second phase will start and so on.

This model assumes that everything is carried out and taken place perfectly as planned in the previous stage, and there is no need to think about the past issues that may arise in the next phase. This model does not work smoothly if there are some issues left at the previous step. The sequential nature of the model does not allow us go back and undo or redo our actions.

This model is best suited when developers already have designed and developed similar software in the past and are aware of all its domains.

### b) Iterative Model

This model (**Fig. 3**) leads the software development process in iterations. It projects the process of development in cyclic manner repeating every step after every cycle of the SDLC process.

The software is first developed on very small scale and all the steps are followed and taken into consideration. Then, on every following iteration, more features and modules are designed, coded, tested and added to the software. Every cycle produces a soft-

ware, which is complete in itself and has more features and capabilities than that of the previous one.

After each iteration, the management team can do work on risk management and prepare for the next iteration. Because a cycle includes small portions of a whole software processes, it is easier to manage the development process, but it consumes more resources.

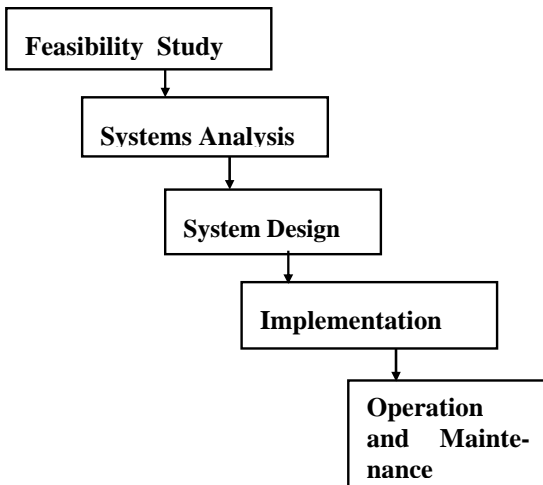


**Fig.2:** Basic waterfall Model

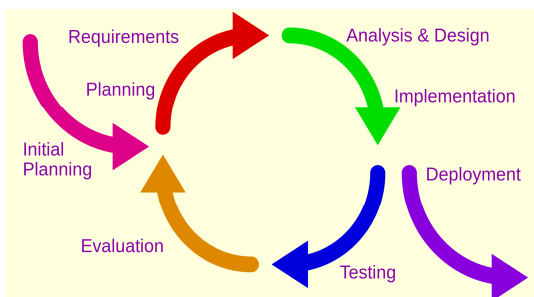


**Fig.3:** Iterative Model

### c) Spiral Model

Spiral model (**Fig. 4**) is a combination of both an Iterative Model and a SDLC model. It can be seen as if you choose a SDLC model and combine it with a cyclic process (Iterative Model).

This model considers risk, which often goes unnoticed by most other models. The model starts with determining objectives and constraints of the software at the start of one iteration. The next phase is of prototyping the software. This includes risk analysis. Then, one standard SDLC model is used to build the software. In the fourth phase of the plan, the next iteration is prepared.

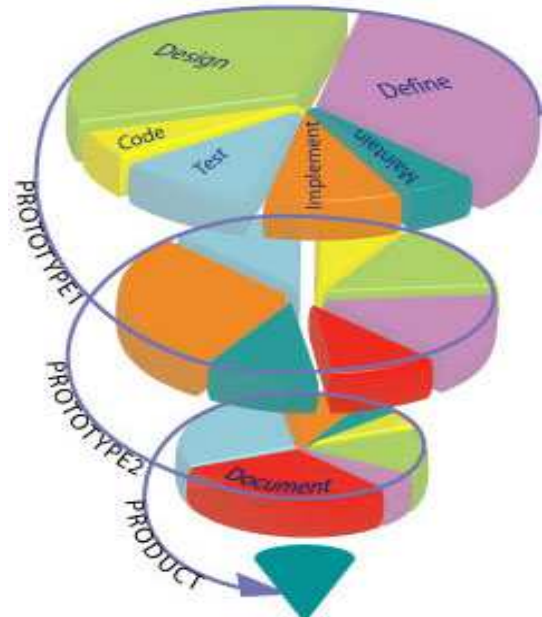


**Fig.4:** Spiral Model

## 3. THE METHODS OF ANALYSIS AND DESIGN OF INFORMATION SYSTEMS<sup>8)</sup>

### (1) Structured Analysis

The Structured Analysis/Structured Design (SASD) approach is the traditional approach of software development based upon the Waterfall model. The phases of development of a system using SASD are:

- Feasibility Study
- Requirement Analysis and Specification
- System Design
- Implementation
- Post-implementation Review

#### a) Advantages

The Structure Analysis focuses on data rather than the procedures as in Structured Analysis.

The principles of encapsulation and data hiding help the developer to build systems that cannot be tampered by other parts of the system.

The principles of encapsulation and data hiding help the developer to develop systems that cannot be tampered by other parts of the system.

It allows effective management of software complexity by the virtue of modularity.

It can be upgraded from small to large systems at a greater ease than in systems following structured analysis.

### b) Disadvantages

The functionality of the Structure Analysis is restricted within objects. This may pose a problem for systems which are intrinsically procedural or computational in nature.

It cannot identify which objects would generate an optimal system design.

The object-oriented models do not easily show the communications between the objects in the system.

All the interfaces between the objects cannot be represented in a single diagram.

### (2) Object-Oriented Analysis

Object-Oriented Analysis (OOA) is the procedure of identifying software engineering requirements and developing software specifications in terms of a software system's object model, which comprises of interacting objects. This tutorial will help you understand the basics of object-oriented analysis and design along with its associated terminologies.

Now, we will look at the relative advantages and disadvantages of Structured Analysis approach and Object-Oriented Analysis approach.

### a) Advantages

As it follows a Top-Down approach in contrast to Bottom-Up approach of Object-Oriented Analysis, it can be more easily comprehended than OOA.

OOA is based upon functionality. The overall purpose is identified and then functional decomposition is done for developing the software. The emphasis not only gives a better understanding of the system, but also generates more complete systems.

The specifications in it are written in simple English language, and hence can be more easily analyzed by non-technical personnel.

### b) Disadvantages

In traditional Structured Analysis models, one phase should be completed before the next phase. This poses a problem in design, particularly if errors crop up or requirements change.

The initial cost of constructing the system is high, since the whole system needs to be designed at once, leaving very little option to add functionality later.

It does not support reusability of code, so the time and cost of development is inherently high.

## 4. CONCLUSION

The paper presents an overview of the analysis and design of systems with the basic contents included. There are many types of different information systems, such as: management information systems, websites, e-commerce systems, etc. Each system will correspond to a particular method of development.

The development of information systems in general including is seen as a life cycle with phases: identification, specification, design, integrated installation, maintenance and removal. The waterfall Model and spiral model and the models used.

Method development of Object-Oriented software has many advantages compared to Structure-Oriented approach. The specific phase in the life cycle of software development is the Object-Oriented analysis, Object-Oriented design and object-oriented programming.

## REFERENCES

- 1) Kendall, Kenneth E., et al. *Systems analysis and design*. Vol. 2. Prentice-Hall, 1992.
- 2) Ba, N. X., *Phân tích và thiết kế hệ thống thông tin*, 2<sup>nd</sup> edn, Đại học Quốc Gia Hà Nội, 2004.
- 3) Paul, Z., *Transaction Processing Systems (TPS): Batch and Real-Time Systems*, viewed 14 November 2015, <http://study.com/academy/lesson/transaction-processing-systems-tps-manual-and-automated-systems.html>
- 4) Laudon, Kenneth C., and Jane P. Laudon. "Management information systems: managing the digital firm." New Jersey 8 (2004).
- 5) Paul, Z., *Executive Information Systems (EIS): Upper Management Decision-Making Tools*, <http://study.com/academy/lesson/executive-information-systems-eis-upper-management-decision-making-tools.html>
- 6) Turban, Efraim, J. Aronson, and Ting-Peng Liang. *Decision Support Systems and Intelligent Systems* 7 " Edition. Pearson Prentice Hall, 2005.
- 7) Blanchard, Benjamin S., Wolter J. Fabrycky, and Walter J. Fabrycky. *Systems engineering and analysis*. Vol. 4. Englewood Cliffs, New Jersey: Prentice Hall, 1990.
- 8) Whitten, Jeffrey L., Victor M. Barlow, and Lonnie Bentley. *Systems analysis and design methods*. McGraw-Hill Professional, 1997.

(Received November 15, 2015)

# The Golden Rules of User Interface Design

LE Duc Binh<sup>1</sup>, NGUYEN Thi Mai<sup>1</sup> and TRINH Bao Ngoc<sup>2</sup>

<sup>1</sup>Student, Faculty of Information Technology, Hanoi University  
(Km9, Nguyen Trai, Thanh Xuan, Hanoi, Vietnam)  
E-mail:{ducbinh, sorrows294}@mail.com

<sup>2</sup> Professor, Faculty of Information Technology, Hanoi University  
(Km9, Nguyen Trai, Thanh Xuan, Hanoi, Vietnam)  
E-mail: ngoctb@hanu.edu.vn

## Abstract

As information technologies mediate many of the activities we now perform routinely, the user interface of a software plays an important part on effectiveness of human-computer interaction. User-interface design is a central issue for the usability of a software product. This paper is based on the Shneiderman's Eight Golden and other selective researches on user interface design. One of the goals of this paper is to provide new rules and principles on user interface design that can guide designers in the right direction to improve the usability of a system and make software more intelligent while designing

**Keywords:** Usability, Golden rules, User interface, Heuristics

## 1. INTRODUCTION

Today, user interface is found at almost every place where digital technology exists, right from computers, mobile phones, cars, music players, airplanes, ships etc. User interface is part of software and is designed such a way that it is expected to provide the user insight of the software. User interface provides fundamental platform for human-computer interaction. User interface is the front-end application view to which user interacts in order to use the software. Designers should apply the appropriate design rules and principles for systems usability.

The guideline Shneiderman's Eight Golden Rules of interface design is collections of design principles are derived base on experience by many developers and can be applied into programs after being refined. If a software system is able to design a good set of user interfaces that are created under the golden principles of software quality, then it is likely that the software system will be widely appreciated and used by the intended user.

The objective of this paper is to design and develop usable user interface by utilizing usability principles and rules on user interface designing based on Shneiderman's Eight Golden Rules and other studies. This paper is an ideal reference for veteran and novice educators, researchers, students, and practitioners in the field of user interface design who require access to current information in this emerging field.

## 2. METHODOLOGY

When designing any user interface, we should follow design rules and principles for designing and evaluating UI. Usability principles and rules give the direction to the designer to produce usable systems. The International Standard Organization (ISO) defines standard usability of a products as the extent so that users can achieve their goals effectively and efficiently. In Human Computer Interaction, in order to promote usability, the principles can be applied to the design of an interactive system with 3 main categories

- **Learnability**– the ease with which new users can begin effective interaction and achieve maximal performance.
- **Flexibility**– the multiplicity of ways in which the user and system exchange information.
- **Robustness**– the level of support provided to the user in determine successful achievement and assessment of goals.

In the following, there are so many rules and principles are available to focus its own strength on usability principles. The guideline proposed by Shneiderman who Eight Golden Rules is also one of the most important and useful one. These collections of design principles are derived base on experience by many developers and can be applied into programs after being refined. However, to make sure cover all the key principles of interface design and achieve the best satisfaction, Shneiderman's principle is not exactly

right. From this above discussion and comparison, we offer the collection of guideline based on the usability principles in this study.

**Table 2.1** show the attribute allocation of 2 guidelines to usability principles which very crucial for any development of system

Usability Principles	Rules of this study	Shneiderman's Rule
<b>1. Learnability</b>		
<input type="checkbox"/> Predictability	Design for error	
Operation visibility	KISS, Visibility	Design Dialog to Yield Closure
<input type="checkbox"/> Synthesizability		
Immediate/eventual honesty	Feedback, Visibility	Offer Informative Feedback
<input type="checkbox"/> Simplicity	KISS, Memory-Load Reduction	Reduce Short-Term Memory Load
<input type="checkbox"/> Familiarity	Match between System and Real Word	Support Internal Locus of Control, Enable Frequent Users to use Shortcuts
Guessability	Design for error, Match between System and Real Word	Enable Frequent Users to use Shortcuts
Affordance	Affordance	
<input type="checkbox"/> Generalizability	KISS	Reduce Short-Term Memory Load
<input type="checkbox"/> Consistency	Be Consistent	Strive for Consistency
<b>2. Flexibility</b>		
<input type="checkbox"/> Dialogue initiative		
System/user pre-emptiveness	Feedback, Place the user in control	Offer Informative Feedback, Design Dialog to Yield Closure
<input type="checkbox"/> Multithreading		
Concurrent vs. interleaving	Visibility	
Multi-modality	Flexibility and Efficiency of Use	
<input type="checkbox"/> Task migratability	Visibility	
<input type="checkbox"/> Substitutivity		
Representation multiplicity	Flexibility and Efficiency of Use	Support Internal Locus of Control
Equal opportunity	Place the user in control	Enable Frequent Users to use Shortcut
<input type="checkbox"/> Customizability		
Adaptability by users	Place the user in control, Flexibility and Efficiency of Use	Enable Frequent Users to use Shortcut
Adaptability by system	Flexibility and Efficiency of Use	
<b>3. Robustness</b>		
<input type="checkbox"/> Observability		
Browsability	Flexibility and Efficiency of Use	
Static/dynamic defaults	Design for error, Memory-Load Reduction	
Reachability	Design for error	Permit Easy Reversal of Actions
Persistence	Be consistent	Strive for Consistency
Operation Visibility	Visibility	Offer Informative Feedback, Design Dialog to Yield Closure

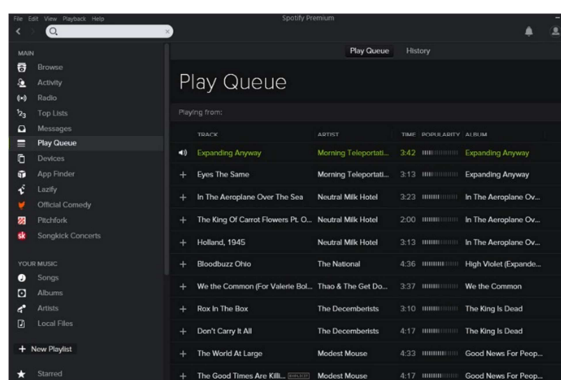
<input type="checkbox"/> Recoverability		Closure
Reachability	Design for error	Offer Simple Error Handling
Forward/backward recovery	Place the user in control, Design for error	Offer Simple Error Handling, Permit Easy Reversal of Actions
Commensurate effort	Design for error	Offer Simple Error Handling
<input type="checkbox"/> Responsiveness		
Stability	Flexibility and Efficiency of Use	
<input type="checkbox"/> Task conformance		
Task completeness	Visibility	Design Dialog to Yield Closure
Task adequacy	Visibility, Flexibility and Efficiency of Use	

### 3. GOLDEN RULES

#### 3.1 Match between system and the real word

The meaning of this first rule is the image of the system perceived by users should match the model the users have about the system. This rule specifically mention on the language, words, or concept and terms that should be familiar to the intended audience to display on the screen. The organization of information needs to arrange as natural as possible based on what users accustomed to seeing in the real world.

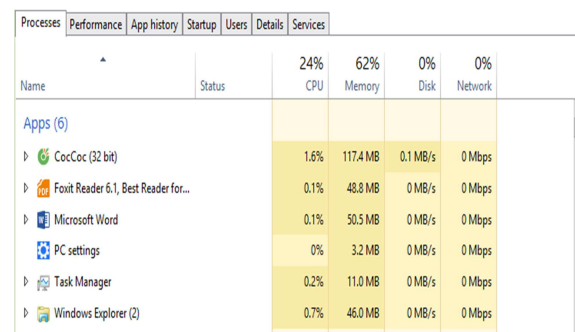
**For example:** Spotify uses words and concepts like “Queue”, “Playlist”, and “History”, “Lists” etc. All of these are things we’re familiar with from the real world, and they are words used in music listening offline too.



#### 3.2 Visibility

Visibility is the concept of communicating to the user what is happening inside the app. They should know roughly what is going on, even if they are not directly involved in that process, if it is relevant for them to know.

**For example:** Progress bars (either in line format or in a “step 1 out of 3” format), hour glass, breadcrumbs, and confirmation messages



#### 3.3 Place user in the control

The availability of control by user is very important because they always want to be the one who in charge to the system but not be controlled by the system. The interface should give them some degree of control to do their tasks quickly and efficiently such as:

- Allow users to use either the keyboard or mouse
- Allow users to customize the interface
- Provide meaningful paths and exits
- Make the user interface transparent

**For example:** Gmail lets me undo sending an email – even after I’ve sent it!

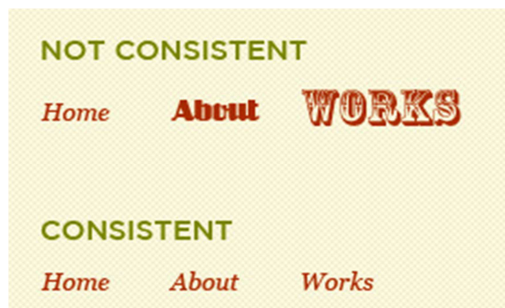


#### 3.4 Be Consistent

The purpose of this rule is to aim for consistency of the program interface, the detail of

the layout and how the interface looks. This rule carries meaning of creating all interface in one specific style, like using similar font size, color and even location of information have to be allocated and content of website; in order to help users to easily find out information and avoid confusion.

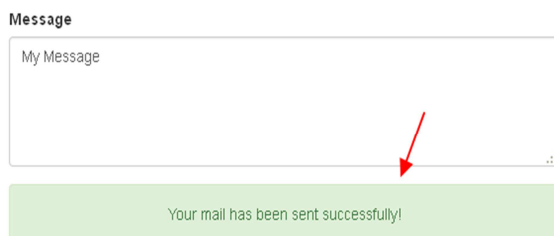
**For example:** users will associate a particular color on your website as the “link color,” they’ll come to recognize the typeface of your body copy



### 3.5 Feedback

System feedback is very important for all kinds of actions. Feedback is about sending back information about what action has been done and what has been accomplished, allowing the person to continue with the activity. Various kinds of feedback are available for interaction design-audio, tactile, verbal, and combinations of these.

**For example:** “Send” button, you may get a confirmation message in a pop-up dialog, and the e-mail will be listed under the “Sent” folder.

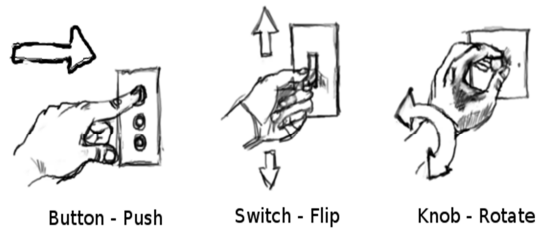


### 3.6 Affordance

Affordance is a term used to refer to an attribute of an object that allows people to know how to use it.

When the affordances of a physical object are perceptually obvious it is easy to know how to interact with it.

**For example:** A mouse button invites pushing (in so doing acting clicking) by the way it is physically constrained in its plastic shell



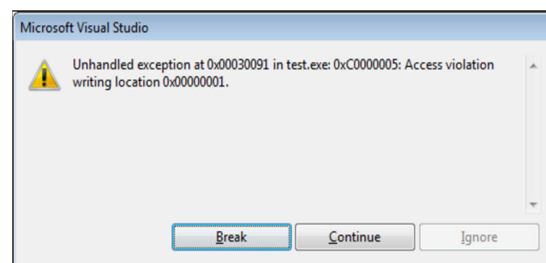
### 3.7 Design for Error

The purpose of this rule is to prevent the error from happening and provide with simple error handling and recovery this. In order to minimizes the ability of happening errors as many as possible, system have to develop to reduce the rate from the errors.

In some case users make error, so this rule is predictable prevention to make sure when error is found, there will be the alternative solutions to handle and recover data.

A default system unchanged message needs to be communicated to the user if an error has happened

**For examples:** Useful error messages (“Your password is incorrect, please ensure your CAPS LOCK key is off”), Form validation highlighting the error field, related links (“Did you mean...”)

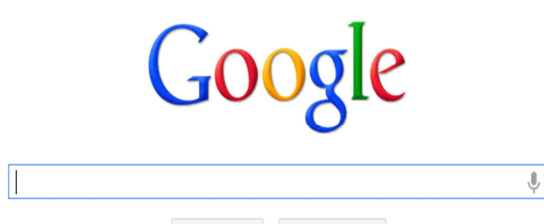


### 3.8 KISS (Keep it simple and straightforward)

The “keep it simple and straightforward” (KISS) principle is a design rule that states that systems perform best when they have simple designs rather than complex ones.

The best interfaces are as simple as they can effectively be.

**For example:** reducing clutter, clear call to actions, and no annoying flashing eye-candy



### 3.9 Flexibility and Efficiency of Use

Design the site in such a way that it can be used efficiently. Make your design flexible, to deal with a variety of situations. Some users are experts, some are novices, so they won't all have the same abilities or needs.

**For example:** when design a website interface, we should select the responsive effects to make the software interface which can adapt all devices.



### 3.10 Memory-Load Reduction

Minimize the user's memory load by making objects, actions, and options visible. The user should not have to remember information from one part of the dialogue to another. Instructions for use of the system should be visible or easily retrievable whenever appropriate by:

- Reduce demand on short-term memory
- Establish meaningful defaults
- Define shortcuts that are intuitive
- Disclose information in a progress fashion

**For example:** You can reduce short term memory load by designing screens where options are clearly visible, or using pull-down menus and icons

**94 56 781029**

**Easier to remember  
if chunked into  
smaller sets**

**94 56 7 810 29**

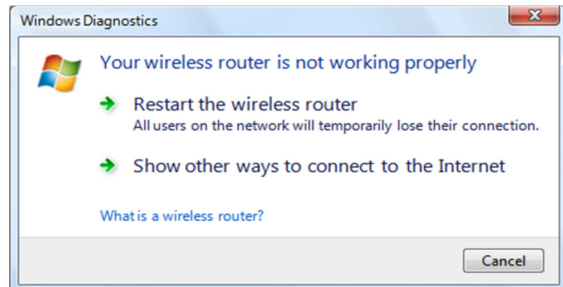
### 3.11 Help and Guidance

The last rule of this study is Help and

Guidance.

This is a very important aspect since the developer cannot aid the user from time to time, so the document is consider as a first level of solution to user when they encounter with problems.

**For examples:** FAQs, "?" icons, advanced search, clear labels on form fields and sections, pop-up help, online / live chat



## 4. CONCLUSION

All in all, this paper is intended to highlight the principles that are currently being used for successfully designing user interfaces, and make appropriate suggestions for betterment of user.

Although considerable effort has been made to base the guidelines on research from a variety of fields—including cognitive psychology, computer science, human factors, technical communication, and usability—other disciplines may provide valuable research that is not reflected in these guidelines.

There are many possible ways in which interface designs based on case studies and research findings. The guidelines may not be applicable to all audiences or contexts and are not fixed rules.

The compliance of user interface design and software quality can be checked. An intelligent software system can be developed in this regard. Therefore, it is suggested that further research can use this paper as a referent and review carefully these rules.

## **REFERENCES**

- 1) Miles, J. W. :" On the generation of surface waves by shear flows", J. Fluid Mech., Vol. 3, Pt. 2, pp. 185-204, 1957.
- 2) Olson, G.M. and Olson, J.S."Human-Computer Interaction: psychological aspects of the human use of computing",Annual Review of Psychology, 2003,page 491-516
- 3) Holzinger, A. (2005) Usability engineering for software developers. Communications of the ACM, , 48(1), pp. 71–74 ,January 29, 2005
- 4) Rubenstein, R. and H. Hersch. "The Human Factor: Designing Computer Systems for People". Massachusetts: Digital Press, 1984.
- 5) Nielsen, J. (2003) Usability 101: Introduction to Usability [online]. Updated 25 August 2003 [accessed 15 June 2007]. Available from: < <http://www.useit.com/alertbox/20030825.html> >.
- 6) Apple Computer, Inc."Macintosh Human Interface Guidelines". Massachusetts: AddisonWesley. 1992.
- 7) Preece, J., Rogers, Y., Sharp," H. Interaction design: beyond human-computer interaction"2002, John Wiley & Sons, New York. pp 6, 12, 13, 27, 166
- 8) Hewett, T., Baeccker, R., Card, S., Carey, T., Gasen, J., Mantei, M., Perlman, G., Strong, G., & Verplank,"Curricula for Human-Computer Interaction", Available at: < <http://sigchi.org/cdg/cdg2.html> >,2004

**(Received November 21, 2015)**

# How Encapsulating Security Payload (ESP) protect your data

TRAN Quang Du<sup>1</sup> and HOANG Thi Minh Ngoc<sup>2</sup>

<sup>1</sup> Student, Faculty of Information Technology, Ha Noi University  
(Km 9, Nguyễn Trãi, Thanh Xuân, Hà Nội, Việt Nam)  
E-mail:quangdutra809@gmail.com

<sup>2</sup> Professor, Faculty of Information Technology, Ha Noi University  
(Km 9, Nguyễn Trãi, Thanh Xuân, Hà Nội, Việt Nam)  
E-mail:ngochtm@hanu.edu.vn

**Abstract** - IPSec supports secure packet transmission at the IP layer and commonly deployed for implementing Virtual Private Network (VPNs). In the other paper, my research team had the brief look at IPSec in general. In this paper, the work will be extended with in-depth analysis about one of the two security services - Encapsulating Security Payload (ESP). The paper delivers a specific look at the structure of the ESP header, then how the packet is transited to provide authentication, confidentiality and data origin. The paper also introduce real case scenario motivated by the security benefits of ESP (VPNs).

**Key Words :** *ESP, security protocol, IPSec, virtual private network.*

## 1. INTRODUCTION

ESP is a protocol that enables secure data encryption, data origin authentication, integrity checking of data. Unlike AH (Authentication Header), which is the other security service provided in IPSec, ESP provides the ability to secret information by encrypting packets at the IP layer. After packing is complete with ESP, all information and encoding and decoding will be in the ESP Header. Both of transport data and encapsulated IP are in protection of ESP; however, except IP header. The encryption algorithm used in protocols such as DES, 3DES, AES.

## 2. ESP PACKET FORMAT

This section discusses about the structure of the ESP packet and what happen during transmission.

The packets for IPv4 and IPv6 have different structure; however, after inserting the ESP, the rule is almost the same, the difference is insignificant.

In the context of IPv4, ESP is placed after the IP Header and before the upper layer protocols, e.g. TCP (Transmission Control Protocol), UDP (User Datagram Protocol). In the IPv6 context, ESP should be placed after some extension headers (hop-by-hop, routing, fragmentation) and before the destination options extension header as it is an end-to-end payload. The destination option ext header, however, could appear before ESP, depending on the semantics desired. All the fields standing behind ESP are encrypted. By that, it may be desirable to place the header after ESP header. If the ESP is implemented in a security gateway, tunnel mode must be used. In

this mode, the entire inner IP packet is protected.

Transport mode seems to be weaker than tunnel mode as the IP Header could be exposed but each mode has pros and cons. For example, when it comes to an end-to-end security, normally communication

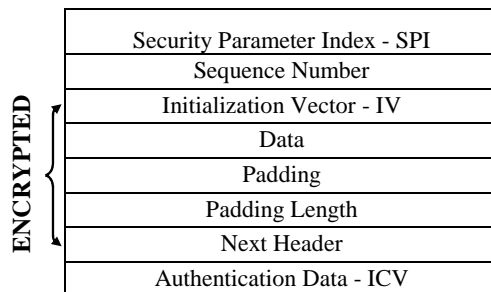


**Fig.1** ESP Packet Format.

between client and server (encrypted telnet for instance), transport mode is rather used.

**Fig.1** above illustrates the structure of the ESP Packet.

The first field is the Security Parameter Index (SPI), which is mandatory and used to identify the SA (Security Association) of the packet. This value is generated by the receiver for an unicast SA and used by itself or by conjunction with the IPSec protocol type (ESP or AH). The next filed is Sequence number, which is a 32-bit counter number. AS the packet is transmitted, the sender must increment this filed. It is initialized to 0 at both sides and never be allowed to cycle. Thus the sender's counter and the

receiver's counter must be reset. The Payload data is the field containing data. This field is mandatory and is an integral number of bytes in length. The field Initialization Vector appears as the algorithm used to encrypt the payload data requires cryptographic synchronization. And in this case, the payload data is placed explicitly in the Payload field and not called out as a separate field in ESP<sup>1)</sup>.

The purpose of using padding field is for the flexibility of the encryption. As the RFC 2046 document states, the padding used to fill the plaintext to match the size of the number of bytes, which is defined by the encryption algorithm. In addition, the padding may be required to ensure the Pad Length and Next Header fields must be right aligned within 4-byte word and the Authentication Data - ICV (optional) terminates on a 4-byte boundary. It is also used to hide the actual length of the payload. The Padding Length field is a mandatory field indicating the pad bytes in the Padding field. This field is limited to 255 bytes, which is not equal to cover the traffic flow confidentiality requirement. Traffic Flow Confidentiality (TFC) Padding is used to address the TFC requirement.

The Next Header field contains information about the data in the Payload field: which version of the IP or what is the next layer TCP-UDP, etc. The value is 8-bit and defined by IANA. To support traffic flow confidentiality, the value 59, meaning "no next header", used to mark the "dummy" packet, which must be discarded by the receiver without prejudice. The Integrity Check Value ICV, an optional field, is computed over the ESP Header, Payload and ESP Trailer. Its presence depends on the selected integrity service<sup>1)</sup>.

### 3. AUTHENTICATION

When conducting business over long distance, it is necessary to know (authenticate) the individual at the other end of the phone, mail, or fax. In the middle ages, a seal guaranteed the authenticity of a document. In modern times, a signed document is notarized with a seal and a signature. In the electronic era, a document is signed using the sender's private encryption key called a digital signature. A signature is authenticated by decrypting the signature with the sender's public key.

There are two primary methods of configuring peer authentication:

#### a) Pre-shared Keys (PSKs)

A pre-shared key value is entered into each peer manually and is used to authenticate the peer. At the end, the PSK is combined with other information to form the authentication key. Each peer must authen-

ticate its opposite peer before the tunnel is considered secure. Pre-shared keys are easy to configure manually but do not scale well, because each IPsec peer must be configured with the pre-shared key of every other peer with which it communicates. And it leads to some problems that need to think about seriously. Due to using pre-shared key, that means each site of peer must know the key before doing anything further. So how can we send the key securely over the Internet? Moreover, with each peer of a connection, a device need one key in order to share to the opposite peer. Supposing in the network, that device has a great number of peers also want to share the key. So that is why the second problem need to deal with is how to manage such great number of keys<sup>2)</sup>.

#### b) RSA signatures

The exchange of digital certificates authenticates the peers. The local device derives a hash and encrypts it with its private key. The encrypted hash is attached to the message and is forwarded to the remote end and acts like a signature. At the remote end, the encrypted hash is decrypted using the public key of the local end. If the decrypted hash matches the recomputed hash, the signature is genuine. Each peer must authenticate its opposite peer before tunnel is considered secure. By using this way, one can definitely solve the problems of number of keys and how to share the key securely.

A third way to accomplish authentication is through RSA-encrypted nonces. A nonce is a random number that is generated by the peer. RSA-encrypted nonces use RSA to encrypt the nonce value and other values. This method requires that the public key of the two peers be present on the other peer before the third and fourth messages of an IKE (Internet Key Exchange) exchange can be accomplished. For this reason, public keys must be manually copied to each peer as part of the configuration process. This method is the least used of the authentication methods<sup>2)</sup>.

To conclude, authentication algorithms produce an integrity checksum value or digest that is based on the data and a key. By this way a receiving device can confirm that a received packet was really sent by a trusted device peer. IPsec has provided variety options for authentication process. The list following is a few authentication algorithms available for IPsec ESP: HMAC-SHA1-96; AES-XCBC-MAC-96 and HMAC-MD5-96.

In stated in ESP, even though encryption and authentication are optional but none of them can be NULL. The goal of all above algorithms is to ensure that the packet is authenticated and cannot be modified in the transit.

## 4. ENCRYPTION

Security has become a basic requirement in computer communication. And encrypting the data provides secure transfer. The file is first translated into a meaningless cipher text then transferred in the configuration of the encryption algorithm. The receiving computer uses a key to translate the cipher into its original form. We have two types of encryption:

Symmetric key algorithms use identical encryption keys for both encryption and decryption. This requires that both sides have access to the keys.

Asymmetric key algorithms use different keys for encryption and decryption. This is preferred to public-key cryptography.

To explain the concept of the symmetric key algorithm, we will have a familiar visualized example to understand how it works:

Alice puts the message into a box locked by the padlock which she has the key. Then she sends it to Bob. Once Bob receives it, he uses an identical copy of Alice's key to open it and read the message. They had met face to face and exchanged this key before in private. Bob can use the same padlock to send his reply.

Symmetric cipher could be divided into stream ciphers and block ciphers. Stream ciphers are based on generating cryptographic key-stream which is used to encrypt one bit or byte at a time. Whereas block ciphers deal with larger chunks of data and require more memory. There are many symmetric algorithms<sup>3)</sup>:

**a) Two-fish:** Two-fish is a block cipher designed by Counterpane Labs. It was one of the five Advanced Encryption Standard (AES) finalists and is unpatented and open source.

**b) Serpent:** Serpent is a symmetric key block cipher that was a finalist in the Advanced Encryption Standard (AES) contest, where it was ranked second to Rijndael. Serpent was designed by Ross Anderson, Eli Biham, and Lars Knudsen.

**c) AES:** Advanced Encryption Standard; it uses the Rijndael block cipher approved by the National Institute of Standards and Technology (NIST). AES was designed by cryptographers Joan Daemen and Vincent Rijmen and replaced DES as the U.S. Government encryption technique in 2000.

**d) Blowfish:** Blowfish is a symmetric block cipher that is unpatented and free to use. It was developed by Bruce Schneier and introduced in 1993.

**e) CAST5:** CAST5 (or CAST -128) is a symmetric-key block cipher used in a number of products, as the default cipher in some versions of GPG and PGP.

**f) RC4:** RC4 is a variable key-size stream cipher

based on the use of a random permutation.

**g) TDES:** TripleDES is an encryption algorithm called Data Encryption Standard that was first used by the U.S. Government in the late 70's. Encrypting PIN number in the ATM and UNIX password encryption using this algorithm.

**h) IDEA:** the International Data Encryption Algorithm is a symmetric-key block cipher designed by James Massey. The algorithm was intended as a replacement for the Data Encryption Standard (DES).

Symmetric encryption require the secret key exchange, which could be a difficulty. Asymmetric encryption in contrast needs no key exchange. The way of sending message of Alice and Bob in the above example now changes. When Alice wants to send Bob a message, she asks him to send his public padlock, this could be done publicly. Alice locks the message with Bob's padlock and send it over to him. Bob then use his private key to open and read the message. The critical advantage of asymmetric algorithm is that Bob and Alice never need to send a copy of their keys to each other so they remain private. The idea is to use public key, which is distributed among the sender and receiver to encrypt the message. The receiver and sender will use their private keys to decrypt the message.

## 5. DECRYPTION

Once the packets come to the receiver's side, they need reassembling. This is the responsibility of the destination node and should be performed prior to the ESP processing. In the RFC document summarization part, we mentioned the steps happen during the process.

The first step is to look up the SA. In order to decrypt the ESP Payload, some elements of the SA must be provided: source and destination addresses of SA, SPI in the ESP Header, encryption and authentication algorithm. The SPI will tell the recipient which SA to use as it has the database of the SAs. Then SA will provide the algorithms and the key used for decryption. If no valid SA exists for the session, the receiver must discard the packet.

Then the recipient will verify the sequence number. This process only performs when the anti-replay service is enabled at the receiver (default mode will be enabled). If the service is not on, then the receiver should notify the sender and this process will not be performed. If the receiver enables the anti-replay service, for each received packet, the receiver must verify the packet contains a sequence number that does not duplicate the sequence number of any other packets received during this session. The packet

should be checked this field first to speed rejection of duplicate packets.

If authentication has been selected, the receiver computes the integrity check value over the ESP packet minus the Authentication Data using the specified authentication algorithm and make sure it is the same as the integrity check value in the Authentication Data field of the packet. If they match then the packet is valid and accepted. Otherwise, the receiver must discard the packet.

The receiver decrypts the ESP Payload Data, Padding, Pad Length, and Next Header using key and algorithm indicated by the SA. The encryption algorithms are supported in IPSec is DES-CBC with key length of 64 bits.

For the case that the authentication is selected, verification and decryption may be performed serially or in parallel. In either cases, the verification process should be finish before the decryption. This order speed the detection and rejection of replayed or bogus packets by the receiver, reducing the impact of denial of service attacks. If two processes perform parallel, the packet accessibility and the reconstruction of the decrypted packet should be taken care of.

These following cases could lead to decryption fail: wrong selected SA due to invalid SPI/ destination address; erroneous pad length or pad value and corrupted ESP packet.

## 6. VPN IMPLEMENTATION

We'll consider ESP through a big picture, which is VPN. Suppose that the staff wants to access the server at the headquarter to finish their report but they are not in the headquarter at the moment. The solution is to deploy VPN. The staff could access to the server at the headquarter in a secure channel anywhere as long as they have internet access and the VPN client service on their computer (VPN client is even installed in the iOS of Apple).

There are some other options for sure, however, VPN seems to be the best choice. The headquarter could build their own lease line, which cost a big budget and not flexible. Or the company could use the cloud service. But they do not have strong confidence about the security issues as the service is provided by the third party. We even have another sort of VPN: Secure Sockets Layer (SSL). This service is quite familiar as the letter "S" in https at the address bar of browsers. In this case, we want to access the data/file sources in the company, which has not been provided through the web interface. SSL VPN does not work in this circumstance. IPSec is likely to be an ideal security solution, we will consider the pros and cons applying it in the fol-

lowing section.

## 7. CONCLUSION

In the IPSec context, using ESP protocol covers almost the security issues. AH header only authenticate the outer header and does not encrypt the payload. AH is used in conjunction with ESP only because of the authenticating the outer IP header in transport mode. Otherwise, ESP is sufficient, especially in tunnel mode. Moreover, since AH is almost redundant, not all of the implementation supports it. For instance, Cisco ASA/PIX version 7.0 and later does not support AH transforms. There are very few cases in which the packet must be strongly protected requiring using both AH and ESP. However, this level of security is rarely used because AH increases the overhead of the packet encrypted by ESP already. In addition, some hardware does not support AH and ESP applied on the same packet either<sup>4)</sup>.

As we known, the transmission of information over the network is accommodating but it also brings the risks to activities of many organizations. Therefore, each organization need to be equipped and build their own tight security system for important data such as: the staff information data or financial reports, projects. In this case, they are highly recommended using IPSEC to for safety of network communication. IPSEC policy will protect the data of organization from the outside risks.

Having strong secure characteristic, ESP also has weakness within itself, not just compared to AH. The Initialization Vector (IV) field in the ESP Header is required to be random and unpredictable to the outside. If choosing IV in a predictable way, there is vulnerability and the plaintext could be exploited using brute force attack. The vulnerability is difficult but not impossible. Another drawback of ESP about the conflict existing ESP and TCP deployed in IP wireless network. "It is impossible for an intermediate gateway outside sender or receiver's security enclaves to analyze an IPSec header to extract TCP flow identification and sequence number. The PEP agent cannot obtain the information needed to generate acknowledgments or retransmit data segments." IPsec tunnel mode and layering principles are unsuitable for new networking services and applications. In these cases, Secure Sockets Layer (SSL) or Transport Layer Security (TLS) can be alternative option. IPSec can have the access to the headers to protect them as being in the kernel, while SSL/TLS cannot do that. However, deploying IPSec could be a problem, and it would result in various things that not working for the user with unknown reasons. The user needs to have the IPSec client

software installed to enable the service. Whereas with SSL/TLS, user can interact with server through Web interface with standard browsers. For that reason, deploying IPSec universally is not realistic.

## REFERENCES

- 1) R. Atkinson, S. Kent.: IP Encapsulating Security Payload (ESP). RFC 2406, IETF, 1998.
- 2) Andrew. M.: Network Security and Virtual Private Network Technologies, Cisco Press, 2004.
- 3) Kan, Y.: Implementation and Evaluation of Secure Industrial Ethernet Communication, M.Sci Thesis, Chalmers University of Technology, 2010.
- 4) Shawn W.: Encapsulating Security Payload: Strengths and Weaknesses. East Carolina University, 2004.
- 5) Dhari K., Ahmed A.: Security Network with Virtual Private Network & (IPSec) Applications. Institute of Research Engineers and Doctors, 2014.

(Received Nov 20, 2015)

# A discussion of a Snake game implementation

Nguyen Thi Thao<sup>1</sup> and TRAN Nguyen Khanh<sup>2</sup>

<sup>1</sup> Student, Faculty of Information Technology, Hanoi University  
(Km9, Nguyen Trai, Thanh Xuan, Hanoi, Vietnam)  
E-mail: thaonguyen4c12@gmail.com

<sup>2</sup> Professor, Faculty of Information Technology, Hanoi University  
(Km9, Nguyen Trai, Thanh Xuan, Hanoi, Vietnam)  
E-mail: khanhtn@hanu.edu.vn

Games are more and more popular with a lot of types nowadays. With the ambition to create for own myself a game, I do this research. My research is the remaking of the classic game Snake as a window application using C# programming language. This program, which was inspired from a snake game in nokia phone version. This game also has two models: classical model and modern model. In each model, the player has a lot of challenge to come over. It is also hoped that this research will be useful reference for students to create their own game.

**Key Words:** snake game, C# programming

## 1. INTRODUCTION

The snake game is created by C# programming language. The main feature of the game is a snake controlled by the player, crawls around the field and “eats” all the foods that appear. After each time the snake successfully “eats” the food, the player will gain certain points and the length of the snake will increase. The game will end whenever the snake bites itself or hits the obstacles. The game will have two game modes: the classic mode and the modern mode. On the classic mode, the snake will simply crawl on a blank field to collect the food until it bites itself and the game will end. On the modern mode, the snake will collect food on different levels. It has to collect a certain amount of food to pass from a level to the next level. On each level, the map will change.

## 2. GAME'S FUNCTIONALITY

- The snake is fully controlled by the player using arrow key on the keyboard.
- The score of the game will be kept track of, if the score are high enough, it will be saved with the player's name and displayed in the high scores section.
- The players are allowed to customize some features of the game such as: sounds volume (background, in game...), snake's skin (optional) and snake's initial speed.

## 3. SPECIFICATION OF FUNCTIONAL REQUIREMENTS

### (1) The GUI

#### a) Main menu

The main menu will be a windows form which contains buttons with certain function, which are:

- New game: initialize a new game.
- High scores: bring up High score form.
- Settings: bring up Settings form.
- Help: bring up Help form.
- About: bring up About form.
- Exit: exit the program

#### b) High scores window

It contains the list of 5 highest scores which have ever been acquired by the players. The list is saved in the text file. This window also has a back button to come back to the main menu.

#### c) Settings window

This is a windows form contains some customizable features of the game for the player to choose:

- Sounds: the player can choose between several levels of sounds, level 0 sound means the sounds is off.
- Snake's initial speed: the movement speed of the snake at the starting point of the game, ranging from 1 to 5.
- Snake's skins(optional): allow player to choose between several snake's textures.

This window also has a back button to come back to the main menu.

All the settings will be saved in a config file.

#### d) Help window

This is simply a window form with some instruction of how to play a game. It has a back button to come back to the main menu.

### e) About window

Similar to the Help window, it contains some information of people who made the game.

### (2) The gameplay

After the player click the “New game” button, first of all, it will bring up a windows form with two options, which are the two game modes for the player. Based on this option, one game mode will be initialized.

#### a) Classic mode

As we mentioned before, in this game modes, the snake will simply crawl in a blank field to collects foods and gain point for the players. And these are some more specific features:

- The speed of the snake is unchanged. It is the same as the initial speed.

- The “food” appears on the field after the previous food had been eaten and it will be at a random location. After the food is eaten, the score will increase by 5 points and the length of the snake is also increased.

- After each 4 regular “foods” was eaten by the snake, there will be a special “food”, which is a bonus of 100 points. However, this bonus point will be disappeared after 5 seconds if it is not consumed by the snake. The amount of bonus points is also decreased over time (optional).

- The game will end when the snake bites itself.

#### b) Modern mode

In this game mode, instead of just a blank field, the snake will have to deal with different levels of obstacles, which are different maps with the system of walls. These are some specific features:

- The food and bonus food mechanism is similar to the Classic game mode.

- The speed of the snake is started at 1 and increase after each time it collect one food. Max speed is 5.

- After the snake has eaten 6 foods (not include the bonus), it will be able to reach to the next level. The total number of levels is 5. The game is always started at level 1. The next levels should be more complicated than the previous levels.

- (Optional)Besides the food system, there is also a special items system. They are similar the foods, but instead of giving points, they give the snake some random special abilities such as wall breaking, speed slowing, length decreasing and so on. These items are randomly appeared between certain amounts of system time after the previous item is appeared. It will disappear after 5 second if it is not consumed by the snake.

- The game will end when the snake bites itself or hits the walls.

### (3) Other features

- The textures of the back ground field are randomized in each new game (optional).

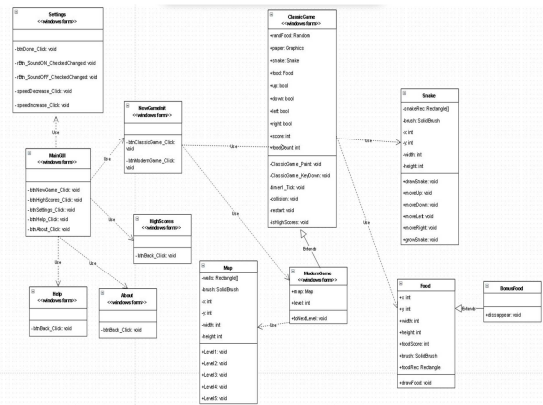
- The background music is randomized in each new

game (optional.)

- There is specific sound for each event in the game such as button clicking, when the snake eats the food and when the game ends.

- After the game ends, there will be a windows form appeared to inform the player about his or her scores. If that is a high score, instead of a normal windows form, it will be a congratulation form and a text box asking for the player’s name to save. After that, another window form will appear with two options which are back to main menu and play another round of new game.

## 4. ANALYSIS



There is the class diagram which shows the classes and the relationship between them. With this Snake game, there are 12 classes: MainGUI, Setting, Help, About, NewGame, HighScore, ClassicGame, ModernGame, Food, BonusFood, Map and Snake. From MainGui, we can connect and control Setting, Help, About, HighScore and NewGame with the one-one relationship. In NewGame, there are also 2 class related more: ClassicGame and ModernGame. In this class, you can choose the type of game you want to play.

There are also 4 objects needed to create: Food, BonusFood, Map and Snake. Food is the object generating the food for the snake. BonusFood is the class which is extended from Food. Furthermore, Snake class is also created in order to make a snake with some functions: constructor, drawSnake, move and getRotate.... Finally, we create Map object to make the game more challenging.

## 4. OBJECTS FOR SNAKE GAME

### 1) Parts of snake

- Head



- Body



- Tail



(2) Food

We have a set of food:



(3) Types of bricks



## 5. PRGRAMMING

### REFERENCES

John Latham, The snake Game Java Case Study,  
2014

# **Solving Notifying General News To Hanoi University Pupils – Hanu News Android Application**

CHU Huu Thanh<sup>1</sup> and NGUYEN Van Cong<sup>2</sup>

<sup>1</sup> Student, Information Technology, Hanoi University  
(Km9, Nguyen Trai, Thanh Xuan, Hanoi, Vietnam)  
E-mail:mrsilver256@gmail.com

<sup>2</sup> Professor, Information Technology, Hanoi University  
(Km9, Nguyen Trai, Thanh Xuan, Hanoi, Vietnam)  
E-mail:congsv@gmail.com

The world is now rapidly growing up and go along with this is the Technology development. People gradually get familiar with software, applications, tools. As a first-year student in my faculty and get lack of experiences, I study android on the internet after finishing IPG course, I myself have created an android application which enables our pupils to read the news from their faculty portal pages and get the notifications if existing updated news. The content of this research demonstrates how I develop my application – Hanu News.

*Key Words : Hanu News, Hanoi University*

## **1. INTRODUCTION**

Nowadays, a lot of software has been applied in the educational system which helps both the lectures and the students. Apart from how to enables IT applications in lessons such as Power Point made by Microsoft or Eclipse application that enables students to write coding statements and compile it, I personally think about how the lectures can notice their students as fast as possible if any changes in time schedule or lecture off happened. The matter is that very few students want to check the portal every single day of their student's life so our University pupils need a tool that could handle it for them. After 3 months acquiring knowledge about android operating system and their application development, I have created an android application which can solve all the problems above. My application also have other features like user friendly interface applying, adding personalization since users can choose their major to receive the updated news and notifications. Finally, it also has mobility feature as I mentioned above.

## **2. RELATED WORKS**

There are some android applications which enable users to fetch the data from websites. However, in most of the case for appealing purposes, the developers tend to put too many things which are unnecessary that cause the page heavy and the application get lagging.

## **3. SOLUTION PROPOSALS**

As we all know about two major mobile operating systems are android OS and IOS, I prefer to work on android platform because of its popularity in our university. After defining the problems, we also have to prepare for the solutions or the goal. The first and also the most important thing is that the application can enable users to read General News from the Portal website. The second, it should help lectures in notifying students as fast as possible.

Honestly, I am just a first-year student who has just finish C basic language course 4 months ago. All other languages are quite hard for me to begin except Java since Java and C language have the same syntax in most cases. At that time, I got no idea about Java language as the PPL – Java basic course - starts quite late. Been through 90 days of getting understanding and practicing android – the similar syntax programming language using the core java - through online guides, I release this application – an object oriented application - even before I was taught about object oriented program 2 weeks. That means I am lack of knowledge and experience but I still can solve the problem by my way so the thing that if it still gets some bugs is reasonable. But I can always find method to fix it.

Our application needs 5 features: parsing, automatically updating and notifying, faculty personalization updated choice, friendly user interface, mobility. The goal is clear and now we need to divide it into 2 main parts or main objects as the whole ap-

plication itself is an object. The first part is parsing HTML content from the Faculty Portal page. Here we got 2 smaller tasks. Firstly, we need to create a list view representing the link of the content page – people read news here. Secondly, content page parsing task. The second part is automatically updating and notifying. Finally, we need a combining object of 2 objects above as the completed application.

## (1) Parsing HTML content from the Faculty Portal page with Jsoup

### (1) Analyzing and fetching the General News to application list view

Starting with Google Chrome which is the most using web browser introduced by Google In-co-operation – about 63.9% people use Google Chrome April 2015<sup>1)</sup>, I try to get the source code of the FIT Portal website by surfing to the web address

<http://fit.hanu.edu.vn/fitportal/mod/forum/view.php?f=4>

via FIT portal in the Generals Announcement.

After reading the source code, I realize all the topic names and the link of the topics are placed in the tag

```
<td class="topic starter"><a href="http://fit.hanu.edu.vn/fitportal/mod/forum/discuss.php?d=3756">Notice on the workshop on 18th April 2015 (for C11, C13 Students) </a></td>
```

Jsoup is a Java library for working with real-world HTML. It provides a very convenient API for extracting and manipulating data, using the best of DOM, CSS, and jquery-like methods<sup>2)</sup>. I use Jsoup to take out the link and the name on the above link and then store them in 2 arrays with in 2 text file.

### (2) Fetching the content page

Now what got the link of the news we want to get the content from so we need a place to let the content appear. We should create a fragment class to represent it. In this class, we also use Jsoup to parse all the contents we want like: topic name, content of the news, profile picture of the author, author name, date and time ...

After that, the content should be shown like figure 1.

### (2) Automatically updating and notifying

Here, I use countdown timer for time checking process, a Service class to run the application in background and Receiver to wake the software on startup.



Fig.1. Showing content in Hanu News Application

### (1) Theory

My method needs a link as the input, using Jsoup we will have 2 base files to make comparisons with the new data files which are also parsed by Jsoup. First, we should create an activity class which let user choose their major. After clicking on the save button, by using the similar method in creating the first object, we got 2 base files which is store name and link. Then, we need 2 more updated files name and link to compare. Now, it is all about comparison. My idea is that we just need to compare the first elements of the array name - name[0] of base file and name[0] of updated file to be exact. If they are different so I replace the base file by 2 new updated files.

### (2) Using Service in android platform

Complete the theory, the work now is on practical. We need something that helps us making comparisons regularly. In android, we need to create a service to handle it. A Service is an application component that can perform long-running operations in the background and does not provide a user interface. Another application component can start a service and it will continue to run in the background even if the user switches to another application<sup>3)</sup>.

### (3) Complete the application with Receiver

A receiver actually is a class which receives the Start on Boot requires from the Manifest file. This means, after booting the device, the receiver class

will start. It just starts and does its function, then it will stop. So if we put the start service command here, the service will automatically start after booting.

## 4. SOLUTION DESIGN

Here, I choose android as the mobile platform because Android was built from the ground-up to enable developers to create compelling mobile applications that take full advantage of all a handset has to offer<sup>4)</sup>.

### (1) Classes

There are some types of class such as service class, receiver class, activity class ...An application contains one or more class which are linked together. Each class contains one or more method, needs an xml file which provides users an interface and requires a declaration in Manifest file to notice the user and get rights to perform in the application.

#### (1) MainActivity class

Main method: input is a Faculty Portal link and output 2 text files. The first file contains array name, and the other has array link.

#### (2) Feed class

Main method: input 2 text files above and output a list view which enables user to click on and turn to content page.

#### (3) Content class

Main method: input is a General News link and output is the content shown in the content page.

#### (4) MyService class

Main method: input is the Faculty Portal link and output is the notifications if any changes are made.

#### (5) MyReceiver class

Main method: start the MyService class on startup if the status text file content is “yes”.

#### (6) Setting class

Main method: Input is the Faculty name and output is a text file which represents the updating status. If the status is “yes”, automatically update mode is on and vice versa.

### (2) Implementation

Go along with android, there are 2 main IDE which can help developers in creating the application: Android Studio and Eclipse with ADT plug-in. Eclipse with ADT plug-in is my IDE choice to work since Eclipse is the essential tools for any Java developer, including a Java IDE, a CVS client, Git client, XML Editor, Mylyn, Maven integration and WindowBuilder<sup>5)</sup>.

## 5. CONCLUSION

In conclusion, I would write about what I have done briefly. From the very first time, I realize a problem is that most students in our campus need a tool which can help them easily get news and updated notifications from the Faculty Portal page. I started to develop an android application with lack of experiences and knowledge but somehow I still can achieve the goal with helps of Eclipse and Jsoup.

My Application now is just only a starting part among my whole idea. In my software, I use object oriented method and java syntax as the basic start and achieve some advantages apart from procedure method such as: It is easier for bug fixing later and more convenient since we can put as many links as we want. That means user can also get the mark tables, research... or other news in their Faculty instead of just General News.

In the future, with more knowledge and experiences, I got 2 more years to develop this application with more functions like registering course, chatting among Hanu students and teachers – a university-scale social networking... which could be very helpful for our pupils.

## REFERENCES

- 1) Refsnes, 2015 . Browser Statics and Trend. Retrieved from [http://www.w3schools.com/browsers/browsers\\_stats.asp](http://www.w3schools.com/browsers/browsers_stats.asp)
- 2) Jonathan Hedley, 2015. Jsoup HTML Parser. Retrieved from <http://jsoup.org>
- 3) Android Developers. Services. Retrieved from <http://developer.android.com/guide/components/services.html>
- 4) The Open Hand Set. Retrieved from [http://www.openhandsetalliance.com/android\\_overview.html](http://www.openhandsetalliance.com/android_overview.html)
- 5) The Eclipse. Retrieved from <http://eclipse.org/downloads/packages/eclipse-ide-java-developers/lunasr2>

(Received November 15, 2015)

# SOCIAL NETWORK ANALYSIS

NGUYEN Viet Anh<sup>1</sup>, NGUYEN Phan Hung<sup>1</sup>, DANG Thai Hoang<sup>1</sup>  
and DO Thi Phuong Thao<sup>2</sup>

<sup>1</sup> Student, Faculty of Information Technology, Hanoi University  
(Km9 Nguyen Trai Road, Thanh Xuan District, Hanoi, Vietnam)  
E-mail:nguyenvietanh168@gmail.com

<sup>2</sup> Professor, Faculty of Information Technology, Hanoi University  
(Km9 Nguyen Trai Road, Thanh Xuan District, Hanoi, Vietnam)  
Email: thaodtp@hanu.edu.vn

In the modern world, when society is developing, the network development trend's analysis cannot be ignored. In fact, it is claimed to be extremely helpful in discovering numerous 'kinship' structure, mobility, contacts amongst the individuals of deviant groups in different societies. It is still the most convenient way to do the task of analysis, there are some restrictions in their applications while usage though (like the performance in normalization of identifiers, the wide range in the social application applied, etc.). However, these would not be the problems to prevent SNA's role from scientists discussing and analyzing the structures for their own projects.

The short report here therefore primarily discuss on how development in social network, from its brief history to the ways for exploring a network in the modern scientist projects applied, particularly notice on the graph theory for displaying the relationships.

## 1. BRIEF PERSPECTIVE

### (1) When and why SNA is born?

There are many sources, from hard to soft materials, stating this issue. Even each might be different, it can be seen that SNA was appeared long ago, but it was not strongly developed until the last century, when there were many requirements in variety of social and scientist fields to it, which includes Mathematics, Anthropology, Psychology, etc. Graph probably was popular thanks to its good and clear design to conveniently solve a bunch of problems (i.e. the shortest and most optimal paths to go through different places, the connection between employees in organizations, the brain connection, etc.).

Without help from SNA, there would be no relief in tackling these challenges, except for extremely brilliant imagination. This means SNA had appeared

to help human beings are easier to facing those hardships with which associated the relationship between objects that brain solely cannot simply imagine.

### (2) What applications they provide?

SNA is excellent in both stimulating good impact and enabling to limit effects from numerous of different social issues.

- For positive development:
  - increase quality customer acquisition
  - improve retention, reduce fee for studying
  - encourage leadership
- For optimizing to prevent deviant problems:
  - defeat terrorism
  - determine crime patterns
  - detect insurance scam
  - uncover conflicts of interest in business

## 2. SNA IN USAGE OF REAL LIFE

### (1) Core terminologies

- Node:
- Tie strength:
- Central measurement
- Key player
- Cluster:

### (2) Analysis strategies used in projects

- Types of network: Ego central and complete networks.

Ego central network: only applied for a sample of objects which was chosen for analyzing, so it will need a suitable statistic analysis (i.e. Estimation theory, Hypothesis theory in statistic respect)

Complete network: applied for summarizing a whole organization, which was synthesizing from different individuals in that, so the proper method here is applying a case study, useful for anyone who haven't experience or do not have good condition to investigate the real life organization.(This normally is obtained by the first type of network).

- Methods to get information for analyzing process:

- Questionnaires
- Interview
- Observation
- Secondary source exploring
- Network data collection

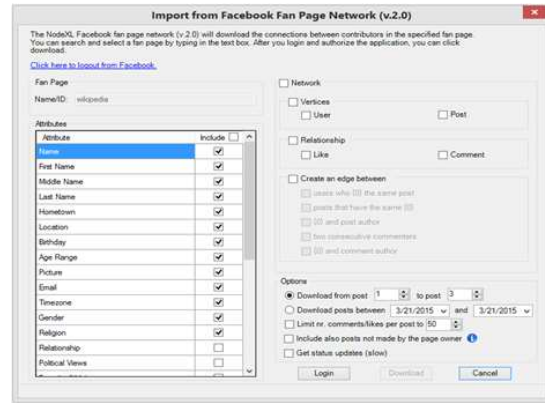
- Ways to show results:

- Matrix of adjunction:
- Graph system
- Applications (Gephi, NodeXL)

### (3) Recommend application (NODEXL)

- A simple way to use yet powerful way for any spreadsheet user to gain the power of network analysis.
- Used for import vectors and edges, stand for users, posts, posters, like...from Timeline, groups(open group only), Fan pages on social network.
- Depict a graph, with variety ways of view.
- Help person to figure out

**Fig. Import from Facebook Fan Page Network**



trends/conclusions: period time of a day people is usually online, posts have the biggest numbers of likes....

## 3. CONCLUSION

Thanks to the help from the analysis tools, NodeXL in specific, it enables more crucial network analyzing works to be done well, by the capability of functioning both analysis and visualization to be combined, with the familiarity in spreadsheet paradigm for handling the data progress. Clearly, SNA is really promising for the future plan and projects, and one of them must include the application to a wide social media data sets range.

## 4. ACKNOWLEDGMENT

We would like to thank our advisors, Mrs Phuong Thao for her help, advice, and mentoring during our graduate career. Without her support and guidance, none of the work presented in this thesis would have been possible. Moreover, we are deeply indebted to her both for showing us how to do successful research, how to mentor students, and how to communicate research results effectively. We suspect that this debt will only grow over time, as we use these skills in our own research career.

## **REFERENCES**

- 1) Smith, W. : Cellular phone positioning and travel times estimates, *Proc. of 8th ITS World Congress*, CD-ROM, 2000.
- 2) Lada Adamic: Social Network Analysis course at <https://www.coursera.org/course/sna>
- 3) Alan E. Mislove: Online Social Networks: Measurement, Analysis, and Applications to Distributed Information Systems 2009.
- 4) Kolli Naimisha: Applications of Social Network Analysis to Community Dynamics
- 5) to Community Dynamics

**2**

# Tic-Tac-Toe Game and Artificial Intelligence

VU Anh Duc<sup>1</sup>, PHAN San Thanh<sup>1</sup> and TA Quang Hung<sup>2</sup>

<sup>1</sup> Student, Faculty of Information Technology, Hanoi University  
(Km 9, Nguyễn Trãi, Thanh Xuân, Hà Nội, Việt Nam)

E-mail: {vuanhduc2c12, jackiehenry1411}@gmail.com

<sup>2</sup> Professor, Faculty of Information Technology, Hanoi University  
(Km 9, Nguyễn Trãi, Thanh Xuân, Hà Nội, Việt Nam)

E-mail: hungtq@hanu.edu.vn

Tic-Tac-Toe - actually a small version of Caro games, is a well-known a very classic game for almost every student in the world. As students studying programming like us, we also very keen on this game. Besides, as we are studying Java programming language, we really desire to develop a real Java game or application project. Thus, we decided to develop the Tic-Tac-Toe game based on Java Programming Language. This paper bases on a real Java Tic-Tac-Toe game project that we implemented into 2 playable modes: player versus player (PvP) and player versus AI which we decided to construct by customizing the famous Minimax algorithm. For the PvP mode, we use XML programming and for the case of player versus AI, we fully focus on Java programming language.

**Key Words :** Tic-Tac-Toe, Java, game, Minimax algorithm, programming

## 1. INTRODUCTION

Tic-Tac-Toe, a small version of Caro game, is a popular game in everywhere. The rules of this game are quite simple so, we decided to learn about this game and how to make an artificial intelligence (AI) for this game. It is challenging to add AI mode to the game so that human can play against computer. After reading materials about AI algorithms, we found that it is possible to make this game using Minimax Algorithm. This is the first time that the authors do research about this algorithm therefore it will contain some unexpected mistakes. The developer team is willing to receive ideas to improve the research.

## 2. ANALYSIS OF THE GAME

We need a 3x3 dimension board with 9 squares. There are two kinds of respective marks “X” and “O” representing for 2 players or human player and computer.

The player who succeeds in placing three respective marks in a horizontal, vertical, or diagonal row wins the game. So we need rules to determine the winner or game is drawn.

Tic-Tac-Toe is game for 2 players so each player can analyze and find the next move of the opponent, so if we want to build a AI for Tic-Tac-Toe, we need know about strategies of this game.

**Win:** If the player has two in a row, they can place a third to get three in a row.

**Block:** If the opponent has two in a row, the player must play the third themselves to block the opponent.

**Fork:** Create an opportunity where the player has two threats to win (two non-blocked lines of 2).

**Blocking an opponent fork:**

*Option 1:* The player should create two in a row to force the opponent into defending, as long as it doesn't result in them creating a fork. For example, if “X” has a corner, “O” has the center, and “X” has the opposite corner as well (**Fig.1**), “O” must not play a corner in order to win (playing a corner in this scenario creates a fork for “X” to win).

*Option 2:* If there is a configuration where the opponent can fork, the player should block that fork.

**Center:** A player marks the center. If it is the first move of the game, playing on a corner gives “O” more opportunities to make a mistake and may

therefore be the better choice. However, it makes no difference between perfect players.

**Opposite corner:** If the opponent is in the corner, the player plays the opposite corner.

**Empty corner:** The player plays in a corner square.

**Empty side:** The player plays in a middle square on any of the 4 sides.

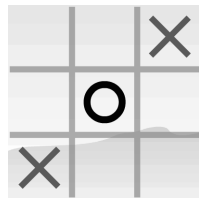


**Fig.1** Example of a situation which may lead to a fork by player "X".

### 3. IMPLEMENTATION OF THE PROJECT

#### (1) The Tic-Tac-Toe game and heuristic AI rules

At first, the authors tried to write many heuristic rules for each of situations can happen, and we set a score (weight) for each of those rules. For instance: at the beginning of a new game, the center square has the biggest priority. Nevertheless, after a long time doing this way, the authors realized that it can't be effective and not scalable. When the board has 9 squares, it is not an issue to write all rules for all possible situations. However, if we extend the board to 10x10 for demonstration, it can be problematic to handle all possible rules.

#### (2) Applying the Minimax algorithm

The Minimax Algorithm is used for all 2-player games. Each player can analyze the opponent's possible next moves. This algorithm uses rules to calculate the "status point" of the recent state of the board. For example: if there are 3 X's in a row the "status point" will increase by 1000 point, else if there are 3 O's in a row the "status point" be will "increased" by -1000. Player X will try to maximize "status point". Meanwhile, player O will try to minimize player X's "status point". Certainly, rules to calculate the "Status point" have many different

weights like 1000, 100, 1. The game program will check all possible next moves of the computer then decide the best move to minimize the human player's "status point". Coming back to strategies of Tic-Tac-Toe which were discussed in section 2, if the computer player only finds the best next moves depending on "status point" of all possible next moves then it only knows how to make a wining move or a create a change move to win for a few next moves. In this case, the AI player can't block the wining moves of human player. With the Minimax algorithm, the AI player can also find what the best moves a human player can make against it are. Doing so, it will be able to prevent the human player from winning. In short, we need to use the Minimax algorithm, a recursive AI algorithm in the Tic-Tac-Toe game.

One of the most important attribute of a recursive algorithm is certainly the number of recursions (the times that the algorithm repeats itself). The authors used an integer variable to hold the data of recursive times called "depth". This "depth" also can be used to classify level of computer AI difficulty (hard, medium and easy). How this depth can do it? In the circumstance that "depth" equals 1, the computer only run Minimax Algorithm for 1 time, so it can only find its wining moves but it can't block the human player's winning moves. When "depth" equals 2, computer can find the wining move and block the wining move of human but it can't find the move to create a **fork** (a strategy in Tic-Tac-Toe game, discussed in section 2). Then, "depth" with a value of 3 can solve this problem. Furthermore, with "depth" equal to 4, the AI player can both create and block **forks**.

#### (3) Building Java GUI for the game

At first, the authors intended to use 9 **JButtons** objects to represent 9 squares on the game board and use **ActionListener** to handle events. However, in future we plan to extend the board to 10x10, so handling 100 **JButtons** is not a good way. For this reason, we decided to use Java graphic drawing line, oval... to create our board and draw our X, O symbol and use **MouseListener** to handle events. This way, the game program can manage events better.

**REFERENCES**

- 1) Eck D. J., Introduction to Programming using Java: Version 6.0.1, 6th, 2012

2) Oracle, The Java Tutorial, 2011

**(Received November 15, 2015)**

# Application of Game theory in Project Management

PHAM Thanh Trung<sup>1</sup>, NGUYEN Minh Quan<sup>1</sup>, and VU Minh Tuan<sup>2</sup>

<sup>1</sup> Student, Faculty of Information System, Hanoi University,  
(Km9 Nguyen Trai, Thanh Xuan, Ha Noi, Viet Nam)  
E-mail:phamtrungzm@gmail.com

<sup>2</sup> Professor, Faculty of Information System, Hanoi University,  
(Km9 Nguyen Trai, Thanh Xuan, Ha Noi, Viet Nam)  
E-mail: tuanvm@hanu.edu.vn

## 1. INTRODUCTION

Conflict is the nature characteristic of the world. We have conflict between sexes, generation, people...We can see the conflict in every aspect, every field of our life: economics, political science, and psychology, as well as logic, computer science, biology and so on...So what lead to these conflict? The answer is the decision making. With every decision we make, there will always be a decision that against our decision. In the past, people try to find the best way to go deeply into the problem, to find a solution for the most difficult question: How to solve the conflict between each decision we made? Before we move to the next part to understand more about Game Theory, I just want to say that Game Theory is very important and necessary for us, especially for people who want to start their own business.

## 2. WHAT IS GAME THEORY

A model of optimality taking into consideration not only benefits less costs, but also the interaction between participants.

Game theory attempts to look at the relationships between participants in a particular model and predict their optimal decisions. This part will give some type of game theory.

### 2.1. Cooperative / Non-cooperative

**Cooperative games:** An example is a cooperative game, when players choose the strategies by a consensus decision-making process. Cooperative game theory also provides useful tools to solve problems in network theory, social choice, and multi-criteria analysis.

#### Non-cooperative games:

Games assigning property rights: rock-paper-scissor; various drinking games

Games in sports: penalty kick in soccer; batter-pitcher duel

Games in media: The Dark Knight, ferry scene; Friends, Season 5, Episode “The One Where Everybody Finds Out”.

Hybrid games contain cooperative and non-cooperative elements. For instance, coalitions of players are formed in a cooperative game, but these play in a non-cooperative fashion.

### 2.2 Simultaneous / Sequential

**Simultaneous games:** An example is the Prisoner’s Dilemma, where the two players have to decide their strategy without knowing what the other player has chosen. Even though the police might not interview each of the prisoners at exactly the same time they are still making their decision without knowing what the other player has chosen.

**Sequential games:** An example is chess. When I am making my move I know what your last move was and can use that information to determine my own strategy. It is important to know who is going to move first in a sequential game as there may be a first mover advantage, or even a first mover disadvantage.

### 2.3 Perfect information and imperfect information

A game of imperfect information (the dotted line represents ignorance on the part of player 2, formally called information set)

Perfect information is often confused with complete information, which is a similar concept. Complete information requires that every player know the strategies and payoffs available to the other players but not necessarily the actions taken. Games of in-

complete information can be reduced, however, to games of imperfect information by introducing "moves by nature".

### **3. APPLICATION: TEAM WORK PROBLEM**

#### **3.1 Problem:**

A group of 3 students including Mr. A, Mr. B and Mr. C is assigned for a project about game theory. They can choose from 2 different topics: "Game theory in specific applications" or "Algorithms of game theory".

A team can have maximum number of member is 3 students, but for each student less than the required number, the team get 1 bonus point. However, because game theory is an extremely difficult topic so no one can finish the project by himself in the required time.

Three students can form a team of 3 to work on 1 topic or split into small groups to work on different topics, but the topics aren't allowed to be similar. That means we can have a team with Mr. A, B and C to work on 1 topic or 2 teams including Mr. A and B work on "Game theory in specific applications" and Mr. C work on " Algorithms of game theory", the team's member and topics can change. Because there are only 2 topics so there is no way for each student to do it separately.

For the option of 3 students, the project can be finished on time and each member get the total mark of the project. For the 2 students team option, the project still can be finished on time, each member gets the total mark of the project plus 1 point bonus. For the 1 student team option, the student can get a high bonus point but because he can't finish the project on time so the result will be a low total mark.

Three students can't decide who will work on which topic and how they will divide the group, so they call a vote. Each member will write down the topic he chose and they will do exactly the same topic they chose. If 3 of them chose 1 topic, they will form a team and do that topic, if 1 of them chose a topic which different from the others, that one will form a team and do the topic himself and the others will form a 2 students team and do the remaining topic.

#### **3.2 Analyze:**

With the example above, we have a normal form

game the 3 players including Mr. A, Mr. B and Mr. C and 2 strategies including "Game theory in specific applications" and "Algorithms of game theory".

We call the strategy of a player chose "Game theory in specific applications" is strategy 1 and strategy of a player chose "Algorithms of game theory" is strategy 2. So we have all results that happen to Mr. A like this:

$$A_{122} = A_{211} = -2, A_{111} = A_{222} = 0 \text{ and } A_{121} = A_{112} = A_{212} = A_{221} = 1$$

The same happens to Mr. B and Mr. C, we have:

$$B_{212} = B_{121} = -2, B_{111} = B_{222} = 0 \text{ and } B_{122} = B_{221} = B_{112} = B_{211} = 1$$

$$C_{112} = C_{221} = -2, C_{111} = C_{222} = 0 \text{ and } C_{212} = C_{122} = C_{211} = C_{121} = 1$$

Assume that Mr. A, Mr. B and Mr. C has the same interest in both topic, so we can call their mixed strategies are:  $p = q = r = (\frac{1}{2}, \frac{1}{2})$ . From this, we find the expected payoff og Mr. A is:

$$A(p,q,r) = -2 * \frac{1}{4} + 0 * \frac{1}{4} + 1 * \frac{1}{2} = 0$$

The same happens to Mr. B and Mr. C expected payoff:

$$B(p,q,r) = -2 * \frac{1}{4} + 0 * \frac{1}{4} + 1 * \frac{1}{2} = 0$$

$$C(p,q,r) = -2 * \frac{1}{4} + 0 * \frac{1}{4} + 1 * \frac{1}{2} = 0$$

Now we will find the Nash equilibrium in this game.

Assume  $p = (a, 1-a)$  is Mr. A mixed strategy, with " $a$ " is the probability of Mr. A chose topic "Game theory in specific applications" and " $a-1$ " is the probability of Mr. A chose topic "Algorithms of game theory".

From this, we have mixed strategy for Mr. B and Mr. C are  $q = (b, b-1)$  and  $r = (r, r-1)$ .

So, Mr.. A's expected payoff will be written in this formula:

$$\begin{aligned} A &= -2[a(1-b)(1-c) + (1-a)bc] + 0[abc + (1-a)(1-b)(1-c)] + 1[ab(1-c) + a(1-b)c + (1-a)(1-b)c + (1-a)b(1-c)] = 1[ab(1-c) + a(1-b)c + (1-a)(1-b)c + (1-a)b(1-c)] - 2[a(1-b)(1-c) + (1-a)bc] = 1[2a(b+c-1) + c + b - 3cb] \end{aligned}$$

		Mr. C			
		Application		Algorithm	
		Mr. B		Mr. B	
		Application	Algorithm	Application	Algorithm
Mr. A	Application	(0,0,0)	(1,-2,1)	(1,1,-2)	(-2,1,1)
	Algorithm	(-2,1,1)	(1,1,-2)	(1,-2,1)	(0,0,0)

**Table 1.** The payoff matrix of the game

And the formula for Mr.. B and Mr.. C are:

$$B = 1[ 2b ( a+c-1 ) + a + c - 3ac ]$$

$$C = 1[ 2c ( a+b-1 ) + a + b - 3ab ]$$

Now we take the case of Mr. A, we can see that b and c are depended on Mr. B and Mr. C strategies. So to find out the maximum of A, we can consider these cases:

-  $b + c > 1$ : A has the maximum value when  $a = 1$ . With  $b > 0$ ,  $c > 0$  and  $a = 1$ , we have  $a + c > 1$ ,  $a + b > 1$ . From this, we have the maximum value of B when  $b = 1$  and the maximum value of C when  $c = 1$ . Because  $a = b = c = 1$  so the Nash equilibrium is  $p = q = r = (1,0)$ . So in this case, the Nash equilibrium happens when all of them chose topic “Game theory in specific applications”.

-  $b + c < 1$ : A has the maximum value when  $a = 0$ . With  $b < 1$ ,  $c < 1$  and  $a = 0$ , we have  $a + c < 1$ ,  $a + b < 1$ . From this, we have the maximum value of B when  $b = 0$  and the maximum value of C when  $c = 0$ . Because  $a = b = c = 0$  so the Nash equilibrium is  $p = q = r = (0,1)$ . So in this case, the Nash equilibrium happens when all of them chose topic “Algorithms of game theory”.

-  $b + c = 1$ :  $A = 1( 1 - 3cb )$  isn't depend on a. If  $a + b$  and  $a + c$  is not 1, so the probability of 3 players maybe 0 or 1. However, we consider the case that  $b + c = 1$  so  $a + b$  and  $a + c$  must equal to 1. From that,  $a = b = c = \frac{1}{2}$ , so the Nash equilibrium is  $p = q =$

$r = (\frac{1}{2}, \frac{1}{2})$ . This is the situation we considered before when Mr. A, Mr. B and Mr. C has the same interest in both topic.

Table 1 presents a payoff matrix of the game. In the matrix, we can clearly see the payoff of each student in each mixed strategy, with Mr. A's payoff in the left, Mr. B's payoff in the middle and Mr. C's payoff in the right.

#### 4. CONCLUSION:

In this research paper, we show that game theory is very suitable to solve conflicts and an example about how take decision in conflict. Game theory shows that in a conflict, everyone can have benefit, no one lose. From this point, game theory can be used in various fields and situations and everyday everyone can use to get benefit for themselves.

#### REFERENCES

- 1) Anthony Kelly, *Decision making using Game Theory, an introduction for Manager*.
- 2) Wang, G. G., & Dobbs, R. L. (2008). Economic Foundation of HRD: Theory and Application. (Special issue). *Advances in Developing Human Resources*, 10.
- 3) Wikipedia:  
[http://en.wikipedia.org/wiki/Nash\\_equilibrium](http://en.wikipedia.org/wiki/Nash_equilibrium).
- 4) William Spaniel, Game Theory 101: What Is a Nash Equilibrium? (Stoplight Game):  
<https://www.youtube.com/watch?v=0i7p9DNvtjk>
- 5) William Spaniel: Game theory 101: rock, paper, Scissor:  
<https://www.youtube.com/watch?v=-1GDMXoMdaY>.

# Multi-objective Optimization using Game Theory and Genetic Algorithm

DO Minh Thu<sup>1</sup>, NGUYEN Minh Hoai<sup>1</sup> and TRINH Bao Ngoc<sup>2</sup>

<sup>1</sup> Student, Special Subject 2, Faculty of Information Technology, Hanoi University  
(Km9 Nguyen Trai, Thanh Xuan, Ha Noi, Viet Nam)

E-mail: {mthu.ctem, hoainm194}@gmail.com  
<sup>2</sup> Professor, Faculty of Information Technology, Hanoi University  
(Km9 Nguyen Trai, Thanh Xuan, Ha Noi, Viet Nam)  
E-mail: ngocbt@hanu.edu.vn

Multi-objective optimization problem is the subject of studying the strategy to satisfy multiple issues, each of which collides with one another. To solve this problem, there have been many researches using game theory and genetic algorithms as an approach. With the mathematical expressions and technique to find the best decision among several opposing ones, together with individuals selecting algorithm, multi-objective optimization research field seem to have great results. In this paper, we discuss the effect of genetic algorithm, based on game theory, in comparison with other algorithms, to solve multi-objective problem. Then, we apply this algorithm on a specific situation in reality to find the best strategy for a company to manipulate their risks management..

**Key Words:** game theory, multi-objective optimization, genetic algorithm, risks management

## 1. INTRODUCTION

The world around us is full of problems that concern more than a single value or objective. An investor composes a portfolio of stocks in order to obtain a high return on his or her investment with a small risk of incurring a loss; an oncologist prescribes radiotherapy to a cancer patient so as to destroy the tumor without causing damage to healthy organs; an airline manager constructs schedules that incur small salary costs and that ensure smooth operation even in the case of disruptions. All three decision makers are in a similar situation—they need to make a decision trying to achieve several conflicting goals at the same time. That is Multi-objective Optimization Problem.

When it comes to conflict analysis and interactive decision, Game Theory is a suitable approach, since it provides general mathematical and logical methods for decision-makers to secure the best outcomes for themselves in an interaction with each other. There have been many thoroughly developed classical methods for solving multi-objective optimization, yet there are still lots of shortcomings in solving high dimension, multimodal problems. Genetic Algorithm appears to be an ideal solution for that. It can handle large space of problem and get a lot of trade-off fronts (possible solutions) in one evolution,

and requires no gradient information and produce multiple optima rather than a single, local optimum.

This research aims to study the effectiveness of genetic algorithm, based on game theory in solving multi-objective optimization problems, a practical multi-objective optimization problem related to risks management is brought in to study. Using genetic algorithm along with game theory, we tried to find the best strategy for a company to manage their investment.

## 2. BASIC CONCEPTS

The Multi-objective Optimization Problem (also called multi-criteria optimization, multi-performance or vector optimization problem) can be defined (in words) as the problem of finding a vector of decision variables which satisfies constraints and optimizes a vector function whose elements represent the objective functions.

Game Theory is the formal study of decision-making where several players must make choices that potentially affect the interest of the other players. In other words, game theory gives mathematical expressions to the strategies of opposing players and offers techniques for choosing the best possible strategy. In game theory, if players agree to cooperate, a Pareto optimum will be an ideal solution because it has the property that if any other solution

is used, at least one player's performance index is worse, or all the players do the same. The same solution concept also applies to multi-objective problems. With cooperative multi-objective optimization, the "compromise solution" should make sure that each objective obtains its maximum possible value although each objective cannot arrive at its own best value. Optimal trade-off among the objectives is sought by using the concept of game theory.

### 3. MULTI-OBJECTIVE OPTIMIZATION USING GENETIC ALGORITHM

The idea of genetic algorithm was inspired by the process of selecting individuals randomly through the impact of the wild's climate and was proposed by John Holland in 1970. If the individual does have a high degree of adaptation to climate change, they will continue to survive; otherwise they will be eliminated. This idea has been applied to solve objective optimization problems by approximately the Pareto test recorded from a number of initial roots.

#### **Step 1:**

- Set:  $t = 0$
- Place:  $t = 0$
- Generate  $N_p > 1$  individuals randomly to form the first population called  $P_t$
- Assess the adaptation of root in population  $P_t$

**Step 2:** Crossover - Using Cross-cultural operators to create the sub population  $Q_t$  as follows:

- Choose 2 roots  $x$  and  $y$  in population  $P_t$  based on adaptability
- Using cross-over operators to generate sub root and add this sub root to  $Q_t$

**Step 3:** Mutation - Use mutations operators to make the change in each root  $x \in Q_t$  with given mutations level.

**Step 4:** Assigning adaptation level to each individual in the population  $x \in Q_t$  based on the value of the objective function and the rejection ability of this test.

**Step 5:** Select  $N_p$  individuals from  $Q_t$  based on their adaptability and put all these roots to the set  $P_{t+1}$ .

#### **Step 6:**

- Stop if the stop condition satisfied (e.g.: the number of individuals in the population, the number generations ...) and give the current population.
- Otherwise  $t \leftarrow t + 1$  and return to step 2

## 4. MULTI-OBJECTIVE RISKS MANAGE

### (1) Problem statement

A new company names eComputer has just come into the in the selling electronics market. As the fund is small and there are no offline store for them yet, eComputer's main business form is electronic retailing – selling computer products via their main website ecomputer.com. Customers can order the product online and pay for them when the products arrive. The company also provides reimbursement service if the real goods do not meet customers' expectation.

Shipping service is provided by a third party, since the company's labor resource is limit at the moment. Fast Transporter, the shipping company in this case, will deal with eComputer's orders and receive shipping fee directly from the customers. This is somewhat a simple form of a supply chain, although the link between the firms is not tight enough.

The computer products eComputer going to sell are imported from other suppliers, ranging from class 1 to class 5, respective to their quality. Products' quality is without denied affects to the royalty of the customers and the benefits of the company. Hence, it is a real problem of choosing which products (from class 1 to class 5) should be sold. The decision of the customers also has great effect on Fast Transporter's profit, and of course the customers' benefit as well. As a new company, eComputer want to try their best to accompany the benefit of three sides: eComputer themselves, Fast Transporter and the customers. They are looking for a strategy that can in one way, bring them the greatest profit, and in another way, make their customers and partner satisfy as well.

### (2) Experiment and results

In Normal Game Theory, no player can do better by choosing a different strategy while keeping the others' strategies fixed.

As there is no dominant strategy in this game, we will try to find the Nash Equilibrium by calculating the expected pay-off of each player's strategies, whose function is:

$$Z = \sum_{k=1}^{m \times n} \sum_{i=1}^m \sum_{j=1}^n a_k \times P(b_i) \times P(c_j)$$

Where:

- $m, n$  are the number of two other players' strategies

- $a_k$  is the pay-off value of current player at strategy  $k^{\text{th}}$
- $P(b_i), P(c_j)$  are the probabilities of strategies  $i^{\text{th}}$  and  $j^{\text{th}}$  of two other players.

As calculated, Nash Equilibrium in this problem is the set:

- Customer with strategy Buy.
- Fast Transporter with strategy Pay-after.
- eComputer with strategy sell Class 5 products.

**Evolutionary Game:** In the Normal Game, each player has decided their own strategy according to the Nash Equilibrium. As a sequence, Customer has joined into the Buy population, Fast Transporter

**Table 1** Customer's expected pay-offs

Buy	Not buy	Return
0,43	0,2	-1,2

**Table 2** Fast Transporter's expected pay-offs

Pay-before	Pay-after	Not Ship
-0,3	1,85	0

**Table 3** eComputer's expected pay-offs

Class 1	Class 2	Class 3	Class 4	Class 5
6,725	5,625	8,225	5,475	10,475

joined Pay-after population and eComputer joined Class 5 population. The probability of each strategy changed, Buy, Pay-after and Class 5 strategy's proportion increased. Eventually, there will be a shift in the optimal strategy if we play the game repeatedly.

The business problem is not a non-repeated game where three players join the game only one times. Therefore, a new kind of reasoning is required to understand how it can be quite rational to ultimately make non-rational choices. To study that, we propose a genetic algorithm that simulates a population of players, each one playing the game a fixed number of times against other randomly chosen players.

**Objective function:** Each player's optimum mixed strategies satisfy

$$\text{Max}\{\min(\sum_{i=1}^m a_{i1}x_i, \sum_{i=1}^m a_{i2}x_i, \dots, \sum_{i=1}^m a_{in}x_i)\}$$

Subject to the constraints

$$x_i \geq 0, i = 1, 2, \dots, m$$

$$\sum_{i=1}^m x_i = 1$$

This problem can be put in the linear programming form as follows.

$$V = \min(\sum_{i=1}^m a_{i1}x_i, \sum_{i=1}^m a_{i2}x_i, \dots, \sum_{i=1}^m a_{in}x_i)$$

Then the problem becomes maximize  $Z = V$   
Subject to

$$\sum_{i=1}^m a_{ij}x_i \geq V, j = 1, 2, \dots, n$$

$$x_i \geq 0, i = 1, 2, \dots, m \text{ and } \sum_{i=1}^m x_i = 1$$

Or in a simple way:

$$\text{Minimize } Z = X_1 + X_2 + \dots + X_m$$

Subject to

$$a_{11}X_1 + a_{21}X_2 + \dots + a_{m1}X_m \geq 1$$

$$a_{12}X_1 + a_{22}X_2 + \dots + a_{m2}X_m \geq 1$$

.

.

$$a_{1n}X_1 + a_{2n}X_2 + \dots + a_{mn}X_m \geq 1$$

all  $X_i \geq 0$  for  $i = 1, 2, \dots, m$

Where

$$Z = \frac{1}{V}, x_i = \frac{x_i}{V}, i = 1, 2, \dots, m$$

**Coding Scheme:** The coding scheme for this problem can be accomplished using a relatively standard coding scheme. The parameters of the search problem are represented as bit strings. The equation is represented collectively as equation (3) and the unknowns are  $x_i$ , for  $i = 1, 2, \dots, n$  and  $0 \leq x_i \leq 1$ , then each parameter is coded as binary strings according to the formula

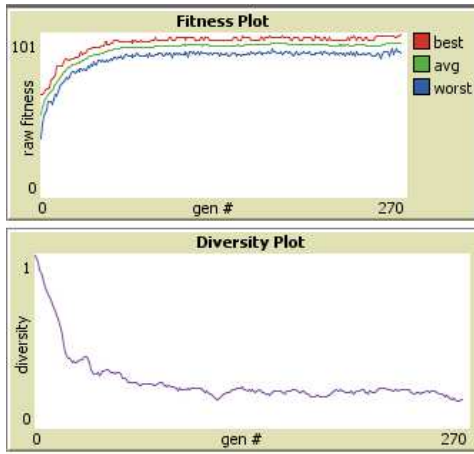
$$P = P_{\min} + \frac{b}{2^i - 1} (P_{\max} - P_{\min})$$

where  $P$  is the parameter to be coded,  $P_{\min}$  is the minimum value of the parameter (in the case of  $x_i$ , the minimum value is 0).  $P_{\max}$  is the maximum value of the parameter (in the case of  $x_i$ , the maximum value is 1).

To solve the problem, we used a genetic algorithm solver in NetLogo. Each run is a simulation of crossover-rate 10 on a population of 200 individuals.

As the mutation value increases, the algorithm is able to explore a larger region of the search space. We can see that, however, the distribution of expected pay-off is not change much. Here is the exact solution by the linear programming.

**Figure 1** Fitness and diversity plot, with mutation-rate = 1.5, generation = 270



In conclusion, as the Nash Equilibrium is quite the same after running Genetics Algorithms, we can

**Table 3** eComputer's expected pay-offs

Optimal strategy	X1	X2	X3
1.285714	0.555556	0.444445	0.000000

say that the best strategy for our three players to follow is:

- The seller company: eComputer imports and sell products of Class 5.
- The shipper company: Fast Transporter delivers products for eComputer with the pay-after contract.
- The customers buy products from eComputer.

Although Class 5 is a good-at-the-moment strategy for eComputer, it is still not a secure one because we have not taken other elements like competitors, government management and so on. As to ethics side, we still advise eComputer to follow a more ensuring strategy in the long term.

## 5. CONCLUSION

In conclusion, we summarize some of the key issues to be studied in this research with the results. In this paper we examine some methods to solve multi-objective optimization. After studied about game theory, we came across a way to solve the multi-objective optimization problem by using game theory with genetic algorithm, and displayed the solution through NetLogo software. Our problem, simply put, is a multi-objective risks management which helps a company manage risks effectively and

create good relationships with partners and gain customer's trust.

**ACKNOWLEDGMENT:** We would like to express the great appreciation to Professor Bao Ngoc Trinh, our respective teacher, who has always been sincere and helpful in our progress of doing this research paper.

## REFERENCES

- 1) Djennas, S. D., Bendimerad, F., Merad, L. and Meriah, S. M., "Genetic Algorithm-Based Synthesis of Three-Dimensional Microstrip Arrays", Vol. 2, No. 3, July 2005.
- 2) Li, T., Zhao, Z. and Zhanesee, K., "A genetic algorithm for the three-dimensional bin packing problem with heterogeneous bins", 2014.
- 3) Tamjidyamcholo, A. and Al-Dabbagh, R. D., "Genetic Algorithm Approach for Risk Reduction of Information Security", 2012.
- 4) Le, H., "Một Lớp Các Phương Pháp Giải Bài Toán Tối Ưu Nhiều Mục Tiêu", 2009.
- 5) Chandu, D. P., "A Parallel Genetic Algorithm for Three Dimensional Bin Packing with Heterogeneous Bins", Vol. 17, No. 1, Nov. 2014.
- 6) Hoque, K. Z., Fang, F. T. and Tat, C. W., "Multi-objective Programming For Pavement Management Using Genetical Algorithms".
- 7) Navidi, H., Khanesar, M. A. and Falahazar, L., "A New Multi-Objective Sorting Algorithm and Its Combination with Game Theory for Optimizing I-beam Engineering System", 2014.
- 8) Turocy, T. L. and Stengel, B., "Game Theory", 2001.
- 9) Firescu, L., "Cooperation in Business - An Application of Game Theory", 2012.
- 10) Jacobson, L. "Creating a genetic algorithm for beginners", 2012.
- 11) Mioc, T. D., "Detecting Equilibria in Game Theory – Evolutionary Approach".
- 12) Devooght, R., "Multi-objective Genetic Algorithm", 2010.
- 13) "Evolutionary Game Theory", 2002, [Online]
- 14) Zhang, S. and Li, K., "A Genetic Algorithm for Solving a Class of Multi-objective Bilevel Programming Problem".
- 15) Sim, K. B., Kim, J. Y., and Lee, D. W., "Game Model Based Co-evolutionary Solution for Multiobjective Optimization Problems", 2004.
- 16) Sim, K. B., Kim, J. Y., and Lee, D. W., "Game Theory Based Coevolutionary Algorithm: A New Computational Coevolutionary Approach", 2004.
- 17) Ismail, I. A., Ramly, N. A. E., Kafrawy, M. M. E. and Nasef, M. M., "Game Theory Using Genetic Algorithms", 2007.
- 18) Riechmann, T., "Genetic Algorithms and Economic Evolution", 1998.
- 19) Cheng, F. Y and Li, D., "Genetic Algorithm and Game Theory for Multiobjective Optimization of Seismic Structures With/Without Control".
- 20) Hamblin, S. and Hurd, P. L., "Genetic algorithms and non-ESS solutions to game theory models", 2006.

(Received November 14, 2015)

# MULTI-PURPOSE ARTIFICIAL INTELLIGENT ASSISTANT HUMANOID GRAPHICAL INTERFACE AND AI APPROACH TO ADVANCED HUMAN COMPUTER INTERACTION

MAI Nguyen Binh Hung<sup>1</sup>, LE Ngoc Hoa<sup>1</sup>, BUI Trong Nam<sup>1</sup> and BUI Minh Ngoc<sup>1</sup>

<sup>1</sup> Student, Faculty of Information Technology, Hanoi University  
(Km9 Nguyen Trai, Thanh Xuan, Ha Noi, Viet Nam)  
Email: akenblack.tudang@gmail.com

Since the dawn of computers, it is essentially important to closing the gap of interaction between humans and machines. Many inventions and innovations have been made and most of them are partially succeeded in creating a bridge of communication between humans and machines. With the introduction of Artificial Intelligent, the standard of Human Computer Interaction are expected to raise to a new level as people can make simple input and the process of information will be handled by A.I. There are some dedicated works of combining A.I and U.I (User Interface) are made but far from success due to the limitations of technology as well the complexity of the A.I algorithms. Our works will introduce sample program of a virtual humanoid assistant called M.A.I.A. (Multi-purposed Artificial Intelligent Assistant). The program we proposed in this page have algorithms of A.I to record the user input (keys, voices, etc.) and translate into different commands. Therefore, this program can make simple conversation and handle some simple tasks in a computer. Unity engine and other graphic tools are used to make the main interface of the program. Our experiments are expected to deliver good results on multiple platform with different scenarios.

## 1. INTRODUCTION

Since the dawn of computer era, Artificial Intelligence has been a major technology subject among scientists and engineers. With the rapid processing speed of a computer brain, It has been successfully applied in many fields and resolved many problems. However, a new challenge emerges: How to interact with the Artificial Intelligence. Some of the first attempts had been made to create an interface for the Artificial Intelligence, but its complexity in operationing is still a high barrier for engineers and users. Therefore, interaction with AI is considered to be unreachable to common users and consumer market.

With the progress of technology, the world had witnessed the introduction of new interface forms such as CLI (command-line) and GUI (graphical), which paved the way for new improvements in Human-Computer interaction as well as AI interaction. At the same time, a new generation of consumer electronic devices emerges with three principles: small, simple and smart. This has led Artificial Intelligence technology into a new issue: it has to be expanded to the new potential consumer market. Its interface designs are required to be user-friendly and functional in daily life tasks.

The main purpose of this work is to introduce a graphical AI interface as an program. Our research scope will mainly focus commands and behaviors in some basic conversations and tasks with user input. The method will be organized as a program and delivered to users via an application. Our expectation is this program will make some simple conversations as a human as well as do some simple tasks without user's intervention.

## 2. PROOF AND PRIOR WORKS

There are many documents and works about Artificial Intelligence and its interface. Domingos (2006) have stated the importance of interface as the answer of Artificial Intelligence progress and "allowing each to benefit from the other". In fact, "The interface layer allows each innovation below it to automatically become available to all the applications above it, without the "infrastructure" researchers having to know the details of the applications, or even what all the existing or possible applications are." (Domingos, 2006)

Wærn in 1997 has questioned the definition of Intelligent Interface. It is considered that the Intelligent Interface employ at least five kinds of technique: "User Adaptivity, User Modelling, Natural Language Technology, Dialogue

Modelling and Explanation Generation". Moreover, the applications of Intelligent Interface has been classified into 3 different categories: "Intelligent Tutoring, Intelligent Help and Intelligent filtering" (Wærn, 1997)

In 2001, Ehlert conducted and researched the Intelligent User Interface (IUI). In his work, he said that "Using techniques from artificial intelligence, IUIs deal with different forms of input and output and try to help the user in an intelligent fashion". Moreover, Ehlert stated that Intelligent User Interfaces are capable to "adapt to the user, communicate with the user, and solve problems for the user". In fact, Ehlert discovered the IUI's ability to learn from a world representative that is measured and drawn by its sensors so that "a certain action or behavior can be generated and communicated to the user".

### **3. MULTI-PURPOSE ARTIFICIAL INTELLIGENT ASSISTANT**

#### **(1) Features**

##### **(a) Concept**

Multi-Purpose Artificial Intelligence Assistant (M.A.I.A) is a program that feature elements of Artificial Intelligence integrated in user interface. It has an interface that use the form of an (customizable) humanoid character as a mean of communication, which is implementable 2D/3D. Moreover, it use a Backend AI to make smart input analyzation that supports Verbal Communication (under development as texts), Voice Command (development in queued) and Image Patterns (future work). This program is developed to make sure that user will feel more comfortable while interacting with Electronic devices.

##### **(b) Mechanism**

It is implied that the fundamental mechanism of AI interface is the way of processing and generating data from user input. Therefore, M.A.I.A consists 3 main Modules:

**Input Manager:** This module is used for Managing and Pre-Processing Input done by users. It requires a Dictionary database that contains Defining Words so that computers can read and analyze the input.

**Processing Components:** This module is used for deeper Input Analyzing and Mapping.

It requires Defining Commands as Mapping tables that assign Verbal Sentences into actual computer's function.

**Designated Objects:** This module is used as method wrappers that have direct access to the OS's functions. Therefore, defining OS Function Wrappers is required to access and execute the commands in the computer.

By gathering all of the input data, the interface will process the data to create the output. This is considered to be identical with the mechanism of computers. Based on different algorithms, the processors detects certain elements in user input as a trigger to call certain data that match those elements. With all of the mentioned mechanisms, the purpose of creating M.A.I.A is to make the way of using Languages' Grammar structures to recognize the need of the users.

#### **(2) System design**

Our proposed system basic architecture design can be classified into 3 phase: Input, Analyze, Output. The Input phase consists of user input manager on different devices. The Analyze phase includes 3 components: Processing component, Word database and Command database. The Output phase contains the designated object as a component that M.A.I.A called via commands.

#### **(3) Implementation**

In our implementation information, we chose to build our prototype in IBM-type Personal Computers on Windows Operating System platform in C# language. The C# language, derived from Java, is well known for its flexibility and strong compatibility of different devices and platforms. For graphical interface, we decided to use the Unity 5.0, Live2D and/or Blender3D for 2D/3D rendering deployment and implementation. Unity is the graphic tool that utilize the C# language so that the interface is inherited the ability of running on multiple platforms.

##### **(a) Input Recognition**

M.A.I.A has the capability of supporting different types of input that can be recognized. The current prototype uses keyboard and voice as the main raw input with the basis of verbal communication. Therefore, text is designated as the main form of refined input for the

interface. It can be imported directly from the keyboard as word command or converted from the voice with an suitable sound recognition algorithm.

### **(b) Input Analysis**

After converting input into text, M.A.I.A will analyze the input to identify the sentence as a command. There are 2 phases in the analysis: Word defining and Text converting.

The first phase of Input Analyzation requires the interface to define the Words for sentences recognition. Therefore, it needs 2 compulsory components: Words and Sentences, which are designed and based on the rules of English grammar.

The Word component is a database consisted of words that used in stating commands. The database must contain the original words and its defined word types as the basis of command and object mappings. Moreover, the synonyms, words that have the same meanings, are added into the database and linked with the original words due to the fact that there are multiple case that users use different words for the same command. This requires database optimization to increase the accuracy of analyzation.

The Sentence component forms the grammar rules with three basic elements: Subject, Action, Object. Subject points to the entity that does the action and Object points to the entity that received the action. Action itself points to the specific behavior that affect the entities. Both Subject and Object can be defined by Nouns and/or Pronouns, but Action or Object are defined with different types of word like Verbs, Adjectives or to be as the sentence can be altered with different structures. These elements are used with the word database to analyze and classify the word type. However, there are some redundant words that are not existed in the database but made no impact to the command, which is common for normal users, especially when using voice as the input. In these situation, M.A.I.A may identify the words as "Anything". However, if there are elements that break the grammar rules (e.g 2 identical elements in a row), the sentence will be designated as "Undefined".

When the Word defining phase is completed, the interface will convert the words into basic sentence. Due to the fact that M.A.I.A use English grammar, particularly the Present Simple tense as the basis, the common structure to use in order and command is that an Action for an Object done by a Subject. When integrate the structure in to M.A.I.A, the program may follow the structure or the elements in the order below:

*Subject + Action + Object*

Then the structure will be used along with the word database to build a command structure. The more amount of words defined in the database, the more accurate the interface recognize. It is expected that the interface will recognize and make use of Keywords and ignore unnecessary texts ("Anything" element).

### **(c) Command Processing**

After analyzed the input as the elements of the command, the program will assign the words into suitable commands which consisted of 2 components: Command components and Designated Objects. Command Components contains specific patterns for function recognition and its mapped functions. It may include the sentence component that follows a single type pattern and the word component that associated with the pattern above. The purpose of Command Components is to execute the function of the sentence structures matched the patterns. Designated Object is placed in the Operation System and contains all the necessary Wrapper Functions for accessing its functions. A command database is required for command mappings as a mapped function of a command must be defined inside the designated object.

## **(4) Limitations and known solutions**

### **(a) Database**

The first problem when implementing the AI interface is database infrastructures. Due to its mechanism, M.A.I.A is mainly depend on Databases, which means code execution requires Database query. Therefore, to execute more complex analyzations, M.A.I.A requires a large quantity of databases. Moreover, the deeper the analyze is, the slower the speed will be. This is considered as a major challenge as the demand of balance between speed and accuracy.

## **(b) Input**

In M.A.I.A, the input component is a crucial factor due to the fact that it is the means of interface control. Therefore, it is important to have a good accuracy in input processing. However, to make correct detection, it requires decent algorithms and hardware, especially when analyzing voices and other types of input. Moreover, when analyzing the text, the interface may lack the flexibility in analyzing unconventional sentences such as omitted words or different tenses.

## **(5) Applications and future expectations**

### **(a) Applications**

With the features mentioned above, M.A.I.A has a great potential with applications on various purposes. It is considered that the most common application is to integrate in devices as assistants. Therefore, the user interface will be better, more natural and more user-friendly. With AI interface, users don't need to do additional actions due to the fact that AI is capable of execute the actions automatically, which the work time will be greatly reduced as the only procedure users need to do is insert their input.. Moreover, the AI assistants can be integrated in multiple platforms, which enables the capability of executing complex tasks in various environment.

### **(b) Future expectations**

#### **Additional input**

In a near future, the input of AI interface will be not limited in current forms such as texts and voices. It will have the capability of importing and detecting inputs from gestures. This input has the mechanism of body movements and face behavior detection and convert. The movements are converted into patterns as the refined input. Different patterns will be assigned to the commands. This can be implemented with additional hardware and API.

#### **Advanced features**

With the progress of technology, the functions of AI interface will be eventually evolved. It will not only act as assistants and smart solutions, but also do the role of advisors. The evolved AI algorithms allow the interface to collect, process the data automatically and execute the commands

without any user interferences. Therefore, the interface can suggest the users with some recommendations and actions based on the current situations.

## **4. CONCLUSION**

In this work, we introduced an Artificial Intelligence interface as the form of a graphical humanoid assistant program, which is organized into a fully working software system. Based on the background knowledge of the Artificial Intelligence and Human-Computer Interaction, we developed our own research strategy with carefully selected method for each part of the system

The input and command process of M.A.I.A (Multi-purpose Artificial Intelligence Assistant) in this work was modeled on C#-based Artificial Intelligence algorithms. The system we proposed has three phases with multiple components, organized into a unified structure. Based on the developed features on the prototype, we believed that our system has the good experimental results with completion of simple tasks on the computer and basic conversations. However, the program still has some problems when importing some types of input and executing few complicated tasks. This is due to the fact that our system has limited database and its queries as well as simple AI algorithms.

The limitations of our system lead us to the chance of enhancing our system in order to reach better results on any situations and devices. The first step towards enhancing our system is the improvement of M.A.I.A, which is the software product that based on this research. After that, we will modify and enhance the algorithm and the database of this product. In recent future, we are planning to extend and implement M.A.I.A to multiple platforms, from mobile devices to game consoles and other electronic utilities.

## **REFERENCES**

- 1) Domingos, P. *What's Missing in AI: The Interface Layer in Artificial Intelligence: The First Hundred Years*, AAAI Press. Menlo Park, CA, 2006. Available at:  
<http://homes.cs.washington.edu/~pedrod/papers/ai100.pdf>
- 2) Wärn, A. *What is an Intelligent Interface?*, Swedish Institute of Computer Science, 1997. Available at:  
<https://www.sics.se/~annika/papers/intint.html>
- 3) Ehrt, P. *Intelligent User Interface, Introduction and Survey*, Mediamatics/Data and Knowledge Systems group

Department of Information Technology and Systems,  
Delft University of Technology, The Netherlands, 2003  
Available at:  
<http://www.kbs.twi.tudelft.nl/docs/report/DKS03-01.pdf>

# “Smart Monkey” Android Game

NGUYEN Van Manh<sup>1</sup>, LUU Ngoc Diep<sup>1</sup>, DO Tram Anh<sup>1</sup>, TA Quang Tu<sup>1</sup>, NGUYEN Viet Hung<sup>1</sup> and NGUYEN Duc Minh<sup>1</sup>

<sup>1</sup> Student, Faculty of Information Technology, Hanoi University  
(Km9, Nguyen Trai, Thanh Xuan, Hanoi, Vietnam)  
E-mail: manh nv@gmail.com

Android is now the most used mobile operating system in the world and an open source software stack for a wide range of mobile devices and a corresponding open source project led by Google. With much influential motivation, especially in Vietnam, we decided to develop a mobile game ourselves. After having a hard time picking a specific game category for our game, we decided to develop a game named “Smart Monkey”, a brain-training and high score based game. We have never experienced in learning and working with Android as well as developing a mobile phone application before. Therefore, in most parts, there are many difficulties we have faced, especially in creating layout and intent despite our familiar zone of coding in Java. However, we overcame it with all of the methods that we came up with in our project, some functions and other solutions as well. A simple Android game has been created including all the main functions and other simple functions.

## 1. PRODUCT DESCRIPTION

### (1) Product depiction and game rule

The game that our group decided to develop is called “Smart Monkey” and it is of the brain-training gaming type. As no exception from most nowadays mobile games, Monkey aims at simple game-play and the main goal of the game is getting the highest score as possible. This game is designed for single player.

The rule of this game is quite simple and straightforward. When user taps the “Start” button, the game will begin and display on the screen nine numbers from one to nine with the random positions. The player is required to memorize all the positions in a short given amount of time. Afterward, it will disappear and then the player’s goal is to replicate the whole nine numbers’ positions precisely before the time runs out. When the player completes filling all the numbers, they can submit by the way of clicking the “OK” button. At this state, there are two use-cases, if the player’s answer is incorrect, the program’s screen will back to the menu and a “Loser!” notification will pop up for informing. Otherwise, the game will advance to the next level and one point will be scored when all positions are matched with the formers. In the event of time is over, the system will automatically submit and check your answer.

### (2) Graphical User Interface

#### a) Relative layout

This is the kind of Layout that allows the developers to initialize the relationship between each child views. In other words, each position of theirs can be located in the comparative with their parents or the siblings. A relative layout is a very powerful utility when designing a user interface and it also improves performance. Therefore, we used this type of layout to design nine buttons in the playing screen while the others are unable to perform this action.

#### b) Button

When the developers want to add a button to the screen, by default the SDK will create a button with the rectangle shape. In order to customize it, in the resource package/drawable, we create an XML file to set the button’s attribute with the round shape and color.

#### c) ImageView

This function is used to display the image file to the various screens and DPIs in different android devices. In this product, we added images to the splash and menu screen.

#### d) TextView

TextView is a basic widget with the purpose of displaying text without allowing the user to modify the content. Thus, we made use of this to present the

randomized set of numbers for the user to memorize. In order for the program to perform this action, we have to customize the textView feature within the button.

#### e) EditText

The EditText control inherits from the TextView control and allows the user to enter and edit the user's input. To use this, we only need to drag and drop this control to the interface and set the text area is in the center of the button by using the gravity attribute.

### (3) Programming

#### a) Generating numbers

As mentioned in the game's description, when the user hits the "start" button, the program will display a screen with the set of random numbers from one to nine; therefore, we need a function to generate all the numbers and put it in different positions. After trying some solutions, we came up with the one that we will create the first ArrayList that contains generated numbers in their orders called *initialList* and then add numbers from one to nine to that ArrayList. Next, we shuffled all the elements of the ArrayList and the program displayed it to the screen.

#### b) Getting user input

When we started to think about the solution to the taking the user's input, first we decided to get it by the means of the user inserts and edits the text directly through the button. However, after getting the input from the user, it was challenging to take that user's answer and check it with the initializing ArrayList, which contains the set of random nine numbers. Finally, we came up with the idea of using the EditText function, which we set the attribute of the text area similar to the buttons' attributes, and then put all the input to a new ArrayList called *resultList*. Below is the code of the function that we used to create a dialog with the numbers whenever the player wants to edit or fill in their answers.

#### c) AsyncTask bar

AsyncTask gives developers the ability to make use of UI thread easily and properly by allowing them to conduct background operations as well as publish results on the UI thread without the need of controlling threads and handlers.

AsyncTask is intended to perform as thread and handler's helper class and does not constitute a generic threading framework. Short operations make the best use of them. In case that the developers have to retain threads working for large amounts of time, a

variety of APIs provided by the *java.util.concurrent* package namely Executor, ThreadPoolExecutor should be used.

An asynchronous task is determined by a background computation thread with its result is published on the UI threat. Three generic kinds - Params, Progress and Result, as well as 4 steps - onPreExecute, doInBackground, onProgressUpdate and onPostExecute are also the elements define this task.

#### d) Result comparison

After accepting user's inputs and save them on a new ArrayList - *resultList*, no matter whether they are completed or not, it needs to be compared with the *initialList*. We decided to take a simple approach by having both of these ArrayList converted into strings since it is easier comparing two string than two ArrayList. The comparison will, then, determine the outcome of the process – if they are matched the game will continue and vice versa.

#### e) Toast notification and intent

We used the toast notification simply for the aim of prompting the user that their answer is correct or not. In the case of their answer is matched with the initializing random numbers that are given from the beginning of the game, the system shall inform to the user with the "well done!" notification. Otherwise, the program will automatically go back to the menu screen and a notification "Loser!" will be shown up. As mentioned in the background knowledge, an intent is a messaging object that can be used to request an action from another app component.

#### f) Storing high scores

Our game is a game with the high score board, therefore, we had to find the solution to store the list of highest scores and it should still remain when the player turns off the game. To do this action, we had to connect to the Android Operating system and saved the highest score to the device's memory.

## 2. FURTHER STUDY

At the moment, the project is still in the stage of development, the game is still very basic. In the near future, we may have some ideas to make the game more interesting and addictive such as upgrading or adding some more features to the game.

We are currently planning to add "Leaderboard". If you are a person who is well familiar to the game play on mobile, in most of the games if you have the internet connection, there will be a section called "Leaderboard". In the video games, the term

“Leaderboard” is typically used to signify the rank among people playing the same game. Players can be ranked against other players, based on the points gained in the game, the number of kills in a game, number of items collected in a game, or other statistics. In our game, it is based on the points which are gained in the game.

Furthermore, we are also considering designing more levels for the game with the difficulty increasing gradually for each level. It will have more than nine buttons for the playing screen. We may call it “advanced levels”. At this stage, it will not only contain numbers but the letters as well. All of them will be randomly arranged in different positions.

In addition, a part that makes the players more addicted to and interested in every game is the sound effect. That’s the reason why we are aiming to add more interesting sound effects for entertainment or for more joy and relaxation in order to attract more players.

After completing and adding some more features to the game, we are going to upload it to Google’s Play Store and plan to develop other kinds of applications in the future.

### 3. CONCLUSION

This is our first experience in learning and working with Android as well as developing a mobile phone application. As a result, we have faced many difficulties in most parts, especially in creating layout and intent in spite of the fact that coding in Java is within our familiar zone. By using ImageView function, Generate number function and some other solutions to the problems, we have created a simple

Android game. The game has not only the main functions, which is the playing methods and rules but also the function of contacting via Facebook, achievements and leader-board.

### REFERENCES

- 1) Android developers n.d., viewed 5 March 2015, <http://developer.android.com/guide/index.html>
- 2) Android-er 2010, “*ProgressBar running in AsyncTask*”, viewed 5 March 2015 [online]. Available at: <http://android-er.blogspot.com/2010/11/progressbar-running-in-asynctask.html>
- 3) Cristian 2015, Full screen activity in Android, viewed 5 March 2015 [online]. Available at: <http://stackoverflow.com/questions/2868047/fullscreen-activity-in-android>
- 4) Google n.d., Google design specification – Color, viewed 5 March 2015 [online]. Available at: <http://www.google.com/design/spec/style/color.html>
- 5) Nagarajan. 2014, Horizontal and Circular Progress Bar in Android, viewed 5 March 2013 [online]. Available at: <http://www.geeks.gallery/horizontal-and-circular-progress-bar-in-android/>
- 6) Pragnesh, G. 2015, Multiple Buttons “onClickListener()” android, viewed 5 March 2015 [online]. Available at: <http://stackoverflow.com/questions/25905086/multiple-buttons-onclicklistener-android>
- 7) Rick, R. 2011, Learning Android Game Programming, 1thedn, Pearson Education Inc., Indiana.
- 8) Ravi T. 2013, How to implement Android Splash Screen, viewed 5 March 2015 [online]. Available at: <http://www.androidhive.info/2013/07/how-to-implement-an-android-splash-screen-2/>

# **Intelligent information system apply for healthcare system in Vietnam**

HOANG Trung Hieu<sup>1</sup>, TRAN Van Doanh<sup>1</sup> and VU Minh Tuan<sup>2</sup>

<sup>1</sup> Student, Faculty of Information Technology, Hanoi University

(Km9, Nguyen Trai, Thanh Xuan, Hanoi, Vietnam)

E-mail: hieuh.t.hanu@gmail.com

<sup>2</sup> Professor, Faculty of Information Technology, Hanoi University

(Km9, Nguyen Trai, Thanh Xuan, Hanoi, Vietnam)

E-mail: tuanvm@hanu.edu.vn

This paper will introduce an intelligent system that was applied the information technology; the system will help to solved the problems of health, management and application of modern advanced equipment in the addressing health problems of Vietnam today. We will focus on two key issues: Give an overview of the healthcare system in Vietnam and introduced the system of health care models that can be applied intelligently to the hospital in Vietnam in the future.

**Key Words:** Intelligent system, healthcare system, Vietnam's hospital.

## **1. INTRODUCTION**

Vietnam is a developing country with a population of over 90 million people, the 3rd most populous country in the Southeast Asian region and 14th in the world. In this stage, developing electronic health is one of the most important fields which are very focused on investment and it is one of the priority areas of the health sector in particular. Since Ministry of health decides to promote the application of information technology in healthcare until now, healthcare system has deployed information technology applications to multiple health activities from central to local levels. But the deployment of information systems still fragmented, the associations among the hospitals still do not have, especially we lack of uniformity in the application of information technology, upgrading

the infrastructure, training of human resources and it has led to applying information technology in health care not promote the best of its ability.

To achieve the objectives and plans of Ministry of Health, we need to have a system that is applied information technology to solve the current problems of healthcare. Developing a management system is so very necessary and essential to improve the quality of state management of health, improve the efficiency of care and protection of people's health.

Based on the study and research on hospital management system as well as the ability of application and development of the system. We would like to introduce an intelligent system that was applied the information technology; the system will help to solve the problems of health,

management and application of modern advanced equipment in the addressing health problems of Vietnam today.

## 2. Current status of healthcare systems in Viet Nam

Despite many positive changes in the healthcare system in Vietnam, the medical industry still meets many difficulties on human resources; finance and especially, many difficulties and challenges in the development of intelligent system in health care. They need to improve a lot about software, hardware, database and network.

## 3. Smart-hospital model

### 3.1 Purposes

The first goal of the hospital intelligent systems to enhance the quality of patient service, build confidence for each patient when health information is stored in a systematic and accurate, thereby contributing to help clinicians increase efficiency in the diagnosis and treatment.

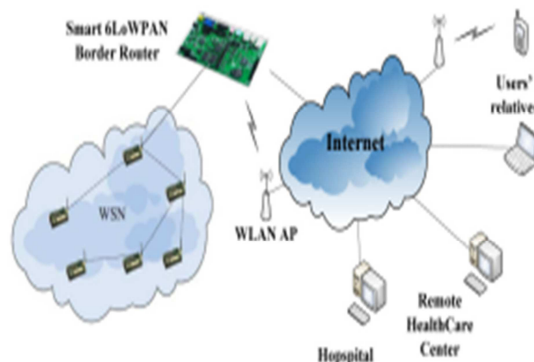
### 3.2 Software

This hospital will be applied a lot of modern software to manage the system, it will have a recognition function to receive the information of person when they go to the hospital, it also have the remote supporting function which will help the patient and provide some useful knowledges for people. And the payment support needs to be added on this system, so that people can pay the bills from the internet. The remote monitoring function of this hospital will help the patient check their status and receive the advice from doctor. To be more convenient, we think that the entire database about the sickness will be stored online, which can help both doctor and patient lookup the information about the patient sickness easily. Moreover, this hospital will also have the monitoring function,

which can help hospitals manage and supervise well the equipment in the hospital, check and ensure the safety of the atmosphere and can manage the amount of drug and condition of equipment in the hospital. This feature helps staff and board of directors of the hospital can easily update and track the status of the whole hospital.

### 3.2 Hardware

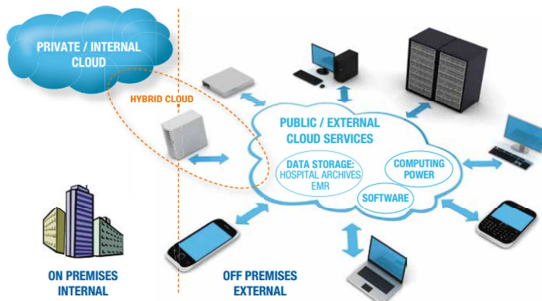
To build and develop models of one intelligent hospital applying of information technology, the hospital need some modern equipment as: computer with high configuration, server system, camera system, identified scanner, self-protected system, Zephyr system. Some of them are already exist on the world, however we will need to develop some of them to be applied on the hospital.



### 3.3 Database

The database of the hospital should be uploaded on the cloud. And the cloud structure may enable both healthcare professionals and patient's access to records and data on tablets, smart phones without the need for access or special settings.

If done properly moving the medical infrastructure to the cloud, will help the industry move health care with a much faster speed compared to current patient information, drug prescription research, development, manufacturing, and many more.



### 3.4 Network

Wireless Sensor Network (WSN) in smart- health model gives a large quantity of real-time vital signs to be processed and make decision of health states. Since it is not enough for one computer to process the huge raw data from many WSNs, we suggest using Grid computing technology to analyze the vital signals. A SensorGrid gateway to connect the WSN with Grid networks has been designed. We proposed and implemented a prototype of a smart 6LoWPAN border router aimed to locally make decisions of health states using a Hidden Markov Model and enable wireless E-health care sensor network to seamlessly connect with IP network. The border router also enables doctors and users' relatives can directly access sensor data on each sensor node or get information from the border router.

### 3.5 Human resources

Employees in the information technology department of the hospital are responsible for the management and application of intelligent hospital model in the hospital. Included specific tasks are:

- Develop implementation plans, develop and apply of intelligent hospital system in hospitals and submission to the Prime Minister for approval.

- Install technology equipment's for the hospital under the approved plan.

- Organize some guiding, training for officials and employees of the hospital, in order to improve the ability to use information technology equipment's in some activities of the hospital.

- Manage and maintain the operation of the system in a stable and efficient way ensuring the connection of information among faculties, departments, Ministry of Health and hospitals in the network.

- Develop and manage the database system of hospital

- Implement measures to ensure the safety and security of information and database system of the organization.

To accomplish these tasks, we propose the Information Technology department (IT) arrange staffing positions as follows:

- Programmers and database management: 7 people.
- Network systems and equipment: Manager: 5 people.
- Training of staff: 2 people.

Staffing in the IT department is expected from 12-15 people including some officers and employees have a specialized university degree accounted for 60% of total IT staff and employees of the rooms.

## 5. CONCLUSION

The intelligent system help the patients and the doctor know exactly the patients' medical history, moreover, this system can create a network among the hospitals which can allow the hospitals share their database with other hospital and also help the patient easier to referral when they need. Besides sharing the database, the smart hospital can also

allow people search information and how to prevent and treat disease. Based on some advance technology the system can be installed the GPS for all devices, equipped some warning devices, some camera to scan the face of people who come in the hospital. This system can also help the hospital manage their finance and human resources effectively; furthermore, if we can apply this system for the hospital we can have a function remote medical.

**ACKNOWLEDGMENT:** We would like to express the great appreciation to Professor Bao Ngoc Trinh, our respective teacher, who has always been sincere and helpful in our progress of doing this research paper.

## REFERENCES

- 1.Zephyr.2015. *Zephyrlife-home*. USA: zephyranywhere.com (<http://zephyranywhere.com/healthcare/zephyrlife-home/>)
2. Brad Swenson.2015. *The new 10 year standard find a more accurate ehr total cost ownership*. USA. Beckershospitalreview.com (<http://www.beckershospitalreview.com/healthcare-information-technology/the-new-10-year-standard-find-a-more-accurate-ehr-total-cost-ownership.html>)
3. Johnson.2015. *Hospital group says illinois lease healthcare*. Chicago: abcnews.go.com (<http://abcnews.go.com/Health/wireStory/hospital-group-illinois-lease-healthcare-31781380>)
4. Ehealth.2015. *Báo cáo khảo sát tiềm năng và nhu cầu phát triển y tế điện tử*. Hanoi ([https://www.google.com/url?sa=t&rct=j&q=&esrc=s&source=web&cd=1&ved=0CB4QFjAA&url=http%3A%2F%2Fjahr.org.vn%2Fdownloads%2FNghien%2520cuu%2FThong%2520tin%2520y%2520te%2FEhealth.doc&ei=rvmCVajDBMPp8AWBqoJo&usg=AFQjCNGAuHd3I\\_0cWCFIrFAwpoSY-NTP3A&sig2=G2KOy\\_xDlesRP\\_OumGlUNA](https://www.google.com/url?sa=t&rct=j&q=&esrc=s&source=web&cd=1&ved=0CB4QFjAA&url=http%3A%2F%2Fjahr.org.vn%2Fdownloads%2FNghien%2520cuu%2FThong%2520tin%2520y%2520te%2FEhealth.doc&ei=rvmCVajDBMPp8AWBqoJo&usg=AFQjCNGAuHd3I_0cWCFIrFAwpoSY-NTP3A&sig2=G2KOy_xDlesRP_OumGlUNA))

Received November 14, 2015

# Robotics for healthcare

TRAN Thi Giang<sup>1</sup>, NGUYEN Thao Quyen<sup>1</sup> and TRINH Bao Ngoc<sup>2</sup>

<sup>1</sup> Student, Faculty of Information Technology, Hanoi University  
(Km9, Nguyen Trai, Thanh Xuan, Hanoi, Vietnam)  
E-mail: {trangieng.hanu, thaoquyen1c12.hanu}@gmail.com

<sup>2</sup> Professor, Faculty of Information Technology, Hanoi University  
(Km9, Nguyen Trai, Thanh Xuan, Hanoi, Vietnam)  
E-mail: ngocbt@hanu.edu.vn

Robots are virtual or mechanical objects that are used in facilitating the occurrence of multiple everyday activities. They have been heavily depended upon in U.S. industry, since 1961, and in health care after the mid-1980s. The virtual and mechanical robots have assisted people in a variety of tasks within and outside the laboratory and operating rooms. Some examples of robot intervention include medication administration, assisting children with autism, telemedicine, and transferring / lifting patients. This paper should serve as an introduction to medical robotic technologies, potential robotics in healthcare and also discuss 5 main areas of robotic application.

**Key Words:** *heath, robotics, intelligent, medical robotic technologies, future*

## 1. ROBOTICS FOR MEDICINE AND HEALTHCARE

Robotics for Medicine and Healthcare is the application of technology whereby systems are able to perform coordinated mechatronic actions (force or movement) on the basis of processing information acquired through sensor technology.

These systems cooperate safely with humans and support the functioning of impaired individuals, medical interference, care and rehabilitation of patients as well as participation of individuals in prevention programmers.

## 2. POTENCIAL OF ROBOTICS

The value of robotics for healthcare could be huge in terms of health, societal and economic benefits. Robotics offer the promise of sustainable and affordable health provision without compromising quality of care. Clear roadmaps are required for the scale of research and development still needed to transform the challenges that exist – technological, financial, ethical, social – into practical and beneficial solutions. The potential is tremendous.

## 3. RESEARCH ROADMAPS FOR ROBOTICS

The basic idea of road mapping is to look for the best way to arrive at a destination. In healthcare, this means dealing with the societal issues, diseases and other medical conditions, which healthcare systems need to cure, care for or prevent, both now and in the future. In relation to robotics, this concerns questions such as which robotic applications will be valued additions to healthcare, which products can meet market needs and which technologies are needed to accomplish them. Some technologies are available, while others need a lot of research and development before they can be applied to the production of a robotic system.

## 4. FIVE AREAS OF ROBOTIC APPLICATIONS

There are many innovation areas that can be considered key product/market combinations and from which five representative areas can be regarded ripe for further investigation and roadmapping

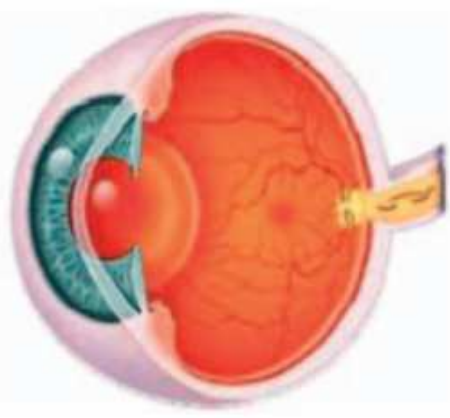
- Smart medical capsules
- Robotised surgery
- Intelligent prosthetics
- Robot-assisted mental, cognitive and social therapy
- Robotised patient monitoring systems;

Each of these specific areas needs to be considered in respect of the key stakeholders and their motives, the key technologies and related research challenges, the expected societal and institutional developments as well as future market trends in order for a

roadmap to be drawn up.

## 5. SMART MEDICAL CAPSULES

A means of ‘journeying’ through the body in a way that causes less discomfort than traditional endoscopy where invasive probes are used. The smart capsule endoscope is a ‘pill’ that is swallowed and then makes pictures of internal systems such as the intestines, while travelling through the body. Robotising the capsules boosts greatly their diagnostic and therapeutic effectiveness and signifies a radical change in medicine. A minirobot (and in the future perhaps a “nanobot”) will be able to move itself, or be externally steered, to have a closer look at internal tissues, take samples or even destroy unwanted tissue. Case in point: In the future, minirobots could be introduced into the eye to perform precision eye surgery under the external control of the surgeon



## 6. ROBOTISTED SURGERY

Robotised surgery will facilitate new types of intervention, e.g., in areas of the human body that are difficult to access. Precision, durability and repeatability enable automation of surgical tasks and facilitate minimally invasive surgery, remote tele-surgery, preoperative planning, surgical training, intra-operative navigation (image-guided surgery) and surgical simulation all from one place. The future: the integration of different robotic systems in broader platforms to assist surgeons and perform surgery autonomously. Case in point: The Da Vinci surgical robot helps the surgeon, who sits at a special console, to perform very precise minimally invasive surgery procedures.

## 7. INTELLIGENT PROSTHETICS

Control systems that facilitate natural movement and intuitive control of arm and leg prostheses, preferably with the same subconscious control as for natural limbs. The future: system autonomy (control by peripheral nervous system) and brain interfacing. Case in point: A future development: the newest experimental hand prosthesis from Otto Bock with individual movement of fingers controlled by nerve signals.



## 8. ROBOT-ASSISTED MENTAL, COGNITIVE AND SOCIAL THERAPY

Social interaction of people with mental, cognitive and social handicaps (e.g., autistic children or elderly people with dementia) is essential to their social participation but proves to be a major challenge for healthcare. Robotised systems can support human care and offer unprecedented therapeutic functionality that will develop or maintain social skills which would not be available without these systems or would vanish. Results can be expected in terms of developing basic social skills through play or maintaining skills to deal with everyday life. These robotic systems can be programmed to generate all kinds of communicative reactions (e.g. sounds and

colors), invite to move or play games, stimulate friendly face expressions and can also learn to adapt to the individual person.



## 9. ROBOTISED PATIENT MORNITORING SYSTEM

Presently, monitoring devices help doctors and nurses to look after patients. This is especially valuable when the patient is at home. However, when unusual situations are detected, it is often difficult to tell from a distance how urgent the situation is, which means that the doctor or nurse has to go to the patient's home. Robotising the present systems will enhance communication and identification of alarming situations. The future will see more remote monitoring and this will help care to become more affordable and efficient.



**ACKNOWLEDGMENT:** We would like to express the great appreciation to Professor Bao Ngoc Trinh, our respective teacher, who has always been sincere and helpful in our progress of doing this research paper.

## REFERENCES

- 1) [http://www.doc.ic.ac.uk/~nd/surprise\\_96/journal/vol4/ao2/report.html#intro](http://www.doc.ic.ac.uk/~nd/surprise_96/journal/vol4/ao2/report.html#intro)
- 2) <http://medicaldesign.com/archive/robotics-healthcare-challenges-and-opportunities-0>
- 3) Jeffey C.Bauer, "The Future of Medical Robotics: Creating Synergy in the Interaction of Patients, Caregivers, and Intelligent Machines".
- 4) Hoque, K. Z., Fang, F. T. and Tat, C. W., "Multi-objective Programming For Pavement Management Using Genetic
- 5) Caroline G.L., Gary R., "ROBOTICS IN HEALTHCARE: HF Issues in Surgery".

(Received November 20, 2015

# The Guidelines for Increasing Conversion Rates for Ecommerce Websites

BUI Thi Ngan<sup>1</sup>, LE Thu Trang<sup>1</sup> and NGUYEN Van Cong<sup>2</sup>

<sup>1</sup> Student, Faculty of Information Technology, Hanoi University  
(Km9, Nguyen Trai, Thanh Xuan, Hanoi, Vietnam)

E-mail: {thuyngan.tb1200, trangle257}@gmail.com

<sup>2</sup> Professor, Dept. of Information Technology, Hanoi University  
(Km9, Nguyen Trai, Thanh Xuan, Hanoi, Vietnam)

E-mail: congnv8192@gmail.com

With the development of Internet, the number of e-commerce websites is increasing dramatically, especially in Vietnam. However, conversion rate, the proportion of visitors who take a desired action of buying products online, are still very low. This problem leads e-commerce companies to figure out the solutions to rise this number. In this article, we provide the base guidelines for any e-commerce websites to increase this important figure by answering two questions including, (1) how to turn the potential customers into the customers, and (2) How to turn the customers into the loyal customers.

**Key Words:** *e-commerce, conversion rates, guideline, psychology, customer relation management*

## 1. INTRODUCTION

Conversion rate is often considered as an essential figure to evaluate the effective of an e-commerce website. It is the percentage of visitors who take a desired action of buying products online. To increase conversion rate, it is necessary to bring convenience, trust and reliability to the customers. It depends on some factors such as the attractiveness of the offer, how well the product is presented, the ease of the process and so on.

## 2. PROBLEM & FACTS

Nowadays, there exists many e-commerce websites all over the world. However, their conversion rate is still very low. In scope of Vietnam, there are hundred thousand companies, and almost all of them want to spread their business on the Internet. Every year, there are still many new ecommerce websites established, and also many of them closed silently. Almost all ecommerce project make no profit. So why? Because of many reasons. People are afraid of buying the products online because of lacking of touch sense, unsuitable with the colors, sizes, shapes of products or advices... In contrast, it is easier for customers to know these properties in brick-and-mortar stores, so they usually choose to buy in offline stores instead of buying online. The average conversion rates of

offline stores is 20-25%, while online conversion rate is much lower, only around 2-10%. The problem is, the e-commerce websites are lacking of the key factors, which help to promote the paying online of user. Many companies are still finding the solutions to solve this problem.

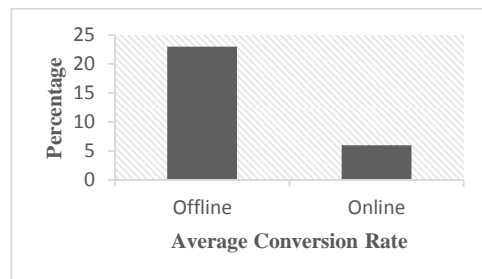


**Fig.1** Average Conversion Rate  
(Marketingsherpa Benchmark 2014).

## 3. GUIDELINES

In this section, we list some solutions based on the analyzing about the human psychology, giving you a theoretical understanding of how our brain be influenced and how to apply these psychological factors to our e-business. Applying psychology factors is reasonable. This has been proved by the success of many worldwide websites. So if your company's ecommerce website still does not work, or if yes, but you want it even better, do checkout

our guidelines below and find your own suggestions.



Fig.2 Psychological Factors.

### (1) How to turn the potential customers into the customers

Who the potential customers are, actually, they are the visitors to our websites. These tips are to promote them to not hesitate with their decisions – to buy/ use your products/ services.

These tips are represented as first coming with a psychology fact, then its application in terms of e-commerce.

#### (1) “People love the sense of control” - provide as much product information as we can

##### a) Bring to the customers the visual information of products such as images, videos, etc.

The product images must be in high quality, zoom-able, clearly, alternated and have detailed views from all angles. The images should be add in context, also shown how to use product. Let's take amazon.com as an example.

Product videos provides the real review and complain about product. Videos can show product more accurately; hence, people are less likely to buy stuffs under false assumptions. Moreover, with the complicated products, it helps save time when introducing about product just in 30 second video.

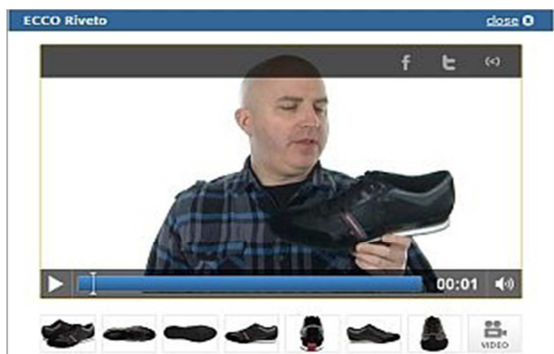


Fig.3 Video of Product Review ([www.zappos.com](http://www.zappos.com)).

##### b) Provide the customer the full product description

The description should contains all the information about product such as material, who's the product for, what will it do and why is that good. With the short description, it provides short and summary about product, if user want to view detailed information, click to long description of product. The more detailed you describe, the more user could imagine how good product is. It is same to view real product if you buy offline (i.e. chotot.vn).

### c) Give customers the chance to evaluate products and view recommendations from other customers

Adding the product review and ratings to each product will be useful to the customers. It helps customers have the overview about product, the feedback from other customers who bought it before. It forms the trust and reliability on product (i.e. bestbuy.com).

### d) Give customer the product comparison feature when they feel confused about choosing some products

Products comparison helps customers have the overview and comparison of products. From that view, they can choose the most suitable product for themselves. Additionally, each product should have product customization for customer to change the color of product into their favorite color or choosing suitable size, other shapes when viewing products.

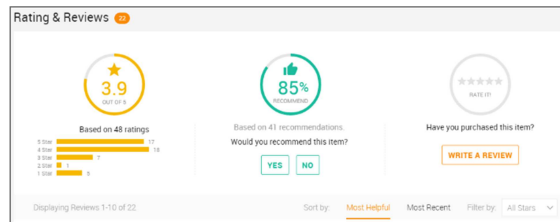


Fig.4 Rating & Reviews ([www.snapdeal.com](http://www.snapdeal.com)).

### (2) “More is better” - give various options and recommendations for users

##### a) Various Options, Versions of Group of Products

In each event, the time and amount of products is limited. For example, the golden week sales all products, the amount of products people can buy in this event are only 5. This thing creates the psychology of user want to compete buying many products.

##### b) Email Personalization

It supports user about the information or any problem about products. User don't have knowledge or how to use, the feeling about product, they can enter personal email in the form. Supporter will immediately chat or send recommendation to email

account of user.

#### c) Automatic Identify Products

In this method, it provides for user the relevant information or combo of products to choose based on history search the user has bought before (i.e. chotot.vn, snapdeal.com).

#### d) Multiple Options

They are Multiple Languages, Multiple Currencies, and Multiple Payment Methods. With Multiple Languages, the foreigner can buy product easily by choosing their language. In website, Multiple Currencies and Multiple Payment Methods allow user to pay online by choose the best options for them such as credit card or cash. Many people are afraid of with the credit card information theft. So there are many options about Payment method for user to choose (i.e. altrec.com).

### (3) “People love convenience” - Friendly User Interface and Instant Supports are the key factors

#### a) Effective search & filter tool

The website should have interactive user interface with good Search and Filter tool. The friendly interface makes customers feel attracted and convenient. Especially some elements related to buying products must be highlighted and noticeable. For example, “Add to Cart”, “Buy”, “Check out” buttons need to be styled standing out from other elements. In addition, each process should have automated guides to guide users from step to step. For instance, with clear payment progress checking, user can easily follow these steps and have successful payment. When the user want to know how much longer something is going to take, only viewing the list of clear progress indicator in the site. Besides, when customers access to the website, they want to find products quickly and accurately. The more products we offer, the better search and filters we need to provide.

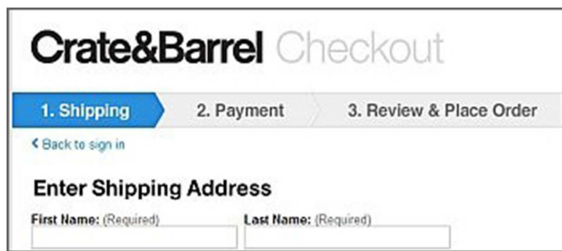


Fig.5 Checking Processes ([www.crateandbarrel.com](http://www.crateandbarrel.com)).

#### b) Direct supports

Bringing direct supports to customers everywhere and every time by offering Live Chat, Live Help, Click-to-Call functions. These services makes us to

assist the customers as soon as they need advice, support or information.

#### (4) “Everyone likes free stuff” - Try the best to increase User Budget Benefits

#### a) Give free shipping for user, it helps reduce the fee in buying products

In many sites applies the order is much more \$100 then user will receive free shipping. In fact, many websites use free shipping method and their conversion rate increase significantly (i.e. 2bigfeet.com; e-tailing.com).

#### b) Provide Sections for Discount, Coupon and Specials

This is attractive more people to buy products when having the selling promotions. User will be attractive with the product is sale or discount. Some people usually look for the Discount, so the advice for some websites should have the section for discount. In some website, if user is returning customer, user will receive the Special, they will receive the priority of price (i.e. stevemadden.com; amazon.com).



Fig.6 Combo of products ([www.snapdeal.com](http://www.snapdeal.com)).

#### (5) “The power of crowd psychology” - Social Network Connections (Facebook, Twitter, Instagram, Youtube, etc.) could bring a huge influence on online buyers

#### a) Like Page button

Every pages in Facebook have the Like button. This activity is very popular. The stores have the owner website and fanpage...when one user likes page on Facebook, the friend in his list can see and can be affected by his action if the page is useful for themselves. This means familiar equal safe and trust (i.e. freaker.vn, cucre.vn).

#### b) Share, Like Post button, Retweet button

All stores and pages in Facebook, they usually create the event for users. In each event, admin requires users to share public or comment to tag friend in event to receive the coupon, discount or free shipping. It is suitable and effective with uncertainty people, same kind of people and inexperience. The more people share, the more people know your products. Using testimonials, social following and subscribing, other social proof

signals will create for user the guarantee about product or service is well respected, widely used and well known which will delete the uncertainty.

## **(2) How to turn customers into loyal customers**

Even when we already have our customer, the enduring value comes from how we maintain the customer relationship. To assure they will come with us the next time. The quantity of products still the most important. Besides, these are the things we need to pay attention.

### **(1) Caring brings satisfy and happiness" - Offer customers more customer care**

In order to serve better, the first thing to do is collecting the customer history data. These data is from various sources such as their order history, phone calls, feedbacks, complaints, etc. Gathering the user experience can classify customers into customer segmentation groups for later data mining and analysis. For example, based on customers' history orders we can recommend for them related products with lower price. Or in the special days, we should send some messages or special gifts to express our caring to our customers.

Moreover, giving priority and discount price for familiar customers is a good option. Everyone loves free stuffs. Give VIP coupons, gifts and value information to customers and public this information to attract more people to become our familiar customers.

### **(2) "Everyone has their own personality" - Each type of customers need to be treated differently**

Based on the customer information analysis, classify customers into customer segmentation groups to figure out each group's needs and values

to our business. These information help us to upgrade the website and improve services to different customer groups. For example, developing the dynamic website that is suitable for different types of customers could bring more satisfaction to the customers.

## **4. CONCLUSION**

The objective of this paper is to minimize the space from visitor to customer of website by providing the method to turn visitors into customers, focusing on managing customer relationship, customer satisfaction and maximize the revenue. This article is based on guideline as a consultant tool that companies can directly apply to their website to improve conversion rate. Two solutions are given in this article: the ways to turn potential customers to customers and how to turn customers to familiar customers.

## **REFERENCES**

- 1) Heathman, Bryan. "*Conversion Marketing*". S.l.: Audioink Publishing, 2012.
- 2) Saleh, Khalid, and Ayat Shukairy. "*Conversion Optimization*". Sebastopol, CA: O'Reilly, 2011.
- 3) "The Ultimate Guide to Increasing Ecommerce Conversion Rates." ConversionXL. April 4, 2012. Accessed November 22, 2015. <http://conversionxl.com/the-ultimate-guide-to-increasing-ecommerce-conversion-rates/>.
- 4) "Continuous Commerce - Meet Magento VN." Meet Magento VN. Accessed November 23, 2015. <http://vn.meet-magento.com/presentation/continuous-commerce/>.
- 5) "Online Persuasion - Meet Magento VN." Meet Magento VN Online Persuasion Comments. Accessed November 23, 2015. <http://vn.meet-magento.com/presentation/online-persuasion/>.

**(Received November 22, 2015)**

# Lecture Archive System Using Web Camera

Yuki TSUTSUURA<sup>1</sup>, Yoshifumi SHIMOSHIO<sup>2</sup>

<sup>1</sup> Student, Department of Information, Communication and Electronic Engineering,

National Institute of Technology, Kumamoto College  
(2659-2 Suya, Koshi, Kumamoto, 861-1102 Japan)

E-mail:te11tsutsuura@g.kumamoto-nct.ac.jp

<sup>2</sup> Professor, Advanced course, National Institute of Technology, Kumamoto College  
(2659-2 Suya, Koshi, Kumamoto, 861-1102 Japan)

E-mail: shimoshi@kumamoto-nct.ac.jp

Recently, the MOOCs become very popular. If we provide a video lecture via the internet, then the cost is very high. They are mainly : (1) cost for making a video and (2) cost for communication cost to send the video. A professional camera operator is needed to make a lecture video and a wide-band network is needed to send a video. This system reduces those costs by using two web cameras. The first camera takes a lecture and extracts a professor's position data and the data is used to control the other camera which takes a lecture focusing a vicinity of the professor. Then the camera takes a lecture automatically and the recorded video does not contain much information.

**Key Words :** e-learning, web camera, lecture archive, data compression, image processing

## 1. INTRODUCTION

Recently the massive open online course (MOOCs) are very popular in the world [1]. In recent years, as most of students have their own smartphone or tablet devices, the system has become very useful for their study. The most famous MOOC is the MIT open courseware and there are many excellent video contents [2]. The contents in the system are very useful for people, especially students, who want to study by themselves via the internet. Therefore we also want to make those video contents for our students. However, it is fairly costly to make lecture video because a camera operator is required. In addition if we watch the video lecture via the internet, then we need wide-band communication link. The communication link cost to send a video lecture using a wide-band link is also costly because the data size is big to send character or graphics information on a blackboard. For those problems, the purpose of this study is to develop a lecture archive system which takes a lecture video in a class automatically, extracts characters and graphics written on a blackboard in the video, and save them as a compressed video data or a still image note data.

The system will be useful for the following cases:

- 1) Professor wants to take his lecture, but there is no staff to help it.
- 2) Students want to watch lecture videos via the internet through a low speed communication link.
- 3) Students do not need to take lecture note, so they can concentrate on professor's talk.
- 4) The note data is helpful for disabled people who are difficult to take note in the class.

The followings are also benefits of preparing a lecture video.

- 5) Students can watch lecture videos for review or when he was absent the class.
- 6) Professor can use the video for flipped class.

## 2. OUTLINE OF SYSTEM

### 2.1 Hardware and software to be needed

This system uses two web cameras connected to a computer. The cameras are set at back and center of classroom as shown in Fig.1 and they capture a lecture and sends the data to the computer. Then, some image processing applied to the data and the processed data will be saved in the computer hard disk. The web camera is controlled by a stepping motor to track professor's movement. As software, Visual C++ 2008 Express Edition and OpenCV 2.1 on Windows 7 are used.

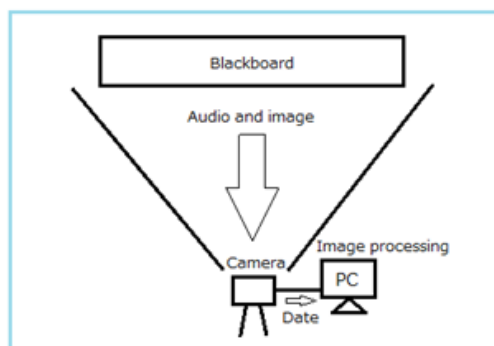


Fig.1 Setup for capturing a lecture.

## 2.2 Function of system

This system has mainly following two functions:

### 1) Recording function

A web camera captures a lecture and save it after image processing. The saved data consists of two kinds of contents: the first one is lecture video containing characters or graphics only which were written on a blackboard in the lecture by professor and the second one is still image note data which was captured every erasing the blackboard surface. The note data can be used instead of a notebook which students usually write.

To reduce a data size, two web cameras are used in this system. The first camera takes a lecture and extracts a professor's position and control the second camera's direction. The second camera takes a lecture focusing the professor. Therefore, the captured video has sufficient resolution to read the characters on a blackboard. If we can extract the professor's movement, then the motor controlled camera will track the professor automatically and the web camera can capture the vicinity of professor.

### 2) Playback function

Several operations are prepared in this function. They are a selecting data file operation, paging operation of note data, and etc.

## 3. SYSTEM DEVELOPMENT

### 3.1 Setting up of development environment

At first, several softwares which are essential to develop this system are installed into a PC and tested whether they work well or not. The recent OpenCV library does not support our web camera, so OpenCV2.1 is used.

### 3.2 Basic image processing

We made a several programs which execute basic image processing. They use OpenCV 2.1. The following functions are implemented.

#### ① Frame image capture

A frame image can be captured from video file or web camera to do some image processing on the frame.

#### ② Recording a video

A processed frame is saved into a hard disk as video file.

#### ③ Gray-scale transformation

A captured color frame image is converted into a grayscale image to save the processing time as the need arises. Usually it takes more time to process a color image than a grayscale image.



Fig.2 Gray-scale

### 3.3 Algorithms used in the system

To make this system, many programs must be built. Now, we have built only two programs which will be explained here.

#### (1) Detection of professor's position

To track a professor's movement to control a camera later, a professor position detection algorithms is developed. Here we use a green image because a blackboard is usually painted by green color. The procedure is shown in Fig.3.

- 1) A green frame image is segmented into 32 images which are divided in vertically. Then each segment is converted into 32 pixel data. One pixel data contains an averaged green value of all pixels in each segment. If professor is there, then the pixel value at there is different from other pixel values except the professor wears a cloth of the same color with the blackboard.
- 2) Every frame, the variation of 32 pixel values is examined and recorded the pixel positon where the pixel value is different from other 31 pixels' value.

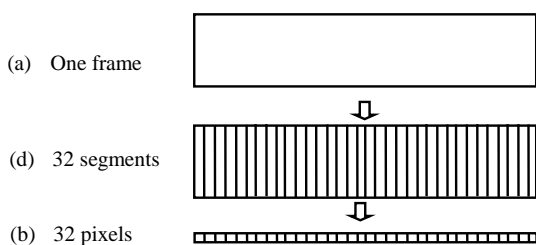


Fig.3 Procedure of detection of professor position.

(2) Extracting a blackboard area from a frame

To reduce the number of pixels for image processing, it is desire to extract the blackboard area only from a frame. To do this extraction, the frame image converted to grayscale image, then all of edge pixels are obtained, and the Hough transformation is executed. By doing those processes, many lines are obtained. A blackboard area can be decided by selecting the lines showing the edge of a blackboard.

#### **4. CONCLUSION AND FUTURE WORKS**

We are developing a lecture archive system which is used for e-learning. It has mainly two functions are 1) recording a lecture by a web camera and 2) save it as a compressed video, a video containing characters or graphs, or a still image note data. In this paper, we

explained the outline of the system and several functions to be developed. At this moment, we have built two programs which detects a professor's position and to obtain lines which show a blackboard area. From now, we have to develop the following programs:

- 1) to extract a blackboard area
- 2) to track a professor's position
- 3) to extract characters or graphics data from an image on a blackboard

To record the vicinity of a professor, a hardware to control a web camera must be build, too.

#### **REFERENCES**

- 1) <http://moocs.com/>
- 2) <http://ocw.mit.edu/index.htm>.

# Redundancy reduction using sparse representation for multi-view images of a light field camera

Taichi SUMI<sup>1</sup> and Yoshimitsu KUROKI<sup>2</sup>

<sup>1</sup> Student, Advanced Engineering School in National Institute of Technology, Kurume College  
(1-1-1 Komorino, Kurume-shi, Fukuoka, 830-8555, Japan)  
E-mail:a3211ts@std.kurume-nct.ac.jp

<sup>2</sup> Professor, Department of Control and Information Systems Engineering in  
National Institute of Technology, Kurume College  
(1-1-1 Komorino, Kurume-shi, Fukuoka, 830-8555, Japan)  
E-mail: kuroki@kurume-nct.ac.jp

**Abstract**—Lytro is a light field camera that US Lytro Inc. has developed. It generates multi-view images by dividing an image by a main lens coordinates of incident lights from information of three-dimensional rays. To reduce the redundancy between frames in a moving image, motion compensated prediction is used. Recently, LIC (Local Intensity Compensation) which extends prediction of the motion compensation to a linear combination consisting of multiple reference blocks has been reported. Moreover, application of sparse solutions has been proposed as a method for improving prediction accuracy with a small number of reference blocks as much as possible. In this paper, we apply the LIC using sparse representation for multi-viewpoint images obtained from light field camera and achieve reduction in redundancy.

**Key Words :***Lytro, Local Intensity Compensation, sparse representation, redundancy reduction*

## 1. INTRODUCTION

Lytro is a camera which can focus on any position by using dedicated software after taking pictures. It is not necessary to focus on each time of capturing as conventional digital cameras. Lytro records light in three-dimensional space from position of an image sensor element and coordinates on a main lens that incident light rays are passing. This feature makes it possible to obtain a distribution of light rays in three-dimensional space as light field. It is also possible to produce multi-view images by decomposing the light field in micro-lenses inside a camera.

Motion compensation prediction is used to reduce the temporal redundancy between frames in video compression. In recent years, LIC (Local Intensity Compensation)[1] has been reported as a new motion-compensation to predict the current block by a linear combination of multiple reference blocks. To decrease coding bits for compression, encoders should approximate a current block with least number of reference blocks. Sparse representation is applicable to LIC when we treat target blocks as original signals and reference blocks as base signals. It has been reported to improve the prediction accuracy.

In this study, the LIC using sparse representation is applied for multi-view images obtained from Lytro to achieve reduction in redundancy.

## 2. LYTRO

Lytro has a CMOS image sensor for acquiring the light field and micro-lens array in contact with image device. The micro-lens array has 330×380 pieces of micro-lens of which diameter is 14 Micrometers. Rays emitted from an object are refracted by the main lens at first. That rays focused on the micro-lens and is recorded in pixels of each image sensor element. 9×9 pixels of the imaging device are provided for each micro-lens. Pixels at same position in the different micro-lens are obtained rays passing through one of sub-apertures in the main lens. So, an image for each partial opening is created, that is, an image for each viewpoint is created by taking out the pixels. The micro-lenses are respectively 9 pieces in the horizontal and vertical direction. total 81 perspectives make images from each view point.

Lytro generates an image that is observed from partial region of the main lens by rearranging the pixels at same position of each micro-lens. Now, we focus on the pixels at same position of different micro-lenses. Lytro generates an image by taking out focused pixels and arranging in 330×380 without change the order as shown in figure 1. This image is equivalent to an image obtained by photographing a subject from a portion of the main lens. After all, a

light field camera generates images of different viewpoints by focusing on different pixels within the micro-lenses.

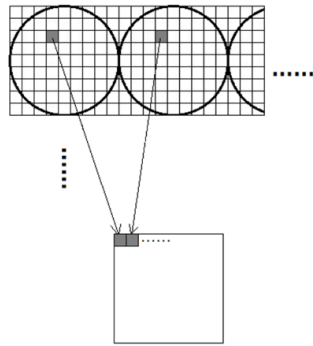


Fig.1. How to generate multi-view images

### 3. LOCAL INTENSITY COMPENSATION USING SPARSE REPRESENTATION

#### (1) Local Intensity Compensation

The LIC is a motion compensation framework which predicts current block using a linear combination of reference blocks as follows:

$$b_p = o + \omega_1 b_{c1} + \cdots + \omega_N b_{cN}, \quad (1)$$

where  $b_p$  is the current block,  $b_{ci}$  is the  $i$ -th reference block ( $i = 1, \dots, N$ ),  $\omega_i$  is the weight coefficient for  $b_{ci}$ ,  $N$  is the number of reference blocks, and  $o$  is the offset. The tasks of the LIC are to select reference blocks and to calculate weight coefficients.

#### (2) Sparse Representation

Let  $y \in \mathbf{R}^M$  be an original signal and  $a_i \in \mathbf{R}^M$ , ( $i = 1, \dots, N, M < N$ ) be an element of the basis vector. The superscript  $M$  is the dimension of the signals and  $N$  is the number of basis vectors. The original signal  $y$  is represented as the following equation:

$$y = Ax, \quad (2)$$

where  $A$  is a matrix, namely a sparse dictionary, containing the list of basis vectors as column vectors and  $x$  is the coefficient vector. To obtain sparse coefficients, sparse representation minimizes the number of non-zero elements of the coefficient vector as  $\hat{x}_0$ . If  $l_0$ -norm, which is the number of non-zero coefficients, of  $x$  is constrained at  $K$ , sparse representation minimizes the square error of the linear combination as follows:

$$\hat{x}_0 = \arg \min \|y - Ax\|_2 \quad \text{subject to } \|x\|_0 \leq K. \quad (3)$$

Equation (3) is called the  $K$ -sparse problem. The exact solutions to Eq. (3) are not obtained within polynomial time because Eq. (3) is NP-hard problems [2].

However, some methods to estimate suboptimal solutions using an iterative algorithm have recently been proposed [3].

#### (3) LIC using Sparse Representation

Assuming that the original signal  $y$  is the current block  $b_p$  and the basis vectors  $a_i$ s are the reference blocks  $b_{ci}$ s, sparse representation is applied to the LIC[4]. The LIC using sparse representation approximates  $b_p$  by solving the  $K$ -sparse problem as below:

$$b_p \sim A \hat{\omega}_0 + o, A = [b_{c0}, \dots, b_{cN}], \quad (4)$$

where  $\hat{\omega}_0$  is the solution of the  $K$ -sparse problem. All the elements of offset  $o$  are the same value, and are given by the mean of the elements of  $b_p - A\hat{\omega}_0$ . The LIC using sparse representation improves prediction accuracy.

## 4. EXPERIMENTS

In this research, multi-view images created by Lytro are verified reducing redundancy by applying the LIC using sparse representation. In experiment, the following two types of image were used as shown in figure 2. 81 multi-view images as experimental images are created from lfp file that Lytro outputs. The block size is set to  $16 \times 16$ . Reference blocks of LIC were entire referable image in method 1-4.

method 1:Forward prediction using a straight-left image

method 2: Bidirectional prediction after the forward prediction from the left in the horizontal direction

method 3: Forward prediction by adding the above image to the method 1

method 4: Bidirectional prediction after forward prediction in horizontal and vertical directions by extending the method 2 in vertical direction

In  $K$ -sparse problem solving in each technique, standard deviation of the prediction error was measured by changing  $K$  from 1 to 5. For comparison, the standard deviation in the case of not applying the LIC was also measured.



(i)Image 1                                   (ii)Image 2  
Fig.2. Experimental images

The results of applying each method to image 1 are shown in figure 3. The results of applying each method to image 2 are shown in figure 4. The horizontal axis of the Fig.3, Fig.4 is the number of reference blocks. Meanwhile, the vertical axis represents the standard deviation ratio for each method at the time of standard deviation are respectively 13.337, 25.094 as 100%. These values are standard deviation in the case of not applying the LIC.

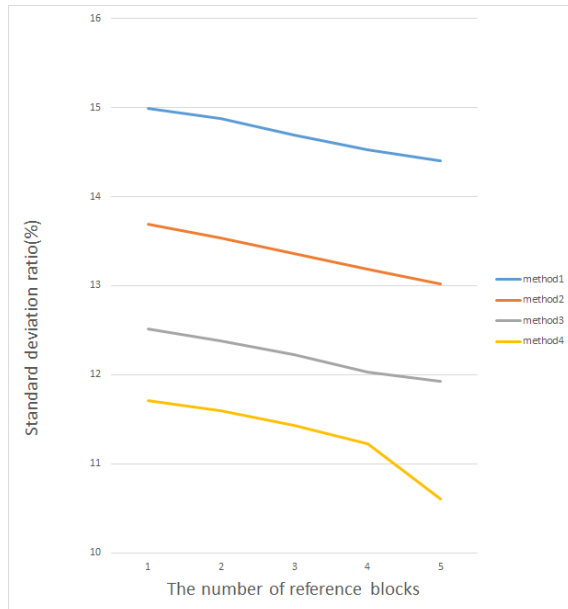


Fig.3. Standard deviation ratio of each method in image 1

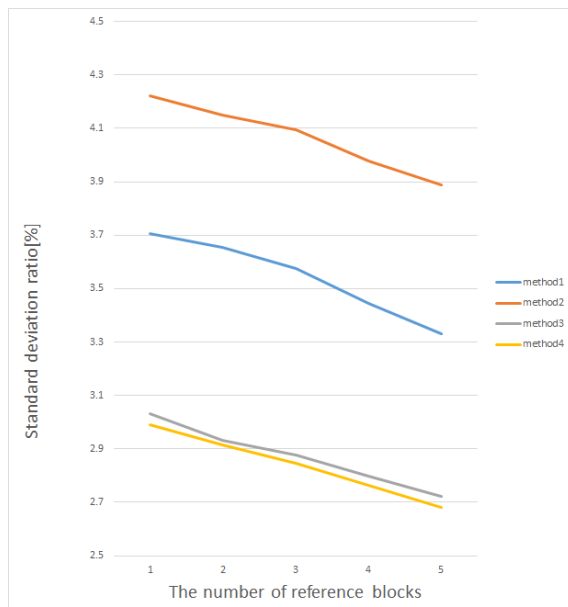


Fig.4. Standard deviation ratio of each method in image 2

From the figures, the more the number of reference blocks, the fewer the standard deviation. In each method, the standard deviation becomes smaller when the number of reference image increases. Furthermore, from Fig.3, correlation in the vertical direction is stronger than that in horizontal direction. So, prediction is more effective in the vertical direction than the horizontal direction. Fig.4 is seen that the correlation in the horizontal direction is low. In addition, differences in the method 3 and method 4 were hardly seen. This is considered the correlation in the vertical direction is very high.

## 5. CONCLUSION

In this paper, motion compensation using a sparse representation is applied for multi-view images that Lytro created. That method reduced redundancy between multi-view images. The motion compensation is applied in the multi-view images by assuming changes in image between the multi-view images to some motion. From the experimental results, the standard deviation of the prediction error image is smaller than the standard deviation of the original image and the redundancy between images is confirmed to have been reduced. As future challenges, prediction error image, the motion vector and the weighting factor should be encoded. Moreover, the evaluation of the coding efficiency is necessary.

## REFERENCES

- 1) N. Spirljan, S. Paschalakis, and P. Wu, "Local intensity compensation for inter prediction in HEVC," Doc. JCTVC-B096, JCT-VC of ITU-T VCEG and ISO/IEC MPEG, Geneva, Switzerland, Jul. 2010.
- 2) J. A. Tropp and S. J. Wright, "Computational methods for sparse solution of linear inverse problems," Proc.IEEE, vol.98, no.6, pp.948-958, Jun. 2010.
- 3) T. Blumensath, "Accelerated iterative hard thresholding," Signal Processing, vol.92, no.3, pp.752-756, Mar. 2012.
- 4) K. Inoue, K. Isechi, H. Saito, and Y. Kuroki, "An Inter-Prediction Method using Sparse Representation for High Efficiency Video Coding," IEICE Trans. Fundamentals, vol.E96-A, no.11, pp.2191-2193, Nov. 2013.



**CONFERENCE SESSION ON**  
**ARCHITECTURE, MECHANICAL, CHEMICAL,**  
**BIOTECHNOLOGY AND MATHEMATIC**



# Experimental Study on Sliding Base-Isolator with Thermal Sprayed Molybdenum in Case of Change the Surface Roughness

Maiko BABA<sup>1</sup> and Satoko ONO<sup>2</sup>

<sup>1</sup> Student, Advanced Architecture Course, National Institute of Technology, Ariake College  
(150 Higashi Hagio-machi, Omuta, Fukuoka, 836-8585 Japan)

E-mail:a47528@ga.ariake-nct.ac.jp

<sup>2</sup> Professor, Department of Architecture, National Institute of Technology, Ariake College  
(150 Higashi Hagio-machi, Omuta, Fukuoka, 836-8585 Japan)

E-mail:satoko@ariake-nct.ac.jp

The purpose of this study is to suggest the sliding base-isolator with weather resistance and wear resistance. For this purpose, the four specimens of various thickness of thermally sprayed molybdenum are produced. The molybdenum is characterized by weather resistance and wear resistance. In the past, these specimens have already been researched the hysteresis behavior by the vibration experiment of sinusoidal wave. However, specimens that changed the surface roughness of the sliding surface have not been researched yet. And therefore, in this study, the surface roughness has increased from about 3 ( $\mu\text{m}$ ) to about 6 ( $\mu\text{m}$ ) by shot blasting was performed to the sliding surface. After that, the effects of the differences in surface roughness in these specimens were investigated by the vibration of horizontal directions. It is confirmed that the residual displacement and the amplitude are greater after shot blasting than before shot blasting by experiment of horizontal vibration.

**Key Words :** Sliding Base-Isolator, Molybdenum, Thermal Sprayed Thickness, Surface Roughness, Hysteresis Behavior

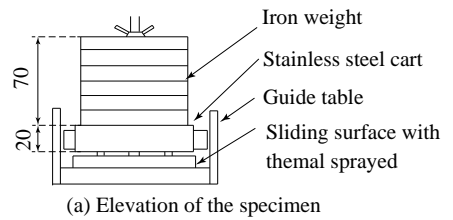
## 1. INTRODUCTION

Base isolation structure can reduce earthquake damage by installing an isolation device between the ground and the base of column for structure. The sliding base-isolator, one of the isolation devices, has the effect in a wide frequency range. However, on the sliding surface of the sliding base-isolator, changes of outdoor environment cause the deterioration and slight earthquake motions cause wears. Therefore, further improvement of the sliding surface is needed.

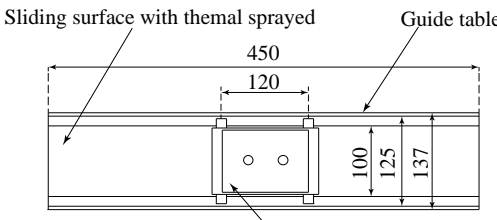
From this background, the present study suggests the sliding base-isolator with weather resistance and wear resistance. The sliding base-isolator on sliding surface is produced by thermal spray of molybdenum. The molybdenum is characterized by weather resistance and wear resistance. In this study, shot blasting was performed to the sliding surface so that the effects of the differences in surface roughness could be detected. After that, the influence of the hysteresis effect on sliding base-isolator based on the differences in surface roughness was investigated by experiment the vibration of horizontal directions.

## 2. SPECIMENS

The shape and size of specimen are shown in Figure 1. The sliding surface thermally sprayed with



(a) Elevation of the specimen



(b) Plan view of the specimen

**Figure. 1** Experiment specimen (unit : mm)

**Table 2** Results of measuring the coefficient of static friction

Thickness of thermal spray ( $\mu\text{m}$ )		100	150	200	250
Initial coefficient of static friction	$W_{\text{water}}(\text{gf})$	2028.2	2171.5	1959.0	1786.6
	$W_{\text{cart}}(\text{gf})$	8494.7			
	$\mu_s$	0.239	0.256	0.231	0.210
Before the shot blasting	$W_{\text{water}}(\text{gf})$	4745.6	3810.8	4251.8	3581.0
	$W_{\text{cart}}(\text{gf})$	8488.6			
	$\mu_s$	0.559	0.449	0.501	0.422
After the shot blasting	$W_{\text{water}}(\text{gf})$	3903.9	3910.0	4151.7	3401.1
	$W_{\text{cart}}(\text{gf})$	8488.6			
	$\mu_s$	0.460	0.461	0.489	0.401

molybdenum is set on the guide table. The thickness of thermal spray on sliding surface is the following four types: 100( $\mu\text{m}$ ), 150( $\mu\text{m}$ ), 200( $\mu\text{m}$ ) and 250( $\mu\text{m}$ ).

The shot blasting was performed to this sliding surface. Arithmetic average roughness measured before and after the shot blasting is shown in Table 1. The surface roughness increased from about 3( $\mu\text{m}$ ) to about 6( $\mu\text{m}$ ) by shot blasting. The stainless steel cart is placed on the sliding surface. This cart has three projections on its bottom and four bearings on its sides. The total weight of the cart is 8492.3(gf), including a steel weight of 5990.0(gf) on it.

### 3. MEASURING THE COEFFICIENT OF STATIC FRICTION

#### A. Measuring Methods

The coefficient of static friction on the sliding surface was measured before the horizontal vibrations. The equipment used in the experiment for measuring the coefficient of static friction is shown in Figure 2. The water vessel via a cable is attached to the front side of the cart. The water is poured at a constant speed into the water vessel. When the cart moves, the pouring of the water is stopped. By

measuring the total weight of the water vessel at that time, the coefficient of static friction is evaluated by this experiment. These procedures repeat five times on the same condition. The sliding surface is managed by wiping with the cloth before and after the all measuring. And, the temperature at the 44 points on the sliding surface is measured for the non-contact thermometer before and after all the experiments.

#### B. Measuring results and discussions

The results of measuring the coefficient of static friction are shown in Table 2. The coefficient of static friction is evaluated from  $W_{\text{water}} / W_{\text{cart}}$ .

First, it is confirmed that the coefficient of static friction are about from 0.40 to 0.49 after the shot blasting in Table 2; coefficient of static friction is decreased before the shot blasting. However, the

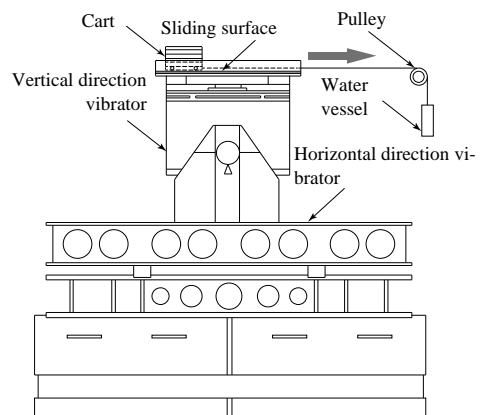


**Figure. 2** Equipment of measuring the coefficient of static friction

**Table 1** Arithmetic average roughness

Thickness of thermal spray ( $\mu\text{m}$ )	100	150	200	250
Before the shot blasting	2.30	3.45	3.21	4.19
After the shot blasting	5.93	5.92	6.71	6.63

fluctuation, which is about  $0.01 \sim 0.02$ , is very small, except the case of  $150(\mu\text{m})$ . Second, in comparison between the “initial” coefficient of static friction and those after the shot blasting, it is confirmed the coefficient after the shot blasting is larger than the “initial” ones. Fluctuations in the coefficient of static friction is about  $0.19 \sim 0.26$ .

## 4. THE VIBRATION EXPERIMENT

### A. Measuring Methods

The equipment of the horizontal directions vibration is shown in Figure 3; the vibration experiment conditions in Table 3. Vibration parameter is the sinusoidal wave frequency (Hz) and maximum acceleration (G). The duration time of vibration is about 60 seconds. Five times are repeated for each cases of experiment. Similar to measuring the coefficient of static friction, the sliding surface is managed by wiping with the cloth at before and after all experiments. In addition, the temperature at the sliding surface is measured for the non-contact thermometer at before and after all the experiments.

### B. Experimental results and discussions

The results of the horizontal vibration after the shot blasting are shown in Figure 4 and Figure 5. Here, the vertical axis is relation displacement (cm), and the horizontal axis is time (sec) in Figure 4 and Figure 5. The relation displacement subtracts the horizontal direction displacement of the vibrator from the horizontal direction displacement of the cart. And, the residual displacement is the horizontal direction displacement of the cart at the end of the experiment. Figure 5 is results before shot blasting. The results of the horizontal vibration after the shot blasting are shown in Figure 4. Here, the vertical axis is relation displacement (cm), and the horizontal axis

is time (sec) in Figure 4.

Results of different case of the thickness of thermal spray are shown in Figure 4 (a) and Figure 4 (b). In the case of the thermal spray thickness of  $250(\mu\text{m})$ , the residual displacement is 5.2 times greater than the case of  $100(\mu\text{m})$ . However, the amplitude is almost the same. Results of different case of the input frequency are shown in Figure 4 (b) and Figure 4 (c). In the case of the input frequency of 5.0 (Hz), the residual displacement is 3.4 times and the amplitude is 0.3 times greater than case of 3.0 (Hz). The result is confirmed in the horizontal vibration experiments before shot blasting. Figure 4 (b) is results of before shot blasting and Figure 4 (d) is results of after shot blasting. Figure 4 (b) and Figure 4 (d) is the same thermal spray thickness and vibration experiment conditions. However, in the case of the after shot blasting, the residual displacement is 2.9 times and the amplitude is 17.2 times greater than case of before shot blasting.

The results of acceleration and time relation are shown in Figure 5. Here, the vertical axis is relation acceleration (G), and the horizontal axis is time (sec) in Figure 5. Acceleration of the cart is gray line and acceleration of the horizontal vibration is red line. Results of before and after shot blasting are shown in Figure 5. Reduction of the acceleration of the cart is greater after shot blasting than before shot blasting. Attenuation rate of the cart acceleration after shot blasting is 19 (%).

One of the results of measuring the temperature on the sliding surface is shown in Figure 6. Here, the vertical axis is temperature ( $^{\circ}\text{C}$ ), the horizontal axis is measuring point in Figure 6. It is confirmed that the fluctuation of temperature on sliding surface is  $2.0(^{\circ}\text{C})$  at most. It is thought that the rise of temperature at the sliding surface does not affect the hysteresis behavior.

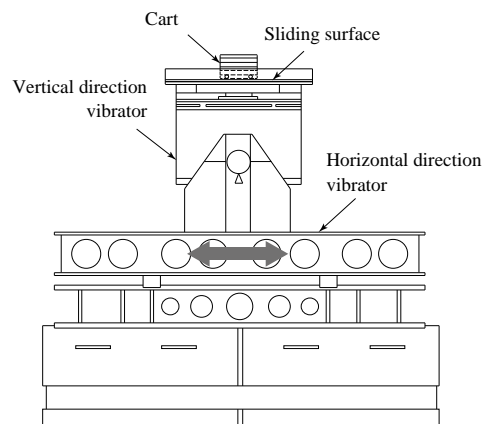


**Figure. 3** Equipment of the horizontal directions vibration

**Table 3** The vibration experiment conditions

No.	input wave	Frequency (Hz)	Maximum acceleration (G)
1	sinusoidal wave	3.0	0.3
2			0.5
3		5.0	0.3
4			0.5
5			0.8

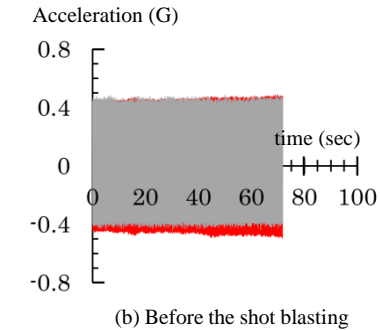
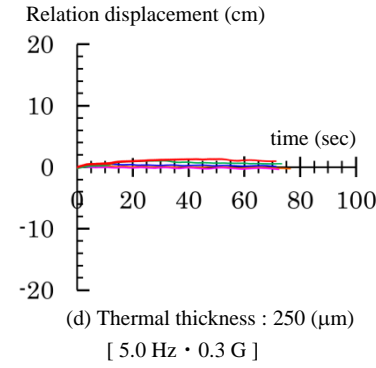
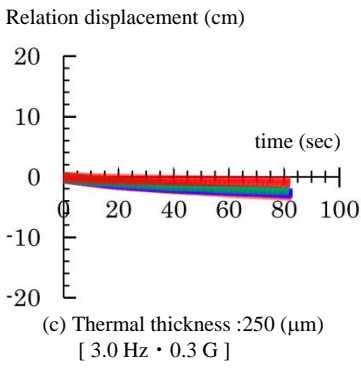
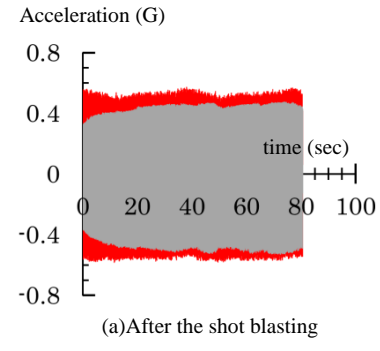
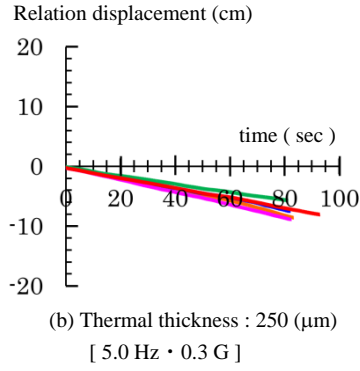
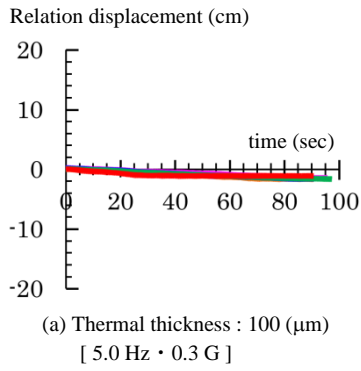


**Figure 4** The relation displacement by horizontal vibration  
[Thermal thickness : 250 $\mu\text{m}$ , (5.0 Hz • 0.5 G)]

## 5. CONCLUSIONS

In this paper, the effects of the differences in surface roughness in these specimens were investigated through the horizontal directions vibration. By the experiment for measuring the coefficient of static friction showed that, in the case of 6 ~ 7 ( $\mu\text{m}$ ) surface roughness, the coefficient are about 0.40 to 0.49. In addition, it is confirmed that the residual displacement and the amplitude are greater after shot blasting than before shot blasting by experiment of horizontal vibration.

## ACKNOWLEDGMENTS

We would like to thank Koei-Techno System Co.,Ltd. and Professor Ryouichi Kawase (department of chemical science and engineering, National institute of technology) for produced the specimens for used in this study.

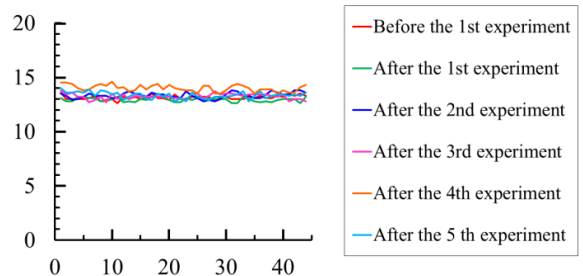


**Figure 6** Result of measuring the temperature  
(Thermal thickness: 250  $\mu\text{m}$ )

## REFERENCES

- [1] R.Nagashoma, S.Miyaji and S.Ono, Experimental Study about Sliding Base-Isolators with the Thermal Sprayed Molybdenum (Part 1) Influence of Dynamic Characteristics on Thermal Sprayed Thickness in Cases of Horizontal Vibration, Summaries of technical papers of annual meeting architectural institute of Japan (B-2), pp.535-536, September 2011.

# Effects of Cyclic Loading on Brittle Fracture in Notched Specimens

Tatsuya IKEDA<sup>1</sup>, Tsutomu IWASHITA<sup>2</sup>

<sup>1</sup> Student, Advanced Architecture Course, National Institute of Technology, Ariake College  
(150 Higashihagiomachi, Omuta, Fukuoka 836-8585, Japan)  
E-mail:a47502@ga.ariake-nct.ac.jp

<sup>2</sup> Associate Professor, National Institute of Technology, Ariake College  
(150 Higashihagiomachi, Omuta, Fukuoka 836-8585, Japan)  
E-mail:iwashita@ariake-nct.ac.jp

To examine the effects of cyclic loading on the decrease in fracture toughness of notched specimens, experiments with three types of loading were conducted : monotonic loading, constant amplitude cyclic loading and monotonic loading after constant amplitude cyclic loading. Test results showed cumulative ductility, which indicated deformation capacity, decreased when ductility amplitude, which indicated amplitude increased. Finally, our findings suggest the possibility that a method proposed in this paper can be used to evaluate the occurrence of brittle fracture for specimens under various loading condition.

**Key Words :** Brittle fracture, Fracture toughness, Notch, Cyclic loading, Cumulative ductility

## 1. INTRODUCTION

A number of brittle fracture occurred at the weld joints in the 1995 Kobe earthquake and Post-earthquake investigations demonstrated that the plastic deformation capacity of steel building frames was significantly reduced by brittle fracture.

Our research group found that the Weibull stress approach can predict the occurrence of brittle fracture more accurately as compare with conventional fracture toughness such as  $K_c$  and  $J_c^{1)}$  because the Weibull stress can consider the plastic constraint. However, our group confirmed the effectiveness of the Weibull stress approach under only monotonic loading. It is important to also consider brittle fracture under cyclic loading since loading can degrade material toughness and induce premature brittle fracture in structures exposed to major earthquakes.

This research focuses on the effects of cyclic loading on the occurrence of brittle fracture. Notched specimens were tested under monotonic loading and two types of cyclic loading—constant amplitude cyclic loading (at one of three amplitudes), and monotonic loading after constant amplitude cyclic loading. Also, to reveal any deleterious effect of cyclic history on fracture toughness, three types of parameters were considered for each type of cyclic loading. Test results interpret mainly in terms of ductility amplitude, which is related to deflection amplitude, and cumulative ductility, which is related to plastic deformation capacity.

This research describes the effects of cyclic loading on the occurrence of brittle fracture in notched specimens based on, for all the specimens, a comparison of the relationship between ductility amplitude and cumulative ductility. Our purpose of research is that a method proposed in this research evaluate the occurrence of brittle fracture under various loading conditions.

## 2. SPECIMENS AND EXPERIMENTS

### (1) Specimens

The geometry of the specimen is shown in Figure 1. The material of the specimens is Japanese Industrial Standard Grade SM490A structure steel. The Each specimen has four notches that are symmetrically located around a loading pin hole at its center. Notch radius is 0.15 mm.

Tensile and Charpy impact test results for the material are shown in Table 1 and Table 2, where  $\nu E_0$  indicates absorbed energy at 0 °C and  $\nu E_{-20}$  that at -20 °C.

**Table 1** Material tensile properties.

Material	Testing temperature (°C)	Yield strength (N/mm <sup>2</sup> )	Ultimate strength (N/mm <sup>2</sup> )	Young modulus (N/mm <sup>2</sup> )
SM490A	-30*	346	604	212805

\*Although the tensile testing temperature was set to -30 °C, experimental tests of the notched specimens were performed at

-20 °C.

**Table 2** Results of Charpy impact tests.

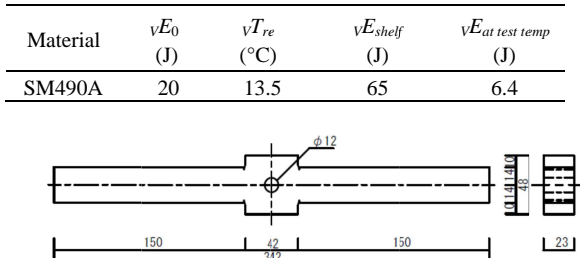


**Figure 1** Specimen dimension.

## (2) Test procedures

The test set-up is shown in Figure 2. The specimen temperature was reduced to -20 °C using a solution of ethanol and dry ice.

The specimen temperature was measured with the thermocouple sensor attached near to the notches of the specimen.

The specimens were tested under three types of loading : monotonic loading (M), cyclic loading (C), and monotonic loading after cyclic loading (Cm). Figure 4 shows the loading patterns. For M specimens, monotonic loading was increased until fracture. For C specimens, constant amplitude cyclic loading was applied to fracture. For Cm specimens, monotonic loading was increased until fracture after one or two cycles of constant amplitude cyclic. Table 3 shows a summary of specimens and loading types. Figure 3 is a photograph of the test apparatus.

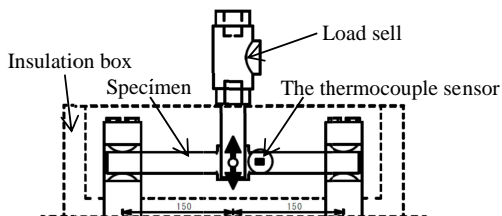


**Figure 2** Test set-up.



**Figure 3** photograph of the test apparatus.

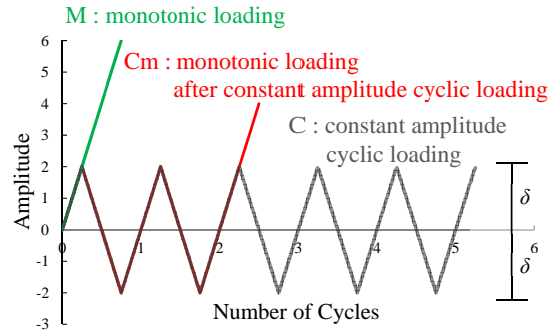


**Figure 4** Loading patterns.

**Table 3** Summary of specimens.

Specimen	Number of specimens	Amplitude, $\pm \Delta\delta/\delta$ (mm)	$\Delta\delta/\delta_p$ , $\mu_p$	Number of cycles, N
M	3	-	-	-
C3.0	5	3.0	0.89	-
C3.7	5	3.7	1.32	-
C4.8	3	4.8	2.05	-
Cm3.0-1	4	3.0	0.96	1
Cm3.0-2	5	3.0	0.92	2
Cm3.7-1	5	3.7	1.42	1

## 3. TEST RESULTS

In the experiments, brittle fracture was observed in all specimens. As mentioned above, every specimen has four notches. When a sample is under load, two of the notches will be in tension and two in compression. Brittle fracture could potentially occur from either of the notches in tension. In actuality, brittle fracture was observed to occur from one of those notches in all specimens. Figure 5 shows a specimen after brittle fracture from a notch.

Figure 6 shows an example of load vs. displacement curve for C and Cm specimens. As shown in the figure, the maximum load in the second cycle is larger than that in the first cycle because of the work hardening of the material. This effect should cause higher stress at the notch tip.



**Figure 5** Fracture from notch.

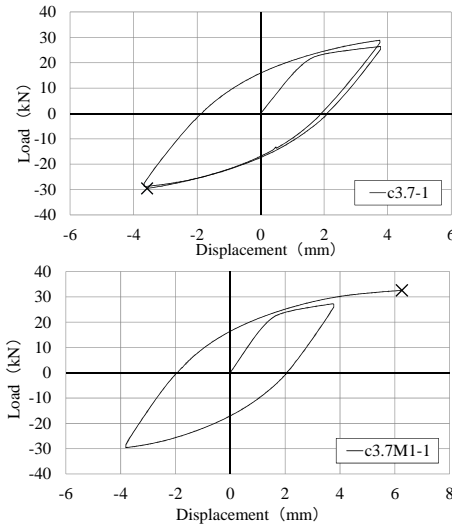


**Figure 6** Load vs. Displacement.

#### 4. EFFECTS OF CYCLIC LOADING ON CUMULATIVE DUCTILITY

##### (1) Cumulative ductility and ductility amplitude

Test results are interpreted in terms of ductility amplitude  $\mu$  and cumulative ductility  $\eta$ . Test data are arranged in the manner of Kuwamura & Takagi (2001). For cyclic loading, the average ductility amplitude  $\mu_p$  are defined as

$$\mu_p = \frac{\Delta\delta_p}{\delta_p} \quad (1a)$$

Here,  $\Delta\delta_p$  is the average displacement amplitude (half-amplitude) and  $\delta_p$  is the elastic displacement at the full plastic load,  $Q_p$ , which is obtained by the general yield point method. A definition of symbols is shown in Figure 7. Because of a slight difference in  $\Delta\delta_p$  by cycle during cyclic loading,  $\Delta\delta_p$  was calculated as average displacement amplitude as follows:

$$\Delta\delta_p = \frac{\Delta\delta_{p1} + \Delta\delta_{p2} + \dots + \Delta\delta_{pn}}{n} \quad (1b)$$

in the case of Figure 7.  $\eta_p$  is cumulative ductility until fracture and is defined as follows:

$$\eta_p = \frac{\Delta\delta_{p1} + \Delta\delta_{p2} + \dots + \Delta\delta_{p,n+1}}{\delta_p} \quad (1c)$$

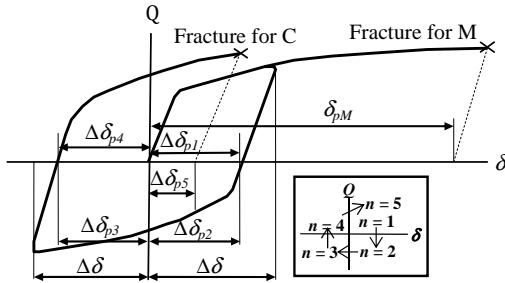
where  $n + 1 = 5$  in the case of Figure 7.  $\eta_p$  for the Cm loading pattern (Figure 8) is also calculated in the same way.  $\eta$  for monotonic loading is defined as  $\eta_{pM}$ :

$$\eta_{pM} = \frac{\delta_{pM}}{\delta_p} = \frac{\delta_f}{\delta_p} - \frac{Q_f}{Q_p} \quad (1d)$$

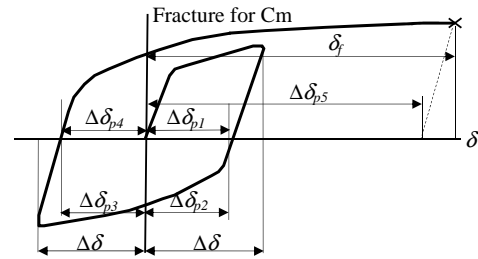
where  $\delta_{pM}$  as shown in Figure 7.

Figure 9 shows cumulative ductility vs. ductility amplitude obtained from C testing. The test results showed cumulative ductility which indicated deformation capacity decreased when ductility amplitude which indicated amplitude increased. Whereas

cumulative plastic deformation values show much scatter, a plot of amplitude versus cumulative plastic deformation shows that average cumulative plastic deformation under constant amplitude loading follows a regression line. Another finding is that the scatter of cumulative plastic deformation values is narrower at higher deflection amplitudes.



**Figure 7** Definition of symbols for M & C loading.



**Figure 8** Definition of symbols for Cm loading.

##### (2) Examination by cumulative ductility

Generally, the ductility  $\eta_{pM}$  of monotonically loaded specimens is not directly comparable to the cumulative ductility  $\eta_{pM}$ , of cyclically loaded specimens. However, we will attempt a comparison by assuming that monotonic loading is a subcategory of cyclic loading. We assume that monotonic loading is cyclic loading under which the specimen fractures during its first cycle because of a large displacement amplitude. Here, we thus assume that cumulative ductility  $\eta_{pM}$  of the M specimens can be expressed in terms of either ductility amplitude  $\mu_p$  or cumulative ductility  $\eta_{pM}$ . Figure 10 is plot of cumulative ductility versus ductility amplitude, with both divided by cumulative ductility  $\eta_{pM}$ . Included are M specimens, which here are used a baseline. The same tendency previously explained in relation to Figure 9 is also observed in Figure 10, even though the latter figure includes monotonic loading results. Here, it is possible that the regression line expresses the occurrence of brittle fracture with various loading types although there is the high degree of scatter.

To examine this possibility, we added the arranged

results for Cm specimens to the plot of Figure 10 to arrive at Figure 11. The results for Cm specimens are divided into two steps. The first step corresponds to the constant amplitude cyclic loading stage ( $n = 1$  to 3 in the case of Figure 12), with the first step having cumulative ductility calculated as  $\eta_{p-1st}$ . This could be interpreted as “stored damage” with respect to material toughness. The second step corresponds to the monotonic loading stage after constant amplitude cyclic loading ( $n \geq 4$  in the case of Figure 12). Second-step cumulative ductility  $\eta_{p-2nd}$  can also be calculated by subtracting  $\eta_{p-1st}$  from  $\eta_p$ . Here, we use the  $\mu_p$  and  $\eta_{p-2nd}$  values of the Cm specimens as, respectively, the first-step and second-step ductility amplitude (i.e., the values on the horizontal axis of Figure 11). More specifically, the axis values are calculated as follows—first-step plots:  $x = \mu_p/\eta_{pM}$ ;  $y = \eta_{p-1st}/\eta_{pM}$ ; and second-step plots:  $x = \eta_{p-2nd}/\eta_{pM}$ ;  $y = (\eta_{p-1st} + \eta_{p-2nd})/\eta_{pM}$ .

As shown in Figure 11, the second-step plots fall across the regression line, with considerable scatter. This suggests a possibility of using this approach to evaluate the occurrence of brittle fracture for specimens under various loading conditions. Admittedly, there remains a problem with scatter. Further research will be needed to closely consider this scatter problem and, by extension, establish an adequate method to evaluate the occurrence of brittle fracture.

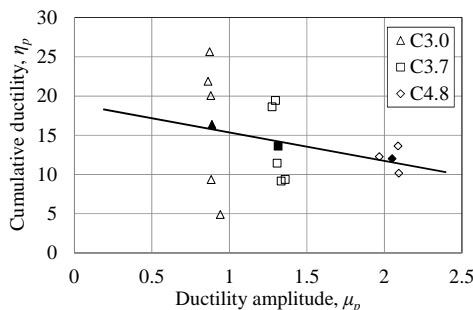


**Figure 9** Cumulative ductility vs. Ductility amplitude.

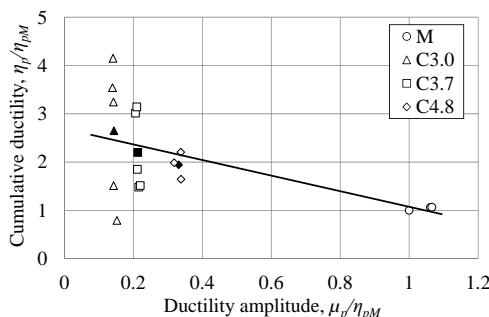


**Figure 10** Cumulative ductility vs. Ductility amplitude with M results.

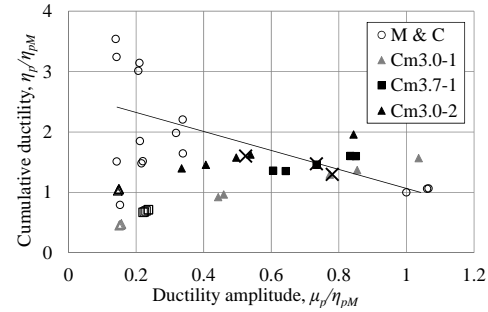


**Figure 11** Cumulative ductility vs. Ductility amplitude with arranged Cm results.

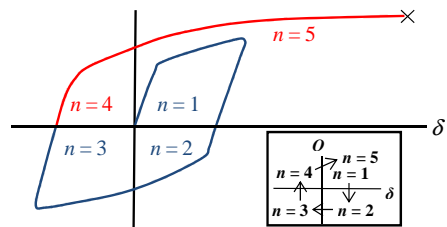


**Figure 12** Diagram of  $\eta_{p-1st}$  and  $\eta_{p-2nd}$  which was divided into 1<sub>st</sub>-step and the 2<sub>nd</sub>-step.

## 4. CONCLUSIONS

This paper focused on the effects of cyclic loading on brittle fracture. Notched specimens were tested under monotonic loading and two types of cyclic loading. When ductility amplitude increased, cumulative ductility prior to brittle fracture decreased in approximately inverse proportion although cumulative ductility values showed wide scatter.

The results suggest the possibility that the method proposed in this paper can be used to evaluate the occurrence of brittle fracture under various loading conditions.

## ACKNOWLEDGMENTS

This research was supported in part by JSPS Grants-in-Aid for Scientific Research (Grant Number: 25820276) and by the MAEDA Engineering Foundation.

## REFERENCES

- Iwashita, T. & Azuma, K. 2012. Effect of plastic constraint on brittle fracture in steel: Evaluation using toughness scaling model. *Journal of Structural Engineering* 138(6): 744-752.
- Kuamura, H. & Takagi, N. 2001. Verification of similitude law of pre-fracture hysteresis. *Journal of Structural and Construction Engineering (Transaction of AJ)* (548): 139-146. (in Japanese)

# Study on “Skeletonics” in Cultural Festival

Kohei KAWAGOE<sup>1</sup>, Hiroyuki SHIRAIWA<sup>1</sup>, Natsuki TAKAGI<sup>1</sup>  
and Akihiro TAKAHASHI<sup>1</sup>

<sup>1</sup> Department of Mechanical Engineering, National Institute of Technology, Miyakonojo College,  
Miyakonojo, Miyazaki, Japan (Yoshio 473-1, Miyakonojo, Miyazaki 885-8567, Japan)

Cultural festival of National Institute of Technology, Miyakonojo College was held in autumn 2014 and an improvement of “Skeletonics” was conducted by student research activities in department of Mechanical Engineering in the college. Prototypes of No.1 to 3 of the “Skeletonics” were fabricated, as results, upper body suit of the “Skeletonics” was developed with attachable in anyone, easy mounting and lightweight. This experience of “Skeletonics” research activities provided major benefits on learning and understanding of machine mechanism for students. In addition, educational contribution using “Skeletonics” was achieved actively in various science events around local area.

**Key Words :** “Skeletonics”, expanding exoskeleton behavior, improvement of linkage mechanics, science education

## 1. Introduction

Our school, National Institute of Technology, Miyakonojo College is located in the Miyakonojo city, in Miyazaki Prefecture in Japan. At present, the college has four departments: Mechanical Engineering, Electrical and Computer Engineering, Chemical Science and Engineering and Architecture. School cultural festival is held each autumn in our college, and the student research activities which makes use of the characteristic of each department is planned as a student event of the festival. The authors are belonging to the department of Mechanical Engineering. Recent year, the research titles of our department were “Power-assisted bicycle (2011)”, “High-speed craft (2012)” and “Gyrocopter (2013)”. In 2014, “Skeletonics” was carried out by author and our classmates.

What is the “Skeletonics”? This is operation enlarging type suit (see chapter 2). Currently, this suit is sold commercially by Skeletonics Inc., but it is limited to a custom-made product. Therefore, authors are aiming to be a generalized “Skeletonics” such as attachable in anyone, easy mounting and lightweight. Through the research activities, effective learning and understanding of machine mechanisms is expected for mechanical engineering student.

## 2. Feature of “Skeletonics”

“Skeletonics” was developed by a couple of guys who graduated from National institute of Technology, Okinawa College in Nago city Okinawa Prefecture in Japan. “Skeltonics” means expanding exoskeleton behavior. Emulating the human body with the use of artificial limbs extensions and linkages which allow for ease of greater movement. Linkage system means that some linkages start moving when one linkage moves. “ Skeletonics” has no actuator. Therefore the operator’s applied load will pass through a system of linked levers in order to magnify movement. At the moment, no body is quite sure of its potentials. Big companies like Google are showing an interest in “Skeltonics”. This subject is sure to become more popular in the future.

## 3. Manufacture

### (1) Prototype No.1

Due to lack of times a low budget our first Prototype was only for the upper body. We designed our 1<sup>st</sup> model 1.5 times than the traditional “ Skeletonics” using wood material.

strapping change the handles to a slide system and now anyway, tall short big or small can operate it



**Fig.1** Linkage structure of the prototype No.1.

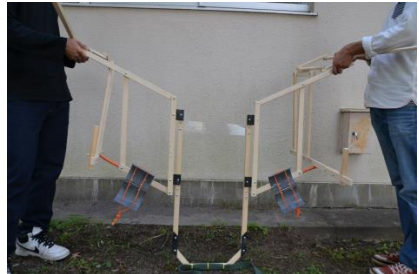


**Fig.3** Prototype No.2 made of “white pine” wood.



**Fig.2** Mounting to the arm of the linkage structure of the prototype No.1.



**Fig.4** Prototype No.2 from the front.

Next we assembled all the mechanic parts. Then we had to trouble shoot some minor problems. In the initial operation testing, great power had to be applied in order to get any movement. This was due to a lack of experience in “Skeletonics”s and a somewhat heavy wooden construction. Some of the linkages would also inhibit movement of other parts.

## (2) Prototype No.2

We tried to design its limbs in such a way, so as to alleviate the need for excessive operational power. We had to find a material which is light and strong but not too expensive. We chose “white pine”. Prototype 2 was better moving but we had other problems, one was the operator had difficulty stitching forward smoothly because the equipment prevented the operator’s arms from moving easily.

And prototype 1,2 were moved by some belts were wound around the operator’s body and caused much pain. We succeeded in reducing the excessive power needed but we had not yet archived our final goals that anybody could put it on and move smoothly.

## (3) Prototype No.3 (Final)

We had a good rethink about all our problems with the P2 and set about re-designing a few features. We re-designed the elbows, did away with some of the



**Fig.5** Prototype No.2 from the behind.

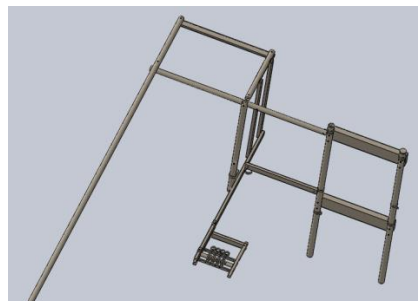


**Fig.6** Three-dimensional CAD sheet of the Prototype No.3.



**Fig.7** Whole structure of the prototype No.3.



**Fig.8** Prototype No.3 from the front.



**Fig.8** Prototype No.3 from the behind.



**Fig.9** Final whole structure of the “Skeletonics” upper body suit made of Aluminum parts.

with ease. Next how to fit the “ Skeletonics” to the human body. We came up with the idea of using a backpack.

This can easily be connected to the “ Skeletonics”. The backpack is easily adjustable to fit different body sizes. Once we had connected P3 to the backpack our prototype was complete. We scaled up our No.3 prototype from 1.5 to 3 times normal human size. We also had to go from wood to aluminum alloy construction in order to keep the weight down and still have a high durability. We added working arms which like artificial limbs were able to grab objects.

At our school festival we took 1<sup>st</sup> prize for our presentation on “Skeletonics”.

We were very pleased that so many people showed an interest in our work and many people tried out our “Skeletonics”. It was a huge hit.

#### 4. At last we reached our goal

We designed and built our own working “Skeletonics” upper body suit. It can be worn by almost anybody and we had the chance to show it to many people both young and old alike. Our next assignment is to simplify putting on and taking of the suit so that one person can do this alone by him. We also have the enormous challenging of designing “Skeletonics” for the lower body and legs and so on.

“Skeletonics” is a perfect teaching aid which enables hands on experience in the use of levers and mechanisms or what’s better known as basic mechanics.

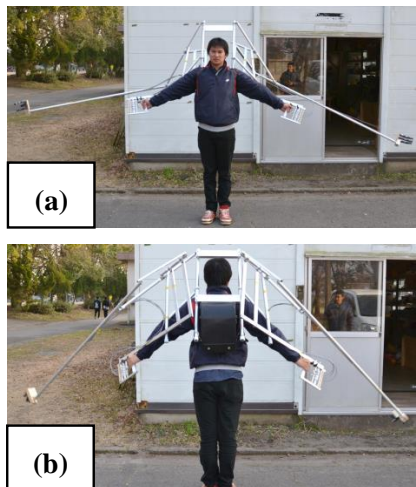


**Fig.10** Final structure of the prototype “Skeletonics” upper body suit made of Aluminum parts from the front, (a) and behind, (b).



**Fig.11** Mounting to the child in cultural festival in autumn 2014.



**Fig.12** Lecture of the “Skeletonics” by students in NIT of Miyakonojo college in the science educational event.



**Fig.13** Local contribution of the science educational event using “Skeletonics”.

## 5. Conclusion

In autumn 2014, improvement of the “Skeletonics” were conducted by student in department of mechanical engineering in NIT of Miyakonojo college. Through the research activities, the following conclusions can be made:

- (1) Improvement of “Skeletonics” of the upper body suit was achieved such as attachable in anyone, easy mounting and lightweight.
- (2) This experience of research activities by “Skeletonics” provided major benefits on learning and understanding of machine mechanism.
- (3) We are actively helping the educational contribution in various science events with local community using “Skeletonics”.

## ACKNOWLEDGEMENT

The Authors thank Ms. Setsuko Hata for constructive comments and suggestions on this article.

## REFERENCES

- 1) <http://skeletonics.com/>, 2015.

# Fatigue Property of Plasma Coating Film as Resistance to Hydrogen Entry and Hydrogen Embrittlement

Kazuki KOJIMA<sup>1</sup>, Hiroshi NISHIGUCHI<sup>2</sup> and Takayuki FUKUDA<sup>2</sup>

<sup>1</sup> Student, Advanced Engineering Course, National Institute of Technology, Sasebo College  
(1-1, Okishinn , Sasebo, Nagasaki 857-1193, Japan)

E-mail:m1116@st.sasebo.ac.jp

<sup>2</sup> Lecturer, Department of Mechanical Engineering, National Institute of Technology, Sasebo College  
(1-1, Okishinn , Sasebo, Nagasaki 857-1193, Japan)

E-mail:hirosin@sasebo.ac.jp

<sup>2</sup> Professor, Department of Mechanical Engineering, National Institute of Technology, Sasebo College  
(1-1, Okishinn , Sasebo, Nagasaki 857-1193, Japan)

E-mail:t-fukuda@sasebo.ac.jp

The present paper deals with fatigue property of plasma coating film as resistance to hydrogen entry and hydrogen embrittlement. In the previous study by Yamabe et al<sup>(1)</sup> hot-dipping method were suggested. However this method shows good resistance against hydrogen entry, high temperature of the molten aluminum has a possibility to influence the strength properties of base metal. In contrast, plasma coating method doesn't give much heat to the material in which temperature increases less than 100 °C. In order to investigate the fatigue properties of the plasma coating film, four-points bending fatigue tests were performed. The surface of the coating part were observed with scanning electron microscope (SEM) to compare the surface morphologies with between before and after the fatigue test. No significant difference was observed in the both before and after the fatigue test. From this result, in the elastic deformation region (less than 3/4 of  $\sigma_y$ ) for S25C steel, the plasma coating film endure  $10^7$  times cyclic loading. By using modified Goodman diagram and tensile strength value for balk A6061,  $\sigma_w$  in case of  $R = 0$  was estimated 96.7 MPa which is greater than that of estimated stress in the aluminum alloy. Furthermore the electric power and sputtering time were changed for adjusting film thickness in order to decreasing sputtering time.

**Key Words :** hydrogen embrittlement , four-points bending fatigue tests,scanning electron microscope (SEM)

## 1. Introduction

In order to solve hydrogen embrittlement (HE) problem, the austenitic stainless steel SUS316L and aluminum alloy A6061-T6 are used as a high resistance materials against HE in a fuel cell vehicle (tank, valve and pipe). However, those materials are too expensive to make fuel cell vehicle popular into the general household. In the present paper, the plasma coating method were suggested as a high resistance to hydrogen entry. This method is considered as a economical method because high cost material will be used only at the surface of the base metal.

In the previous study by Yamabe et al<sup>(1)</sup> hot-dipping method were suggested. However this method shows good resistance against hydrogen entry, high temperature of the molten aluminum has a possibility to influence the strength properties of base metal. In contrast, plasma coating method doesn't give much heat to the material in which temperature increase less than 100 °C.

The thickness of the film formed by the (electric power 300 W, 17 h) was found to be 40 μm by In the previous study of Nishiguchi et al<sup>(2)</sup>.

This study investigates the effect of fatigue loading on the plasma coating film and relationship between sputtering time and coating thickness in order to decrease sputtering time.

## 2. Experiment method

Plasma coating (300 W, 17 h, 40 μm thickness) was applied on specimens having a rectangular cross section(Cross-section of 7.5 mm × 12 mm). JIS-S25C steel (hereinafter, S25C steel) and aluminum alloy A6061 were employed as the base material and coating material, respectively. RF sputtering deposition system was used for the coating. The chamber was evacuated to a base pressure (below  $5 \times 10^{-3}$  Pa) with a molecular pump and a rotary pump. The gas pressure was varied from the base pressure to 10 Pa by feeding Ar gas into the chamber. Distance between the target (S25C steel)

and substrate (A6061) was 50 mm. The temperature at S25C steel surface was from R.T. to 100 °C. The coating condition was 300 W and 17 h. Coated specimen was subjected to four-point bending fatigue test. Stress ratio of fatigue test was 0.048 to 0.091. Frequency was 20 Hz. As shown in Figure 1, the maximum stresses were 1/4, 1/2 and 3/4 of the yield point  $\sigma_Y$  of the carbon steel(266 MPa) Each number of cycles were  $10^7$  times. The surface of the coating part was observed with scanning electron microscope (SEM) to compare the surface morphologies between before and the fatigue test.

Furthermore the electric power and sputtering time were changed for adjusting film thickness in order to decreasing sputtering time.

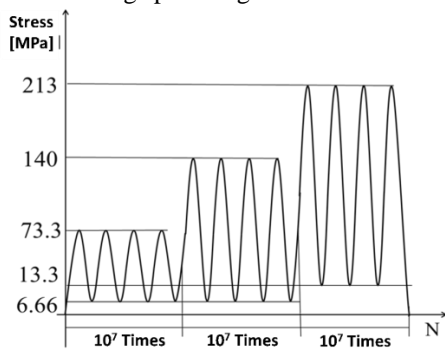


Figure 1 : The relationship between stress and the number of cycles during fatigue test.

### 3. Result and discussion

#### (1) Investigation of the fatigue properties of the coating part

Figure 2 shows the surface morphologies of the coating part observed by SEM. No significant difference was observed in the both before and after the fatigue test. In the previous report, plasma coating was fractured at the starting of plastic deformation of S25C steel under the tensile test<sup>(2)</sup>. In the present fatigue test, it is revealed that in the elastic deformation region (less than 3/4 of  $\sigma_Y$ ) for S25C steel, the plasma coating film endure  $10^7$  times cyclic loading.

From the tensile test of A6061 bulk specimen, the tensile strength,  $\sigma_B$ , was 291 MPa. The fatigue limit of A6061 in case of stress ratio  $R = -1$  can be estimated to 146 MPa by the equation of  $\sigma_w = 0.5 \sigma_B$ . By using modified Goodman diagram,  $\sigma_w$  in case of  $R = 0$  was estimated 96.7 MPa.

The Young's modulus of S25C (206 GPa) is about 3 times that of A6061 (69 GPa). Therefore under the cyclic loading, stress in the coating film can be estimated 1/3 of the stress in base metal (S25C steel). In the present study, the stress in the coating part is estimated 71 MPa (35.7 MPa in stress amplitude) at the maximum. For the further investigation, high

strength material will be used as a base metal. In addition, hydrogen effect on the strength properties of plasma coating will be investigated with the fatigue test for hydrogen-precharged specimen or fatigue test in the high pressure hydrogen gas atmosphere.

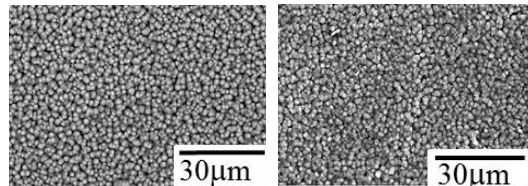


Figure 2 : Surface morphologies of coated parts. (Left: before fatigue test, Right: after fatigue test)

#### (2)The relationship between deposition time and film thickness

Under the sputtering condition, electric power is 300 W, sputtering times,  $T_s$ , are 4 h and 8 h, and distance between the target (S25C steel) and substrate (A6061) was 21.6 mm. From SEM observation of film thickness,  $t = 37 \mu\text{m}$  in case of  $T_s = 4 \text{ h}$ , and  $t = 54 \mu\text{m}$  in case of  $T_s = 8 \text{ h}$ . However, in the previous study,  $t = 40 \mu\text{m}$  in case that  $T_s = 17 \text{ h}$  and the distance between the target and substrate was 50 mm. From these results, the closer the distance between target and substrate is, the earlier the thick coating can be made which causes decreasing sputtering time.

### 4. Conclusion

- (1) The fatigue property of Al aluminum alloy A6061 plasma coating over the S25C steel was investigated. It is revealed that in the elastic deformation region (less than 3/4 of  $\sigma_Y$ ) for S25C steel, the plasma coating film endure  $10^7$  times cyclic loading at the stress ratio 0.048 to 0.091.
- (2) The closer the distance between target and substrate is, the earlier the thick coating can be made which causes decreasing sputtering time.

### 5. References

- 1) Junichiro Y., Saburo M. and Yukitaka M. : Surface coating with a high resistance to hydrogen entry under high-pressure hydrogen-gas environment, *Int. J. Hydrogen Energ.*, Vol. 38, pp. 10141-10154, 2013.
- 2) Hiroshi N., Tamiko O., Hiroharu K. and Takayuki F., Strength of plasma-coating film and effect of plasma coating on hydrogen entry, *Jpn. J. Appl. Phys.*, (to be published)

# Study of the Adhesive Strength for Single Lap Joints in Consideration of Surface Properties

Keita OTA<sup>1</sup>, Genji HOTTA<sup>2</sup>

<sup>1</sup> Student, Advanced Course of Mech Eng., National Institute of Technology, Ariake Colegge  
(150, Higashi-hagio-machi. Omuta.Fukuoka. Japan)  
E-mail:m48104@g.ariake-nct.ac.jp

<sup>2</sup> Professor, Dept., Mechanical Engineering, National Institute of Technology, Ariake Colegge  
(150, Higashi-hagio-machi. Omuta.Fukuoka. Japan)  
E-mail:hotta@ ariake-nct.ac.jp

In this study, shear stress of Single lap joint is considered appearing at the surface properties. Test pieces which have variety of surface properties are used to make the lap joint, and those are done tension test. Result of the test, what surface properties are considered efficiency of adhesive bonding design. We found that surface properties which have uniform surface and unevenness are efficiency of adhesive design.

**Key Words :** shear stress, adhesive strength, lap joint, surface property, adhesive bonding design, tension test

## 1. Introduction

This study examines the relation between shear stress of Single lap joint and the surface properties of joint planes, by regulating the JIS-K6850. Currently, glued connections are used in portable electronic devices which required to be small, space saving and the weight saving is also required in a variety of other contexts. In addition, glued connection can easily join different types of materials.

However, a lap joint may be damaged when a singular stress field occurs at the end of the joint interface. The studies related to over the past few years, several studies have been made on these singular stress fields. For example, FEM analysis by Noda<sup>1)</sup>, and an experiment by Miyazaki<sup>2)</sup>, but little attention has been given to consider surface properties.Koharada's study considers surface properties but it goes no further than doing chemical analysis.

The purpose of this study examines the strength of lap joints according to the test pieces, which have various surface properties, and also clarifies the relationship between these surface properties.

## 2.Material and method

Test pieces in this study employed those from

Park's study<sup>3)</sup>. The dimension of test piece is shown in Fig.1.

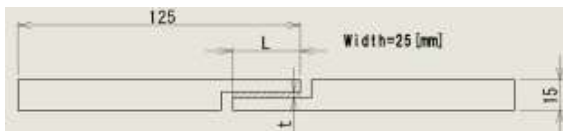


Fig.1 test piecee (unit is [mm])

In Fig.1, "t" is glue line thickness; "L" is adhesion length.In this study,  $t=0.2[\text{mm}]$ ,  $L=18[\text{mm}]$ .This study used test piece material "A2017".

In this study, three kinds of surface properties were prepared. [TYP1], derricking of joint surface is uniform (TYP1 is made by a wire electric discharge machine), [TYP2], is regular (TYP2 is made by milling), and [TYP3], is random. (TYP3 is made by hand finishing with a paper file.) The reason that these types were prepared is to observe influence in the suface exerted strength.

The roughness parameters were determined by a measuring instrument (SJ-201) and getting the roughness curve.

Fig.2 shows a micrograph of each surface property and roughness curve.

The roughness curve horizontal axis is for measurement length, and the vertical for the

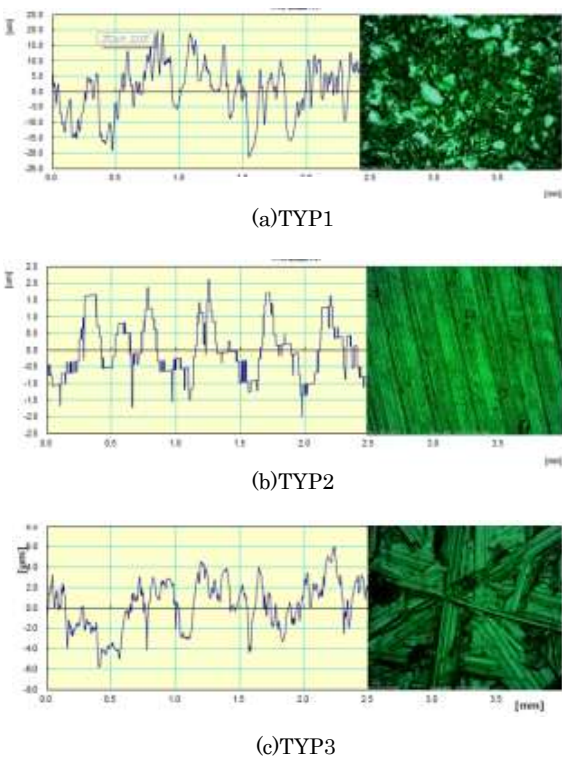


Fig.2 Each test piece of micrograph and roughness curve

surface roughness.

An Epoxy adhesive consisting of two liquids mixtures was used.

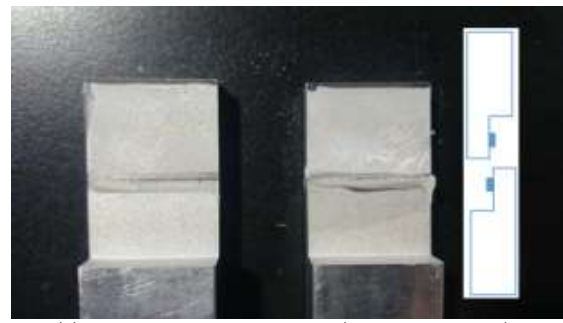
[Adhesion conditions] two liquids are mixed exact ratio(1:1), in a 20°C room, Aging time is 80 hours. Tension test was done in accordance with JIS Z 2241 by a universal testing machine at National Institute of Technology, Ariake College. Cross head speed is 0.5[mm/min]. Shear stress is determined longitudinal shear strength divided adhesion area(unit is [Pa]).

### 3.Result of the test

In TYP1 cohesion failure left adhesion residue on both planes.

But in TYP2 and TYP3, it was observed that adhesive was residual on the adhesion plane of one side only. Fig.3 shows plane of adhesive failure TYP1, TYP2, TYP3 (delamination).Also average roughness (Ra) was sought from the roughness curve.

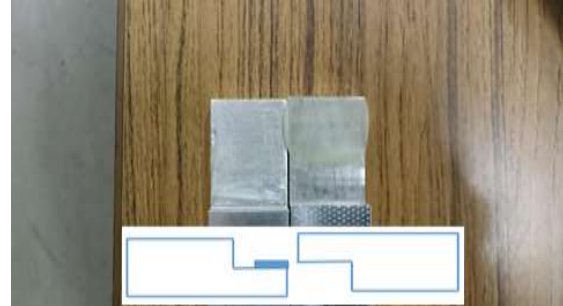
In Fig.4 the relationship between Ra and longitudinal shear strength for each surface property is shown.



(a) TYP1's adhesion residue (cohesion failure)



(b) TYP2's adhesion residue (delamination)



(c) TYP3's adhesion residue (delamination)

Fig.3 Plane of adhesive failure

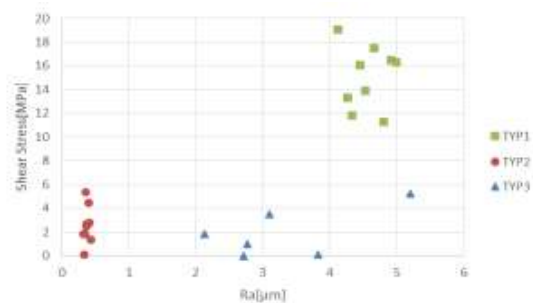


Fig.4 Relationship between Ra and shear stress strength

Fig.4 shows max shear stress value 19.8[MPa] when TYP1 is Ra=4[ μ m]. This value exceeded shear stress that maker has published it (11.1[MPa])In TYP2, the max shear stress value is 5.3[MPa] when Ra=0.36[ μ m]. TYP1 and TYP2 had

stable shear stress values but TYP3 was unstable, also the shear stress of TYP3 is lower than TYP1 and TYP2.

As shown in Fig.3 and Fig.4, it was found that surface properties of TYP1 had the largest shear stress value.

Fig.5 shows changes in shear stress. ( $R_a$  was changed.)

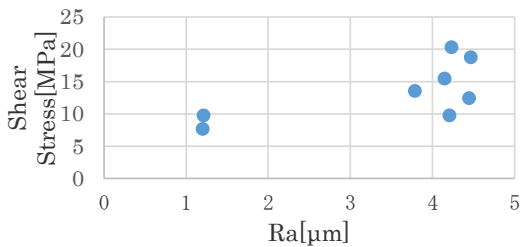


Fig.5 Relarationship between Ra and shear stress

In TYP1, shear stress increases with increasing  $R_a$ .

Determining shear stress was impossible when  $R_a$  was less than  $1.2[\mu\text{m}]$  because of the criteria of stable machining. Also Fig.7 is shown relation number of unevenness in plane of adhesive and shear stress.

Number of unevenness in plane of adhesive was decided by roughness curve.(Fig.6)



Fig.6 How to determine of number of evenness

As shown in Fig.7, shear stress decrease with increasing number of unevenness.

#### 4. Conclusion

Fig.5 shows, when surface properties is such as TYP1 and  $R_a=4\sim 5[\mu\text{m}]$ , genuine shear stress is exhibited. But when  $R_a$  is less than  $4\sim 5[\mu\text{m}]$ , it isn't exhibited.

However, Odahara's journal shows that genuine shear stress is exhibited when surface properties is as mirror( $R_a=10[\text{nm}]$ ).

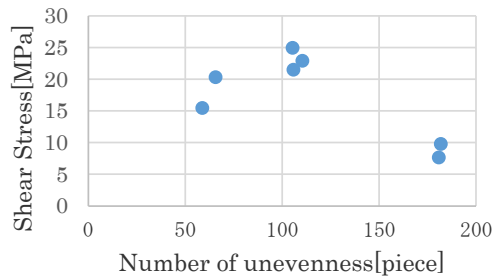


Fig.7 Relationship between number of unevenness and shear stress

These experiment yields that there are safety area and dangerous area of shear stress by surface properties.

When  $R_a$  is less than  $10[\text{nm}]$ , chemical bonding which affect between adhesive and adherend become effective, and also when  $R_a$  is more than  $4[\mu\text{m}]$  and such as TYP1, mechanical adhesion become effective. In surface properties of TYP2 and TYP3, joining is unstable because chemical bonding and mechanical adhesive are difficult to occur. It is assume that occurring singular stress field coincides with delamination, and adhesive was residual on the adhesion plane of one side only.

Fig.7 shows relevant number of unevenness which adhesive percolate through the plane. It is assume that shear stress decrease when too much unevenness.

Adhesive bonding design, it found that finishing work of surface influence of shear stress.

For getting a well trusted plane of lap joint, we should do mirror finish to make large bonding force of chemical bond or we should get unevenness such as TYP1.

That is, to select the relevant planes lead to reliability improvement of adhesive bonding design.

#### 5. References

- 1) Naoaki Noda: Convenient Debonding Strength Elution Based on the Intensity of Singular Stress for Adhesive Joints
- 2) Tatsujiro Miyazaki: Debonding Criterion for Single Lap Joints from the Intensity of Singular Stress Field
- 3) J.-H.Park, J.-H.Chi, and J.-H.Kweon: Evaluating the strength of thick aluminum joints with different adhesive lengths and thicknesses, Composite Structures, Vol. 92, pp. 2226-2235, 2010

# Charpy Impact Property on Wrought Magnesium Alloy at Cryogenic Temperature

Kenta HATANAKA<sup>1</sup>, Akihiro TAKAHASHI<sup>1</sup>, Naoyuki YAMAMOTO<sup>1</sup>, Hiromi MIURA<sup>2</sup>,  
Masakazu KOBAYASHI<sup>2</sup> and Yasuhiro NAKIYAMA<sup>3</sup>

<sup>1</sup>Student, Dept. of Mechanical Engineering., National Institute of Technology, Miyakonojo College  
(473-1, Yoshio-cho, Miyakonojo-city, Miyazaki 885-8567, Japan)

<sup>2</sup>Dept. of Mechanical Engineering, Toyohashi University of Technology  
(1-1, Tempaku-cho, Toyohashi-city, Aichi 441-8580, Japan)

<sup>3</sup>Dept. of Mechanical Engineering., National Institute of Technology, Kagoshima college  
(1460-1, Shinko, Hayato-cho, Kirishima-city, Kagoshima 899-5193, Japan)

Research on mechanical properties of the magnesium alloys at low temperature is few. In this study, deformation and fracture behavior of the magnesium alloy at cryogenic temperature were investigated. As received rolled AZ31B magnesium material was used. Charpy impact test was carried out at temperatures of range from 77K (-196°C) to 293K (20°C) with loading velocity of approximately 4.76 m/s for standard size V-notch specimen. Impact load-displacement responses of the alloy tested at 293 K and 77 K were evaluated. Failure begin of both specimens was achieved at maximum load,  $P_{max}$  and toughness at 77 K was degradable compare with that at 293 K. From observation results of crack path behavior, formation energy of fracture surface of specimen tested at 293 K was higher than that tested at 77 K.

**Key Words :**wrought magnesium alloy, impact test, low temperature, absorbing energy, fracture behavior

## 1. INTRODUCTION

Light-weight materials have a high potential for weight reduction to improve fuel consumption and emissions in transportation and logistics industries. The automobile industry made a voluntary commitment to reduce fuel consumption by 25 % in comparison with 1990 levels by the year 2005 [1]. Therefore, there is a growing trend to substitute these nonferrous materials for conventional steel and cast irons especially in automobile industrial field. Compared to steel structural materials, the mechanical property of nonferrous materials, such as aluminum, titanium and magnesium base alloys under impact loading is much less investigated. In general, the number of research on dynamic deformation and failure of magnesium alloys is not many. The knowledge of dynamic deformation response of the light-weight structures is essential in improving and developing product resistance to shock loading, for crashworthiness, safety, and reliability. For important information used as the basis of mechanical design, the three point bending properties under the moderate impact loading condition have been extensively measured by Charpy impact testing machine. Due to its simple and convenient nature, the Charpy impact test has been used widely for

screening of materials. However, structures have been designed on the basis of strength at quasi-static strain rate and at ambient temperature without considering a Charpy impact test result. In this paper, the purpose of this investigation is to evaluate fundamentally impact toughness and fracture morphology on wrought AZ31B magnesium alloy tested at cryogenic temperature by Charpy impact testing machine.

## 2. EXPERIMENTS

The material used in this study was a rolled AZ31B magnesium alloy of thickness of 10 mm, received from OSAKA FUJI CORP. (Amagasaki, JAPAN). The chemical composition of is presented in Table 1. Table 2 shows tensile properties and Vickers hardness of the alloy.

Fig.1 shows Charpy impact testing machine (TOKYO Kouki Ltd, capacity 170 J) in this study. Initial impact velocity was 0.8 m/s by low blow test to avoid oscillations accompanying with inertial loading [2].

Charpy impact test was conducted in accordance with JIS Z 2242 method. Standard V-notched Charpy specimen was prepared with dimensions of 10 mm ×

10mm × 55 mm and notch depth of 2 mm, and machined perpendicular to the rolling direction as shown in Fig.2.

Impact tests were carried out at various temperatures of 77 K (-190°C), 123 K (-150°C), 183 K (-90°C), 223 K (-50°C) and 293K (20°C). Liquid cryogens such as dry ice, isopentane (2 – methylbutane) and liquid nitrogen were used to achieve various prescribed temperatures as shown in Fig.3 [3,4]. To determine testing temperature, a cooling curve was measured for dummy sample of the rolled AZ31B alloy attaching a thermocouple before Charpy test. After having reached a testing temperature, specimen was moved on the machine anvil, and then the impact test was conducted within one second. An accurate impact test that held a temperature change of a testing specimen when conveyed it to the anvil was carried out carefully. In addition, impulse,  $E_{\text{impulse}}$  as a kind of absorbing energy was calculated by load-time curve obtained from specimen attached strain gage as shown in Fig.4. This measurement was described in reference [5]. Yield load,  $P_y$  and maximum load,  $P_{\max}$  in the Charpy impact property were determined from the load-time curve obtained by the specimen attaching a strain gage.

**Table 1** Chemical Composition of the AZ31B in used study.

Al	Zn	Mn	Fe	Si	Cu	Ni	Mg
3.0	0.7	0.1	≤	≤	≤	≤	Bal.
8	6	5	0.10	0.10	0.10	0.10	

**Table 2** Tensile property and Vickers hardness of rolled AZ31B magnesium alloy used in this study.

<b>Yield stress (MPa)</b>	153
<b>Tensile strength (MPa)</b>	218
<b>Elongation (%)</b>	12
<b>Vickers hardness (HV)</b>	60



**Fig.1** Configuration of Charpy testing specimen.

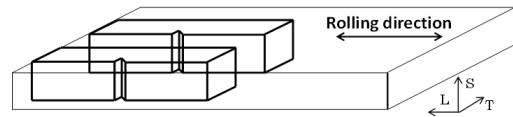


**Fig.2** Charpy impact testing machine used in this study.

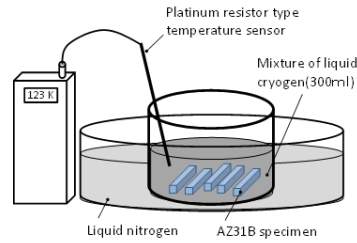


**Fig.3** Schematic illustration of the specimen cooling method to achieve various prescribed temperatures.

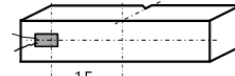


**Fig.4** Schematic showing attachment position of a strain gage on specimen surface for impulse,  $E_{\text{impulse}}$ .

### 3. RESULTS AND DISCUSSION

Typical load-time curves of the Charpy impact specimen at room temperature and cryogenic temperature of 77 K are shown in Fig.5, from which their respective yield load,  $P_y$ , maximum load,  $P_{\max}$  and absorbing energy,  $E_{\text{impulse}}$  were measured. Yield load at 77 K is approximately 4.5 % higher than that at room temperature, but maximum load is 13 % lower than at room temperature. According to research on Wang et al., on Mg-rare earth alloys [6], yield strength increased while ductility decreased as the testing temperature degreased. Elastic compliances at different testing temperatures are almost same. On the other hand, the impulse,  $E_{\text{impulse}}$  is expressed as follows equation (1):

$$E_{\text{impulse}} = E_{i,\text{impulse}} + E_{p,\text{impulse}} \quad (1)$$

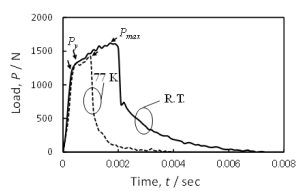
where  $E_{i,\text{impulse}}$  and  $E_{p,\text{impulse}}$  are impulse component of crack initiation and crack propagation, respectively in shown in Fig.6. It can determine each impulse value to measure area in the load-time curve using planimeter. Fig.7 shows change of the entire impulse,  $E_{\text{impulse}}$  at room temperature and 77 K for the rolled AZ31B specimen. The impact impulse at 77 K was 1.38 N · s and approximately 63 % lower than that at room temperature. The  $E_{i,\text{impulse}}$  at room temperature and 77 K accounted for about 59 % and 75 % of the impulse,  $E_{i,\text{impulse}}$ . It was found that crack propagation component does not nearly exist at 77 K, and most of the overall impulse until fracture was occupied by crack initiation component.

Fig.8 represents the absorbing energy,  $E_{t,dial}$  and the lateral expansion rate, L.E. versus testing temperature for the Charpy impact specimen in used study. As result from equation (1) calculation, the absorbing energy at 77K was approximately 54% lower than that at room temperature. The energy showed a tendency to decrease linearly as decreasing temperature. This shift in energy absorption with temperature means embrittlement in used material. In previous study, cryogenic absorbing energy of AZ61 magnesium extruded alloy showed degradation of 55 % compare to room temperature absorbing one [7].

Lateral expansion on the compression side of the Charpy impact specimen occurs and undergoes a transition from small values at low temperature to large values at high temperature. It is well known that lateral expansion and ductility of material have strong correlation and this increase in observed plastic deformation is consistent with the absorbing energy trend [8]. As results, lateral expansion at 77 K was 47 % lower than that at room temperature. That of 77 K and 123 K is almost same, but lateral expansion represented a tendency to degrease like a change of the absorbing energy monotonically. It is interesting to note that these results were shown to be in relative agreement with the degradation of cryogenic toughness in Fig.8. According to previous study by authors, lateral expansion at 83 K of extruded AZ61 magnesium alloy was 46 % lower than that at room temperature [7]. This shift in lateral expansion with temperature also means embrittlement in rolled AZ31B.

Fig.9 shows photographs of the crack propagation path of the lateral specimen surface after impact test at room temperature, (a) and at cryogenic temperature, (b). In Fig.9 (a), intensive plastic deformation was ahead of notch bottom, and then crack path was not straight and made a wide detour with ductility large shear lip.

On the other hand, In Fig.9 (b), the whole plastic zone size was small compare with Fig.9 (a), and crack propagation behavior keep in a straight, thus it has a marked tendency toward brittle fracture.



**Fig.5** Typical load-time curves obtained from the Charpy impact test at room temperature and 77 K.

**Table 3** Charpy impact properties of AZ31B specimen at room temperature and 77K.

	R.T.	77 K
Yield load, $P_y$ (N)	1177	1290
Peak load, $P_{max}$ (N)	1605	1418
Impulse, $E_{impulse}$ ( $N \cdot s$ )	3.71	1.38
Absorbing energy, $E_{t,dial}$ (J)	7.4	3.4

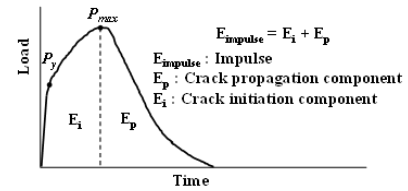


**Fig.6** Schematic diagram for the impulse evaluation by load-time curve obtained from instrumental impact test.

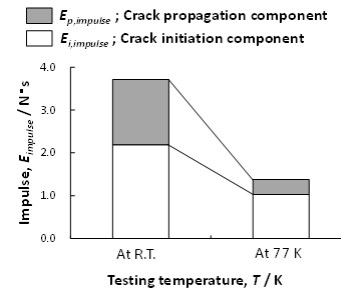


**Fig.7** Change of the impact impulse,  $E_{impulse}$  of the rolled AZ31B specimen tested at room temperature and 77 K.

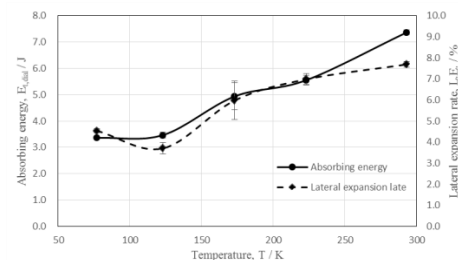
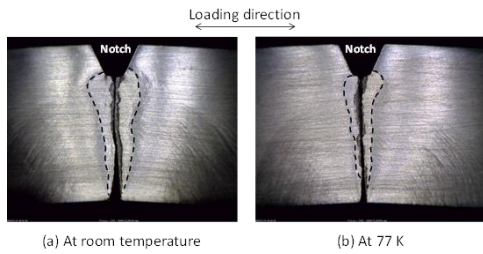


**Fig.8** Relationship between absorbing energy,  $E_{t,dial}$ , Lateral expansion rate and testing temperature.

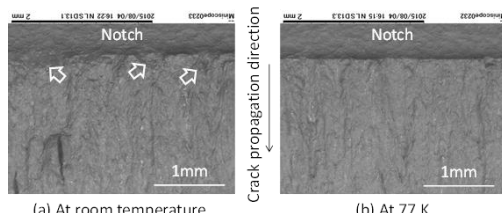
Fig.10 shows appearance of fracture surface near notch root after impact test at room temperature, (a) and at cryogenic temperature, (b). In Fig.10 (a) at room temperature, there was unevenness on the entire surface in comparison with Fig.13 (b) at 77 K. Arrows in Fig.10 (a) means the growth region of ductile shear fracture zone. The fracture surface of this shear zone between the notch root and dashed line is relatively smooth and approximately 45 degree angle with the surface as shown in Fig.11. Ductile shear zone area at room temperature is larger than that at cryogenic temperature. Larger shear zone ahead of the notch-tip can be explained increasing of absorbing energy during impact fracture process. These observation results were in good agreement with the impact absorbing energy in Fig.8 obtained from impact tests. Moreover, the plastic zone size of crack-tip increases as a result of decreasing yield load,  $P_y$  at room temperature as shown in Table 3, leading to a blunt crack front to improve intrinsic toughening.

Fig.12 shows the crack propagation zone of

specimen tested (a) at room temperature and (b) 77 K.



**Fig.9** Schematic showing impact crack propagation path of the rolled AZ31B magnesium specimen tested at room temperature, (a) and 77K, (b).



**Fig.10** Schematic showing impact crack initiation region near notch root of the rolled AZ31B magnesium specimen tested at room temperature and 77 K, (b). Arrows indicate intensively growth of ductile shear zone.

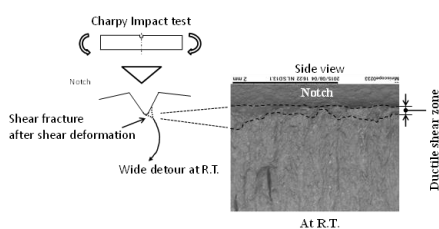


**Fig.11** Schematic illustration of the occurrence mechanism of the ductile shear zone in a front of notch-tip in this study.

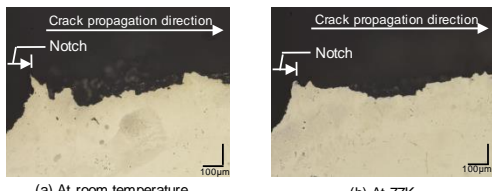


**Fig.12** Schematic showing impact crack propagation near notch root of specimen tested (a)room temperature and 77K

#### 4. CONCLUSION

In this study, impact test at cryogenic temperature was conducted for the rolled AZ31B magnesium alloy, which impact toughness and fracture morphology was investigated and evaluated fundamentally. The results of this work can be summarized as follows.

- (1) In rolled AZ31B magnesium alloy, yield load,  $P_y$  at 77 K is approximately 4.5 % higher than that at room temperature, but maximum load,  $P_{max}$  is

13 % lower than at room temperature. Cryogenic impact toughness at 77 K,  $E_{t,dial}$  showed degradation of approximately 54 % compared to room temperature toughness. In addition, the impact impulse,  $E_{impulse}$  at 77 K was 1.38 N · s and approximately 63 % lower than that at room temperature.

- (2) The lateral expansion rate at 77 K was 47 % lower than that at room temperature. Lateral expansion represented a tendency to decrease like a change of the absorbing energy monotonically.
- (3) At room temperature, intensive plastic deformation was observed in the ahead of notch bottom, and then crack path was not straight and made a wide detour with ductility large shear lip. On the other hand, at 77 K, the whole plastic zone size was small compare with the fracture morphology at room temperature, and crack propagation behavior keep in a straight, thus it has a marked tendency toward brittle fracture as test temperature becomes cryogenic atmosphere.

#### REFERENCES

- 1) D. Engelhart, D. and C. Modl, "Die Entwicklung des Audi A2," Conference Paper on Technologien um das 3L-Auto, pp. 16-18, 1999.
- 2) T. Kobayashi, "Progress in the Instrumented Charpy Impact Test," Materials Science Research International, vol.8, No.3, pp.141-150, 2002.
- 3) Takahashi, T. Kobayashi, H. Toda and T. Mizutani, "Effect of Testing Temperature from Cryogenic to High Temperatures on Dynamic Fracture Properties in 5083 Aluminum Alloy," J. J. Ins. Of Light Metals, vol. 50, No.8 pp.386-391, 2000.
- 4) Takahashi, K. Murayama, N. Yamamoto, T. Toyohiro and Y. Todaka, "Impact Behavior at Low Temperature of Severe Plastic-Deformed Pure Iron Treated by High Pressure Torsion," Proceedings of the 2nd Japan-Thailand Friendship International Workshop on Science, Technology and Education, vol. 2, pp. 213-216, 2012.
- 5) L. Wang, T. Kobayashi, H. Toda and M. Hayakawa, "Effects of Loading Velocity on Fracture Toughness of a SiCw / A6061 Composite at Elevated Temperatures," Mater. Trans. JIM, vol.40, No.10, pp.1056-1062, 1999.
- 6) H. Wang, S. Dong and G. Lu, "Study of Tensile Properties of Mg-Rare Earth Alloys at Cryogenic Temperatures," Vision, Image and Signal Processing, Protection of Materials and Structure from the Space Environment, vol. 32, pp. 381-388, 2013.
- 7) Takahashi, N. Yamamoto and T. Toyohiro, "Fundamental Study on Impact Toughness of Magnesium Alloy at Cryogenic Temperature," Inter. J. of Innovations Eng. Tech., Special Issue, pp.7-14, 2015.
- 8) T. H. Courtney, "Mechanical Behavior of Materials," McGraw-Hill International Editions, p.436, 2000.

# Synthesis and Characterization of Novel Aromatic Polymer with Benzoxazine Functionality

<sup>1</sup>Mizuki Otsuka , <sup>2</sup> Nobuyuki Furukawa

<sup>1</sup>Student, Advanced Engineering Course of complex Engineering, National Institute of Technology, Sasebo College  
(1-1 Okisin-tyou, Nagasaki 857-1193, Japan)  
E-mail:cb1505@st.sasebo.ac.jp

<sup>2</sup>Professor, Department of Chemical and Biological Engineering, National Institute of Technology, Sasebo College  
(1-1 Okisin-tyou, Nagasaki 857-1193, Japan)  
E-mail:n-Furukawa@sasebo.ac.jp

In this study, a new class of thermosetting polymers or oligomers, polybenzoxazines were synthesized from various aromatic diamines, bisphenol-A and paraformaldehyde by Mannich reaction condition. It was found that introduction ratio of benzoxazine structure in the polymer backbone were influenced by solvent polarity and structure of diamine components, probably due to effect on the polymerization rate. Self-standing films from the benzoxazins were prepared by solution cast method. Furthermore, the polymer properties such as thermal reactivity, thermal and mechanical properties were characterized.

**Key Words:** Polybenzoxazine, Thermosetting resin, Thermal properties

## 1. INTRODUCTION

Recently, many kinds of high performance thermosetting resins are developed and used for electronic industries. They are required various properties such as stability and reliability under condition of high temperature and high humidity.

Benzoxazine is a new thermosetting resin. The reaction proceeds by ring-opening polymerization. It surpasses conventional materials in mechanical strength, thermal stability and durability under humid environment.

However, toughness of benzoxazine which was lowered depending on increase of the cross linking density and happened reduction of volatile components under 300 °C were reported in previous studies.<sup>(1)</sup> So, we have to improvement its brittleness.

High polymer benzoxazine precursors have been synthesized from diamine, bisphenol-A and paraformaldehyde. They have many various prepare such as heat-resistant, low moisture and low shrinkage during curing.

In this research, aromatic polymers which contained benzoxazine functionality in the main chain structure, thermal and mechanical

properties of the functional aromatic polymers were analyzed. The several kinds of polymers revealed free standing and flexible properties.

## 2. EXPERIMENTAL

### (1) Syntheses of polybenzoxazine precursors

Polybenzoxazine, which were thermosetting precursors were prepared by Mannich reaction pathway as shown in Figure1. BAPP (0.1mol), bisphenol-A (0.1mmol) and paraformaldehyde (0.4mol) were mixed together in methanol and refluxed for 10 h. After the reaction mixture was treated by 1N NaHCO<sub>3</sub> aqueous solution for removing unreacted BPA, solid state product was obtained. The product was washed several times with water and dried under vacuum condition. We had used diamine monomers with three phenylene group such as ODA and MDA, and with four phenylene group such as BAPP, BAPS and BODA (see Fig.2).

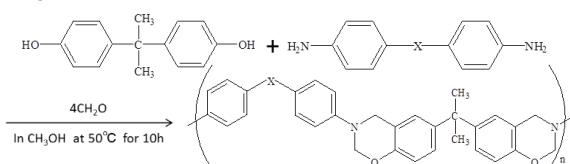


Fig.1 synthesized of polybenzoxazine

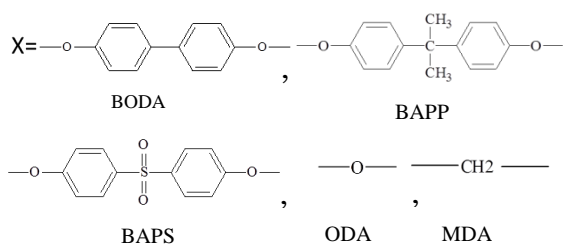


Fig.2 Each of amines

Firstly, we had researched about solvent effect for polymerization reaction and for benzoxazine ring formation into the polymer backbone.  $\text{CHCl}_3$ , dioxane and N,N-dimethylacetamide (DMAc), methanol were used as solvent on the synthesis of polybenzoxazine.. Secondly, we had researched about influence of difference of diamine structure on the reaction.

### (2) Preparation of precursor films

The polybenzoxazine product (5g) was dissolved in dioxane (25g), and the solution was cast on glass plate. Then, solvent was removed by pre-heating at  $50^\circ\text{C}$  for 10 h. Heat treatment of the precursor films at 105, 140, 200 and  $240^\circ\text{C}$  for 1h each gave brown transparent polybenzoxazine films.

### (3) MEASURMENTS

The structure of precursor was analyzed by NMR and FT-IR. The thermal properties were measured by DSC, TG/DTA and DMA.

### 3. RESULTS AND CONCLUSION

The average molecular weight ( $M_w$ ) of the polybenzoxazine was estimated from GPC. The molecular weight was in the range of 1000-300 which is not so high (so-called oligomer), as shown Table1.

Table.1 molecular weight of the precursor

	Chloroform	Methanol	Dioxane	DMAc
Mn	907	3108	2663	1466

The rate of introduction benzoxazine ring and methylene unit into the oligomer was calculated based on results of  $^1\text{H-NMR}$  analysis as shown in Table 2. We founded that synthesis using Chloroform and Methanol as reaction solvent, is given much benzoxazine ring introduction than other solvents. The results was considered that Mannich reaction was accelerated because of the effect of acidity on

phenolic group of BPA (self-acid catalyst is promoted the reaction).

Table2. The rate of introduced oxazine ring and methylene

Standard	The ratio	Chloroform	Methanol	Dioxane	DMAc
Aromatic ring	ring structure	19.8	31.5	2.62	5.82
	introduction of methylene	32.5	31.5	14.9	5.82
Methyl group	ring structure	22	37.6	2.26	7.44
	introduction of methylene	36.2	37.6	12.9	7.44

The  $^1\text{H-NMR}$  was also measured to confirm the structure. The aromatic protons appeared at range of 6.6-7.3ppm. The characteristic peaks assignable to methylene ( $\text{O}-\text{CH}_2-\text{N}$ ) and methylene of oxazine ( $\text{Ar}-\text{CH}_2-\text{C}$ ) was observed at 5.2and 4.5ppm, respectively. Also, the methyl proton proton of BPA and methylene proton appeared at 1.6 and 3.7 ppm, respectively, confirming the formation of precursor.

TG-GTA and DMA profiles of the Precursor are shown in Fig. 4 and Fig. 5.

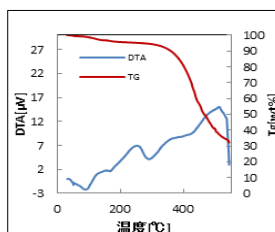


Fig. 4. TG/DTA of polybenzoxazine precuesor

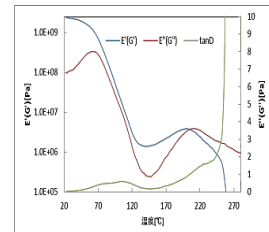


Fig. 5. DMA of polybenzoxazine film cured at  $140^\circ\text{C}$

The polybenzoxazine (BPA/BAPP)  $T_g$  was found at  $106^\circ\text{C}$  from  $\tan\delta$  ( $E''/E'$ ) in Fig. 4. The polybonzoxazine precursor was heated up to  $140^\circ\text{C}$ , and it was given yellow film. We understood that the curing reaction happened at  $250.1^\circ\text{C}$  in Fig.5.

In addition, it was found that the molecular weight was influenced from structural difference of diamines, probably due to the reactivity of amino-group, as shown Table3.

Table.3 molecular weight of the precursor

	BODA	BAPS	ODA	MDA	BAPP
Mn	1834	1950	15675	12636	3108

We though that synthesis used two ring diamine was better than four ring diamine.

### REFERENCE

- 1)A.Sudo, R.Kudoh, H.Nakayama,K.Arima and T.Endo, Macromolecules, Vol.41, p9030(2008)
- 2)T.Takeichi, T.Kano, T.Agag, Polymer, Vo.46, p12172(2015)

# Effect of Lactic acid bacteria on Awamori spirits quality

Shoya ARAKAWA<sup>1</sup>, Masato MIYAHIRA<sup>2</sup>, Shinya IKEMATSU<sup>3</sup>, Makoto MIYAGI<sup>4</sup>  
and Yasutomo TAMAKI<sup>5</sup>

<sup>1</sup> Student, Advanced Course of Bioresources Eng., National Institute of Technology, Okinawa College  
(Henoko 905, Nago-city, Okinawa 905-2171, Japan)

E-mail: ac144802@edu.okinawa-ct.ac.jp

<sup>2</sup> Student, Graduate School of Environmental Science, Hokkaido University  
(N10-W5, Kita-ku, Sapporo, Hokkaido 060-0810, Japan)

E-mail: miyahira@eis.hokudai.ac.jp

<sup>3</sup> Professor, National Institute of Technology, Okinawa College  
(Henoko 905, Nago-city, Okinawa 905-2171, Japan)

E-mail: ikematsu@okinawa-ct.ac.jp

<sup>4</sup> Student, Advanced Course of Bioresources Eng., National Institute of Technology, Okinawa College  
(Henoko 905, Nago-city, Okinawa 905-2171, Japan)

E-mail: ac144811@edu.okinawa-ct.ac.jp

<sup>5</sup> Associate Professor, National Institute of Technology, Okinawa College  
(Henoko 905, Nago-city, Okinawa 905-2171, Japan)

E-mail: tamaki@okinawa-ct.ac.jp

Awamori is the traditional distilled spirits brewed in Okinawa. It is made from indica rice, and fermented with black koji and yeast. One of awamori's attractivity is "Aging" by maturing. Awamori changes to a mellow flavor and smell by aging. Flavor compounds of aged awamori are well known. Vanillin is one of the typical aged awamori flavor compounds that has sweet vanilla flavor. It has been reported that vanillin is produced when ferulic acid derived from raw material rice is converted into 4-vinyl guaiacol (4-VG) by acid of awamori mash and heat from distillation, the 4-VG gets oxidized in distillate.

In this study, we focused on the lactic acid bacteria many of which exist in awamori mash and grows on the early stage in fermentation awamori mash, and searched the strain producing 4-VG which is a precursor of vanillin. Subsequently, we brewed awamori to use the highest conversion rate strain. In addition, we evaluated manufacturing process to analyze the typical awamori flavor compounds for our brewed awamori by HPLC and GC/MS.

As a result, first, we isolated 181 lactic acid bacteria strains from awamori mash. Of these, 22 strains can convert from ferulic acid to 4-VG. Especially, strain T13 which has the highest 4-VG conversion rate was estimated to be *Lactococcus lactis*. When it is cultured in 100ppm ferulic acid containing MRS liquid medium, the rate from ferulic acid to 4-VG was 89.2%. Next, by the brewed awamori to use strain T13, we found that this awamori significantly increased in 4-VG.

In conclusion, we discovered that lactic acid bacteria in awamori mash relates to changing flavor compounds composition. In addition, it is suggested that we can produce flavor rich awamori to use lactic acid bacteria.

**Key Words :** Awamori, spirits, fermentation, lactic acid bacteria, vanillin, flavor, bioconversion

## 1. INTRODUCTION

Awamori is a traditional distilled spirits in Okinawa, made from Thai rice. One of Awamori's attractivity is "aging" by maturing. Maturing makes smooth taste and flavor, increase quality. One of aged Awamori's typical flavor compound is found-

ed vanillin<sup>1)</sup> (Fig.1). Brewing Awamori that have these characters, fermentation of mash relate not only koji and yeast but also lactic acid bacteria and so on<sup>2)</sup>. Changing of These bacterial flora may affect Awamori quality. But, it is not well known.

In this study, we focused on the lactic acid bacteria many of which exist in awamori mash and grows

on the early stage in fermentation awamori mash, and searched the strain producing 4-vinylguayacol (4-VG) which is a precursor of vanillin. Subsequently, we brewed awamori to use the highest conversion rate strain. In addition, we evaluated manufacturing process to analyze the typical awamori flavor compounds for our brewed awamori.

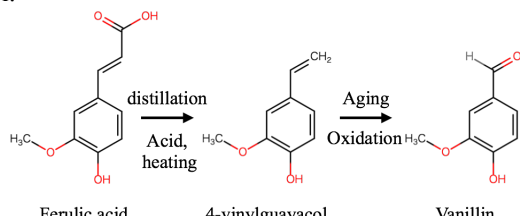


**Fig.1** Process of producing vanillin

## 2. METHODS

### (1) Isolation lactic acid bacteria from Awamori mash

#### a) Isolation lactic acid bacteria

We picked up mash from some Awamori breweries in Okinawa. It continued first fermented day to after five days. Mash 0.5g were mixed 0.1M phosphoric acid buffer (pH7.2) 4.5ml, and shaked 30 seconds. After that, there were serially diluted and inoculated on MRS agarose solid medium. Incubate condition was 24 hours on 30°C under anaerobic condition. Colonies that can make halo were picked up by sterile toothpicks, preserved as stub culture on refrigerator. And counted colonies on plates, calcurnated total viable bacterial counts of lactic acid bacteria.

#### b) Exam of changing ferulic acid to 4-VG

Picked lactic acid bacteria added 100ppm ferulic acid / MRS medium. After incubated 48 hours, measured amounts of ferulic acid and 4-VG.

#### c) Genetic analysis

We identified expected strain species by 16S rRNA region analysis. It was used BLAST for homology search. Sequence was used CEQ8800 (Beckman Coulter), DTCS Quick Start Master Mix (Beckman Coulter).

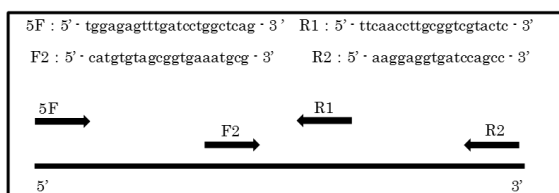


**Fig.2** Primers and 16S rRNA amplified region

### (2) Brewing Awamori using lactic acid bacteria

Brewing process of Awamori separates four steps. At first, making Koji (solid fermentation of rice), second, fermentation of mash, and third, distillation, the last, maturing. We brewed Awamori by that process. In addition, we tried co-fermentation lactic acid bacteria and mash flora in mash. Considering that lactic acid bacteria usually is low alcohol resistance, we examined 4-VG content to delay adding yeast. And furthermore, considering Awamori quality changing by to delay adding yeast, we examined only to delay adding yeast.

Mash fermentation period was 15 days, continued sampling mash.

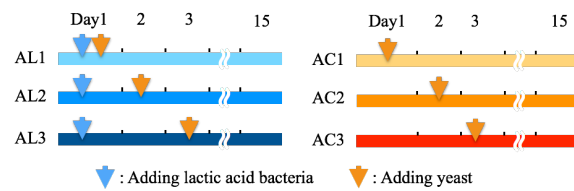


**Fig.3** Fermentation of Awamori mash

### (3) Analysis of flavor compounds

These are showed tables of each analysis conditions below. Mash and distilled Awamori were filtered by using 0.45um filter as necessary.

#### a) Ferulic acid, 4-VG and vanillin

Table 1 Analysis condition of ferulic acid, 4-VG and vanillin	
Instruments	Nexera (SHIMADZU)
Column	XBridge Shield RP18, 4.6mm x 50mm, 3.5μm
Mobile phase	A : 50mM acetic acid-sodium acetate buffer (pH4.0) B : acetonitrile or methanol
Speed	1.0mL/min
Coloum temp.	30°C
Injection	3uL
Detection	PDA (ferulic acid : 320nm, 4-VG : 258nm, vanillin : 280nm)

**Table 2** Gradient condition

Time (min)	A (%)	B (%)
0.0	90	10
7.0	70	30
12.5	20	80
15.0	90	10
20.0	90	10

#### b) Low boiling point flavor compounds

Low boiling point flavor compounds are main flavor compounds in Awamori.

**Table 3** Analysis condition of low boiling point flavor compounds

Instruments	GCMS-QP2010 ultra (SHIMADZU)
Column	HS : Trubomatix110 (PerkinElmer)
Vaporizing temp.	Stabliwax 60m x 0.25mm x 0.50um 200°C
Coloum temp.	60°C→5°C/min→120°C→8°C/min→ 200°C
Ionization	EI (200°C)
Injection	3 μl
Carrier gas	He (23.0cm/sec)

### c) Organic acid

Organic acid becomes the parameter of judging the performance of koji and a state of mash.

**Table 4** Analysis condition of organic acids

Instruments	G7100A (Agilent Technologies)
Column	Fused silica capirally 75um, 72cm
Buffer	α -AFQ133
Coloum temp.	25°C
Preparation	Run at Buffer, 300sec
Voltage	-20.0kV
Injection	Apply presstre (50mbar, 4sec)
Detection	DAD (Sig.=350nm, Ref.=230nm)

### d) Alcohol concentration

Alcohol concentration is the parameter of judging the progress of alcohol fermentation in mash.

**Table 5** Analysis condition of alcohol concentration

Instruments (mash)	GC/MS-QP2010 Ultra (SHIMADZU)
Column	HS : Turbomatrix110 (PerkinElmer)
Vaporizing temp.	Stabilwax 60m x 0.25mm x 0.50μm 200°C
Column temp.	60°C→20°C/min→200°C
Ionization	EI (200°C)
Injection	3 μl
Carrier gas	He (23.0cm/sec)

## 3. RESULTS

### (1) Isolation lactic acid bacteria from mash

#### a) Isolation lactic acid bacteria

We isolated 181 lactic acid bacteria strains from awamori mash. There were not any viable lactic acid bacteria after day 4.

**Table 6** Number of isolated lactic acid bacteria strains

Brewery	A	B	C	D	E	F
Number	148	0	0	0	0	33

**Table 7** Number of total viable lactic acid bacteria

Brewery	Day1	Day2	Day3	Day4	Day5
A	5.3x10 <sup>5</sup>	3.3x10 <sup>8</sup>	8.5x10 <sup>7</sup>	0	0
F	3.3x10 <sup>2</sup>	2.3x10 <sup>3</sup>	8.0x10 <sup>2</sup>	0	0

#### b) Exam of changing ferulic acid to 4-VG

Of 181 all lactic acid bacteria strains, 22 strains can convert ferulic acid to 4-VG. Some chromatogram are showed Fig.4.

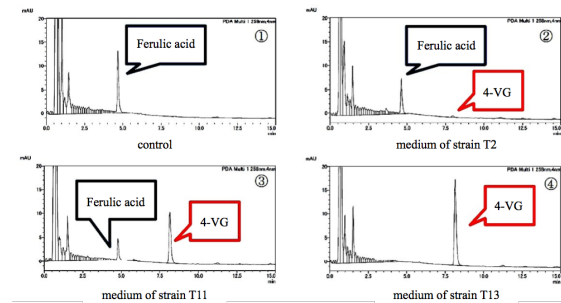


Fig.4 Chromatogram of exam

#### c) Genetic analysis

We identified 3 strains. Then, one is *Lactobacillus plantarum*, the other is *Lactococcus lactis*. *Lactobacillus* is a putrefactive lactic acid bacteria, but *Lactococcus* is not<sup>3)</sup>. Therefore, we tried to brew Awamori to use T13 strain.

**Table 8** Result of 16S rRNA analysis

T02	<i>Lactobacillus plantarum</i>
T11	<i>Lactococcus lactis</i>
T13	<i>Lactococcus lactis</i>

#### (2) Analysis of flavor compounds in Awamori

Awamori mash to use T13 strain, alcohol concentration increased 15% over in Day15. It was had much citric acid than acetic acid. Therefore, it is suggest that to use T13 strain don't affect mash fermentation.

Concentration of each low boiling point flavor compounds in distilled Awamori is not mush different due to use T13 strain.

Ferulic acid and vanillin in distilled Awamori were not detected. Concentration of 4-VG was increase as to delay adding yeast, it reached up approximately 4 times of control.

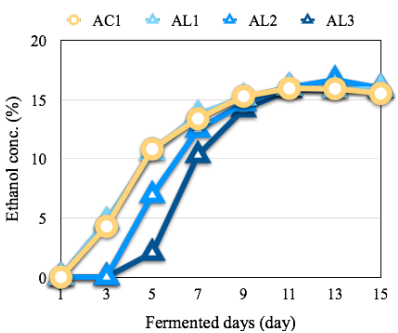


Fig.5 Changing alcohol concentration in Awamori mash

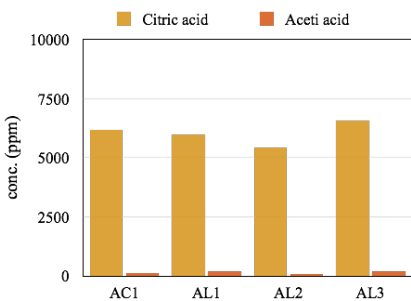


Fig.6 Concentration of organic acids in Awamori mash

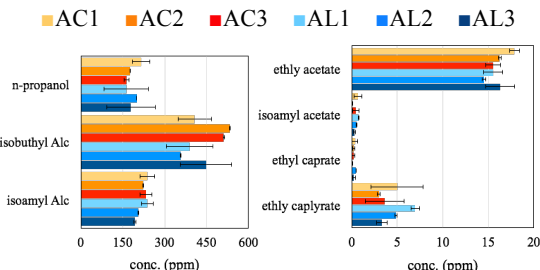
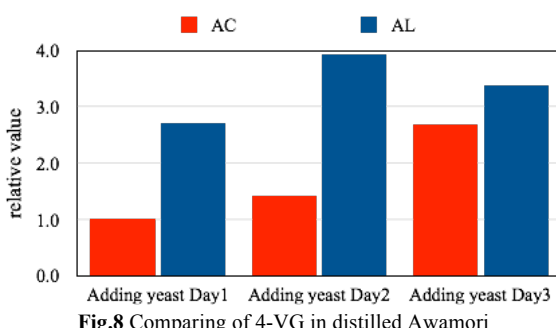


Fig.7 Concentration of low boiling point flavor compounds in distilled Awamori



#### 4. DISCUSSION

##### (1) Effects of lactic acid bacteria in mash and to delay adding yeast

Lactic acid bacteria is regarded as to cause pufification, but on the other hand, it can make a flavor compound 4-VG in this study. It show relation on

lactic acid bacteria and Awamori quality.

Lactic acid bacteria from Awamori mash can't be isolated after fermentation period Day4. It is suggested that growth of lactic acid bacteria is prevented by provided yeast in usual brewed Awamori. In the fact, to delay adding yeast is slow to increase alcohol concentration (Fig.5), and these Awamori has much 4-VG than control (Fig.8). Therefore, lactic acid bacteria in Awamori mash needs low alcohol concentration to produce 4-VG.

There is not much different at low boiling point flavor compounds due to delay adding yeast (Fig.7), but at 4-VG concentration, increased as to delay adding yeast regardless of adding lactic acid bacteria (Fig.8). So that, it is suggested that 4-VG is produced at early fermentation period in low alcohol concentration. In addition, it shows that can make much more 4-VG by to use lactic acid bacteria.

##### (2) Producing 4-VG rich Awamori

Our new production method can brew 4-VG rich Awamori that approximately 4 times than control (Fig.8). And so, we develop production method of 4-VG rich Awamori. Maturing this Awamori, will become vanillin rich Awamori.

#### 5. CONCLUSION

We discovered that lactic acid bacteria in awamori mash relates to changing flavor compounds composition. In addition, we develop production method of 4-VG rich Awamori.

**ACKNOWLEDGMENT:** I am grateful to Prof. Tamaki and Mr.Miyahira for helpful comments and suggestions. Special thanks also go to Prof. Ike-matsu and Mr.Miyagi who provided technical help.

#### REFERENCES

- Significance and production mechanism of vanillin in Awamori, Takuya Koseki, Kimio Iwano, *Journal of the Brewing Society of Japan*, Vol.93, p.510-517, 1998
- Isolation and Characteristics of Lactic Acid Bacteria in Japanese Spirit Awamori Mash. Sayaka Watanabe, Makoto Kanauchi, et. al., *J. Am. Soc. Brew. Chem.* 65(4), p197-201, 2007.
- Quality specificity of Awamori mash, Takeshi Tamaki, Yoshiharu Takamiya, Chosei Takaesu, Mutsuko Simoji, *Journal of the Brewing Society of Japan*, Vol.81, p130-132, 1986

(Received July 1, 2009)

# On the study of the infinite decimal

Koki MURAOKA and Jo IDE

Students, National Institute of Technology, Kurume Colege

(Komoriono 1-1-1, Kurume city, Fukuoka 830-8555, Japan)

E-mail : y4-matsuda@kurume-nct.ac.jp

We have tried to calculate the value of the infinite decimals which are expressed by various progressions – arithmetical progression , geometrical progression , Fibonacci progressions and so on. Moreover the interesting numerical line has been obtained as the extension of this study. In this paper we would like to describe these process of the study and some results by this thesis.

**Key Words :** the infinite decimal , arithmetical progression , geometrical progression ,Fibonacci progression, recurrence formula, numerical line

## Preface

We had interested in the equation

$$0.123456789(10)(11)(12) \cdots = \frac{10}{81} \quad (1)$$

More than 2 digits of the integer move up at the previous place. Then we have tried to calculate the value of the infinite decimals which are expressed by various progressions.

## 1. The value of the infinite decimal which are expressed by the arithmetical progression

Let  $a, d$  be the integers , and

$$A_1(a, d) =$$

$$0.a(a+d)(a+2d) \cdots (a+(n-1)d) \cdots ,$$

$$A_2(a, d) =$$

$$0.0a0(a+d)0(a+2d) \cdots 0(a+(n-1)d) \cdots$$

Then , the next theorem is obtained.

### Theorem 1.

$$A_1(a, d) = \frac{9a+d}{81}, \quad A_2(a, d) = \frac{99a+d}{9801}$$

### Proof .

If  $|r| < 1$  , then

$$\sum_{n=1}^{\infty} r^n = \frac{r}{1-r} (=S(r)) ,$$

$$\sum_{n=1}^{\infty} nr^n = \frac{r}{(1-r)^2} (=T(r))$$

$$A_1(a, d) = \sum_{n=1}^{\infty} \frac{a+(n-1)d}{10^n}$$

$$\begin{aligned} &= (a-d) S\left(\frac{1}{10}\right) + d T\left(\frac{1}{10}\right) \\ &= (a-d) \frac{1}{9} + d \frac{10}{81} = \frac{9a+d}{81} , \\ A_2(a, d) &= \sum_{n=1}^{\infty} \frac{a+(n-1)d}{100^n} \\ &= (a-d) S\left(\frac{1}{100}\right) + d T\left(\frac{1}{100}\right) \\ &= (a-d) \frac{1}{99} + d \frac{100}{9801} = \frac{99a+d}{9801} \end{aligned} \quad \square$$

### Example 1 .

$$0.123456789(10)(11)(12) \cdots = A_1(1,1) = \frac{10}{81}$$

((1) is showed.)

$$0.01020304050607080910 \cdots = A_2(1,1) = \frac{100}{9801} ,$$

$$0.13579(11)(13) \cdots = A_1(1,2) = \frac{11}{81}$$

## 2. The value of the infinite decimal which are expressed by the geometrical progression

Let  $a, r$  be the real numbers , and

$$R_1(a, r) = 0.a ar ar^2 ar^3 \cdots ar^{n-1} \cdots ,$$

$$R_2(a, r) = 0.0 a 0 ar 0 ar^2 \cdots 0 ar^{n-1} \cdots$$

Then, the next theorem is obtained.

### Theorem 2.

$$R_1(a, r) = \frac{a}{10-r} \quad (|r| < 10) ,$$

$$R_2(a, r) = \frac{a}{100-r} \quad (|r| < 100)$$

### Proof .

$$\begin{aligned}
R_1(a, r) &= \frac{ar^0}{10} + \frac{ar^1}{10^2} + \frac{ar^2}{10^3} + \cdots + \frac{ar^{n-1}}{10^n} + \frac{ar^n}{10^{n+1}} + \cdots \\
&= \frac{a}{10} + \frac{a}{10} S\left(\frac{r}{10}\right) = \frac{a}{10} + \frac{a}{10} \times \frac{\frac{r}{10}}{1 - \frac{r}{10}} \\
&= \frac{a}{10} + \frac{ar}{10(10-r)} = \frac{a}{10-r}
\end{aligned}$$

Similarly

$$\begin{aligned}
R_2(a, r) &= \frac{a}{100} + \frac{a}{100} S\left(\frac{r}{100}\right) \\
&= \frac{a}{100} + \frac{a}{100} \times \frac{\frac{r}{100}}{1 - \frac{r}{100}} = \frac{a}{100-r} \quad \square
\end{aligned}$$

### Example 2 .

$$\begin{aligned}
0.1248(16)(32)(64)\cdots &= R_1(1,2) = \frac{1}{8}, \\
0.01020408\cdots &= R_2(1,2) = \frac{1}{98}
\end{aligned}$$

### 3. The value of the decimals which are expressed by the recurrence formula .

#### Theorem 3.

Let the progression  $\{a_n\}$  be expressed by the recurrence formula

$$a_{n+2} + pa_{n+1} + qa_n = 0$$

(  $p, q$  are the constant numbers)

and

$$1 + px + qx^2 \neq 0, \lim_{n \rightarrow \infty} x^n = 0$$

then

$$\sum_{n=1}^{\infty} a_n x^n = \frac{a_1 x + (a_2 + a_1 p)x^2}{1 + px + qx^2}$$

#### Proof.

Let

$$P = \sum_{k=1}^n a_k x^k$$

then

$$\begin{aligned}
&(1 + px + qx^2)P \\
&= a_1 x + (a_2 + a_1 p)x^2 \\
&\quad + (a_3 + a_2 p + a_1 q)x^3 + \cdots \\
&\quad + (a_n + a_{n-1} p + a_{n-2} q)x^n \\
&\quad + (a_n p + a_{n-1} q)x^{n+1} + a_n q x^{n+2}
\end{aligned}$$

As

$$\begin{aligned}
a_3 + a_2 p + a_1 q &= 0, \cdots, \\
&\sim \downarrow \sim \quad \sim \downarrow \sim
\end{aligned}$$

$$\begin{aligned}
&(1 + px + qx^2)P \\
&= a_1 x + (a_2 + a_1 p)x^2 + \\
&\quad (a_n p + a_{n-1} q)x^{n+1} + a_n q x^{n+2}
\end{aligned}$$

Therefore

$$P = \frac{a_1 x + (a_2 + a_1 p)x^2 + (a_n p + a_{n-1} q)x^{n+1} + a_n q x^{n+2}}{1 + px + qx^2}$$

As  $\lim_{n \rightarrow \infty} x^n = 0$ ,

$$\sum_{n=1}^{\infty} a_n x^n = \lim_{n \rightarrow \infty} P = \frac{a_1 x + (a_2 + a_1 p)x^2}{1 + px + qx^2} \quad \square$$

**Example 3.** Fibonacci progression is expressed by the next recurrence formula :

$$a_1 = a_2 = 1, a_{n+2} = a_n + a_{n+1}.$$

Put

$$a_1 = a_2 = 1, p = q = -1, x = \frac{1}{10},$$

to the formula in theorem 3, we get

$$0.112358(13)(21)(34)(55)(89)(144)\cdots = \frac{10}{89}$$

**Example 4.** The arithmetical progression are expressed by the next recurrence formula :

$$\begin{aligned}
a_1 &= a, a_2 = a + d, \\
a_{n+2} - 2a_{n+1} + a_n &= 0.
\end{aligned}$$

Put

$$p = -2, q = 1, x = \frac{1}{10}, \frac{1}{100}$$

to the formula in theorem 3, we get

$$\begin{aligned}
A_1(a, d) &= \frac{ax + \frac{1}{10} + (a+d+a \times (-2)) \times \left(\frac{1}{10}\right)^2}{1 + (-2) \times \frac{1}{10} + \left(\frac{1}{10}\right)^2} \\
&= \frac{10a - a + d}{100 - 20 + 1} = \frac{9a + d}{81}, \\
A_2(a, d) &= \frac{ax + \frac{1}{100} + (a+d+a \times (-2)) \times \left(\frac{1}{100}\right)^2}{1 + (-2) \times \frac{1}{100} + \left(\frac{1}{100}\right)^2} \\
&= \frac{100a - a + d}{10000 - 200 + 1} = \frac{99a + d}{9801}
\end{aligned}$$

These values are correspond with the values of theorem 1.

**Example 5.** The geometrical progression are expressed by the recurrence formula :

$$a_1 = a, a_2 = ar,$$

$$a_{n+2} - (r + 1)a_{n+1} + ra_n = 0 .$$

Put

$$p = -(r + 1), q = r, x = \frac{1}{10}, \frac{1}{100}$$

to the formula in theorem 3, we get

$$R_1(a, r) = \frac{ax^{\frac{1}{10}} + (ar + a \times (-r-1)) \times (\frac{1}{10})^2}{1 + (-r-1) \times (\frac{1}{10}) + (\frac{1}{10})^2 \times r}$$

$$= \frac{9a}{90-9r} = \frac{a}{10-r} ,$$

$$R_2(a, r) = \frac{ax^{\frac{1}{100}} + (ar + a \times (-r-1)) \times (\frac{1}{100})^2}{1 + (-r-1) \times (\frac{1}{100}) + (\frac{1}{100})^2 \times r}$$

$$= \frac{99a}{9900-99r} = \frac{a}{100-r}$$

These values are correspond with the values of theorem 2.

#### 4. On the interesting numerical line

About the calculation with the regularity the next theorems are obtaind.

##### Theorem 4.

$$1 \times 9 + 2 = 11$$

$$12 \times 9 + 3 = 111$$

$$123 \times 9 + 4 = 1111 \quad (2)$$

$$1234 \times 9 + 5 = 11111$$

• • • • • • • •

$$123456789 \times 9 + 10 = 1111111111$$

$$123456789(10) \times 9 + 11 = 111111111111$$

• • • • • • • •

##### Proof of (2).

Put

$$S = 0.0123456789(10)(11)(12) \dots ,$$

$$10000S = 123.456789(10)(11)(12) \dots$$

Get the difference

$$9999S = 123.444 \dots$$

As  $S = \frac{1}{81}$  from (1)

$$9999 \times \frac{1}{81} = 123 + \frac{4}{9} , \quad 1111 \times \frac{1}{9} = 123 + \frac{4}{9} .$$

When 9 is hung on the both sides ,

$$123 \times 9 + 4 = 1111$$

So (2) is showed.

Other equations ars showed similarly.  $\square$

##### Theorem 5.

$$1 \times 9 + 2 = 1 \times 11$$

$$13 \times 9 + 4 = 11 \times 11$$

$$135 \times 9 + 6 = 111 \times 11$$

$$1357 \times 9 + 8 = 1111 \times 11$$

$$13579 \times 9 + 10 = 11111 \times 11$$

$$13579(11) \times 9 + 12 = 111111 \times 11 \quad (3)$$

• • • • • • • •

##### Proof of (3).

Put

$$T = 0.13579(11) \dots ,$$

$$1000000T = 13579(11).(13)(15)(17) \dots$$

Get the difference

$$999999T = 13579(11).(12)(12)(12) \dots$$

As  $T = \frac{11}{81}$  from example 1

$$999999 \times \frac{11}{81} = 13579(11) + \frac{12}{9} ,$$

$$111111 \times \frac{11}{9} = 13579(11) + \frac{4}{3}$$

When 9 is hung on the both sides ,

$$13579(11) \times 9 + 12 = 111111 \times 11$$

So (3) is showed .

Other equations ars showed similarly.  $\square$

## Conclusion

Let the progression  $\{a_n\}$  be determined by the recurrence formula

$$a_{n+2} + pa_{n+1} + qa_n = 0 \\ (p, q : \text{constant numbers})$$

and

$$1 + px + qx^2 \neq 0, \lim_{n \rightarrow \infty} x^n = 0$$

then, from theorem 3

$$\sum_{n=1}^{\infty} a_n x^n = \frac{a_1 x + (a_2 + a_1 p)x^2}{1 + px + qx^2}.$$

Put  $x = \frac{1}{10}$ , then

$$\sum_{n=1}^{\infty} \frac{a_n}{10^n} = \frac{(p+10)a_1 + a_2}{100 + 10p + q}$$

The denominator of this decimal is obtained by the next translations :

$$a_{n+2} \rightarrow 100, a_{n+1} \rightarrow 10, a_n \rightarrow 1.$$

For example, the denominator of

$$0.123456789(10)(11)(12)\dots = \frac{10}{81}$$

is obtained by

$$a_{n+2} - 2a_{n+1} + a_n = 0 \rightarrow$$

$$100 - 20 + 1 = 81.$$

We would like also to continue the study of the infinite decimal now.

## REFERENCES

- 1) Tomio Ueno, Kazuuno wadai jitenn, Tokyodo Syuppan, 1995, pp. 288-289.
- 2) Shinpen Kosen no Sugaku 1~3, Morikita Syuppan, 2012. (The mathematics text of our school)

(Received October 29, 2015)